12-19-2008

Development of a Borehole Log Signature for Oceanic Anoxic Events and Its Application to the Gulf of Mexico

Asani Brewton
University of New Orleans

Development of a Borehole Log Signature for Oceanic Anoxic Events and Its Application to the Gulf of Mexico

A Thesis

Submitted to the Graduate Faculty of the
University of New Orleans
in partial fulfillment of the
requirements for the degree of

Master of Science
in
Earth and Environmental Sciences

by
Asani Brewton

B.S. Elizabeth City State University, 2005

December 2008

ACKNOWLEDGEMENTS

It is with sincere thanks that I would like to acknowledge the following people: Dr. William Busch, Dr. Mark Kulp, Dr. Mark Hanan, Minerals Management Services, Ron Bowser, Holly Karrigan, Fran Wiselady, Mary Rather, the people of Digital Formations Inc., Angie Josey, Stephen Pomes, Cathy Moser, David Cooke, Rose Hampton, Mary Malouse, Kevin Karl, Davin Marin, Dr. Kaiyu Liu, Robert Witrock, Phil Smith, and the MMS Public Information employees. Without any one of these people this project would not have been completed. I cannot thank you enough.

TABLE OF CONTENTS

LIST OF FIGURES

LIST OF TABLES

ABSTRACT

Oceanic anoxic events (OAEs) are periods in Earth's history when oceans were depleted in dissolved oxygen and characterized by deposition of organic-rich sediments. The Oceanic Drilling Program (ODP) has drilled through OAEs in a number of areas worldwide, collecting core and borehole log data. This project attempts to identify a characteristic signature from known ODP OAE sections using these data and to apply the signature to identify OAE intervals in Gulf of Mexico wells where cores are lacking. Additionally, pseudo density curves were generated from ODP logs and compared to bulk density logs to determine if the deviation between the two would aid identification of OAE intervals. A general, though not fool proof, signature of high gamma ray, uranium, neutron porosity and low density was seen in nearly all of the ODP holes. Using this signature 20 potential OAE intervals were identified in the Gulf of Mexico.

Key Words: Cretaceous, anoxic, organic-rich, oceanic anoxic event, pseudo density, log characteristic, gamma ray, uranium, density

INTRODUCTION

Oceanic anoxic events (OAEs) are defined as periods of time marked by the global deposition of organic-rich, finely laminated, black, fine-grained sediments accompanied by a spike in the $^{12}C/^{13}C$ ratio and a decrease in the $^{87}Sr/^{86}Sr$ ratio resulting from the depletion of dissolved oxygen (Tskios et al., 2004; Weissert et al., 2004). They are known to correlate with the presence of anomalous quantities of trace metals, emplacement of large igneous provinces (LIPs) and extinction events (Snow et al., 2005; Hallam et al., 1999; Weissert et al., 2004). Oceanic anoxic events are also marked by the presence of geoporphyrins that point to diazotrophic cyanobacteria (green sulfur bacteria) as primary producers during their formation and thus a euxinic water column (Ohkouchi et al., 2006; Pancost et al., 2004).

Two main OAEs occurred during the Cretaceous, the Selli Event, or OAE 1a (~120 Ma), and the Bonarelli Event, or OAE 2 (~92 Ma) (Pancost, et al., 2004). In addition to these two events there are several minor OAEs during the Cretaceous thought to be relatively confined to the Atlantic Ocean, which was much narrower during that period and more susceptible to anoxia by cut off from oceanic circulation by the formation of underwater igneous plateaus (Fig. 1) (Dean, 1999). Among these is OAE 3, the most recent OAE. Oceanic anoxic event 3 has the least clearly defined time span of the OAEs, ranging from the Middle Coniancian stage (~89 Ma) to the Early Santonian stage (~86 Ma). In addition to being the latest OAE, it is also the longest at roughly 3 m.y. versus all other OAE periods that are roughly 1 m.y. in duration (Wagreich, 2006). A third major OAE occurred in the Early Jurassic during the Toarcian stage (~183 Ma).

Oceanic anoxic events are well documented in cores from the Pacific and the Atlantic Oceans, obtained through drilling by the Deep Sea Drilling Project (DSDP) and the Ocean Drilling Program (ODP). The DSDP, and to a greater extent, the ODP also used wireline logging to characterize the sections they drilled. However, only limited attempts have been made to use the borehole logs to develop criteria to recognize OAE sediment intervals. A set of logging criteria integrated with core data from known OAE intervals could be used to identify OAEs in boreholes from areas where only logging data are available. Development of these criteria would be especially valuable in the Gulf of Mexico where there is an abundance of logging data but core samples are commonly unavailable. While OAEs are known from the Gulf of Mexico through seismic records and cores collected in Alabama (Liu, 2005) and in outcrops

from the Sierra Madre Oriental, Mexico (Montanez, 2006), documentation of OAEs in the Gulf of Mexico is limited.

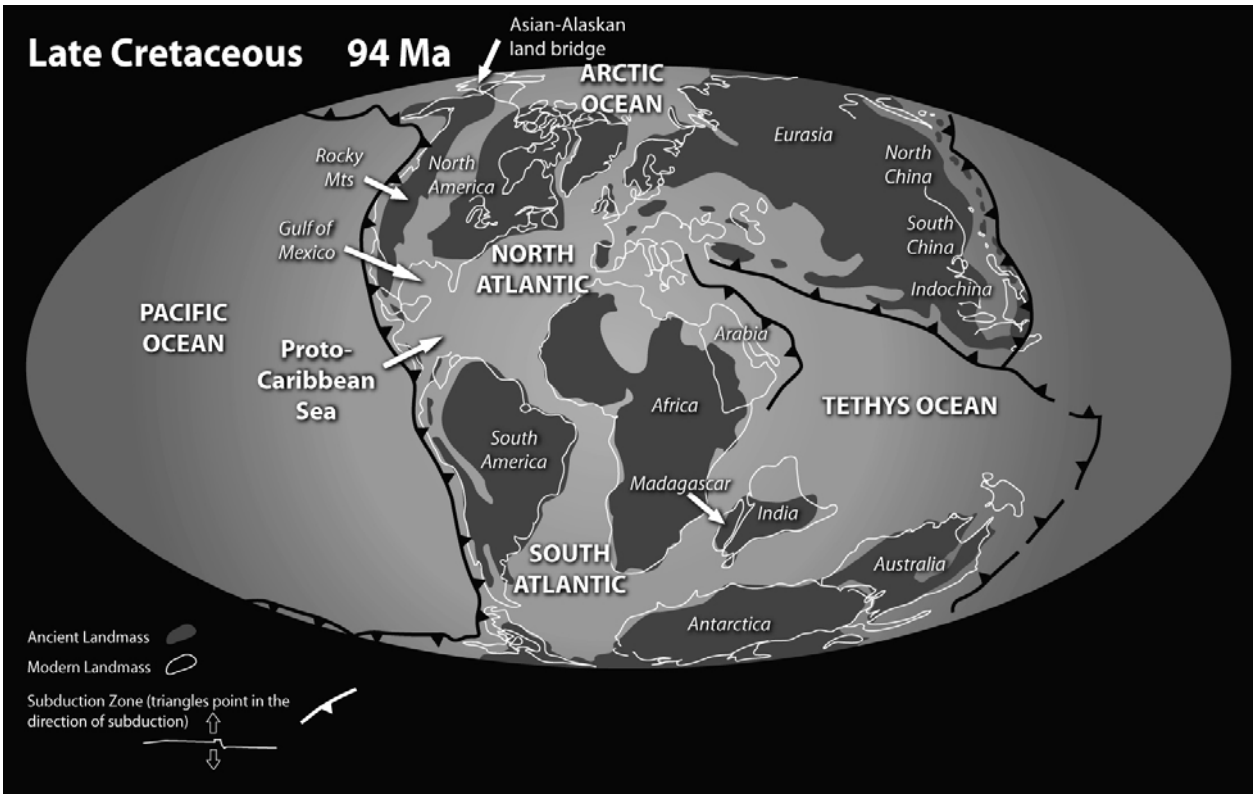

Figure 1. Late Cretaceous paleogeography (modified from http://scotese.com/cretaco.html).

Whereas the signature of OAEs in ODP borehole logs is expected to be applicable to borehole logs from the Gulf of Mexico, there are differences between the two data sets that might affect how the signal appears in the Gulf of Mexico logs. Most of the ODP sites are areas where sediments were deposited under more open marine conditions as opposed to the Gulf of Mexico well sites where sediments were deposited in a continental margin, carbonate-dominated shelf setting. It is anticipated that the Gulf of Mexico wells will show expanded OAE intervals as sedimentation rates at the continental margin are expected to be higher. However, the higher sedimentation rate of carbonate sediments may cloud the borehole log signature developed for the ODP sites. Additionally, there is wide variation in the types of sediment that were deposited at the ODP sites during OAE intervals. Whereas OAEs are most commonly associated with black shales, the organic-rich lithologies encountered at the ODP sites range from shales and mudstones, to limestones, porcellanites, and chert or other siliceous deposits of radiolarians and diatoms.

Oceanic anoxic events are significant for a number of reasons. First they document the earth under greenhouse conditions (Jenkyns, 2003). With today's focus on global warming the insight into what initiated the onset of OAEs and what triggered their ending is invaluable. Second, the high organic carbon content of these rocks frequently makes them ideal source rocks for hydrocarbon reservoirs (Liu, 2005). As such, the ability to identify a lithologic sequence deposited during an OAE within the Gulf of Mexico, without the cost of coring, would be an aid to hydrocarbon exploration. This project attempts to identify a characteristic signature within ODP borehole logs from known OAE sections and to apply that signature to identify potential OAE associated lithologies within the Gulf of Mexico.

The objectives of this study are to define a set of log response criteria that could be used as an indication of the presence of intervals deposited during an OAE. The criteria would be assembled by the examination of wireline data acquired by the ODP over intervals established by paleontology and core data as having been deposited during OAEs. These criteria then will be applied to Gulf of Mexico wireline logs through lithologies bio-stratigraphically dated as having been deposited during Aptian, Albian, Cenomanian, Turonian, Coniancian, and Santonian stages of the Cretaceous to identify intervals likely to have been deposited under OAE conditions.

METHODS

Data Sources

Two main sources of data were used for the comparison of OAE intervals in ODP and Gulf of Mexico boreholes: (1) core and log data from the ODP database and Initial Reports volumes and (2) non-proprietary Gulf of Mexico borehole logs from the Minerals Management Service.

ODP Sites

Ocean Drilling Program holes that penetrated OAE intervals and that were used in this study are summarized in Table 1 and Figure 2. The sites listed in Table 1 represent only a portion of the DSDP and ODP sites that contain sediments deposited during OAEs. A number of DSDP sites containing OAE sediments were identified; however, none of these sites have borehole logs corresponding to the cored intervals. Additional ODP sites containing sediments of Cretaceous age were identified, but they do not have intervals appearing to have been deposited during OAEs. Only those ODP sites that contain previously identified OAE intervals were used in this study.

Not all of the ODP sites that contain sediment intervals deposited during OAEs met the borehole log requirements for this study, and they were excluded. Sites that were chosen have all the needed borehole logs for the majority of the sections in which corresponding sediments deposited during OAEs were recovered. Data provided by the ODP include gamma ray logs, resistivity logs, density logs, neutron porosity logs, sonic logs and data from a wide range of sedimentological, geochemical, and paleontological analyses of core samples. These data were examined and used to generate the borehole log signature to be used to identify OAEs in the Gulf of Mexico.

Table 1. Ocean Drilling Program holes that penetrate sediments deposited during Oceanic Anoxic Events.

Leg	Hole	Location	Ocean
103	641C	Galicia Bank	NE Atlantic
159	959D	Cote d'Ivoire-Ghana Margin	Equatorial NE Atlantic
171B	1052E	Blake Nose	NW Atlantic
198	1207B	Shatsky Rise North	NW Pacific
198	1213B	Shatsky Rise North	NW Pacific
207	1258C	Demerara Rise	Equatorial NW Atlantic
207	1261B	Demerara Rise	Equatorial NW Atlantic

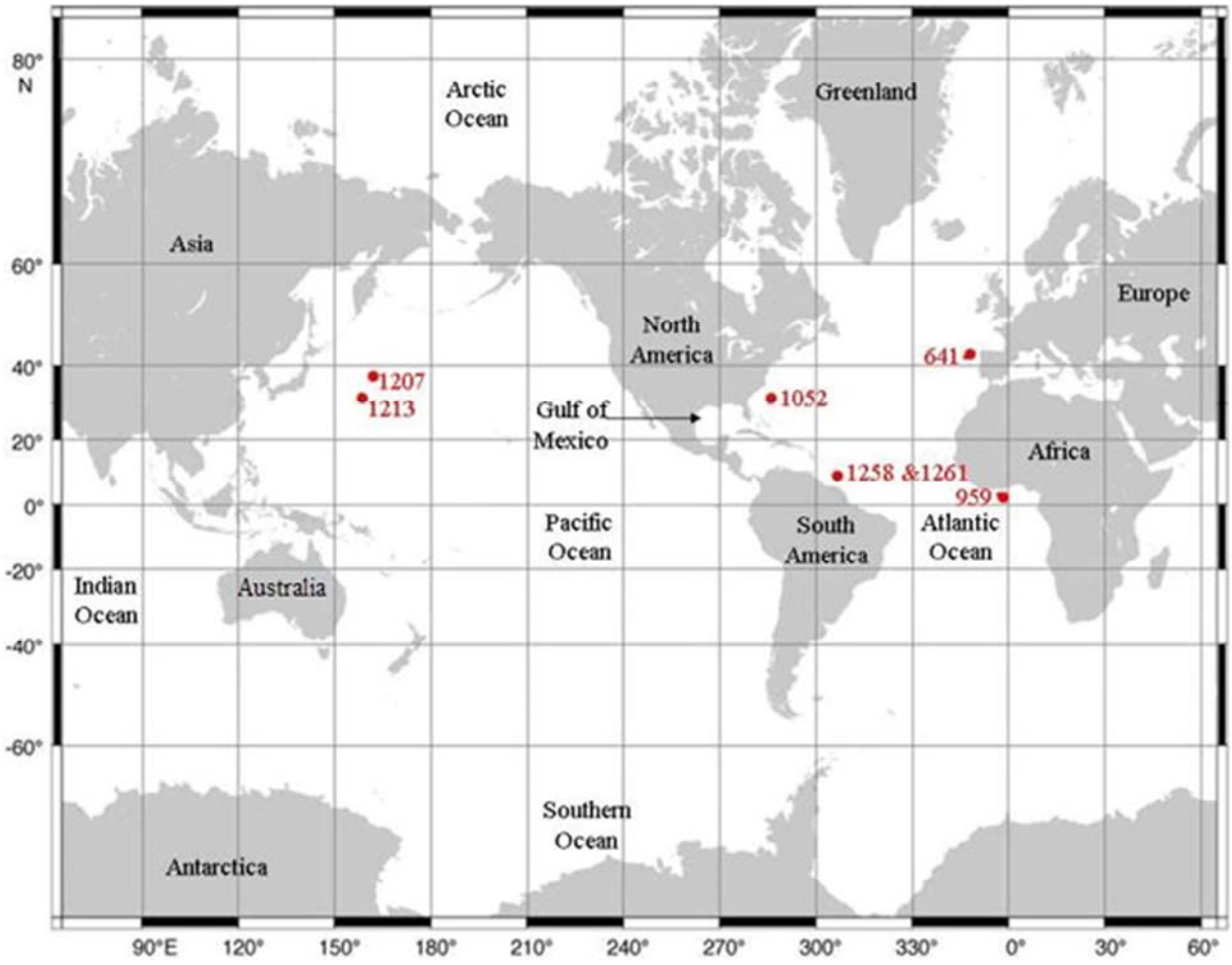

Figure 2. ODP sites with OAEs (modified from http://www-odp.tamu.edu/sitemap/odpmap.gif).

Gulf of Mexico Wells

Non-proprietary Gulf of Mexico wells that are available from the Minerals Management Service and that penetrate sediments of Cretaceous age are summarized in Table 2 and Figure 3. These wells were chosen based on searching all publicly available paleontology reports for those wells that contain index fossils of Coniancian, Santonian, Turonian, Cenomanian, Albian or Aptian age. Additionally wells that penetrated the Tuscaloosa Formation, based on formation data available in some paleontology reports, were examined. The Tuscaloosa Formation has been shown to be associated with OAE deposition on land in the Gulf of Mexico region (Liu, 2005). Using these criteria 35 wells were originally identified as possibly containing OAEs. This number was pared down to eight wells that have the highest number of index fossil data points for time control and the borehole logs necessary to compare with the ODP sites and to create pseudo density curves. Data provided by Minerals Management Service include gamma ray logs, resistivity logs, density logs, neutron porosity logs, mud logs, sonic logs and paleontology reports.

Table 2. Well names and locations for data provided by the Minerals Management Service in the Gulf of Mexico Area.

API	Well name	Side Track	By Pass	Area Code[1]	Blk #
177244005200	002	00	00	MP	264
177244005400	006	00	00	MP	253
177244006300	001	00	00	MP	222
608164003700	001	00	00	VK	30
608224000600	001	00	00	DD	166
608224001400	003	00	00	DD	162
608224001700	001	00	00	DD	529
608224002200	001	00	00	DD	284

[1] DD=Destin Dome; MP=Main Pass Area; VK=Vioska Knoll. See Figure 3, Map of the Gulf of Mexico showing Minerals Management Service protractions.

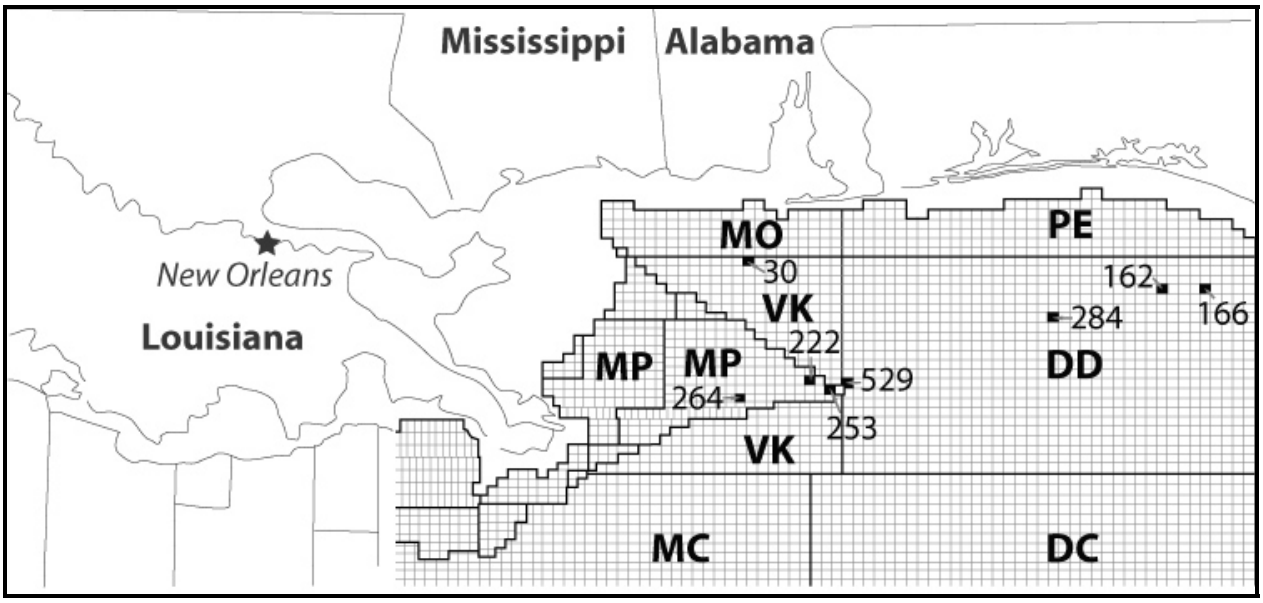

Figure 3. Gulf of Mexico showing Minerals Management Service protractions (modified from http://www.gomr.mms/gov/homepg/1pg/lsesale/Visual1.pdf). DD=Destin Dome; DC=DeSoto Canyon; MC=Mississippi Canyon; MO=Mobile; MP=Main Pass Area; PE=Pensacola; VK=Vioska Knoll.

Data Analysis

Data analysis involved four steps: (1) the available ODP data were examined in detail for possible signatures indicative of deposition during an OAE; (2) gamma ray and spectral gamma ray borehole logs and organic carbon data from core analyses were compared to establish a correspondence with OAEs; (3) the petrophysical analysis software LESA was used to produce and test pseudo bulk density curves for use in identifying OAEs; and (4) the signature that was compiled using ODP borehole logs was applied to non-proprietary logs from the Gulf of Mexico to identify intervals likely to have been deposited during an OAE.

Logging Tool Summary

In order to understand the use of each of the logging tool readings being examined for this study, a brief, generalized summary of how the tools work and what they read is necessary. A listing of all log types used in the analysis of ODP holes and Gulf of Mexico wells is presented in Table 3.

Table 3. Borehole Logs Available from ODP and MMS Databases.

Log Name	Abbreviation	Measures	Units	Approx. Tool Vertical Resolution (m)
Total Gamma Ray	Gr	Naturally occurring radioactivity	GAPI	0.152
Corrected Gamma Ray	CGR	Naturally occurring radioactivity minus radioactivity attributed to uranium	GAPI	0.152
Thorium Gamma	Th	Radioactivity associated with thorium	GAPI	0.152
Potassium Gamma	K	Radioactivity associated with potassium	GAPI	0.152
Uranium Gamma	U	Radioactivity associated with uranium	GAPI	0.152
Resistivity/Dual Induction	ILD	Measures conductivity	OHMM	0.91
Neutron Porosity	NPHI	Measures neutron density of hydrogen atoms	V/V	0.39-0.5
Bulk Density	RHOB	Measures the electron density	g/cm3	0.3
Acoustic/Sonic	Sonic	Measures the rate of travel of sound waves through material	μs/ft	0.6

The gamma ray log records "the intensity of the natural gamma radiations emanating from the formations penetrated by the borehole versus depth" (Bassiouni, 1994). While all rocks have some degree of radioactivity, radioactive elements are often concentrated in clay minerals, which are the building blocks of shales.

Some gamma ray tools allow for the distinction between the three most common sources of natural gamma radiation: potassium, thorium and uranium. These distinct components make up a spectral gamma ray log. Potassium, K^{40}, a common constituent of clay minerals, is the most abundant radioactive element (Bassiouni, 1994). Because uranium readily binds to organic matter, organic-rich sediments display high gamma ray counts. Using the general assumption that a high gamma ray signal implies high clay content, organic-rich sediments are sometimes mistakenly interpreted as having a high clay content. For this reason some gamma ray readings are given in total gamma ray and or corrected gamma ray form. The corrected gamma ray subtracts the effect of the uranium from the total gamma ray reading, as this can be useful in certain oil and gas exploration situations.

Each individual gamma ray tool gives a different reading through a given lithology based on its size and the efficiency of the tool (Ellis, 2007). This variation led to the need for a standardized means of documenting gamma ray log readings. All gamma ray tools are now calibrated to the same standard set of units, GAPI. The API stands for the American Petroleum Institute who developed the standard by which all gamma ray logs are compared. Calibration involves normalizing of the gamma ray tool against a standard pit with various zones of concrete at known concentrations of potassium, thorium and uranium. These zones are meant to represent twice the radiation of a typical shale, or 200 GAPI (Ellis, 2007). Typical gamma ray log responses for some of the most common lithologies are shown in Figure 4.

The gamma ray log, while one of the most highly used tools in the logging field, does have some drawbacks. The logging tool will not detect all gamma radiation. A gamma ray tool that is considered very efficient may only detect 50-60% of the gamma radiation within a rock (Bassiouni, 1994). Therefore, the potential for gamma radiation to go undetected is high. Another drawback is the reading range of the tool. The gamma ray tool averages radiation over a 0.152 m (0.5 ft) interval. Many thin beds of various radiation outputs may then be averaged together giving a misleading interpretation of what is actually present. In order to read properly, the tool must stay within the center of the borehole. This is frequently complicated by the borehole quality, angle of inclination, and various other mechanical problems associated with drilling. Increases in temperature also affects the ability of the tool to read efficiently.

Bulk density is measured by a tool that is applied to the borehole wall as opposed to being centrally located within the borehole as a gamma ray tool is. It works by directing gamma rays into the formation and then counting the gamma rays that are backscattered to the detector. Since the gamma rays lose energy as they encounter electrons within the formation, the amount of backscatter is inversely related to the electron density of the formation (Foster, 2006). Essentially, a rock with a higher density will funnel fewer gamma rays back to the detector (Bassiouni, 1994). The electron density can then be corrected to give the rock's bulk density and is recorded in units of g/cm^3. The average grain densities of several sedimentary rock components are listed in Table 4.

Because the tool must be applied directly to the rock formation it cannot be run through the drill pipe or in cased holes. The vertical resolution of the tool is ~0.3 m (1 ft). The tool is

very sensitive to the borehole shape. Even microrugosity that goes undetected by the caliper tool can cause the density readings to be suspect.

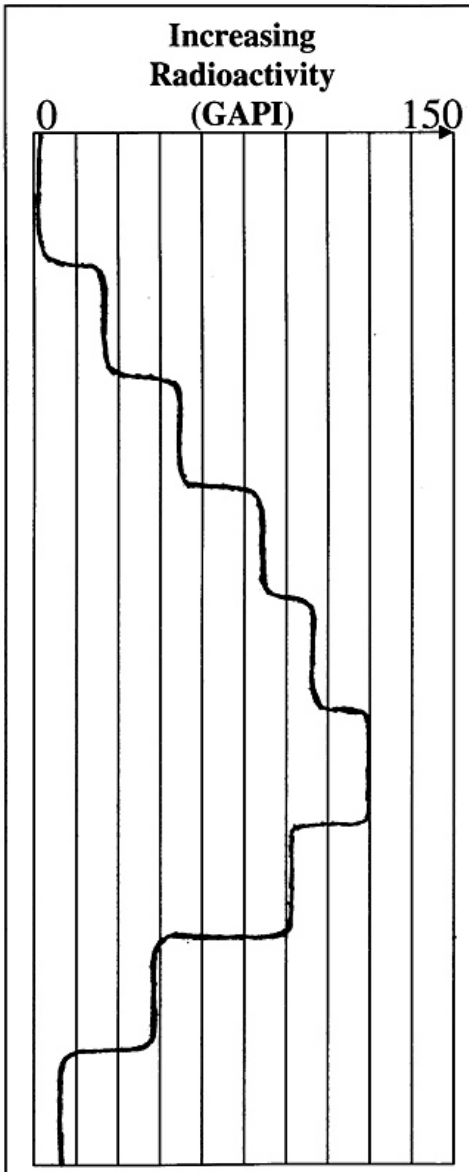

Lithology	Average Becquerel (Bq)
Evaporites	Not Available
Clean Sand	0.152
Shaley Sand	0.259
Interbedded Sand and Shale	0.500
Shale	0.752
Black Marine Shale (Organic Rich)	0.967
Black Limey Shale	0.611
Limey Shale	0.252
Limestone	0.141

Figure 4. Diagram comparing typical log response in GAPI units to average radioactivity measured in becquerels (Bq) with a Geiger counter for common sedimentary rocks (modified from Bassiouni, 1994; Russel, 1944; and Schlumberger, 1972).

Table 4. Average grain densities for several sedimentary rock components.

Component	Average grain density (g/cm^3)
Organic matter	1.06
Lithogenic material	2.71
CaCO3	2.71
Opal	2.10

The neutron porosity tool estimates porosity based on the hydrogen content of the rock. The tool bombards the rock with neutrons and detects the rate at which energy is lost by the neutrons. The smaller the nucleus struck by the neutrons the greater the energy loss. Because a hydrogen atom is nearly the same size as a neutron, the energy of the rebounded neutrons is directly related to the hydrogen content of the rock. In sediments and sedimentary rocks, most hydrogen is in the pore fluids. This relationship allows for the determination of porosity (Foster, 2006 and Bassiouni, 1994). The tool units are in volume per volume (V/V).

Like the density tool, the neutron porosity tool must be applied directly to the borehole wall. The vertical resolution depends on the specific neutron porosity tool used but ranges between 0.39 m (1.29 ft) and 0.5 m (1.63 ft) (Foster, 2006). One draw back to this tool is that companies calibrate it in standard limestone units. Where sandstone is the dominant lithology each company uses its own computer modeling to calibrate the tools, and the resulting values cannot be compared accurately between companies.

Sonic logs provide an indirect means of calculating formation porosity by recording the velocity at with sound travels through rocks adjacent to the borehole. An electronic pulse is used to generate a sharp sound impulse. The transit time of the impulse through the rock is recorded continuously through the borehole. The log is recorded as transit time, the inverse of velocity, in μs/ft. The vertical resolution is ~0.61 m (2 ft).

Resistivity logs deal with a lithology's ability to resist electric current. The resistivity of a formation is inversely related to the electrolyte content of the pore fluid. Oil and gas in the pore space of a rock and the solid rock constituents do not conduct electricity well. As a result, hydrocarbon saturated rocks and low porosity rocks show a high resistivity. Clays commonly have bound water absorbed to the mineral surfaces, and even though this water is immobile, it

typically retains its electrolytic properties. Thus rocks rich in clay minerals, such as shales, tend to read as less resistive.

The resistivity tool works by applying an electrical current to the rock and recording the degree to which it conducts electricity. The typical vertical resolution range for resistivity tools commonly used today a ~0.91 m (3 ft) to ~0.3 m (1 ft) (Foster, 2006 and HRLA high-resolution Laterolog Array Tool, 2000). The resolution depends on the specific tool being used.

OPD Data Processing

The ODP log data were obtained from the database maintained by the Integrated Ocean Drilling Program (IODP) Borehole Research Group at the Lamont Doherty Earth Observatory. Core data were obtained from the ODP Janus database maintained by the IODP U.S. Implementing Organization (USIO) at Texas A & M University. The data were converted into Excel files where they were quality checked for any potential errors or missing data points. The data were then placed into individually made Lasso (.las) files for use in the petrophysical software Log Evaluation System Analysis, Version 7.0 (LESA), produced by Digital Formations, Inc. Before being used to establish a borehole log signature, the data were examined again, this time with the LESA software, to determine if there were any potential tool or human errors.

Ocean Drilling Program borehole log data evaluated for an OAE signature include gamma ray, resistivity, bulk density, neutron porosity, and sonic logs (Table 3). Lithology and paleontology descriptions were used to verify the presence of sediments deposited during OAEs. Depths for OAE intervals were taken from the Initial Report volumes for each of the ODP sites. After depths for OAEs were established, borehole log responses through these intervals were examined for a signature that repeated in each of the ODP holes. The petrophysical analysis software LESA was used as a means of displaying the data for comparison among borehole logs. Spectral gamma ray logs were examined to explain the response of the total gamma ray log through OAE intervals. Intervals determined to be “hot” shales, those with an especially high gamma radiation level were examined to determine if the radioactivity resulted from the presence of uranium, which typically correlates with the organic content of the sediments (Lüning and Kolonic, 2003).

Total and Spectral Gamma Comparison with Carbon Data

The significance of the total and spectral gamma ray tool responses were evaluated in part by comparing their output with organic carbon values determined for core samples. In order to compare the gamma ray responses with organic carbon weight percentages determined from core analyses, the depths assigned to the core values had to be adjusted to account for uncertainty in the depth associated with less than 100% core recovery. The ODP assigns core depths by assuming that the top of the cored interval corresponds to the top of the drilled interval for a given core. Because of this assumption, the uncertainty in the depth of a core sample could be as large as the length of the drilled interval for which core was not recovered. For each organic carbon sample a depth range was established by adding the length of no recovery for a core to the assigned depth for a sample. Once the depth ranges for the organic carbon values were determined, the gamma ray and uranium gamma ray values through those intervals were averaged so that a value-to-value comparison would be possible.

Pseudo Bulk Density Log Generation

In addition to examining the borehole logs for a signature characteristic of sediments deposited during OAEs, a second technique was used to identify organic-rich sediment intervals. Bulk density logs were compared with pseudo bulk density logs. The pseudo density logs were created from gamma ray, resistivity, and porosity curves by means of a neural network of the original data logs using the program *Esteem* within the LESA software. *Esteem* is designed to generate a missing curve based on being "trained" by the input of valid curves. Initially the program is fed curves like gamma ray, resistivity, and neutron porosity and based on the responses of these curves it predicts what a chosen outcome curve should look like for a particular borehole. In this case *Esteem* was asked to generate a bulk density curve, creating what is referred to a pseudo bulk density curve. Differences between the bulk density and the pseudo bulk density, referred to as density anomalies, were examined to identify intervals of organic-rich sediments. It was expected that negative anomalies (measured bulk density – pseudo density) would be a potential indicator of high organic content.

In the hope of better establishing the correlation between lithology and deviation from bulk density a core-by-core average deviation was then obtained for all of the ODP holes (Appendix B). Using the naming classification standards as a means of determining approximate carbonate to quartz to clay content in each core, the cores were then compared to the average deviation for that segment of the hole (Shipboard Scientific Party, 2004c).

Analysis of Gulf of Mexico Logs

The Gulf of Mexico data were processed in a manner similar to that of the ODP data. The data were first placed in Excel spreadsheets to examine for obvious data errors. A Lasso file was designed for each well, and the data were loaded into the file for use in the LESA software. The data were quality checked again for errors or missing points. The paleontology reports for the individual wells provide depths for the occurrence of index fossils, which were used to narrow the section of the well log to be examined. The depth ranges that were examined for sediments potentially deposited during OAEs were determined from the first appearance datum (FAD) and last appearance datum (LAD) for each index fossil. The index fossils were chosen to provide depth ranges that include all sediments possibly deposited during the desired intervals. Non-proprietary Gulf of Mexico wells that met the age requirements for OAEs but were not used in this study because they did not meet other selection criteria are listed in Appendix A.

Mud logs, where available, were used to further refine the selection of potential OAE sediment intervals. After the set of wells with potential OAE intervals was narrowed based on the paleontology reports, the well logs were compared with the OAE signature established for the ODP holes to check for the presence of OAE sediments. In instances where the signature appears to occur in the Gulf of Mexico wells, the lithology descriptions from the mud logs were used to infer the lithology of the interval matching the signature.

RESULTS

Ocean Drilling Program Holes

Sediments deposited during OAEs were examined at seven ODP sites, Sites 641, 959, 1052, 1207, 1213, 1258 and 1261. The holes that were logged at these sites include Holes 103-641C, 159-959D, 171B-1052E, 198-1207B, 198-1213B, 207-1258C and 207-1261B.

Hole 103-641C is located northwest of the Iberian Peninsula in the west Galicia Margin in a water depth 4640.0 m. The hole penetrated sediments ranging from Barremian to Cenomanian in age. From Late Jurassic to Early Cretaceous the Galicia margin depositional environment was a shallow-water carbonate-platform. The platform began breaking up during the Early Cretaceous, and the area became dominated with a basin-and-range topography, allowing for rapid subsidence. With the water level rapidly increasing deposition below the calcite compensation depth (CCD) began as early as the Barremian (Boillot, 1987). By the Late Aptian the region had moved into a post-rift, gradual subsidence setting. Four major lithologies were recovered in Hole 103-641C: (1) Barremian- to Aptian-age silt and sand turbidites and shallow-water limestones; (2) Aptian-age thin calcareous turbidites and black shales; (3) Aptian-age marlstones and conglomerates; and (4) Albian- to Cenomanian-age black and dark-green claystone (Shipboard Scientific Party, 1987) (Appendix B). There was a brief hiatus in deposition between Aptian- and Albian-age lithologies.

The Albian black claystone is considered to be associated with deposition during one or more OAEs. While the claystone does have trace amounts of fish debris, the primary organic carbon components are of terrestrial origin. Organic matter accounts for 1%-2% of the claystone (Boillot, 1987). The upper boundary of Albian- to Cenomanian-age black shales is at 150.9 meters below seafloor (mbsf) and continues through to the lower boundary at 202.6 mbsf for a thickness of 51.7 m (Table 5).

Reliable log readings were acquired from ~130.0-196.0 mbsf (Appendix C). Additional logging for this hole was obtained by reading through the drill pipe, which inhibits the effectiveness of the gamma ray logging, density and neutron density logging tools. The first core taken in Hole 103-641C was at 150.0 mbsf. This core is 90.0 m deeper than the last core taken in Hole 103-641A, leaving a section where lithology cannot be accounted for within the logged

interval. The lower boundary of the Albian black claystone is beyond the depth of the last logged interval. The total gamma ray and uranium gamma ray GAPI values increase significantly through this lithology. The average gamma ray reading through lithologies not associated with deposition during an OAE is 31.0 GAPI. The average gamma ray reading through the black shales is 86.2 GAPI. The uranium average through this interval is 3.9 GAPI versus the non-OAE associated lithologies where it averages 0.9 GAPI (Table 6). In particular, there is a significant spike in the total gamma ray of 157.2 GAPI and in the uranium gamma ray of 12.2 GAPI at ~160.0 mbsf. At this same depth, there is a matching decrease in bulk density and increase in neutron porosity when compared to the rest of the black shale interval. Bulk density values are given for these depths; however, there are no shallower density values for comparison within this hole. Neutron porosity values are not the highest that are seen through the hole, but are comparatively higher than those seen in the interval immediately preceding the black shale (Table 7).

Hole 159-959D is in the eastern equatorial Atlantic Ocean, in the Cote d'Ivoire-Ghana transform continental region. The hole is in 2090.7 m of water. There are five lithologic units described in Hole 159-959D (Appendix B): (1) A mix of Pleistocene- to Early Miocene-age nannofossil ooze with chalk, a foraminifer nannofossil ooze with chalk, and a nannofossil and chalk with clay deposited in a basin with cyclic variations in the bottom water oxygen content; (2) Early Miocene to Late Paleocene cherts, diatomite, and porcellanite deposited during a period of relatively high primary productivity; (3) Late Paleocene to Early Coniancian black claystones and claystones with nannofossils deposited in a pelagic environment; (4) Early Coniancian to Early Turonian and older sandy limestone, sandy dolomite, calcareous sandstone, and limestones with a downhole coarsening trend indicative of shifting from a more shallow depositional setting to a basinal setting; and (5) Late Albian quartz sandstone and silty claystone from a shallow shelf environment (Shipboard Scientific Party, 1996).

Hole 159-959D has concentrations of organic matter in both Lithologic Units 2 and 3. However, in both instances the origin of the organic matter cannot be determined. In the case of Lithologic Unit 3, which contains black claystones deposited during OAE 3, the organic matter has been oxidized and is highly degraded (Mascle, 1996). Lithologies associated with deposition during OAE 3 have an upper boundary at 1024.0 mbsf and a lower boundary at 1043.3 mbsf for a thickness of 19.3 m (Table 5).

Table 5. Description of organic-rich intervals in ODP holes.

Hole	Depth (mbsf)	Depth (ftbsf)	Age[1]	OAE	Lithology of organic-rich sediment interval
103-641C	150.9-202.6	495.1-664.7	Albian	N/A	Massive black claystone, laminated black claystone, gray claystone, black and dark greenish gray claystone interbedded, greenish gray claystone-lightly bioturbated and faintly laminated, grayish green massive claystone.
159-959D	1024.0-1043.3	3349.7-3422.9	Late Santonian-Early Coniancian	3	Black claystone, parallel laminated, numerous dolomite crystals in upper portion, pyrite aggregation forms some laminations. Burrows disturb laminations slightly, pyrite disseminated throughout.
171B-1052 E	510.6-656.0	1681.5-2182.0	Late Albian	OAE 1d	Dark claystone, black shale, calcareous claystone, silty claystone, clayey limestone with foraminifers and quartz and clayey siltstone. These alternate beginning and ending with black "shale." Are rich in pyrite, contain clay with calcareous nannofossils, fine silt sized quartz, fish remains, and organic debris. Has terrigenous material. There is a lot of calcium material judging from the core descriptions.
198-1207B	565.0-574.0	1853.7-1883.2	Aptian	1a	Dark yellowish brown organic carbon rich claystone. Limestone flanks this interval above and below.
198-1213B	256.8-266.4	842.3-874.0	Aptian	1a	Organic carbon rich clayey porcellanite with minor altered tuff.
207-1258C	397.5-449.6	1304.1-1477.9	Turonian-Middle-Late Albian	2	Upper portion is mostly composed of organic carbon rich black shales and black limestones. The upper portion contains complete OAE 2. This is separated from a bottom portion by a Middle Albian disconformity. See Below.
207-1258C	449.6-484.9	1474.9-1590.8	Late-Early Albian	1d?	The bottom portion consists of organic carbon rich claystones with phosphatic concretions. The bottom portion is possibly OAE 1d but there are insufficient biomarkers to say definitively.
207-1261B	563.0-659.2	1847.1-2162.7	Santonian-Late Cenomanian	2	Calcareous claystone (black laminated) with organic matter, clayey chalk with nannofossils and organic matter, glauconitic limestone with phosphatic nodules, and clayey limestone. The organic claystone is interbedded with limestone.

Table 6. Gamma ray and uranium mean values for lithologies associated with OAEs and lithologies not associated with OAEs.

Hole	Depth (m)	Mean Gr in non-OAE lithologies (GAPI)	Mean Gr in OAE lithologies (GAPI)	Peak Gr in OAE lithologies (GAPI)	Mean U in non-OAE lithologies (GAPI)	Mean U in OAE lithologies (GAPI)	Peak U in OAE lithologies (GAPI)
103-641C	150.9-202.6	31.0	86.2	157.2	0.9	3.9	12.1
159-959D	1024.0-1043.3	41.0	117.9	207.1	2.9	9.7	12.4
171B-1052E	510.6-656.0	23.7	50.5	71.7	1.2	1.8	3.2
198-1207B	565.0-574.0	10.4	19.3	83.0	0.5	1.1	6.4
198-1213B	256.8 - 266.4	11.0	33.7	79.3	0.3	1.5	5.1
207-1258C	397.5-449.6	23.7	85.7	220.2	0.5	8.8	25.4
207-1258C	449.6-484.9	23.7	140.4	409.9	0.5	14.2	47.9
207-1261B	563.0-659.2	35.2	82.8	150.8	0.8	8.0	15.3

Table 7. Trends in borehole logs content in OAE sediment intervals in ODP holes.

Hole	Depth (mbsf)	Gr peak	U peak	RHOB decrease	NPHI increase	Sonic decrease
103-641C	150.9-202.6	Y	Y	Y	Y	N/A
159-959D	1024.0-1043.3	Y	Y	Y	Y	N/A
171B-1052 E	510.6-656.0	Y	N	N	N	Y
198-1207B	565.0-574.0	Y	Y	Y	Y	N/A
198-1213B	256.8-266.4	Y	Y	Y	Y	N/A
207-1258C	397.5-449.6	Y	Y	Y	Y	Y
207-1258C	449.6-484.9	Y	Y	Y	Y	Y
207-1261B	563.0-659.2	Y	Y	Y	Y	Y

Figure 5. Hole-159-959D gamma ray logs. The upper boundary of OAE 3 is indicated with the thick red line and the lower boundary is marked with a light green line.

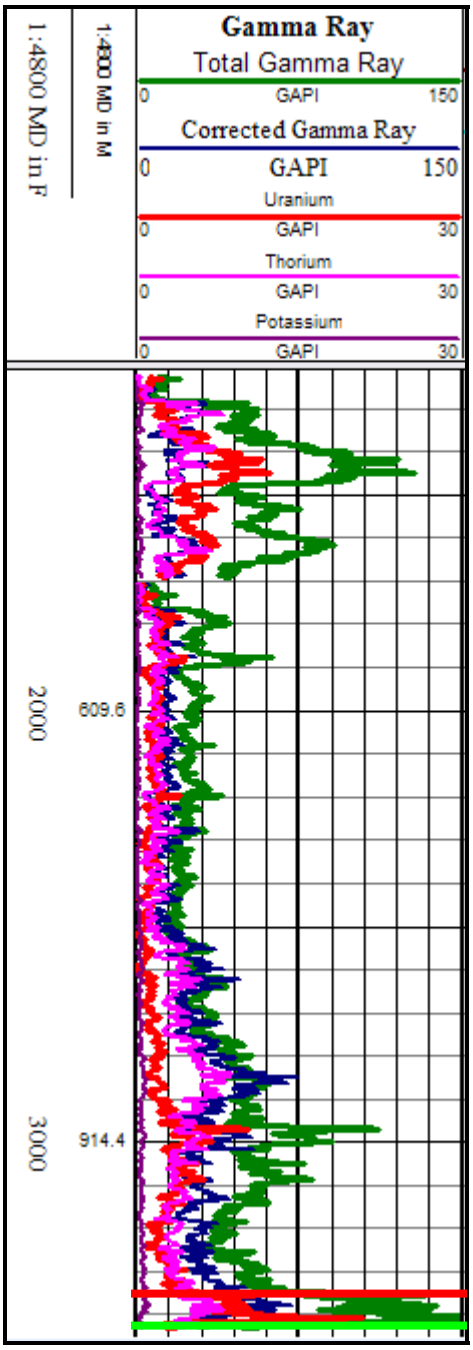

Logs were acquired from 373.8-1047.1 mbsf in Hole 159-959D (Appendix C). There are three instances where the gamma ray and uranium readings increase significantly as compared to the rest of the hole (Fig. 5). All three of these instances are related to increases in organic material within Lithologic Units 2 and 3. The average gamma ray reading for lithologies not

associated with deposition during OAE 3 is 41.0 GAPI units. This average includes lithologies with comparatively high organic matter within Lithologic Unit 2. The average gamma ray reading for 1024.0-1043.3 mbsf is 117.9 GAPI (Table 6). While all three lithologies with organic matter did show increases in gamma ray readings compared to the rest of the hole, the gamma ray is significantly higher through the sediments associated with deposition during OAE 3. The peak gamma ray reading for Hole 159-95D occurs in this interval at 207.1 GAPI. The average uranium reading for the hole is 2.9 GAPI. This average includes uranium measurements through non-OAE associated organic-rich lithologies. The average uranium reading for 1024.0-1043.3 mbsf is 9.7 GAPI units, with a peak of 12.4 GAPI units. There is a sustained slight decrease in bulk density and increase in neutron porosity through the Albian black claystone when compared to the rest of the hole. However, there are many instances of significantly lower density throughout the hole (Table 7).

Hole-171B-1052E is located east of the Florida-Georgia border on the Blake Nose. The Blake Nose is a salient on the eastern margin of the Blake Plateau and gently ramps down to the Blake Escarpment (Shipboard Scientific Party, 1998). It is located in 1345.2 m of water. Hole 171B-1052E was drilled without coring to 140.0 mbsf. As a result the uppermost unit at Site 1052, Pleistocene to Middle Eocene nannofossil ooze (0-~129 mbsf), was not recovered in Hole 171B-1052E The lithologic units described for Hole 171B-1052E begin with Subunit IIA and include (Appendix B): (1) Middle Eocene nannofossil chalk and foraminifer chalk with chert layers deposited with a dominance of pelagic sediment; (2) Middle-Early Eocene porcellanite calcareous claystone deposited with a dominance of pelagic sediment; (3) Late-Early Paleocene nannofossil claystone, calcareous claystone with chalk, and nannofossil, foraminifer, and calcareous chalk with clay deposited with a dominance of pelagic sediment; (4) Late Maastrichtian clayey nannofossil chalk and nannofossil chalk with clay deposited with a dominance of pelagic sediment; (5) Late Maastrichtian nannofossil chalk or nannofossil chalk with clay deposited with a dominance of pelagic sediment; (6) Cenomanian-Late Albian silty claystone and clayey siltstone with nannofossils deposited in a hemipelagic environment; (7) Late Albian laminated black shale, clayey limestone with foraminifer and quartz, and silty claystone deposited in a deepening upward environment during a global transgression event under dysoxic to anoxic conditions; and (8) Late Albian clayey siltstone, silty claystone, siltstone

with carbonate grains, bioclastic and lithic grainstone deposited in a shallow marine environment near the storm wave base (Norris, 1998).

The organic material in the black shale associated with deposition during OAE 1d is of terrestrial origin (Shipboard Scientific Party, 1998). However, it also includes some fish remains. This interval is also high in calcareous material and contains fine silt-sized quartz grains as well. The lithologies associated with OAE 1d have an upper boundary at 510.6 mbsf and a lower boundary at 656.0 mbsf for a thickness of 145.4 m. Through this interval the amount of organic carbon present fluctuates from 0.18%-0.20 % of the black shale (Table 5). It should be noted that of all the segments containing OAE associated lithologies in the ODP holes, it is only in Hole 171B-1052E that the organic carbon content doest not exceed 1% of the weight of the rock.

Figure 6. Hole 171B-1052E gamma ray, density, neutron porosity and sonic log responses. Horizontal red line marks the upper boundary of the Late Albian black shale sequence. This lithology extends below the logged interval.

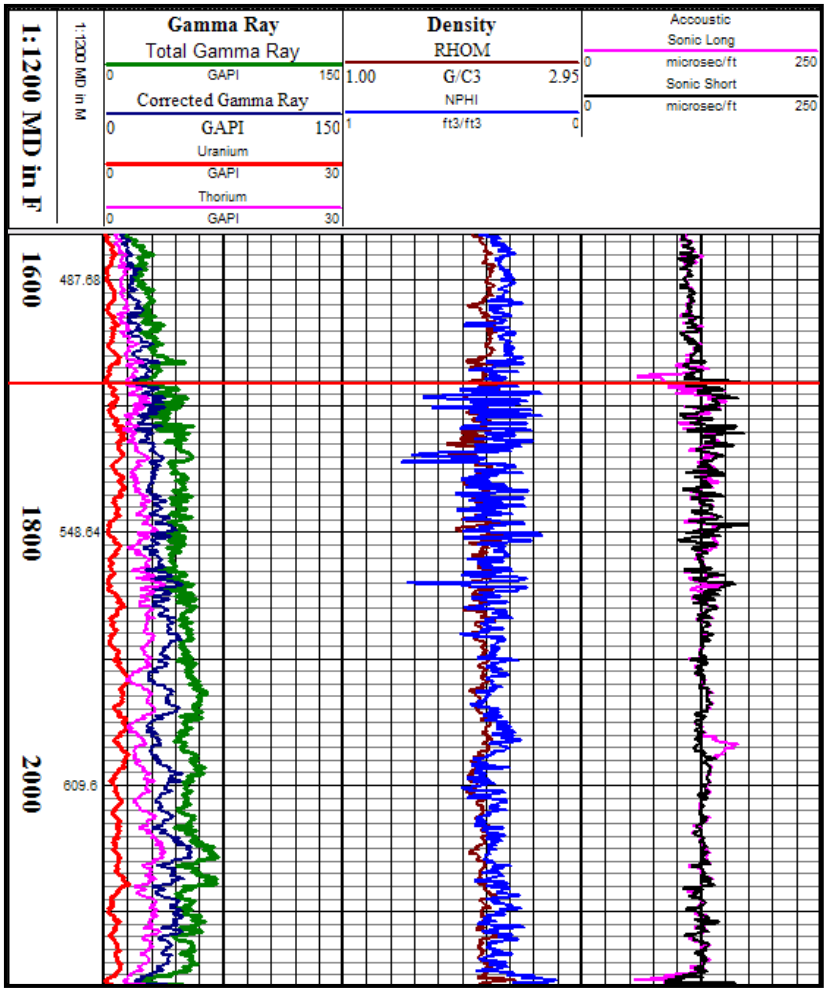

The total gamma ray peaks in the black shale at 71.7 GAPI with an average of 50.5 GAPI (Fig. 6) (Appendix C). This average is higher than the total gamma ray average of 23.7 GAPI for the hole. The total gamma ray is higher than the corrected gamma ray value throughout the black shale, but not as dramatically as is seen in other OAE segments of ODP logs. Elevated thorium levels are present throughout the black shale as well. The uranium reading through the black shale has an average of 1.8 GAPI, which is closely matched by the average uranium reading for the total well of 1.2 GAPI. The peak uranium reading through this interval is 3.2 GAPI (Table 6). The average bulk density through the black shale is not low compared to the rest of Hole 171B-1052E. However, this interval shows considerable variation between the peaks and lows of bulk density readings through this interval when compared to the rest of the logged interval. Similarly, the neutron porosity does not show as more porous compared to the rest of the logged interval, but does show a greater range in readings through the black shale interval than are seen elsewhere in the hole. The sonic log shows mildly slower velocities through this interval (Table 7).

Hole 198-1207B is in 3100.8 m of water located near the most elevated central part of the Northern High of Shatsky Rise in the northern Pacific Ocean (Bralower, 2002). Hole 198-1207B was drilled without coring to 157.0 mbsf. Three lithologic units were identified at Site 1207 (Appendix B). Lithologic Unit 1 is Holocene-Middle Miocene nannofossil ooze, nannofossil ooze with diatoms, clayey nannofossil ooze mostly deposited under oxic conditions, often dominated by glacial-interglacial cycles. A manganese crust near the bottom of the unit indicates episodic or long-term exposure of the seafloor capping the Cretaceous sediments. Lithologic Unit 2 includes Campanian-Turonian nannofossil ooze and chalk interbedded with chert or chert nodules. These sediments are dominantly pelagic in origin and are characterized by deposition from slumping and erosion from bottom currents sweeping over the rise. Lithologic Unit 3 is Cenomanian-Barremian nannofossil limestone and chert. Within this unit there is a 45 cm layer of organic carbon rich mudstone. Lithologic Unit 3 shows signs of being frequently swept by bottom currents during its formation (Shipboard Scientific Party, 2002a).

Within the nine meters of alternating lithologies associated with OAE 1a is a 45 cm layer of organic-rich black shale. The amount of organic carbon (C_{org}) measured within this interval ranges from 1.7 % to 34.0 %. The organic material is composed of marine algae and bacteria

(Shipboard Scientific Party, 2002a). The upper boundary of this unit as seen in the logs is at 565.0 mbsf and the lower boundary is at 574.0 mbsf (Table 5).

There are two spikes in the total gamma ray for Hole 198-1207B (Fig. 7; Appendix C). The first spike is at 163.7 mbsf and has matching spikes in corrected gamma ray and thorium. This first spike is a normal clay mineral-rich nannofossil ooze. The second spike coincides with the organic-rich mudstone. The average total gamma ray reading through this interval is 19.3 GAPI, with a peak reading of 83.0 GAPI. The average total gamma ray reading through the hole is 10.4 GAPI, including the first spike in the total gamma ray. The corrected gamma ray through the second total gamma ray spike only reaches a peak of 31.8 GAPI. The thorium increases significantly less through this interval as compared with the thorium increase seen at the first spike in total gamma ray. The average uranium reading through the mudstone associated with OAE 1a is 1.1 GAPI with a peak of 6.4 GAPI (Table 6). While the bulk density is not at the lowest measurements seen through the hole at the organic-rich black shale, there is a definite decrease in density readings correlating with the spike in total gamma ray. There is also an increase in neutron porosity at the spike in total gamma ray; however, these values are not the most porous seen in the hole (Table 7).

Hole 198-1213B also is located in the northern Pacific Ocean on the Shatsky Rise. This hole is on the southern flank of the Southern High, and is in 3883.0 m of water (Shipboard Scientific Party, 2002b). Like Hole 198-1207B, the sediments at Site 1213 were deposited in a pelagic environment. There are four lithologic units described at Site 1213 (Appendix B): (1) Holocene-Early Pliocene nannofossil ooze with clay that is interbedded in cycles with clayey nannofossil ooze; (2) Santonian-Cenomanian nannofossil ooze pale orange in color and a red chert; (3) Early Cenomanian-Berriasian chert, limestone, and porcellanite; and (4) an undated sequence of at least three diabase sills (Shipboard Scientific Party, 2002b). Hole 198-1213B was drilled without coring to 189.7 mbsf, the uppermost part of Lithologic Unit 3.

Oceanic anoxic event 1a has an upper boundary of 256.8 mbsf and a lower boundary of 266.4 mbsf for a thickness of 9.6 m. Within this interval the C_{org} ranges from 2.87% to 25.17%. The OAE 1a interval occurs within the clayey porcellanite subunit of Lithologic Unit 3 (Table 5). Unlike the comparable unit associated with OAE 1a in Hole 198-1207B, this interval at Site 1213 is heavily bioturbated. The organic material in these sediments is of algal and bacterial origin (Shipboard Scientific Party, 2002b).

Figure 7. Hole 198-1207B; gamma ray, density and neutron porosity log responses. A thick red line indicates the upper boundary of sediments associated with OAE 1a. A thick light green line indicates the lower boundary of sediments associated with OAE 1a.

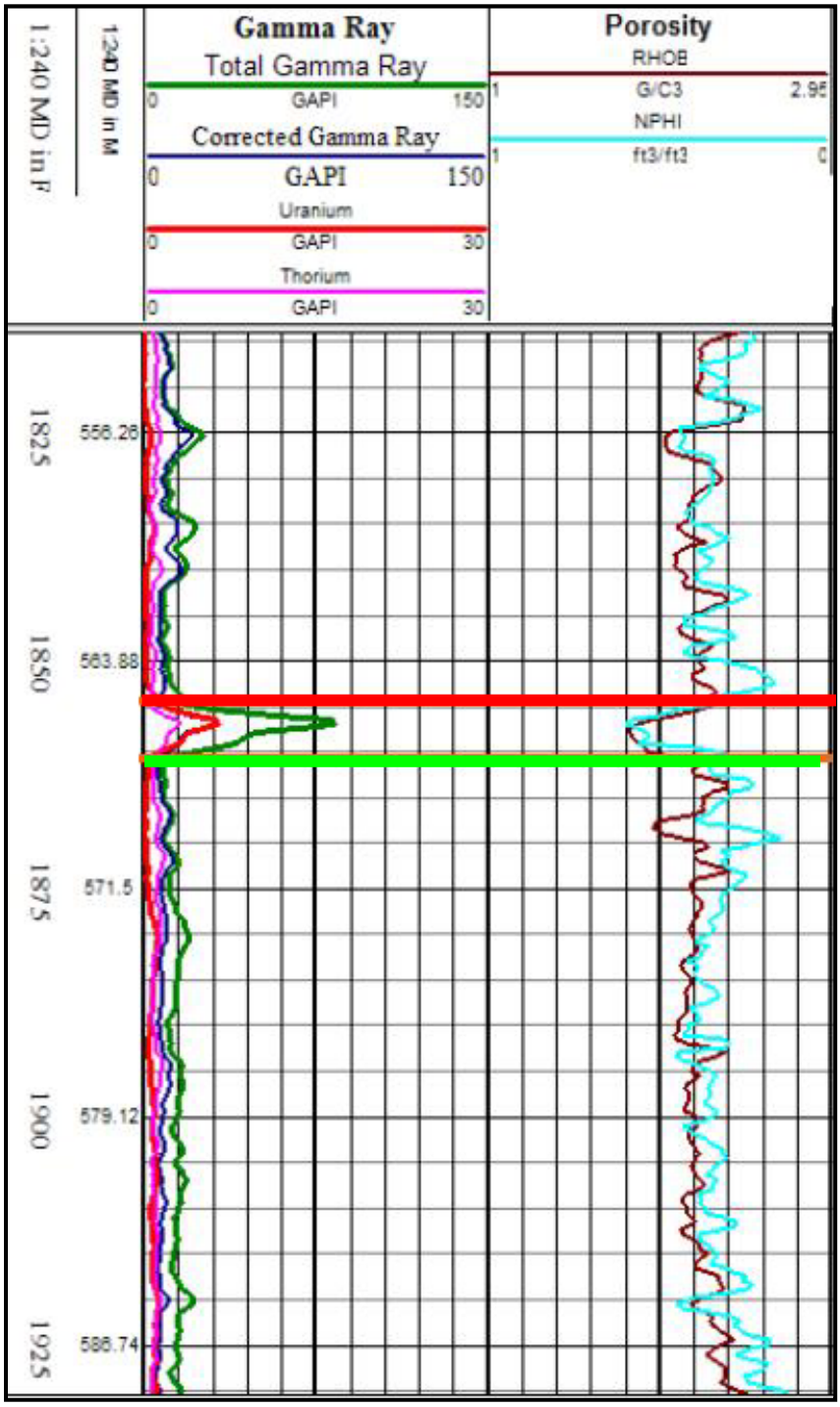

The only peak in gamma radiation for Hole 198-1213B is between 256.8 and 266.4 mbsf. The peak is in both total gamma ray and uranium. The average total gamma ray through lithologies not associated with OAE 1a is 11.0 GAPI. The average through the organic-rich interval is 33.7 GAPI with a peak of 79.3 GAPI. The average uranium value for the logged interval not associated with OAE 1a is 0.3 GAPI. The average uranium value through the lithology associated with OAE 1a is 1.5 GAPI, with a peak of 5.1 GAPI (Table 6). The density values through this interval are not the lowest in the total logged interval, but do display a localized decrease coinciding with the largest peak in total gamma ray. Additionally, there is a localized increase in neutron porosity at the peak in total gamma ray (Table 7).

Hole 207-1258C is located ~380 km north of Suriname in 3192.2 m of water on the western slope of Demerara Rise (Shipboard Scientific Party, 2004a). Five lithologic units were identified in this hole (Appendix B): (1) Middle Miocene-Early Oligocene nannofossil ooze with foraminifers of pelagic origin; (2) Middle Eocene-Maastrichtian nannofossil chalk with foraminifers and calcareous chalk with foraminifers of pelagic origin; (3) Campanian-age calcareous nannofossil clay; (4) Turonian-Middle Late Albian black shale, chalk and limestone that is finely laminated and gives off a strong petroliferous odor; and (5) Early Albian phosphatic calcareous claystone with organic matter associated with synrift deposition in a sheltered shallow marine environment with occasional tempestites (Shipboard Scientific Party, 2004a).

Both Lithologic Units 4 and 5 have abundant organic material. Lithologic Unit 4 is associated with OAE 2. It is 52.1 m thick and has an upper boundary of 397.5 mbsf and a lower boundary of 449.6 mbsf. The organic material in this interval has Type II kerogen, indicative of marine origin (Shipboard Scientific Party, 2004a). It also has abundant fish scales and bone fragments throughout. The C_{org} content ranges from 2.62% to 16.64 %. Lithologic Unit 5 is suggested to be associated with OAE 1d; however, there are insufficient biomarkers to make this association conclusively. The upper boundary for this interval is 449.6 mbsf and the lower boundary is 481.9 mbsf for a thickness of 35.3 m. The lower boundary is beyond the base of the logged interval. The organic carbon content ranges from 1.88% to 36.63% and the organic material is of marine origin (Table 5).

The average total gamma ray reading for lithologies not associated with an OAE in Hole 207-1258C is 23.7 GAPI. This includes several shalely intervals throughout the total logged interval. The average uranium reading not associated with deposition during an OAE is 0.5

GAPI. The average total gamma ray reading through the lithologies associated with OAE 2 is 85.7 GAPI, with a peak of 220.2 GAPI. The average uranium reading associated with OAE 2 is 8.84 GAPI, with a peak of 25.4 GAPI (Table 6). Whereas there are several intervals with bulk density readings lower than those associated with an OAE, the values seen through OAE 2 are considerably lower than the density of most lithologies in the hole. The average gamma ray reading through the lithologies associated with what is potentially part of OAE 1d is 140.4 GAPI, with a peak of 409.9 GAPI. The average through available uranium logs for this interval is 14.2 GAPI, with a peak of 47.9 GAPI (Table 6). The bulk density values through what is potentially OAE 1d are the lowest seen in the hole. Through this same interval the neutron porosity values are the highest that are seen in the hole (Table 7). The sonic log shows a mild decrease in velocity through both OAE segments.

Hole 207-1261B also is located on Demerara Rise. It is on the northwest slope of the rise in 1899.7 m of water. This hole has five lithologic units that differ from the five units at Hole 207-1258C. The units are (Appendix B): (1) Pleistocene-Late Miocene nannofossil ooze, nannofossil clay, and clayey nannofossil ooze of pelagic origin in an open marine environment; (2) Middle Eocene-Early Eocene calcareous chalk, nannofossil chalk and limestone of pelagic origin in an open marine environment; (3) Late Paleocene-Late Campanian nannofossil chalk with clay and claystone with nannofossils that is low in organic carbon and is of pelagic origin in an open marine environment; (4) Santonian-Late Cenomanian calcareous claystone with organic matter, clayey chalk with nannofossils, and clayey limestone of shallow marine origin; and (5) Albian or younger quartz sandstone whose subangular grains indicate a high energy, near shore depositional environment (Shipboard Scientific Party, 2004b).

The 96.2 m organic-material-rich interval in Lithologic Unit 4 is associated with OAE 2 (Shipboard Scientific Party, 2004b). It has an upper boundary of 563.0 mbsf and a lower boundary of 659.2 mbsf. The organic carbon content ranges from 7.76% to 16.09% of the total rock. The organic material is of marine origin and consists primarily of algal material (Shipboard Scientific Party, 2004b) (Table 5).

The average total gamma ray reading through lithologies not associated with OAE 2 is 35.2 GAPI (Fig. 8; Appendix C). The average through the claystone with organic matter is 82.8 GAPI, with a peak of 150.8 GAPI. The average uranium reading through lithologies not associated with OAE 2 is 0.8 GAPI. The average associated with OAE 2 is 8.0 GAPI, with a

peak of 15.3 GAPI (Table 6). Compared to the immediately surrounding lithologies, bulk density and sonic logs are consistently lower, and neutron porosity higher, through the interval associated with OAE 2 (Table 7).

Figure 8. Hole 207-1261B gamma ray, density, neutron porosity and sonic log responses. Red horizontal line marks the upper boundary of lithologies associated with OAE 2. This interval continues deeper than the available borehole logs.

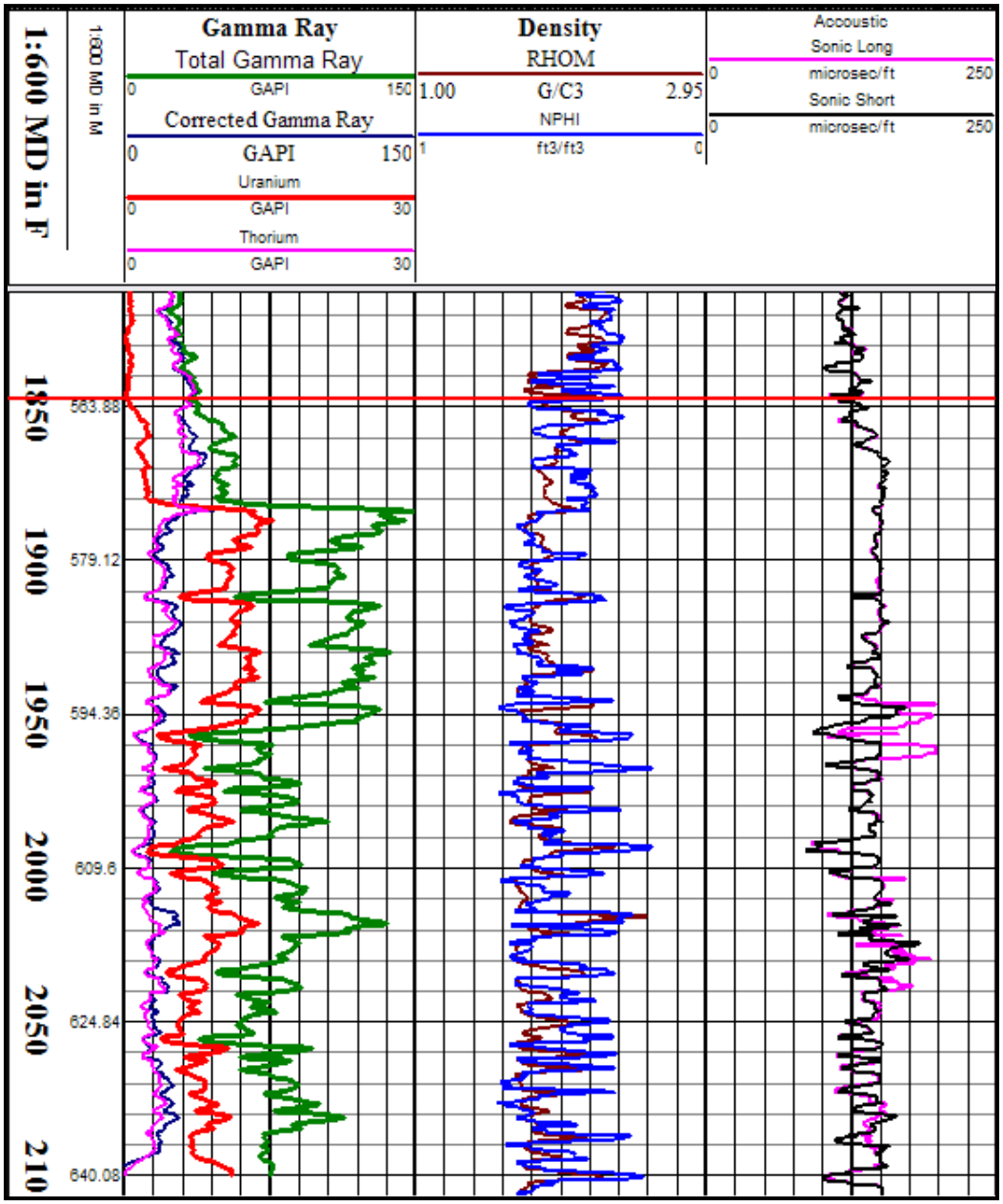

Organic Carbon Data and Gamma Ray Logs

Visual inspection of the logs and organic carbon data show a general trend of increased total gamma ray and uranium gamma ray readings in areas rich in organic material (Fig. 9). In order to better understand the relationship between gamma ray response and the organic content, the gamma ray value for each organic carbon datum was plotted against the weight percent of the organic carbon for core samples from all of the ODP holes in this study. Table 8 lists the range and mean organic carbon content for ODP holes.

Table 8. Organic carbon content through OAE intervals in ODP wells.

Hole	Depth (mbsf)	Mean C_{org} through OAE (%)	Corg Range (%)
103-641C	150.9-202.6	2.26	0.22-19.74
159-959D	1024.0-1043.3	3.14	0.09-7.19
171B-1052 E	510.6-656.0	0.52	0.00-0.91
198-1207B	565.0-574.0	N/A	N/A
198-1213B	256.8 -266.4	12.76	2.87-25.17
207-1258C	397.5-449.6	9.05	2.62-16.64
207-1258C	449.6-484.9	6.43	1.88-36.63
207-1261B	563.0-659.2	10.5	7.76-16.09

Figure 9. Hole 207-1258C. Close up of gamma ray logs and C_{org} (wt%) in sediments deposited during OAE 2 and 1d.

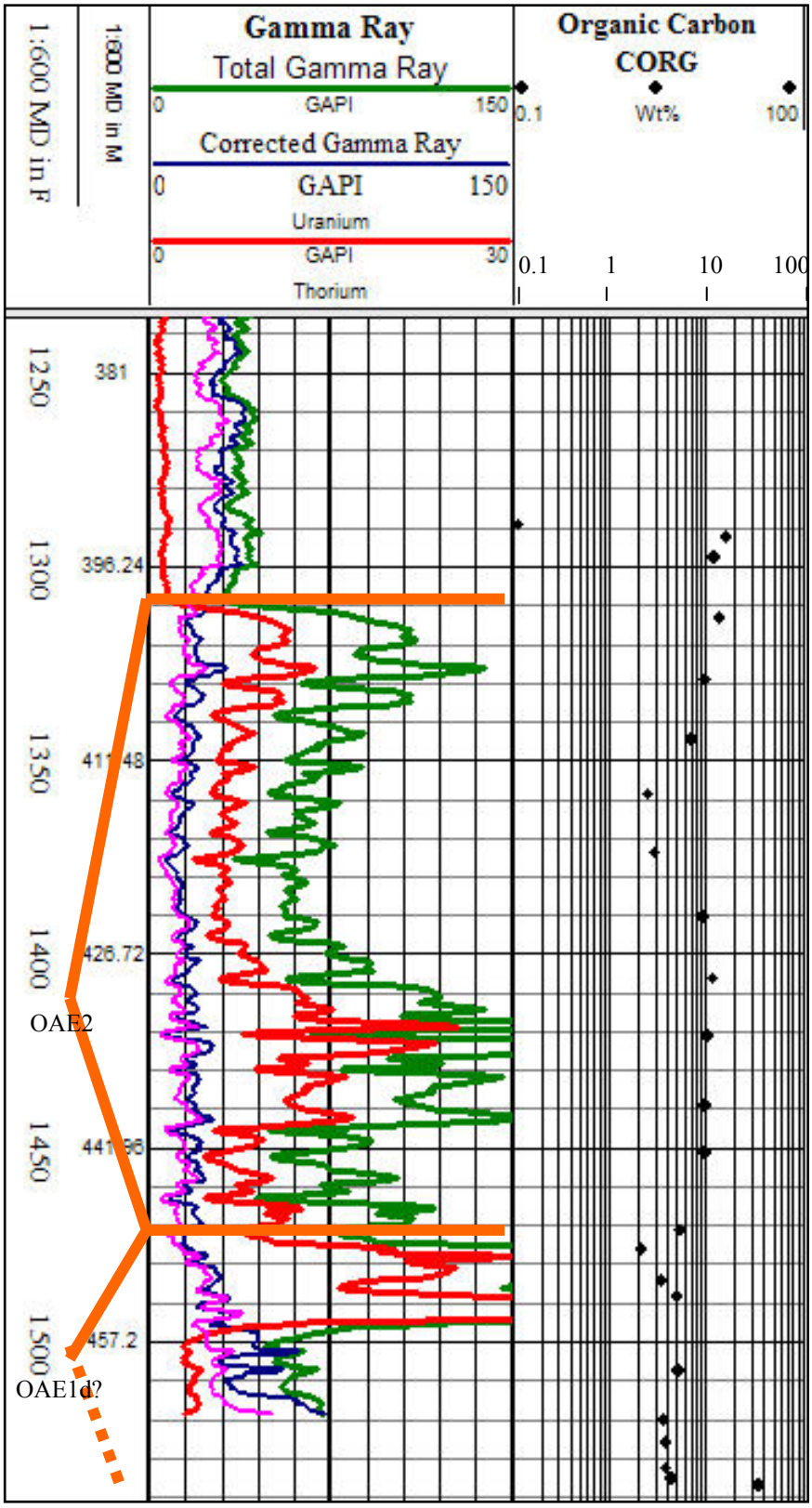

A correlation between organic carbon content and total gamma ray response is lacking (Fig. 10). The plot of Corg and total gamma ray is characterized by a concentration of points with Corg less than 2% and gamma ray values from near zero to 90 GAPI. At organic carbon contents greater than 2% there are fewer and more widely scattered data. Although there appears to be a general trend of increasing gamma readings with increasing organic content, the R^2 value is only 0.2. Outlying points fit into two categories. First are points with gamma ray readings greater than 200 GAPI but less than 6% C_{org}. Second are points with greater than 10% C_{org} and total gamma readings less than 100 GAPI. All data points fitting these two sets of outlying point categories were checked to ascertain their validity. Only one point was found to be questionable, as a result of core disturbance and was removed from the data set.

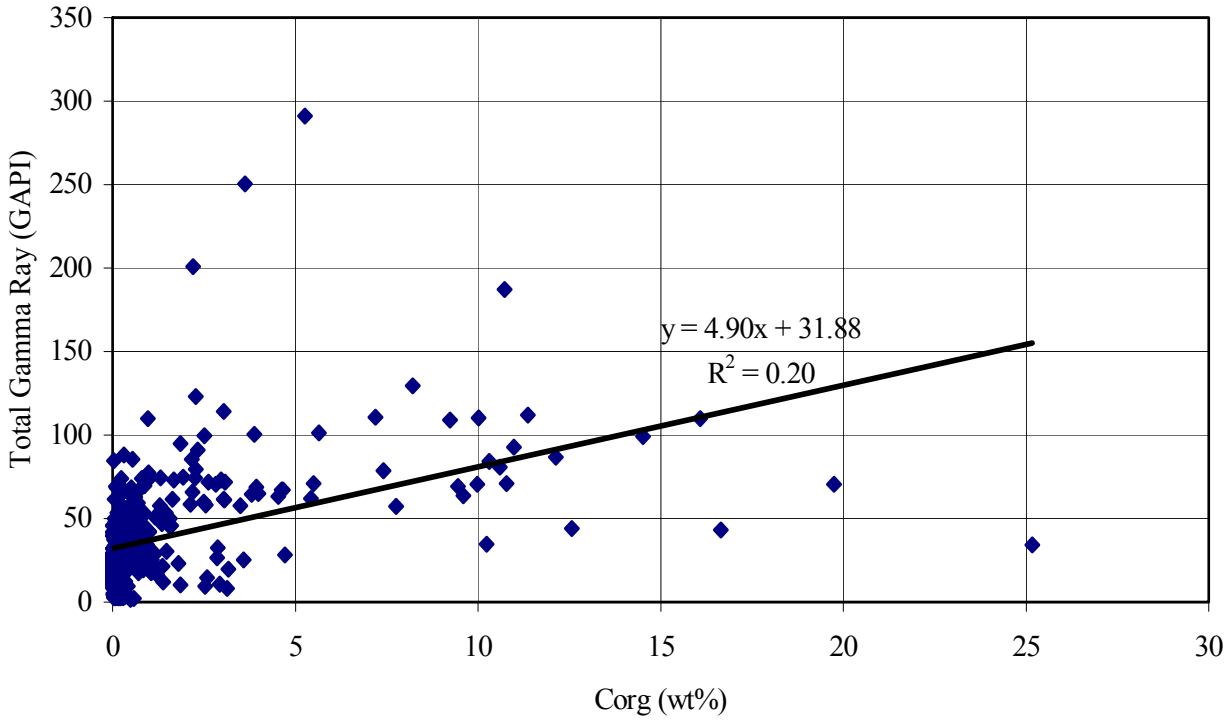

Figure 10. Total gamma ray versus organic carbon for all ODP holes used in the study.

Because uranium binds to organic matter a relationship between C_{org} and uranium was expected (Bassiouni, 1994 and Schlumberger, 1972). There does appear to be a general trend between Corg and uranium (Fig. 11). The R^2 value for C_{org} and uranium is 0.25, which is higher than for the plot of C_{org} and total gamma ray; however, the correlation is weak. The plot of C_{org} and uranium is characterized by a concentration of points with C_{org} less than 2% and uranium less than 3 GAPI. At organic carbon contents greater than 2% there are fewer and more widely scattered data. Again, there are two categories of outlying points. First are points with uranium

gamma ray readings greater than 15 GAPI and less than 6% $C_{org.}$ Second there are points with C_{org} greater than 7% and uranium gamma ray readings less than 10 GAPI. All data points fitting these two sets of outlying point categories were checked to ascertain their validity. Again, only one point was found to be questionable and was removed from the data set. This point was the same data point removed from the plot of C_{org} and total gamma ray.

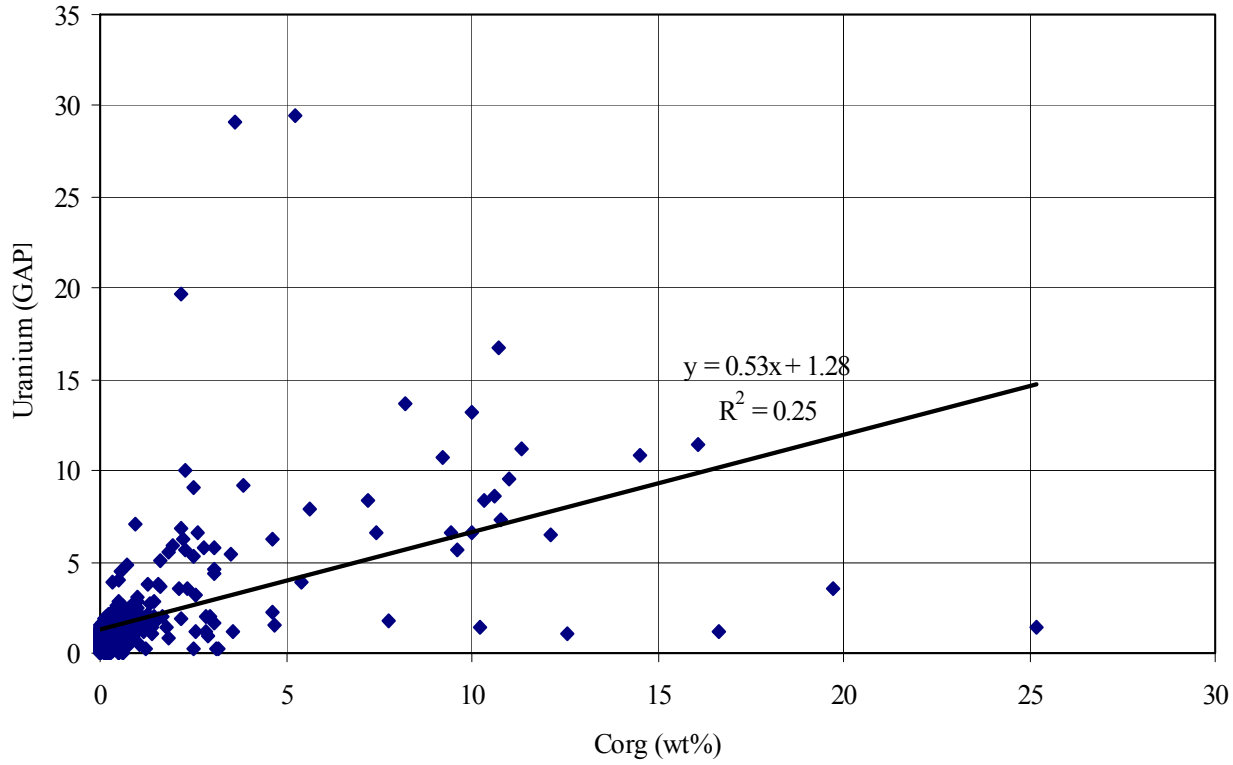

Figure 11. Uranium gamma ray versus organic carbon.

In another attempt to examine the relationship between organic content and gamma ray response, the total gamma ray values were plotted against the uranium gamma values (Fig. 12). While the gamma ray data points used in Figures 10 and 11 were averaged to make point-to-point comparisons with the organic carbon data, all total gamma and uranium gamma ray readings were used in the creation of the plot in Figures 12a and 12b. These plots show distinct differences between sediments deposited during OAEs and those sediments deposited during non-OAE intervals. The non-OAE lithologies have a maximum uranium reading of 13 GAPI and do not exceed 150 GAPI in total gamma ray values. Lithologies deposited during an OAE have uranium values that can exceed 40 GAPI and nearly a third of the total gamma ray readings are of values greater than 150 GAPI. There were two general groupings of data points within that apply to both OAE sediments and non-OAE sediments. Firstly, there is a steeply sloping

group of data points with uranium values less than 3 GAPI. The second group is largely limited to sediments deposited during OAEs. This group runs up the middle of the plot with increasing total gamma ray values correlating with increasing uranium values.

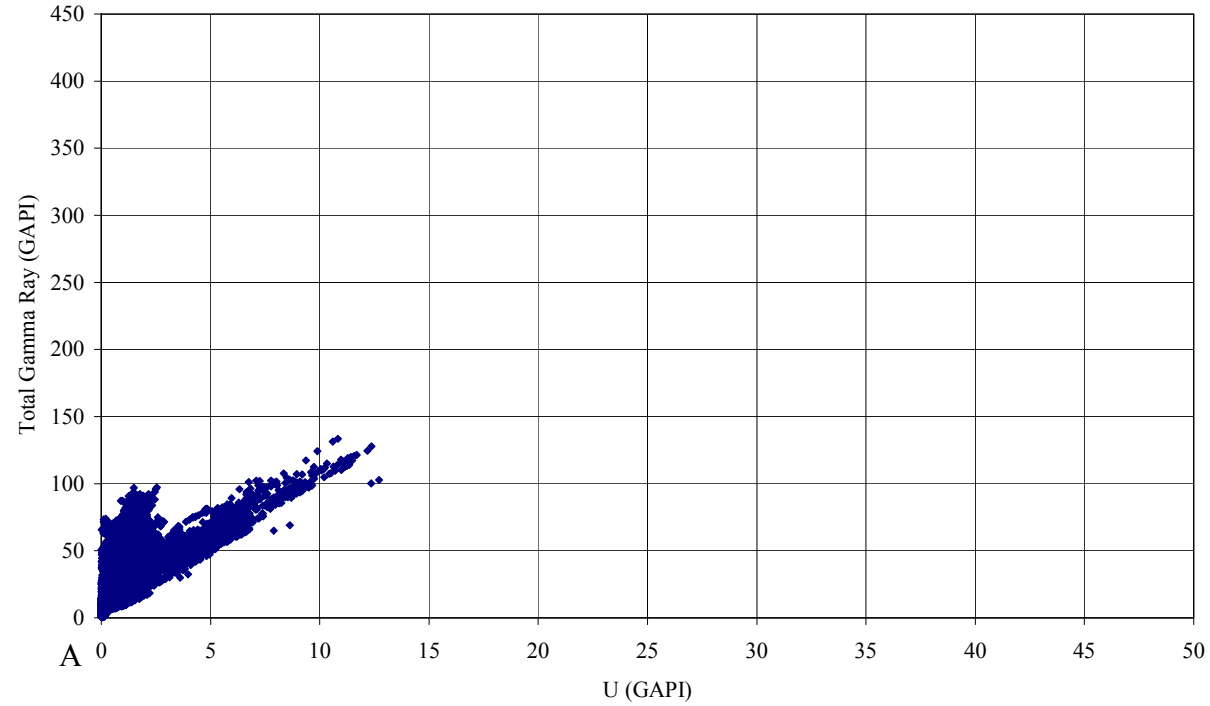

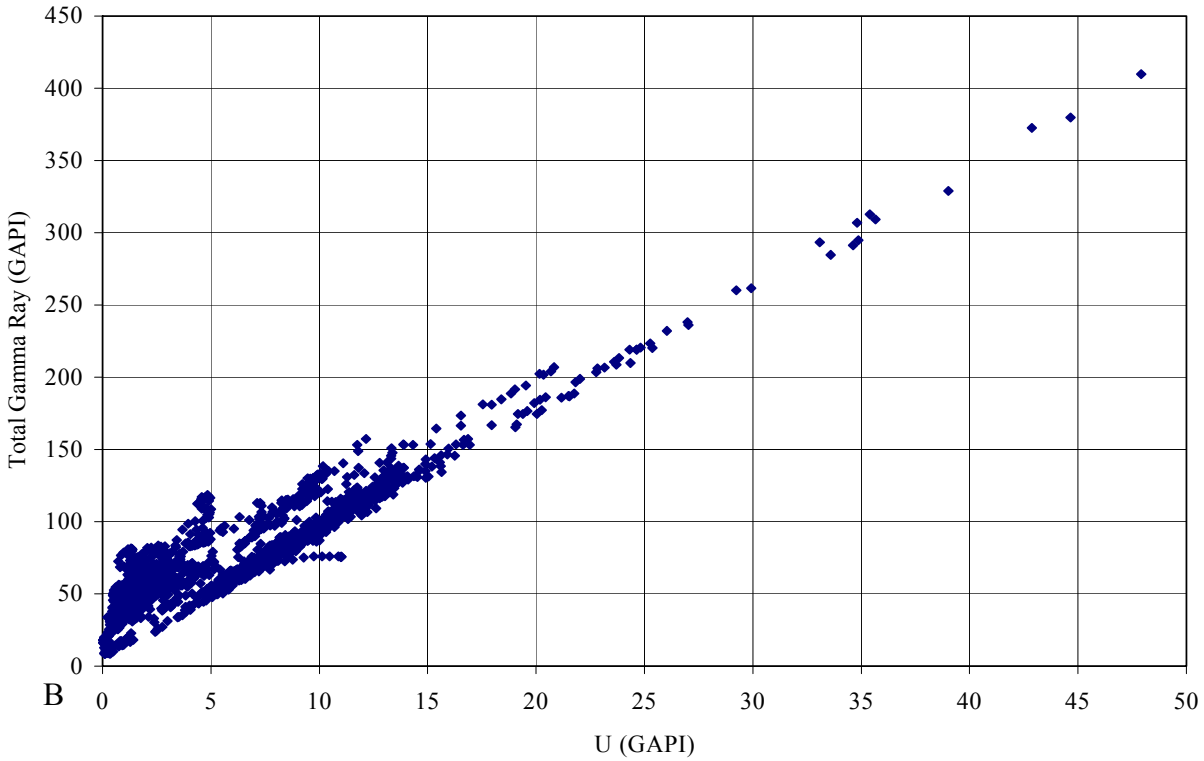

Figure 12. (a) Total gamma ray versus uranium through lithologies not associated with deposition during an OAE. (b) Total gamma ray versus uranium through lithologies deposited during an OAE.

Gulf of Mexico Wells

The sediments penetrated by the Gulf of Mexico wells have a fairly similar depositional history because of their close proximity to one another. The wells are located in the northern part of the Gulf of Mexico, just east of the mouth of the Mississippi River. The oldest sediment in any of the Gulf of Mexico wells is Late Jurassic. This age roughly coincides with the formation of the first true oceanic crust within the basin as the Yucatan block separated from the North American block and moved southward (Gore, 1992; Darnell, 1990). By this time the Louann Salts already had been deposited and the basin had become a relatively stable province. The deeper central Gulf of Mexico continued to undergo subsidence. During the Cretaceous, the rim of the Gulf of Mexico was dominated by the deposition of carbonates and evaporates (Gore, 1992; Darnell, 1990). Following the Cretaceous, deposition in the northern part of the Gulf of Mexico switched to prograding clastic wedges. Deposition at the site of the Gulf of Mexico wells used in this study currently is dominated by sediment provided by the Mississippi River.

Well 177244005200 is located in Main Pass Block 264. It is approximately 61.5 km southeast of New Orleans (Fig. 3). Dated rocks range from Pliocene to Albian in age (Appendix F). There is one interval that is possibly associated with deposition during an OAE (Appendix E). It ranges from Santonian to Cenomanian in age and is composed of black shale (Table 9). This interval shows a moderate increase in gamma ray readings. The mean gamma ray reading through sediments not associated with deposition during an OAE is 51.5 GAPI. The mean for non-OAE sediments includes several shaley intervals younger than Cretaceous age. The mean gamma ray reading through this interval is 55.3 GAPI. The peak through this interval is 70.6 GAPI (Tables 10 and 11). The black shale potentially associated with deposition during an OAE shows only a very slight decrease in density compared to the immediately surrounding lithologies. There is a marginal increase in neutron porosity for this interval (Appendix G).

Table 9. Lithology and age of Gulf of Mexico wells containing OAE intervals. See Figure 3 for the location of the wells.

Well	Block	Dominant lithology	Age	Age of OAE interval	OAE lithology
177244005200	Main Pass 264	sands, shales, limestone, chalk	Pliocene to Albian	Santonian to Cenomanian	black shale
177244005400	Main Pass 253	chalk, limestone, occasional shale or sandstone	Late Paleocene to Aptian	Albian to Aptian	dark gray to black limestone
177244006300	Main Pass 222	shales, sandstone, limestone	Early Pliocene to Albian	Cenomanian to Albian (2 intervals)	dark gray shale, calcareous shale
608164003700	Vioska Knoll 30	limestone, shales	Late Oligocene to Albian	Turonian to Cenomanian	black calcareous shale, limestone
608224000600	Destin Dome 166	shale, sandstone, limestone, salt	Maastrichtian to Late Jurassic	Turonian to Cenomanian	sandy, limey shale (Tuscaloosa Fm.)
608224001400	Destin Dome 162	shale, limestone, anhydrite	Late Oligocene to Late Jurassic	Albian to Aptian (5 intervals)	shale, calcareous shale
608224001700	Destin Dome 529	siltstone, limestone	Middle Eocene to Late Jurassic	Albian to Aptian	limestone, shale, siltstone
608224002200	Destin Dome 284	shale, sandstone, limestone	Early Pliocene to Valanginian	Coniancian to Santonian (2 intervals)	black shale (Tuscaloosa Fm.)

Table 10. Mean gamma ray values for lithologies potentially deposited during OAEs and non-OAE lithologies.

Wells	Avg. Gr in non-OAE lithologies (GAPI)	Avg. Gr in OAE lithologies (GAPI)	Peak Gr in OAE lithologies (GAPI)
177244005200	55.3	51.5	70.6
177244005400	37.9	39.6	68.8
177244006300	34.1	63.0	83.8
608164003700	47.5	67.1	76.6
608224000600	49.2	55.9	67.5
608224001400	52.2	112.7	153.9
608224001700	35.2	62.6	94.1
608224002200	36.1	42.6	62.6

Table 11. Log response through lithologies potentially deposited during an OAE.

Well	Depth (mbsf)	Gr Peak	RHOB Decrease	NPHI Increase
177244005200	4402.8-4405.9	Y	Y	Y
177244005400	4434.8-4526.3	Y	Y	Y
177244006300	2970.3-2982.5	Y	Y	Y
	3314.7-3320.8	Y	Y	Y
608164003700	2802.6-2808.1	Y	Y	Y
608224000600	1489.6-1495.0	Y	N	N
608224001400	1384.7-1386.8	Y	Y	Y
	1937-1938.5	Y	Y	Y
	1981.5-1983.6	Y	N	N
	2066.8-2068.4	Y	N	N
	2810.6-2813.6	Y	N	N
608224001700	5251.7-5253.2	Y	Y	Y
	5363.0-5373.6	Y	Y	Y
	5643.4-5649.5	Y	Y	Y
	5669.3-5671.6	Y	Y	Y
	5681.2-5692.1	Y	Y	Y
	5730.2-5732.1	Y	Y	Y
	5752.5-5789.2	Y	Y	Y
608224002200	1883.7-1888.2	Y	N	N
	1917.2-1956.8	Y	Y	Y

Well 177244005400 is located in Main Pass Block 253. This block is approximately 75 km southeast of New Orleans (Fig. 3). The youngest rocks are Late Paleocene in age and the oldest are Aptian (Appendix F). There is one interval possibly associated with deposition during an OAE. It is in dark gray to black limestone and is Albian to Aptian in age (Table 9; Appendix E). This interval spans from an upper boundary at 4434.8 mbsf to a lower boundary at 4526.3 mbsf and shows a moderate increase in gamma ray compared to non-shaley intervals within the well. The mean gamma ray value for lithologies not associated with deposition during an OAE is 37.9 GAPI. The mean includes several shaley intervals younger than Cretaceous age. The mean gamma ray value for the black limestone potentially deposited during an OAE is 39.6 GAPI with a peak of 68.8 GAPI (Table 10). The bulk density decreases sharply at several points through this interval (Table 11). Decreases in density correlate with increases in neutron porosity (Appendix G).

Well 177244006300 is located in Main Pass Block 222. It is approximately 71.3 km southeast of New Orleans (Fig. 3). The dated rocks within this well range from Early Pliocene to Albian (Table 9; Appendix F). The mean gamma ray reading for lithologies not associated with deposition during an OAE is 34.1 GAPI. There are two intervals whose sediments were possibly deposited during OAEs (Appendix E). The mean gamma ray reading through these intervals is 63.0 GAPI with a peak of 83.8 GAPI (Table 10). The first is a Turonian- to Cenomanian-age calcareous shale that has an upper boundary of 2970.3 mbsf and a lower boundary of 2982.5 mbsf. There is a sharp decrease in density and a moderate increase in neutron porosity through this interval (Table 11; Fig. 13). The second section within the well potentially associated with deposition during an OAE is an Albian-age black, calcareous shale. The section of interest has an upper boundary of 3314.7 mbsf and a lower boundary of 3320.8 mbsf. There is a sharp decrease in density and an increase in neutron porosity through this interval.

Well 608164003700 is located in Vioska Knoll Block 30. This block is roughly 58.0 km east northeast of New Orleans. The youngest dated lithology is Late Oligocene in age and the oldest dated lithology is Albian in age (Appendix F). The mean gamma ray reading for lithologies not associated with deposition during an OAE is 47.5 GAPI. The mean value includes several shales with much higher gamma ray readings than those in the lithology potentially associated with deposition during an OAE. There is one interval possibly associated with deposition during an OAE (Appendix E). It is in black calcareous shale and limestone and

ranges in age from Turonian to Cenomanian (Table 9). The upper boundary for this interval is at 2802.6 mbsf and the lower boundary is at 2808.1 mbsf. The mean gamma ray value for this interval is 67.1 GAPI and the peak is 76.7 GAPI (Table 10). The increase in gamma ray values through this section is only slight. The decrease in density is moderate as is the increase in neutron porosity (Table 11).

Figure 13. Well 177244006300; gamma ray log, density and neutron porosity response through the total logged interval on the lefy and a detailed view through Turonian-Cenomanian-age calcareous shale potentially associated with OAE deposition on the right. The upper boundary of the section of interest is indicated with a red line and the lower boundary is indicated with a light green line.

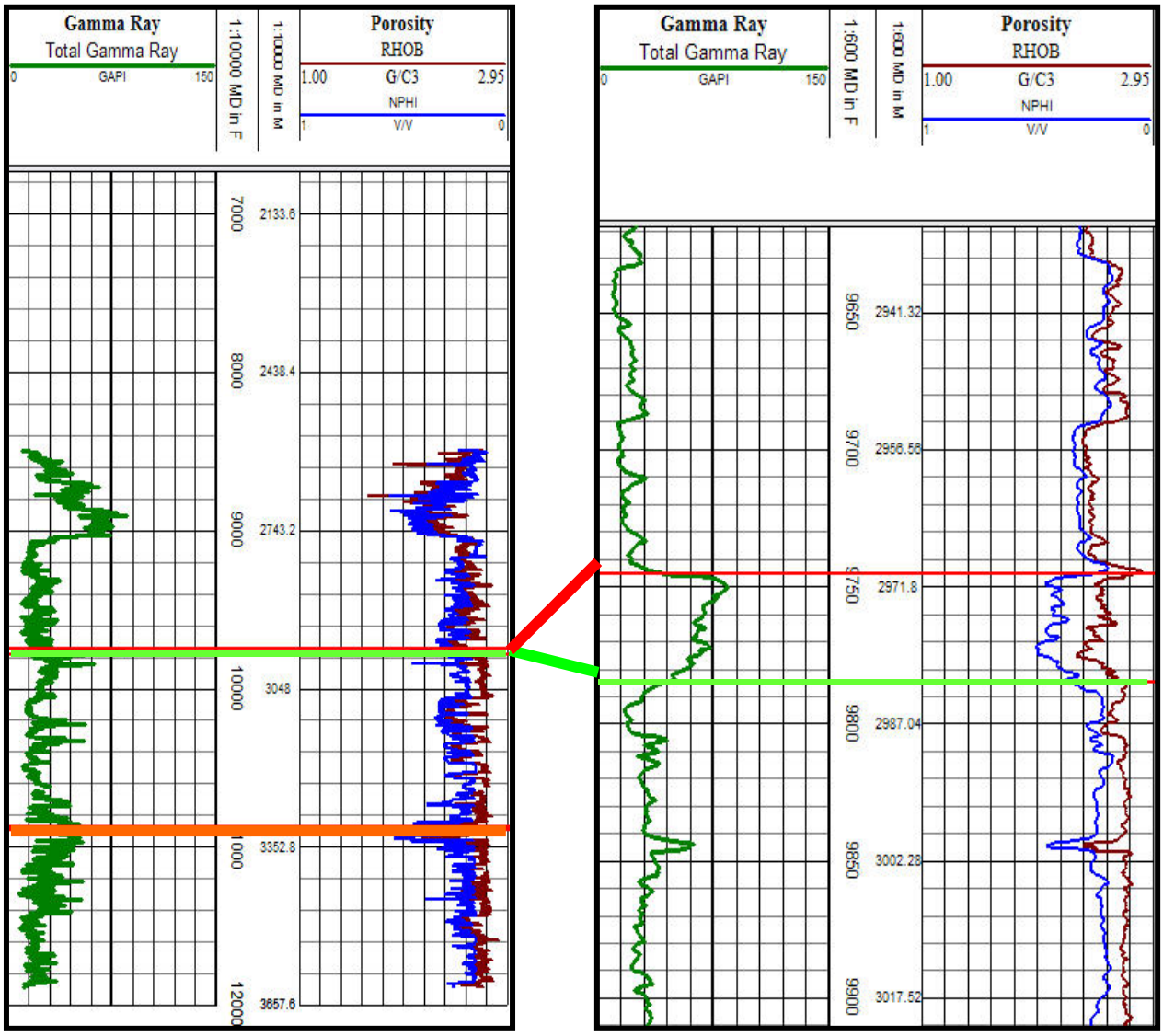

Well 608224000600 is located in Destin Dome Block 166 and is approximately 103.1 km east of New Orleans (Fig. 3). The youngest rocks dated within this well are Maastrichtian aged and the oldest are Jurassic aged (Appendix F). The mean gamma radiation for lithologies not associated with deposition during an OAE is 49.2 GAPI (Table 10). There is one possible interval associated with deposition during an OAE (Appendix E). Its upper boundary is at 1489.6 mbsf and its lower boundary is at 1495.0 mbsf. This interval is part of the Tuscaloosa Formation and is a sandy, limey shale of Turonian to Cenomanian age (Table 9). The gamma ray values show only a slight increase. There are many younger and older intervals in the well with considerably greater gamma ray values (Fig. 14). The mean gamma ray reading through this interval is 55.9 GAPI with a peak of 67.7 GAPI. The density values do not show a decrease through this interval, there is even a slight increase. Likewise, the neutron porosity does not increase through this interval and at times decreases (Table 11).

Figure 14. Well 608224000600; gamma ray log, density and neutron porosity response through the total logged interval and detail through Turonian-Cenomanian-age Tuscaloosa Formation shale potentially associated with OAE deposition. The upper boundary of the section of interest is indicated with a red line and the lower boundary is indicated with a light green line.

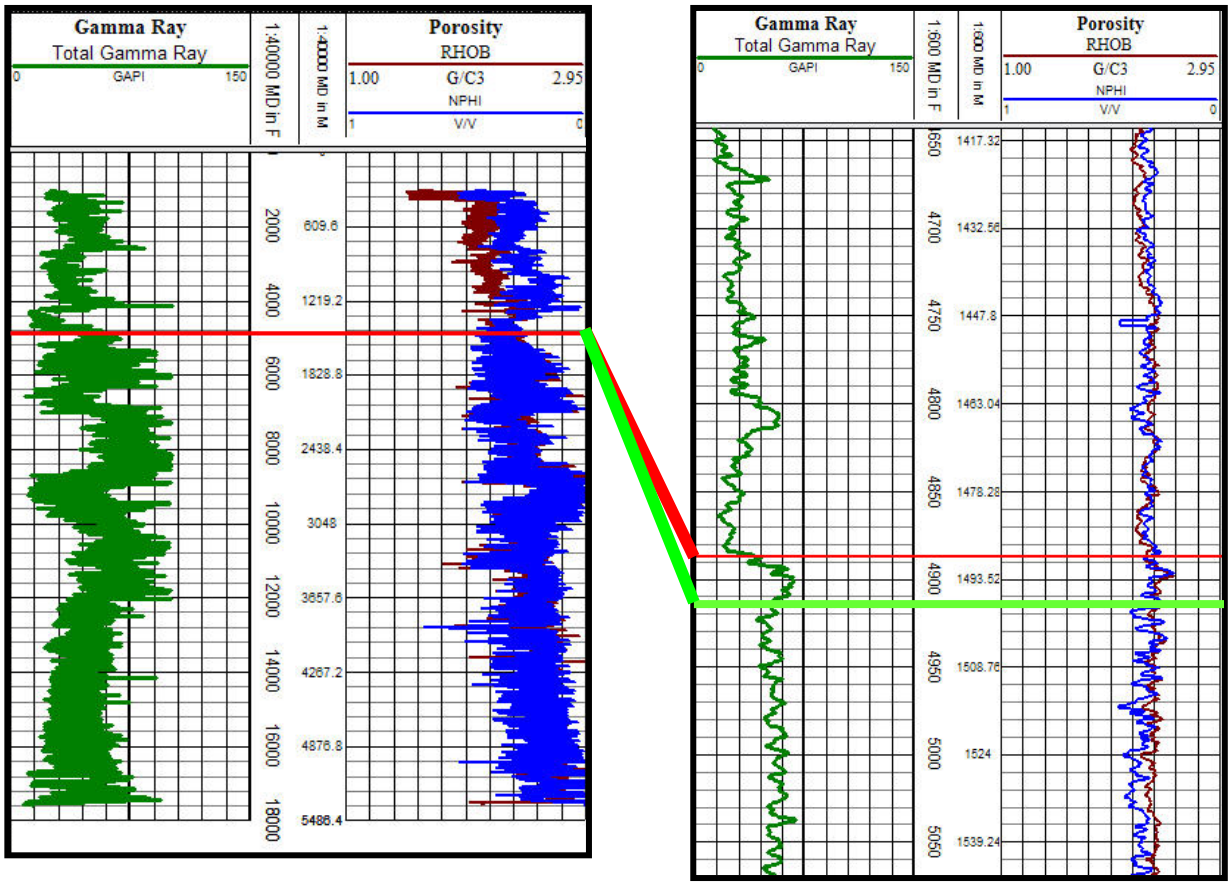

Well 608224001400 is in Destin Dome Block 162. This block is roughly 128.4 km east of New Orleans (Figure 3). The youngest dated lithology in the well is Late Oligocene in age and the oldest is Late Jurassic in age. The mean gamma ray value for lithologies not associated with deposition during an OAE is 52.2 GAPI (Table 10). This well has five intervals whose sediments were possibly deposited during an OAE. The mean gamma ray reading through these intervals is 112.7 GAPI with a peak of 153.9 GAPI. The depths and lithologies for these intervals are listed in Table 9. The intervals generally are composed of shales to calcareous shales and range in age from Albian to Aptian. The first two of these intervals show decreases in density and increases in neutron porosity (Table 11). The remaining three intervals do not show decreases in density or increases in porosity (Figs. 15 and 16; Appendix G).

Figure 15. Well 608224001400; gamma ray log, density and neutron porosity response through the total logged intervala and detail through Albian-age shale potentially associated with OAE deposition. The upper boundary of the section of interest is indicated with a red line and the lower boundary is indicated with a light green line.

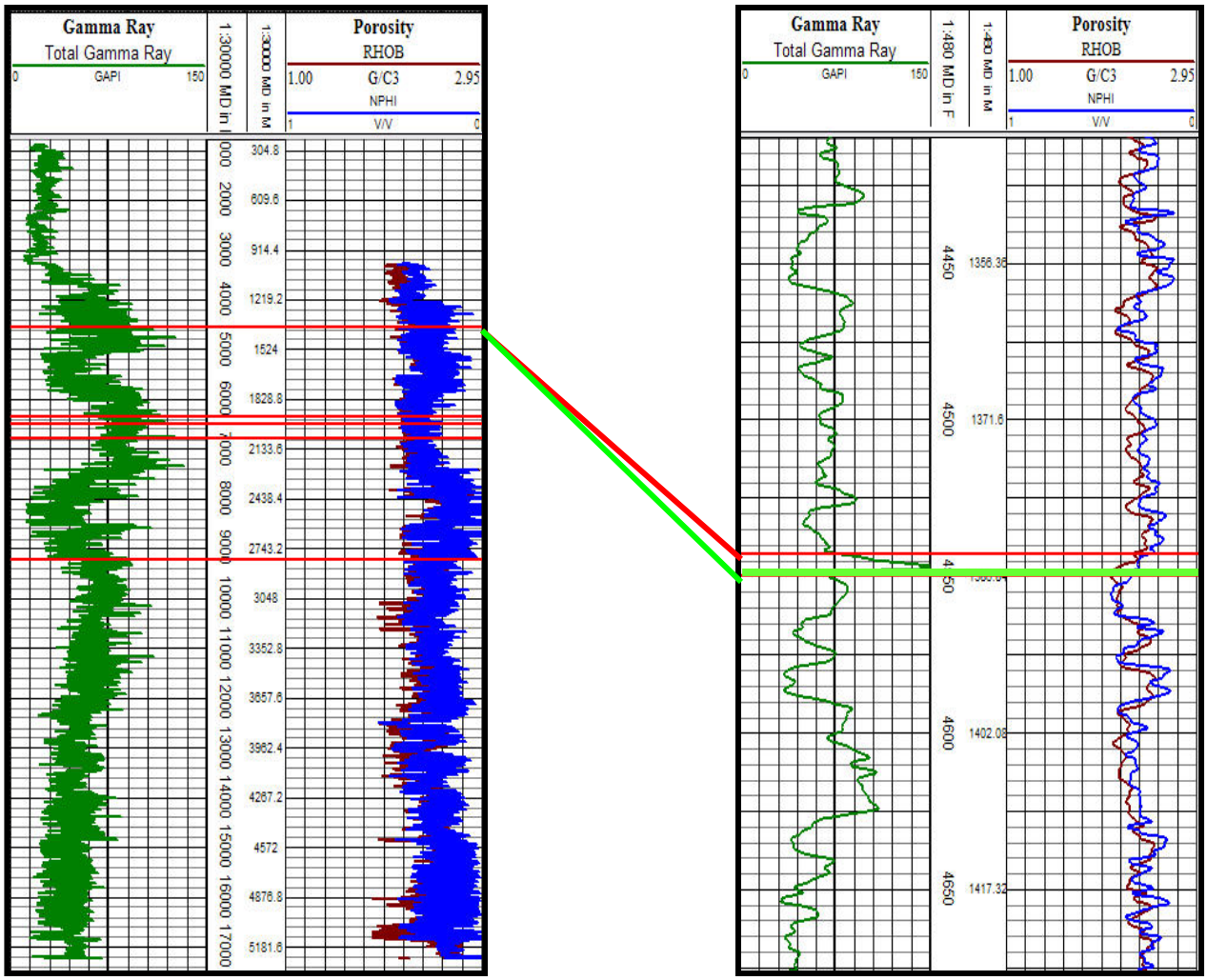

Figure 16. Well 608224001400; gamma ray log, density and neutron porosity response through total logged interval and detail through Aptian-age shale potentially associated with OAE deposition. The upper boundary of the section of interest is indicated with a red line and the lower boundary is indicated with a light green line.

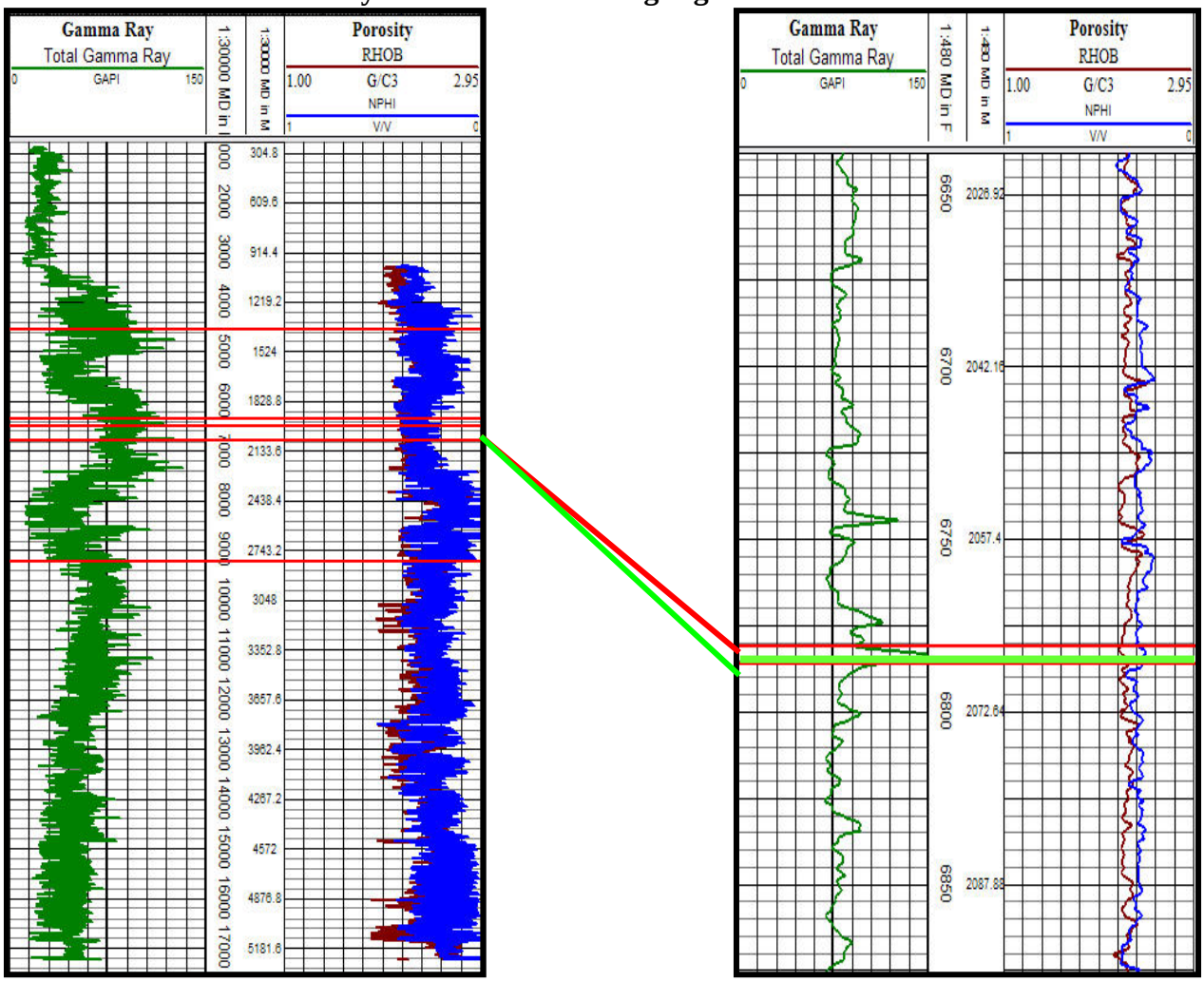

Well 608224001700 is in Deston Dome Block 529, which is located ~77.9 km southeast of New Orleans (Fig. 3). The dated rocks in the well range from Middle Eocene to Late Jurassic in age (Appendix F). The mean gamma ray value for lithologies not associated with potential deposition during an OAE is 35.2 GAPI. There are seven intervals that may be associated with deposition during an OAE (Appendix E). The mean gamma ray value through these intervals is 62.6 GAPI with a peak of 94.1 GAPI (Table 10). The lithologies for these intervals range from limestone to shale to siltstone and are Albian to Aptian in age (Table 9). The density decreases and the neutron porosity increases through each of these intervals (Table 11; Fig. 17; Appendix G).

Figure 17. Well 608224001700; gamma ray log, density and neutron porosity response through the total logged interval and detail through multiple Aptian-age limestones and siltstone potentially associated with OAE deposition. The upper boundaries of the sections of interest are indicated with red lines and the lower boundaries are indicated with light green lines.

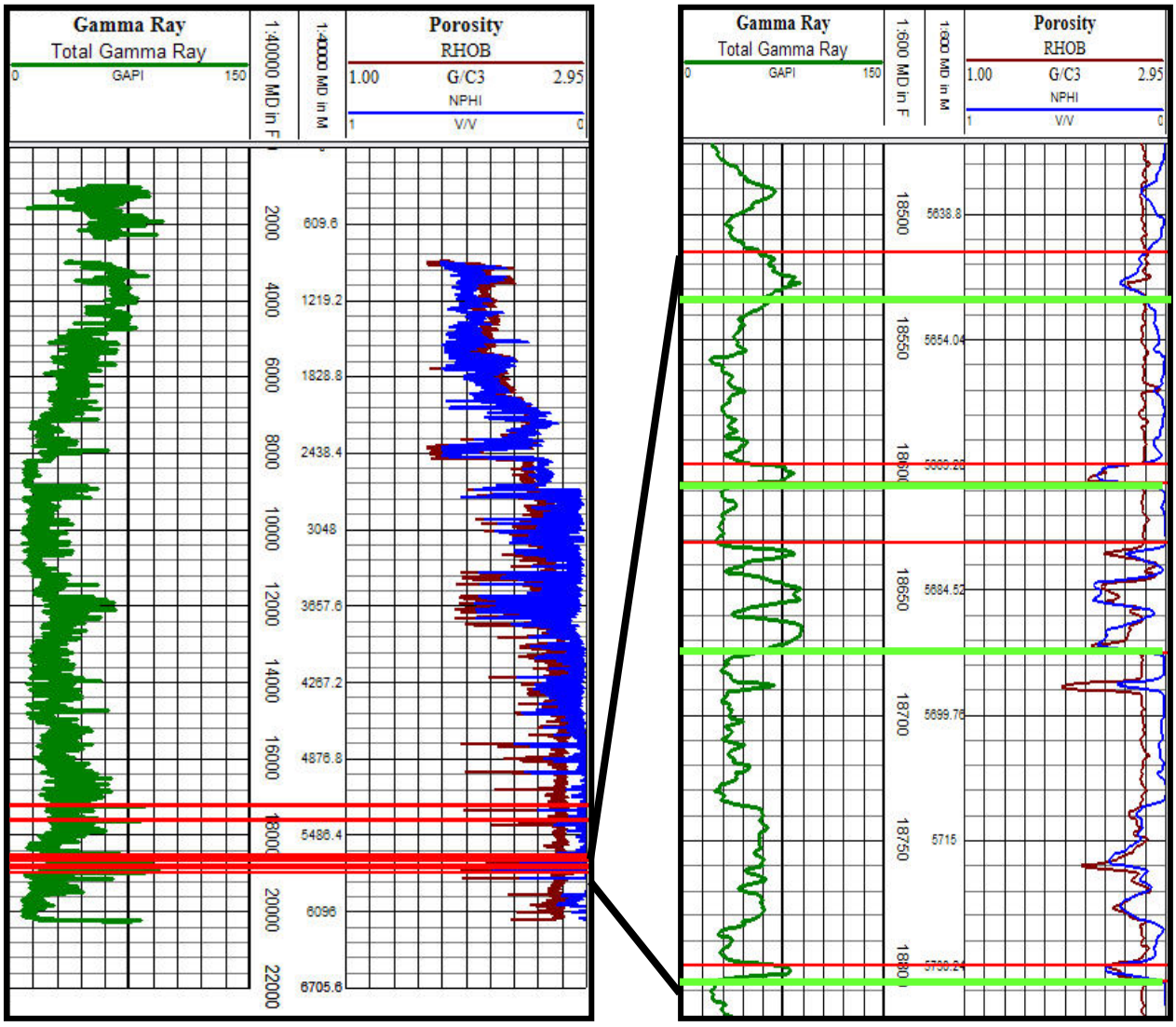

The last well in Destin Dome used in this study is in block 284. This block is located approximately 112.7 km east of New Orleans. The youngest dated lithology is from the Early Oligocene and the oldest dated lithology is Valanginian in age (Appendix F). The mean gamma ray reading for lithologies not potentially associated with deposition during an OAE is 36.1 GAPI. There are two possible intervals associated with deposition during an OAE (Appendix E). These intervals are in black shale, one of which is part of the Tuscaloosa Formation (Table 9). These black shales are Coniancian to Santonian in age. There is very little increase in gamma

ray readings. The mean gamma ray reading through these intervals is 42.6 GAPI with a peak of 62.6 GAPI (Table 10). The first black shale does not show a decrease in density or an increase in neutron porosity. The second black shale, which is part of the Tuscaloosa Formation, does show a slight decrease in density and a slight increase in neutron porosity (Table 11; Fig. 18; Appendix G).

Figure 18. Well 608224002200; gamma ray log, density and neutron porosity response through total logged interval and detail through Santonian-Coniancian-age calcareous black shale and Tuscaloosa Formation black shale potentially associated with OAE deposition. The upper boundaries of the interested log segments are indicated with thick red lines and the lower boundaries are indicated with light green lines.

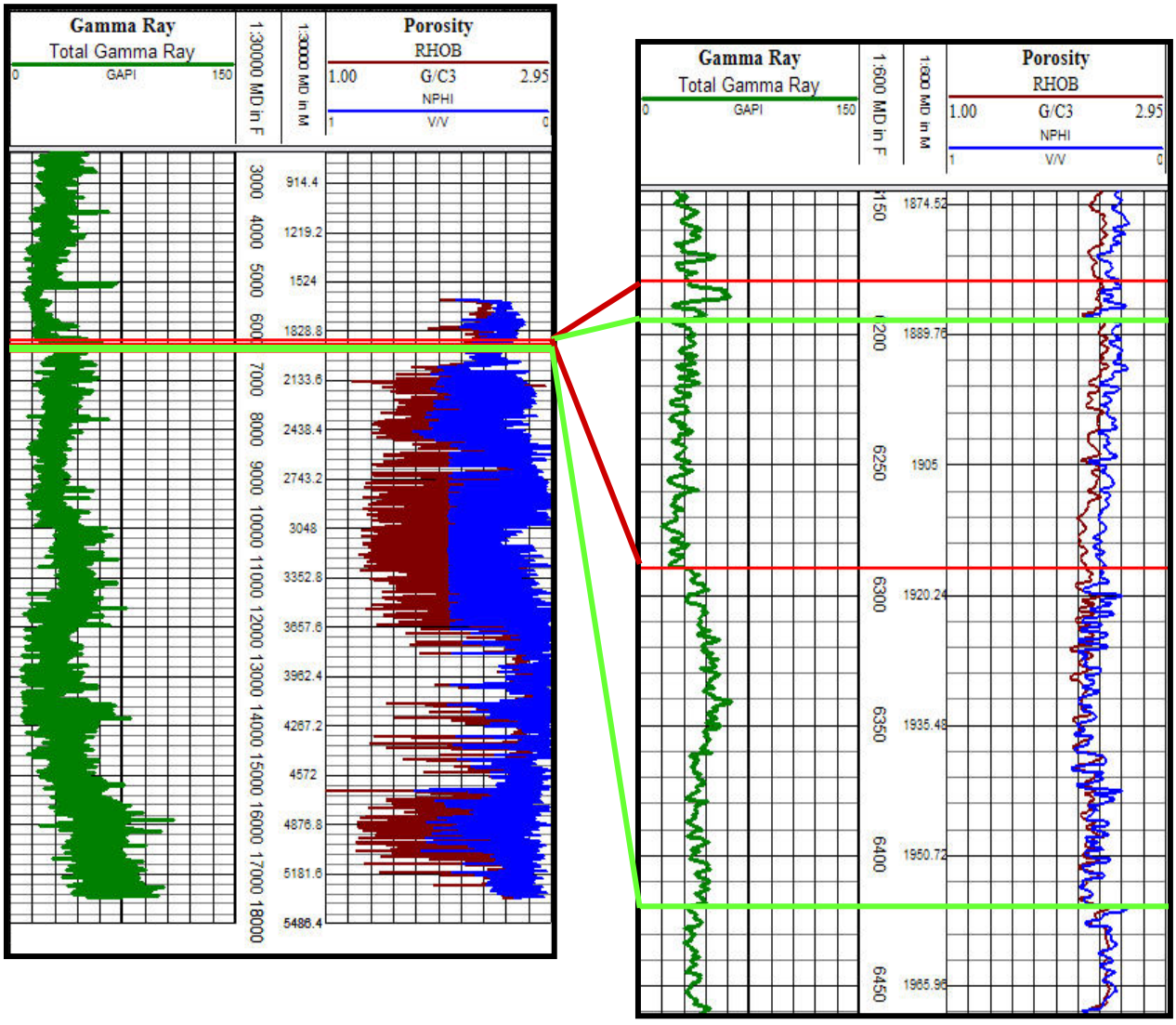

Pseudo Density Deviation from Bulk Density

A clear pattern for the deviation of the pseudo density from the bulk density does not exist for sediments deposited during OAEs. The deviation was negative 54% of the time and positive 43% of the time, with the average deviation through the segment deposited during an OAE as 0 the remaining 3% of the time (Tables 12 and 13). There is a correlation between organic matter and density deviation. The more organic material present, the more negative the deviation of the pseudo density from the bulk density curve (Fig. 19).

Table 12. Mean density deviation from bulk density through all intervals associated with deposition during an OAE for ODP holes.

Hole	Depth (mbsf)	Mean density deviation (g/cm^3)
103-641C	150.9-202.6	0.004
159-959D	1024.0-1043.3	0.004
171B-1052 E	510.6-656.0	0.000
198-1207B	565.0-574.0	-0.032
198-1213B	256.8-266.4	-0.023
207-1258C	397.5-449.6	-0.018
207-1258C	449.6-484.9	0.004
207-1261B	563.0-659.2	-0.007

Table 13. Mean density deviation from bulk density through all intervals potentially associated with deposition during an OAE for the Gulf of Mexico wells.

Well #	Area	Block	Depth (m)	Depth (ft)	Mean Density Deviation (g/cm^3)
177244005200	MP	264	4402.8 - 4405.9	14445.0 - 14455.0	-0.070
177244005400	MP	253	4434.8 - 4526.3	14550.0 - 14850.0	0.015
177244006300	MP	222	2970.3 - 2982.5	9745.0 - 9785.0	-0.035
			3314.7 - 3320.8	10875.0 - 10895.0	0.134
608164003700	VK	30	2802.6 - 2808.1	9195.0 - 9213.0	-0.017
608224000600	DD	166	1489.6 - 1495.0	4887.0 - 4914.0	0.013
608224001400	DD	162	1384.7 - 1386.8	4543.0 - 4550.0	-0.019
			1937.0 - 1938.5	6353.0 - 6365.0	-0.047
			1981.5 - 1983.6	6501.0 - 6508.0	-0.032
			2066.8 - 2068.4	6781.0 - 6786.0	-0.037
			2810.6 - 2813.6	9221.0 - 9231.0	0.012
608224001700	DD	529	5251.7 - 5253.2	17230.0 - 17235.0	-0.062
			5363.0 - 5373.6	17595.0 - 17630.0	-0.071
			5643.4 - 5649.5	18515.0 - 18535.0	0.204
			5669.3 - 5671.6	18600.0 - 18607.5	-0.015
			5681.2 - 5692.1	18639.0 - 18675.0	0.137
			5730.2 - 5732.1	18800.0 - 18806.0	0.048
			5752.5 - 5789.2	18873.0 - 18995.0	-0.074
608224002200	DD	284	1883.7 - 1888.2	6180.0 - 6195.0	0.110
			1917.2 - 1956.8	6290.0 - 6420.0	0.190

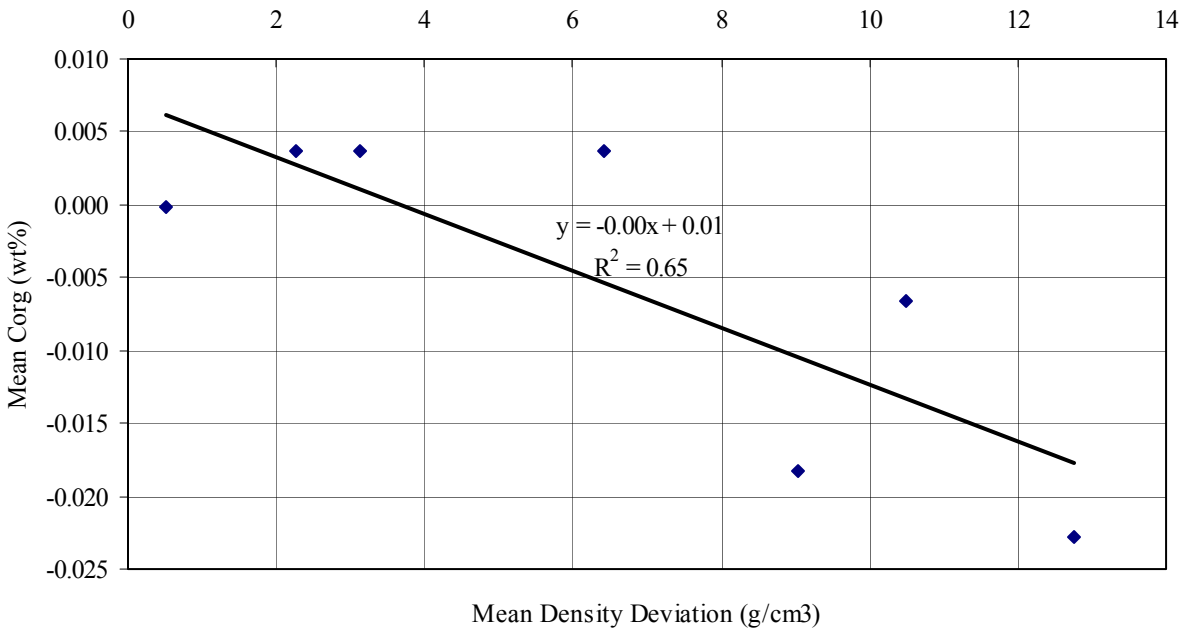

Figure 19. Mean organic carbon % versus the mean density deviation through OAE lithologies in the Ocean Drilling Program holes.

Despite not showing a clear indication of OAE deposits the deviation of the pseudo density curve from the bulk density curve did appear to show a pattern based on lithology (Appendix B). Initially the pseudo density deviation from the bulk density was plotted against depth and then for intervals showing a marked tendency for either positive or negative deviation the lithology over that interval was established from the core descriptions. By labeling the lithologies present to the graph of the deviation amount a pattern started to take shape. Within the ODP wells there was a moderate correlation between a negative deviation and quartz material and a correlation between positive deviation and calcareous material (Figs. 20 and 21). Unfortunately there was little correlation between clay material and deviation (Appendices D and H).

Figure 20. Hole 103-641C deviation of pseudo density from bulk density with lithology descriptions.

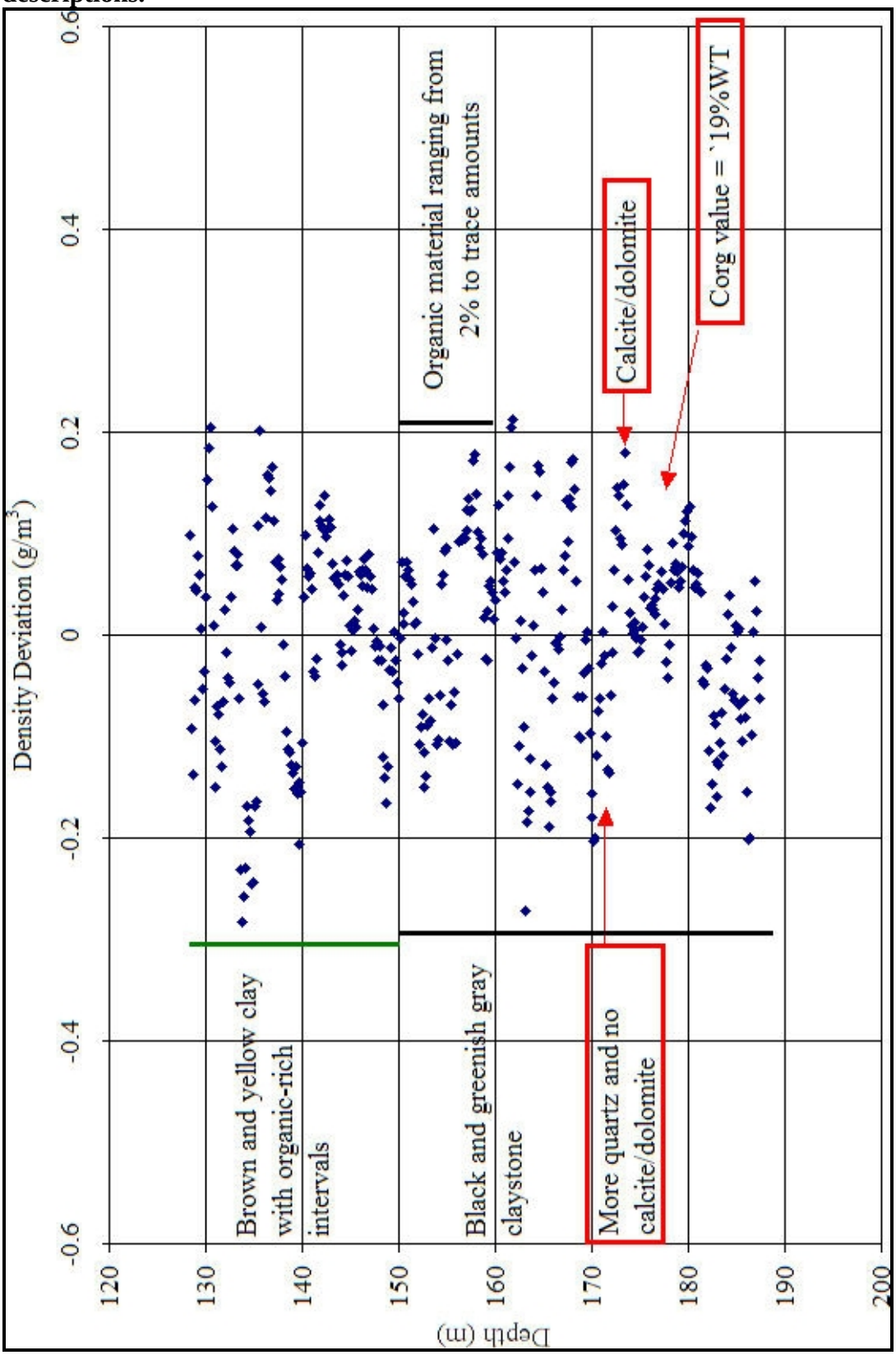

Figure 21. Hole 171B-1052E deviation of pseudo density from bulk density through Late Albian lithologies associated with OAE deposition, with lithology information.

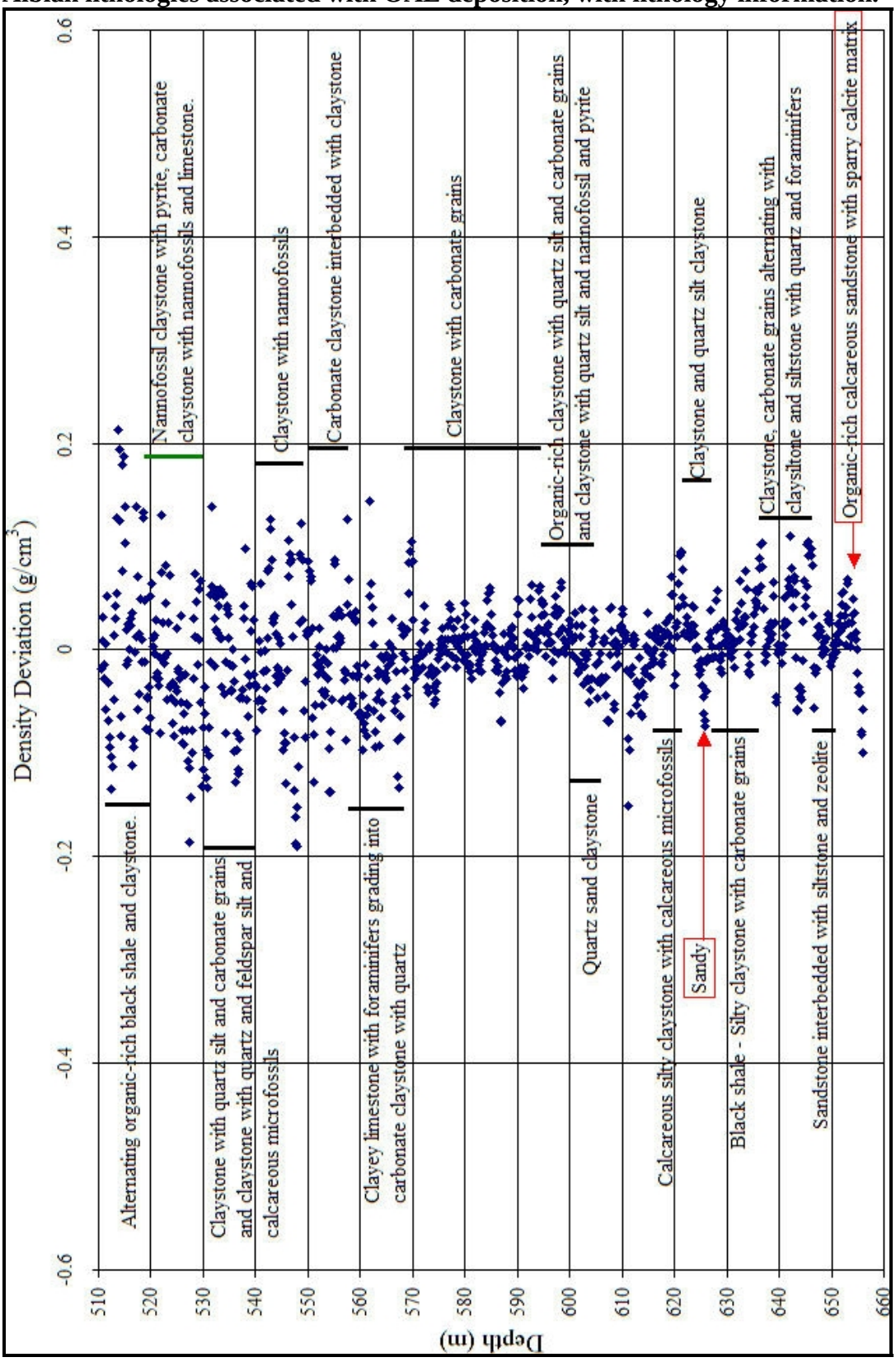

DISCUSSION

Log Signature

It was expected that this study would find that OAEs characteristically would have a comparatively high gamma ray signal, especially uranium influenced values, and corresponding low density, high neutron porosity and low sonic velocity. These expectations were based in part on the understanding that organic matter is typically rich in uranium, which should elevate the gamma ray readings (Bassiouni, 1994 and Ellis, 2007). The density expectation was based on the organic content being considerably less dense than lithic material and thus lowering those values. The average grain density of organic matter is 1.06 g/cm^3 (Logan, 1987). The average grain density of lithic material is 2.71 g/cm^3 (Klass, 2002). It was expected that the neutron porosity would increase as a result of the open fabric characteristic of organic-rich sediments and the higher hydrogen content of organic material. The sonic values were expected to decrease as a result of the low velocities typical of organic matter (Passey, 1990). It was unclear what kind of response the resistivity values might show in the OAE intervals, but as resistivity is a common curve generated when holes are drilled it was examined for a pattern that might be added to the overall borehole log signature of sediments deposited during an OAE.

The known OAE intervals in the ODP holes typically show a spike in the gamma ray values for the hole. Also, as expected, the uranium and neutron porosity values increase significantly, while the density and sonic values decrease through the OAE sediment intervals (Figs. 10 and 11). One exception to this pattern within the ODP holes occurs in Hole 171B-1052E in which the uranium alone does not seem to account for the increase in gamma radiation, and there is not a corresponding decrease in the density (Fig. 12). This exception may have to do with the black shale associated with OAE deposition in Hole 171B-1052E being interbedded with calcareous and silica rich lithologies. Another possible explanation for the difference between Hole 171B-1052E and the other OAEs segments in ODP wells may lie in the organic carbon content. The organic carbon content in this hole never goes above 1wt %; whereas the segments deposited during OAEs in other ODP wells have organic carbon contents significantly higher throughout the OAE interval. Hole 171B-1052E contains rocks deposited during OAE 1d, a minor OAE confined more to the Atlantic Ocean. It may be that the position of Hole 171B-

1052E allowed it to be less significantly affected during this time period. Alternatively, productivity might not have been as high at this particular site as opposed to other sites during the OAE interval.

A discernable signature is not present in the resistivity curves for the ODP holes. This lack of a signature is likely the result of the bound water found shales, which tends to affect resistivity readings. A summary of the information on the log responses of the ODP holes and a description of the lithology through the OAE intervals can be found in Tables 6 and 7.

Correlation Between Organic Carbon and Gamma Ray Response

It was expected that there would be a significant correlation between organic carbon content and gamma ray values. This was expected because of the apparent correlation seen when the bore hole logs were plotted next to the organic carbon content as seen in Figure 9 (Appendix C). Additionally, previous work done by Bell, et. al. in 1940, as well as work by Zelt in 1985, established a linear relationship between total organic carbon and uranium. However, an obvious correlation is not present within the data set established using the ODP holes (Fig. 10; Fig. 11). There are a several explanations for the lack of correlation.

One explanation is shale effect. Clay can contain up to 30-70% radioactive material in the form of potassium, thorium, and uranium (Schlumberger, 1972). Shales and mudstones rich in clay minerals are easily recognizable from sandstones or calcareous rocks that typically contain considerably less radioactive material. The type of radioactive material varies widely from deposit to deposit, and knowing the source of the radiation provides an indication of the composition of the rock. This indirect means of determining composition is why the spectral gamma radiation tool is used to differentiate between radiation produced by thorium, potassium and uranium. A high total gamma ray value may represent normal shale that reads with a high gamma ray due to its thorium or potassium content, both of which are very common in the clay minerals. Potassium-40 is the most abundant naturally occurring radioactive material and accounts for nearly all the gamma radiation encountered in rocks (Bassiouni, 1996 and Foster, 2006). As a result, an enrichment in clays within the holes and wells would affect the gamma ray log results.

Another aspect of the lack of correlation between organic content and gamma ray values is that what constitutes a high total gamma ray reading in one borehole would not necessarily be regarded as a high value in another hole. There are many reasons for this including differing lithologies, borehole shape effect, temperature of the hole, and the possibility that the tool is not correctly calibrated or that the tool is not effectively reading the gamma radiation the lithology is emitting (Bassiouni, 1994). While sediments deposited during OAEs are generally called black shales, not all deposits of an OAE are shale or mudstone. Some of the sediments are highly calcareous material, which would have the effect of lowering the gamma ray reading.

Total gamma ray and uranium gamma ray readings also are skewed by the averaging effect of the tool that reads the amount of radiation the rock is emitting. The gamma ray tool averages gamma radiation over a 0.15 m (0.5 ft) interval. Oceanic anoxic events can be associated with beds that are only millimeters thick. Often the organic-rich rocks associated with OAEs are interbedded with other lithologies such as carbonates or sandstones. Carbonates and sandstones generally contain little radioactive material compared with shales or organic-rich rocks. Thus averaging by the gamma ray tool over these interbedded lithologies may give a misleadingly low gamma ray response through the OAE interval.

In addition to the averaging effect of the gamma ray tool, the manner in which the point-to-point values were generated for each C_{org} datum from the ODP cores may have a detrimental effect on the correlation. Because the exact depth for each C_{org} point could not be established as a result of incomplete cores, the gamma ray values were averaged over the range of potential depths for the C_{org} datum. Averaging at times occurred over a meter or more, and the value obtained by averaging over these depths may not be representative of the gamma response at the true depth of the C_{org} datum.

The variation in lithologies in which the organic material accumulated during OAEs also caused outlying values in both the plot of total gamma ray versus C_{org} and uranium versus C_{org}. Values with very high gamma ray readings and relatively low C_{org} values are likely the result of deposition in lithologies not only rich in uranium as a result of organic material, but also rich in potassium and thorium rich clays. For example, in Hole 207-1258C there is a data point with a total gamma ray reading of 291.0 GAPI, a uranium reading of 29.5 GAPI and a C_{org} value of only 5.26 %. In this case the value occurs in black nannofossil clay rich in organic material. The high total gamma ray values, while partially the result of the high uranium values, are also

product of the potassium- and thorium-rich clay material. The uranium values are likely high as a result of the organic matter, but there also may be uranium present in the clay material not associated with organic matter. Oxygen-deficient systems frequently produce authigenic uranium as a result of reduction and precipitation from uranium enriches ocean waters. This can lead to uranium concentrations higher than those where the source of uranium is primarily detrital (Lüning and Kolonic, 2003).

Data points where the organic carbon content is particularly high but the total gamma ray and uranium gamma ray are relatively low is likely the result of deposition of organic-rich material in lithologies that are otherwise low in radioactive material. One such point is found in Hole 198-1213B. Here the C_{org} reaches 25.17%, yet the total gamma ray reading only reaches 34.0 GAPI and the uranium value is 1.4 GAPI. In this case the organic material occurs in 15 – 68 cm beds of porcellanite, which is interbedded with non-organic-rich porcellanite and chert. The radioactivity of these thin beds would be averaged with the very low radioactive porcellanite and chert beds, thus lowering the gamma ray readings. While these data points are still valid, with the majority of the data points focused around 100 GAPI or less in the total gamma ray, 10 GAPI units or less in the uranium readings, and an organic carbon content of 5% or less, the data becomes skewed by the outlying points.

These points seem to show lower amounts of uranium having a larger effect on the total gamma ray value. This is not likely the case however. Within this group there are two lithology type sub-groups. First those points with total gamma ray readings of 70.0 GAPI or lower and uranium values of 3 GAPI are lower reflect lithologies such as sandstone and limestone with little radioactivity. For example, in Hole 103-641C at 664.0 mbsf the total gamma ray reads as 60.0 GAPI and the uranium is only 1.7 GAPI and the lithology is that of a sandstone with glauconite pellets. The second lithology sub-group contains clay-rich lithologies whose main radioactive component is potassium or thorium. These points show total gamma ray values of 70.0 GAPI or higher but still have uranium readings of less than 3.0 GAPI. For example, within Hole 207-1261B there are several instances of total gamma ray readings of 90.0 GAPI or higher corresponding to uranium values of less than 2.0 GAPI within a nannofossil clay lithology.

The group of data points that make the right arm of the V-shape on the plot of the non-OAE plot consists of more organic-rich lithologies that contain more uranium. The majority of these points within the non-OAE plot are from Hole 171B-1052E through black nannofossil clay

and from Hole 159-959D through a black claystone with organic matter and a black porcellanite with organic matter. The large difference between the OAE rocks and the non-OAE rocks in Figures 12a and 12b lies in the uranium content. The OAE lithologies still have the same right arm of the V-shape seen in both plots; however, the right arm in the OAE plot extends through much higher uranium readings. The right arm on the plot for OAE lithologies represents the highly organic-rich sediments through the intervals deposited during OAEs.

Borehole Log Signature Applied to the Gulf of Mexico Wells

Once the signature from the ODP holes was established it was then applied to eight wells in the Gulf of Mexico that met the age criteria for containing lithologies deposited during OAEs. The eight wells contain twenty intervals that potentially were deposited during OAEs. While the majority of these intervals follow the signature identified in the ODP holes, a relative spike in the gamma ray, a decrease in density and an increase in neutron porosity, there are some differences between the ODP holes and the Gulf of Mexico wells.

While it was hoped that the Gulf of Mexico wells would show OAE intervals with expanded thicknesses, the lithologies that were potentially deposited during an OAE range from a few meters to at most several tens of meters in the Gulf of Mexico wells. None of the Gulf of Mexico wells come close to the thickness of 155 m seen in Hole 171B-1052E from the ODP data set. The thinness of the segments potentially deposited during OAEs in the Gulf of Mexico may be the result of a number of factors. The Gulf of Mexico wells are closer to land during OAEs than the sites of the ODP holes. The shallower position may have allowed for earlier reoxygenation of the waters. Alternatively, the sites of the Gulf of Mexico wells were dominated by the deposition of carbonate material. This carbonate material may have diluted the organic material being deposited.

While the individual intervals seen in the Gulf of Mexico are typically comparably thin, in well 608224001700 there are several pulses that meet the log signature criteria developed in the ODP holes over a 300-meter thickness that ranges in age from Aptian to Albian. Without the availability of a more detailed chronology for these sediments it is not possible to tell if these represent separate OAE events, such as the minor OAE 1b, 1c, and 1d, or if they are an expanded package over a single OAE. The presence of such an expanded package could potentially bring invaluable insight into the timing and mechanics of OAEs.

Most of the Gulf of Mexico wells show prominent spikes in the gamma ray within the well; however, there are instances where the lithology is known to be black shale and yet the gamma ray only shows a moderately shaley signal. For instance, in well number 608224002200 in Destin Dome Block 284 there are two intervals known to be black shales from the mud logs. Additionally, one of these intervals is known to be the Tuscaloosa Formation from the paleontology report. Yet both intervals show only the slightest increase in gamma radiation compared to the rest of the well (Fig. 18). These lithologies also show traces of limestone and sandstone, both of which may be affecting the gamma ray because they tend to lack radioactive material. It may be that the increase in non-clay lithic material in these instances, as well as in other Gulf of Mexico wells where the lithology points to OAE conditions during deposition but the borehole logs do not give a definitive indication of OAE intervals, has caused the signature to be dampened within these wells. It should be noted that while the signature is dampened, the density did decrease slightly and the neutron porosity increased slightly through this interval in well 605224002200, though not to the degree generally seen in the more pelagic sediments of the ODP holes. In addition, while the density does generally decrease in the potential OAE intervals for the majority of the Gulf of Mexico wells, it does not decrease as intensely as it does in the ODP holes.

While every attempt was made to keep the results of the Gulf of Mexico data as accurate as possible, there are several factors that must be kept in mind when applying the results to other wells. Without the aid of spectral gamma ray logs it is impossible to determine if the increase in gamma radiation is the result of uranium enrichment. The high gamma ray intervals may be clays rich in thorium or potassium. The lithology estimates are highly questionable because the descriptions cover depths ranging from fifty to one hundred feet; whereas, OAE intervals can be as thin as a few millimeters to centimeters thick. Additionally, the tendency for borehole logs from the Gulf of Mexico to need adjustments to improve accuracy may diminish the ability to properly identify potential lithologies deposited during OAEs.

For this study, it is assumed that the gamma ray logs for the Gulf of Mexico wells are total gamma ray logs; however, there is the possibility that one or more of these logs may have been corrected gamma ray logs. In areas where the use of a corrected gamma ray log is common, it is not unusual to refer to it simply as the gamma ray log without an indication that it is a corrected gamma ray log. This practice is not common in the Gulf of Mexico. For this

reason logs labeled as gamma ray logs were assumed to be total gamma ray logs. However, it is possible that there are instances where the gamma ray log does not show a peak through a section known to be black shale from the mud logs as a result of the log not being a total gamma ray log. Examples of the difference in log response between a total gamma ray log and a corrected gamma ray log is shown in Figures 5 through 9.

A main difference in data control between the ODP holes and wells from the Gulf of Mexico lies in the lithology descriptions. The ODP holes all have core reports with lithology descriptions covering all cored intervals. The Gulf of Mexico lithology descriptions come from mud logs, with minimal descriptions that cover in most cases over 30 meters and are taken from fragments of rock (cuttings) that float up as drilling mud is circulated during the drilling of a well. These cuttings may get trapped in places as they float up and may arrive later than expected, making it seem as if they come from deeper in the well. Where the material is not well consolidated, the pieces may circulate in the mud and not reach at all the person observing and documenting the cuttings. Therefore a wide margin of error was granted when fitting lithologies from the mud logs to borehole log responses from the wells. Every effort was made to accurately label lithologies for potential OAE intervals within the Gulf of Mexico wells, but incorrect labeling may account for areas labeled as containing black shales that do not give the expected response on the borehole logs.

Lastly, while the care taken during the administration of logging tools during the ODP expeditions can be relied on to have given accurate responses, this attention to detail is not always the case in the Gulf of Mexico logs, or in any industry produced logs. Ordinarily logs come with some form of error that needs to be corrected for before they are most useful. Tool failure or human errors are the most common inaccuracies. In addition to these problems, it is not unusual to see various logs within a well that need to be depth matched to one another, adjusting the depths for one type of log to match the readings of a more reliable log. Often the adjustment required is less than a meter, but absolutely necessary to assure that assessments made using those logs are correct.

Another issue that affects many logs is borehole wandering. Wandering often happens when different segments of a well are logged at different times for a number of reasons. One segment of a gamma ray log, for example, will show all lithologies at an obvious offset from those run by a different tool or at a different time. Most petrophysical analysis equipment comes

with software to make these adjustments because of the frequency with which they occur. No obvious issues of this nature were observed in any of the logs used in this study.

Pseudo Density versus Bulk Density

Because of the striking characteristics of the log response through lithologies deposited during OAEs it was hypothesized that pseudo density curves built from these borehole logs would show a significant deviation from the true bulk density values logged through these sections. Because the gamma ray and neutron porosity values are elevated to such a degree through these intervals it was expected that a neural network generated pseudo bulk density would read as significantly less dense than the true bulk density. The limited number of log types available for the Gulf of Mexico wells restricted the number of curves that could be used to produce pseudo density curves for a comparison between ODP and Gulf of Mexico data sets. However, in addition to the pseudo density curves built from the ODP holes to test for a signature that might be applied to the Gulf of Mexico wells, other pseudo density curves were created using all available log types for each of the ODP holes. The additional logs did not change the pseudo curves enough to warrant their use in producing a suitable curve.

The results of the pseudo density curve comparison to the bulk density curve are the opposite of what had been expected. The pseudo density most often is higher than the bulk density through the intervals associated with OAEs; however, no true correlation between pseudo density and OAEs exists. The expectation that the elevated gamma ray and elevated neutron porosity would decrease the density value in the pseudo density curve was unfounded. A possible reason for the disparity could be that these values are not sufficiently elevated to affect the pseudo density curve in the manner expected. Another possibility is that the assumptions about the effect of an elevated gamma ray and elevated neutron porosity on the pseudo density curve are incorrect. Also, the wide variation of lithologies deposited during OAEs may play a large role. A limestone does not have the same density as shale, for example, and this variation may be shown in range of pseudo density deviations seen in OAEs.

While there is no clear pattern between OAEs and pseudo density curves, there is a link between increasing organic carbon content and pseudo density deviation from bulk density becoming more negative within the OAE intervals. The pseudo density logs would then be

reading as denser through areas that were especially rich in organic material. Not all sediments deposited during an OAE would be equally rich in organic material, possibly as a result of varying rates in productivity. An example would be the variation between the organic-rich unit associated with deposition during OAE 1a at ODP site 198, in Holes 1207B, 1213B and 1214A (Bralower, T.; et al., 2002). Therefore the pseudo density deviation would vary within sediments deposited during an OAE. This variation in lithology may be why a clear pattern in pseudo density curves for OAE intervals as a whole may not exist. Whereas the results are not what were expected, the data obtained from the study is still potentially useful in the gauging the organic richness of a lithology known to have been deposited during an OAE. Gauging organic richness would require further study into the effect of organic material on a pseudo density curve.

The affect of lithology on the pseudo density curve was an unexpected result. The tendency for calcareous material to read as more dense in the pseudo density curve and for the siliceous material, such as siliceous micro fossils, quartz, and sandstone, to read as less dense than its true bulk density may just be a result of the difference in densities between these two materials. Calcareous material has a general density of 2.71 g/cm^3 while siliceous material has a general density of 2.65 g/cm^3. This difference might be enough to build the pattern seen in ODP pseudo density curves. There also is the possibility that this apparent pattern is a fluke. While the lithologies present in the ODP holes fit this pattern most of the time, they did not do so frequently enough to warrant it being called a strong correlation (Appendix B). Also, the deviations were averaged over full core lengths, which may skew the data. Additionally, the amount of siliceous versus calcareous material present per core was established by estimating based on how the lithology was named in the core description. This interpretation of the sediment type can lead to erroneous assumptions about the lithic components within a core. Therefore, while an interesting pattern does seem to exist, more research is needed to make use of the pattern in establishing lithology where cores are not available.

CONCLUSIONS

Oceanic anoxic events are of great scientific importance not only as a means of hydrocarbon production, but also as a window into a time when the earth was under severe greenhouse conditions. The intent of this study was to characterize a borehole log signature indicative of sediments deposited during an OAE and to use that signature to recognize OAE lithologies within the Gulf of Mexico. It was believed that because of the high organic content of lithologies deposited during OAEs and the known effects of organic matter on the response of different logging tools that identification of a characteristic signature would be possible. The borehole logs in the ODP holes largely meet the expectations of what an OAE would look like in the logs. In nearly all the holes examined the gamma ray, especially the uranium-derived gamma response, increases significantly through the sections associated with OAEs as a result of the tendency for organic material to accumulate uranium. The bulk density decreases through these intervals as a result of the density of organic matter being lower than that of lithic material. The open fabric characteristic of organic material results in an increased neutron porosity. However, these characteristics do not hold true in all of the ODP holes, specifically Hole 171B-1052E. There is only a slight increase in the gamma ray readings for this hole, and this increase is in large part to the result of the potassium and thorium in the clayey sediments in which the organic matter is present.

While the pseudo density curves generated for this study are not as beneficial in the identification of OAEs as was hoped, the lithologic association found in the deviation of these curves from a true bulk density curve opens an avenue for future research. With a more precise lithologic description at the meter or smaller scale these deviations might yet prove to have a direct link.

Because of the immense variation in lithologies rich in organic material as a result of deposition during an OAE, it is not possible to convincingly identify these deposits solely based on borehole logs over intervals that have been constrained chronologically. While the borehole log signature that was developed works well more often than not, the lack of the signature does not indicate that OAE-related organic-rich intervals are not present. Thus applying this signature to wells in the Gulf of Mexico may still provide a good initial indication of the presence of lithologies associated with deposition during OAEs. Within the Gulf of Mexico eight wells were

identified that potentially contain OAE intervals. Within these eight wells 20 intervals meet either in total, or in part, the characteristic log signature documented for the ODP holes. The sections potentially deposited during OAEs are consistently thinner than those that are present in the ODP holes, although within some wells several pulses occur that might be linked to separate smaller events or an expanded package of a singe OAE. Without more precise chronologic constraint within these wells it is not possible to determine if expanded packages are present as was hypothesized for in the Gulf of Mexico. However, the presence, solely within the publicly available data, of so many intervals potentially deposited during OAEs in the Gulf of Mexico makes the Gulf of Mexico a prime location for future studies, especially should privately owned oil and gas industry data become available.

REFERENCES

Arthur, M., and Schangler, S., 1979. Cretaceous 'oceanic anoxic events' as causal factors in development of reef-reservoired giant oil fields. *AAPG Bulletin*, 63:870-885.

Bassiouni, Z., 1994. *Theory, Measurement, and Interpretation of Well Logs*. *SPE Textbook Series Vol. 4.* Society of Petroleum Engineers, Inc.

Bell, K. G., Goodman, C., Whitehead, W. L., 1940. Radioactivity of sedimentary rocks and associated petroleum. *AAPG Bulletin*, 24:1529-1547.

Boillot, G., Winterer, E.L., Meyer, A.W., et al., 1987. *Proc. ODP, Init. Repts.,* 103: College Station, TX (Ocean Drilling Program). doi:10.2973/odp.proc.ir.103.1987

Bralower, T. J., Premoli Silva, I., Malone, M. J., 2002. *Proc. ODP, Ini. Repts.,* 198: College Station, TX (Ocean Drilling Program). doi:10.2973/odp.proc.ir.198.2002

Clavier, C., Heia, A., Scala, C. Effect of pyrite on resistivity and other logging measurements. *Trans. of the SPWLA Ann. Log. Symp.,* 17:34.

Darnell, R. M. and Defenbaugh, R. E., 1990. Gulf of Mexico: Environmental overview and history of environmental research. *American Zoologist,* 30:3-6.

Dean, W. and Arthur, M., 1999. Sensitivity of the North Atlantic Basin to cyclic forcing during the early Cretaceous. *Journal of Foraminiferal Research,* 29:465-486.

Ellis, D. and Singer, J., 2007. *Well logging for earth scientists*. Dordrect, The Netherlands: Springer.

Erba, E., 1994. Nannofossils and superplumes: The early Aptian "nannofossil crisis. *Paleoceanography*, 9:483-501.

Erba, E., 2004: Calcareous nannofossils and Mesozoic oceanic anoxic events: *Mar. Micropaleontol*., 52:85-106.

Erbacher J., Huber B. T., Norris R. D., 2001. Increased thermohaline stratification as a possible cause for an ocean anoxic event in the Cretaceous period. *Nature*, 409:325-327.

Foster, E., 2006. *Well Log Interpretation* (short course manual). Tulsa, Oklahoma: *Petroskills, LLC*.

Gore, R. H., 1992. *The Gulf of Mexico*. Pineapple Press, Inc., Sarasota, Florida. 384.

Hallam, A., 1999. Discussion on oceanic plateau formation: A cause of mass extinction and black shale deposition around the Cenomanian-Turonian boundary. *Jour. Geol. Soc.*, 156:208.

HRLA high-resolution *Laterolog Array Tool*. Schlumberger, 2000. [Online]. Available from the World Wide Web: <http://www.slb.com/media/services/evaluation/petrophysics/resistivity/hrla.pdf>. [Cited 2008-09-21]

Jenkyns, H., 2003. Evidence for rapid climate change in the Mesozoic-Palaeogene greenhouse world. *Phil. Trans. R. Soc. Lond.,* 361:1885-1916.

Klass, C., and Archer, D. E., 2002. Association of sinking organic matter with various types of mineral ballast in the deep sea: Implications for the rain ratio. *Global Biogeochem. Cycles,* 16:1116, doi:1110.1029/2001GB001765.

Larson, R. L., and Erba, E. 1999. Onset of the mid-Cretaceous greenhouse in the Barremian-Aptian: Igenous events and the biological, sedimentary, and geochemical responses. *Paleoceanography*, 14:663-678.

Leckie, R. M., Yurectich, R. F., West, O. L. O., Finkelstein, D., and Schmidt, M., 1998. Paleoceanography of the southwestern Western Interior Sea during the time of the Cenomanian-Turonian boundary (Late Cretaceous). In Dean, W. E., and Arthur, M. A. (Eds.), *Stratigraphy and Paleoenvironments of the Cretaceous Wester Interior Sea Way, USA, Concepts Sedimentol. Paleontol*. 6, Soc. of Sediment. Geol., 101-126.

Leckie, R. M., Bralower, T. J., and Cashman, R., 2002. Oceanic anoxic events and plankton evolution: Biotic response to tectonic forcing during the mid-Cretaceous. *Paleoceanography*, 17:1041.

Liu, K., 2005. Upper Cretaceous sequence stratigraphy, sea-level fluctuations and Oceanic Anoxic Events 2 and 3, Gulf of Mexico. *Stratigraphy*, 2:147-166.

Logan, B. E., and Hunt, J. R., 1987. Advantages of microbes of growth in permeable aggregates in marine systems. *Limnol. Oceanogr.*, 32:1034-1048.

Lüning, S., & Kolonic, S. (2003). Uranium spectral gamma-ray response as a proxy for organic richness in black shales: applicability and limitations. *Journal of Petroleum Geology*. *26:2,* 153-174.

Lyle, M., Wilson, P.A., Janecek, T.R., et al., 2002. *Proc. ODP, Init. Repts.,* 199: College Station, TX (Ocean Drilling Program). doi:10.2973/odp.proc.ir.199.2002

Mascle, J., Lohmann, G.P., Clift, P.D., et al., 1996. *Proc. ODP, Init. Repts.,* 159: College Station, TX (Ocean Drilling Program). doi:10.2973/odp.proc.ir.159.1996

Montanez, I., 2006. Orbitally tuned C and N isotopic records of Aptian Oceanic Anoxic Event1a in northeastern Mexico and Deep Sea Drilling Project Site 398, North Atlantic Ocean. *Eos Trans. AGU*, 87:52.

New Oceans Begin to Open. Earth History [Online]. Available from the World Wide Web: <http://www.scotese.com/cretaceo.htm>. [Cited 2008-03-16]

Norris, R.D., Kroon, D., Klaus, A., et al., 1998. *Proc. ODP, Init. Repts.*, 171B: College Station, TX (Ocean Drilling Program). doi:10.2973/odp.proc.ir.171b.1998

Ohkouchi N., Kitazato H., Kashiyama Y., Kuroda J., Ogawa N. O., 2006. An importance of diazotrophic cyanobacteria as a primary producer during Cretaceous Oceanic Anoxic Event 2. *Biogeosciences Discussions*, 3:575-605.

Pancost, R. D. 2004. Further evidence for the development of photic-zone euxinic conditions during Mesozoic oceanic anoxic events. *Jour. Geol. Soc.*, 161:353-364.

Passey, Q. R., Creaney, S., et al., 1990. A practical model for organic richness from porosity and resistivity logs. *The Amer. Ass. Of Pet. Geo. Bul.*, 74:12 1777-1794.

Russell, W., 1944. The total gamma ray activity of sedimentary rocks as indicated by geiger counter determinations. *Geophysics*, 2:180-216.

Schangler, S. O., and Jenkyns, H. C., 1976. Cretaceous oceanic anoxic events: Causes and consequences. *Geol. Mijnbouw*, 55:179-184.

Schangler, S. O., Jenkyns, H. C., PremoliSilva, I., 1981. Volcanism and vertical tectonics in the Pacific Basin related to global Cretaceous transgressions. *Earth Planet. Sci. Lett.*, 52:435-449.

Sclumberger, 1972. *Log Interpretation, Volume I – Principles*. New York, NY: *Schlumberger Limited*.

Shipboard Scientific Party, 1987. Site 641. *In* Boillot, G., Winterer, E. L., Meyer, A. W., et al., *Proc., Init. Repts., ODP*, 103: College Station, TX (Ocean Drilling Program), 571-649.

Shipboard Scientific Party, 1996. Site 959. *In* Mascle, J., Lohmann, G. P., Clift, P. D., et al., *Proc., Init. Repts., ODP*, 159: College Station, TX (Ocean Drilling Program), 65-150.

Shipboard Scientific Party, 1998. Site 1052. *In* Norris, R.D., Kroon, D., Klaus, A., et al., *Proc. ODP, Init. Repts.*, 171B: College Station, TX (Ocean Drilling Program), 241-320. doi:10.2973/odp.proc.ir.171B.106.1998

Shipboard Scientific Party, 2002a. Site 1207. *In* Bralower, T.J., Premoli Silva, I., Malone, M.J., et al., *Proc. ODP, Init. Repts.*, 198: College Station, TX (Ocean Drilling Program), 1–140. doi:10.2973/odp.proc.ir.198.103.2002

Shipboard Scientific Party, 2002b. Site 1213. *In* Bralower, T.J., Premoli Silva, I., Malone, M.J., et al., *Proc. ODP, Init. Repts.,* 198: College Station, TX (Ocean Drilling Program), 1–110. doi:10.2973/odp.proc.ir.198.109.2002

Shipboard Scientific Party, 2004a. Site 1258. *In* Erbacher, J., Mosher, D.C., Malone, M.J., et al., *Proc. ODP, Init. Repts.,* 207: College Station, TX (Ocean Drilling Program), 1–117. doi:10.2973/odp.proc.ir.207.105.2004

Shipboard Scientific Party, 2004b. Site 1261. *In* Erbacher, J., Mosher, D.C., Malone, M.J., et al., *Proc. ODP, Init. Repts.,* 207: College Station, TX (Ocean Drilling Program), 1–103. doi:10.2973/odp.proc.ir.207.108.2004

Shipboard Scientific Party, 2004c. Explanatory notes. *In* Erbacher, J., Mosher, D.C., Malone, M.J., et al., *Proc. ODP, Init. Repts.,* 207: College Station, TX (Ocean Drilling Program), 1–94. doi:10.2973/odp.proc.ir.207.102.2004

Snow, L. J., Duncan, R. A., and Brawlower, T. J., 2005. Trace element abundances in the Rock Canyon Anticline, Pueblo, Colorado, marine sedimentary section and their relationship to Caribbean plateau construction and oxygen anoxic event 2. *Paleoceanography,* 20. doi:10.1029/2004PA001093.

Tsikos, H. 2004. Carbon-isotope stratigraphy recorded by the Cenomanian-Turonian Oceanic Anoxic Event: correlation and implications based on three key localities. *Jour. Geol. Soc.,* 161:703-709.

Visual 1, Active Leases and Infrastructure October 2007, Gulf of Mexico Outer Continental Shelf [Online]. Available from the World Wide Web: <http://www.gomr.mms.gov/homepg/lsesale/Visual1.pdf>. Cited [2008-03-17]

Wagreich, M. 2006. OAE3 and Upper Cretaceous oceanic red beds (CORB). *Geophysical Research Abstracts,* 8:02799.

Weissert, H., 2004. Volcanism, CO_2 and palaeoclimate: a Late Jurassic-Early Cretaceous carbon and oxygen isotope record. *Jour. Geol. Soc.*, 161:695-702.

Zelt, F. B., 1985. Natural gamma-ray spectrometry, lithofacies, and depositional environments of selected Upper Cretaceous marine mudrocks, western United States, including Tropic Shale and Tununk Member of Mancos Shale. Ph.D thesis, Princeton University, 284p.

APPENDIX A - GULF OF MEXICO WELLS WITH INDEX FOSSILS OF SANTONIAN, CONIANCIAN, TURONIAN, CENOMANIAN, ALBIAN, OR APTIAN AGE

Table A-1. Gulf of Mexico wells with index fossils of Santonian, Coniancian, Turonian, Cenomanian, Albian, or Aptian age.

API	Well name	Side Track	By Pass	Area Code[1]	Block Number
177242002700	002	00	00	MP	253
177242012700	004	00	00	MP	253
177244005200	002	00	00	MP	264
177244005400	006	00	00	MP	253
177244006300	001	00	00	MP	222
177244006800	001	00	00	MP	221
177244008400	002	00	00	MP	220
177244008500	001	00	00	MP	223
177244032900	001	00	01	MP	183
177244067600	001	00	00	MP	171
177254060900	001	00	00	MP	97
608154000700	A001	00	00	MO	823
608154000900	001	00	00	MO	826
608154001700	001	00	00	MO	1006
608154002800	A001	00	00	MO	821
608154002900	001	00	00	MO	862
608154003700	001	00	00	MO	999
608154005200	A001	00	00	MO	872
608164003700	001	00	00	VK	30
608164009300	001	00	00	VK	117
608164014601	002	01	00	VK	826
608164016100	001	00	00	VK	737
608164020600	001	00	00	VK	253
608164020800	001	00	01	VK	818
608214000000	001	00	00	PE	973
608214000200	002	00	00	PE	948
608224000000	001	00	00	DD	162
608224000600	001	00	00	DD	166
608224001200	001	00	00	DD	360
608224001400	003	00	00	DD	162
608224001600	001	00	01	DD	31
608224001700	001	00	00	DD	529
608224001800	001	00	00	DD	563
608224002200	001	00	00	DD	284
608234000000	001	00	00	DC	512

[1]Area Code Abbreviations: MP=Main Pass; MO=Mobile; VK=Vioska Knoll; PE=Pensacola; DD=Destin Dome; DC=Desoto Canyon.

APPENDIX B - OCEAN DRILLING PROGRAM SUMMARIES

Lithologic descriptions follow standard sediment phase diagrams used by the ODP(e.g. Shipboard Scientific Part; 2004c). Where multiple lithologies are present within a core, multiple ranges of constituent parts are provided.

Table B-1. Hole 103-641C (Galicia Bank; water depth 4640.0 m; total depth 305.3 mbsf; interval logged 130.0-196.0 mbsf).

Lith. unit	Lith. unit depth (mbsf)	Lith. unit depth (fbsf)	Description	Age[1]	Mean density dev. (g/cm^3)	Clay (%)	$CaCO_3$ (%)	Quartz (%)	Fit[2]?
II	53.6-53.9 Hole A	175.9-176.8	Black zeolitic clay corg rich.	Cen-Alb	N/A	N/A	N/A	N/A	
IIIA	53.9 - 63.6 Hole C	176.8-208.7	Greensih gray and gray nannofossil marl and calcareous clay badly disturbed by drilling.	Cen-Alb	N/A	N/A	N/A	N/A	
IIIB	150.9-202.6 Hole C	495.1-664.7	Massive black claystone, laminated black claystone, gray claystone, black and dark greenish gray claystone interbedded, greenish gray claystone-lightly bioturbated and faintly laminated, grayish green massive claystone. Corg 1-2% wt.	Alb	0.002	100-90	N/A	N/A	n
IIIB	150.9-199.0	495.1-652.9	Black and greenish gray claystone, massive and laminated	Alb	0.002	100-90	N/A	N/A	n
IIIB	199.0-208.7	652.9-684.7	Black and greenish gray claystone, and granule conglomerate	Alb- L Apt	N/A	N/A	N/A	N/A	
IV-V	208.7-228.0	684.7-748.0	Marlstone, calcareous claystone and calcarenite	L Apt	N/A	N/A	N/A	N/A	
V	228.0-237.6	748.0-779.5	Interbedded black and greenish gray claystone, carbonate-sand turbidites	E Apt	N/A	N/A	N/A	N/A	
V-VI	237.6-266.5	779.5-874.3	Calcareous microturbidites, marlstone and clayey limestone, contains organic matter and plant debris	E Apt-L Barr	N/A	N/A	N/A	N/A	
VI	266.5-276.2	874.3-906.2	Clayey limestone, calcareous microturbidites, and turbidites	L Barr	N/A	N/A	N/A	N/A	
VI	276.2-305.2	906.2-1001.3	Clayey limestone, calcareous microturbidites, marlstone, debris flow and slump deposits	L Barr	N/A	N/A	N/A	N/A	

[1]Age abbreviations: Cen=Cenomanian; Alb=Albian; Apt=Aptian; Barr=Barremian; L=Late; M=Middle; E=Early

[2]Fit refers to whether the mean density deviation fits the overall lithology pattern: y=yes, n=no; m=mixed lithology

Table B-2. Hole 159-959D (Cote d'Ivoire Ghana Margin; water depth 2090.9 m; total depth 1158.9 mbsf; interval logged 538.0-927.0 mbsf).

Lith. unit	Lith. unit depth (mbsf)	Lith. unit depth (fbsf)	Description	Age[1]	Mean density dev. (g/cm^3)	Clay (%)	$CaCO_3$ (%)	Quartz (%)	Fit[2]?
II	417.8-812.3	1370.7-2665.0	Diatomite, chert, porcellonite.	E Olig-L Pal	-0.018	N/A	N/A	N/A	y
IIA	417.8-427.3	1370.7-1401.9	Clayey diatomite with radiolarians,diatomite with clay, radiolarians, and organic matter-interbedded with nannofossil chalk and clay.	E Olig	-0.065	25-50, 10-25	N/A	75-50	y
IIB	427.3-484.6	1401.9-1589.9	Black chert and claystone. Organic matter throughout both making up to 20% bulk weight.	M-E Olig	-0.004	N/A	N/A	N/A	y
IIB	427.3-475.0	1401.9-1558.4	Clayey diatomite with radiolarians, diatomite with clay, radiolarians and organic matter, chert, porcellanite with clay	M-E Olig	-0.016	100-90, 0-10, 0-10, 10-25	N/A, N/A, N/A, 90-75	0-10, 100-90, 100-90, N/A	y
IIB	475.0-484.6	1558.4-1589.9	Chert, bituminous porcellenite with zeolite	M-E Olig	0.055	0-10, 0-10	0-10, 100-90	100-90, 0-10	m
IIC	484.6-812.3	1589.9-2665.0	Porcellanite with micrite and clay.	M-E Olig	-0.019	10-25	90-75	N/A	n
IIC	484.6-561.8	1589.9-1843.2	Porcellanite with clay and porcellanite	M-E Olig	-0.028	10 -25, 0-10	90-75, 100-90	N/A	n
IIC	561.8-600.2	1843.2-1969.5	Porcellanite, porcellanite with clay, porcellanite with micrite	L-M Eoc	-0.043	0-10, 10-25, 0-10	100-90, 90-75, 100-90	N/A	n
IIC	600.2-609.7	1969.5-2000.3	Porcellanite, porcellanite with organic matter, micritic porcellanite	M Eoc	-0.117	N/A	100-90	N/A	y m
IIC	609.7-764.2	2000.3-2507.2	Porcellanite with varying amounts of clay and micrite	M Eoc	-0.025	N/A	N/A	N/A	n m
IIC	764.2-812.3	2507.2-2665.0	Micritic porcellanite, porcellanite with nannofossil chalk, micritic chalk and chert	M Eoc-L Pal	0.053	N/A	100-90, 0-10	N/A, 100-90	y m
III	812.3-1043.3	2665.0-3422.9	Black claystone and claystone with nannofossils. Dark color = high pyrite concentrations	L Pal	0.037	N/A	N/A	N/A	m
III	812.3-831.6	2665.0-2728.4	Micrite nannofossil claystone, micrite claystone and black claystone	Maast	0.068	90-75, 100-90	10-25, N/A	N/A	y m
III	831.6-995.4	2728.4-3265.8	Black to gray claystone with varying amounts of glauconite, pyrite and organic matter	Maast	0.034	N/A	N/A	N/A	n

Lith. unit	Lith. unit depth (mbsf)	Lith. unit depth (fbsf)	Description	Age[1]	Mean density dev. (g/cm^3)	Clay (%)	$CaCO_3$ (%)	Quartz (%)	Fit[2]?
III	995.4-1005.0	3265.8-3297.2	Claystone and claystone with dolomite and barite, dark gray, faintly laminated to massive, pyrite is disseminated or occurs as fracture fill. Burrows in massive portions of the sediment.	Maast-L Sant	0.011	100-90, 90-75	0-10, 10-25	N/A	n
III	1005.0-1014.7	3297.2-3329.0	Claystone medium dark gray, massive to faintly laminated, disseminated pyrite throughout, some pyrite enrichments along laminae and as fracture fill, kaolinite fills some small cracks	Maast-L Sant	0.071	100-90	N/A	N/A	n
III	1014.7-1024.1	3329.0-3359.9	Claystone, meidum dark gray, massive to faintly lamanated, shell fragments and plant debris occur in laminated portions, which also contain glauconite, pyrite, and some calcite. Burrows occur in non-laminated portions. Dolomite fills some fractures. Some flecks of Kaolinite present. Fish debris present around 1016m.	Maast-L Sant	0.072	100-90	frac fill	N/A	m
III	1024.1-1033.7	3359.9-3391.4	Black claystone, parallel laminated, numerous dolomite crystals in upper portion, pyrite aggregation forms some laminations. Burrows disturb laminations slightly, pyrite disseminated throughout.	Sant-Con	0.023	100-90	frac fill	N/A	m
III	1033.7-1043.3	3391.4-3422.9	Nannofossil claystone with glauconite, claystone with nannofossils, and nannofossil claystone. Brown and black phosphatic nodules occur in the very middle and bottom most portions of this interval. Some clayey dolomite and nannofossil claystone with dolomite found in the core catcher.	Sant-Con	-0.016	90-75	10-25	N/A	y m
IV	1043.3-1081.7	3422.9-3548.9	Sandy limestone, sandy dolomite, calcareous sandstone.	E Tur	N/A	N/A	N/A	N/A	
IV	1043.3-1053.0	3422.9-3454.7	Sandy limestone and sandy dolomite	E Tur	N/A	N/A	N/A	N/A	
IV	1053.0-1062.7	3454.7-3486.6	Calcareous sandstone and conglomerate	L Alb	N/A	N/A	N/A	N/A	

Lith. unit	Lith. unit depth (mbsf)	Lith. unit depth (fbsf)	Description	Age[1]	Mean density dev. (g/cm^3)	Clay (%)	$CaCO_3$ (%)	Quartz (%)	Fit[2]?
IV	1062.7-1081.7	3486.6-3548.9	Limestone and dolomitic limestone	L Alb	N/A	N/A	N/A	N/A	

[1]Age abbreviations:Olig=Oligocene; Eoc=Eocene; Pal=Paleocene; Maast=Maastrichtian; Sant=Santonian; Con=Coniacian; Tur=Turonian; Cen=Cenomanian; Alb=Albian; L=Late; M=Middle; E=Early

[2]Fit refers to whether the mean density deviation fits the overall lithology pattern: y=yes, n=no; m=mixed lithology

Table B-3. Hole 171B-1052E (Cote d'Ivoire Ghana Margin; water depth 1345.3 m; total depth 673.3 mbsf; interval logged 220.0-657.6 mbsf).

Lith. unit	Lith. unit depth (mbsf)	Lith unit depth (fbsf)	Description	Age[1]	Mean density dev. (g/cm^3)	Clay (%)	$CaCO_3$ (%)	Quartz (%)	Fit[2]?
II	140.0-204.0	459.3-669.3	Nannofossil chalk and foraminifer chalk with chert layers and porcellanitic calcareous claystone	M Eoc-L Pal	N/A	N/A	N/A	N/A	
III	204.0-301.6	669.3-989.5	Nannofossil claystone and calcareous claystone with zeolite, calcareous claystone, nannofossil and calcareous chalk with clay and foraminifer chalk. NOTE-contains ash layer, base = K/T boundary. GR low here but UR higher than K or Th.	L-E Pal	N/A	N/A	N/A	N/A	
III	204.0-213.6	669.3-700.8	Zeolitic nannofossil claystone with carbonate grains and pyrite alternating with carbonate claystone	L-E Pal	N/A	N/A	N/A	N/A	
III	213.6-223.2	700.8-732.3	Nannofossil claystone with zeolite and pyrite alternating with carbonate claystone	L-E Pal	N/A	N/A	N/A	N/A	
III	223.2-232.8	732.3-763.8	Nannofossil claystone to carbonate claystone with nannofossil claystone	L-E Pal	N/A	N/A	N/A	N/A	
III	232.8-242.4	763.8-795.3	Clayey nannofossil chalk with zeolites alternating with carbonate chalk with zeolite	L-E Pal	N/A	N/A	N/A	N/A	
III	242.4-252.0	795.3-826.8	Clayey nannofossil chalk that grades into carbonate chalk with clay and nannofossils	L-E Pal	-0.067	25-50, 10-25	75-50, 90-75	N/A	m
III	252.0-261.7	826.8-858.6	Nannofossil chalk with foraminifers, clay, and carbonate grains	L-E Pal	-0.052	10-25	90-75	N/A	n
III	255.0-255.1	836.6-836.9	Altered ash with biotite	L-E Pal	-0.065	N/A	N/A	N/A	N/A

Lith. unit	Lith. unit depth (mbsf)	Lith unit depth (fbsf)	Description	Age[1]	Mean density dev. (g/cm^3)	Clay (%)	$CaCO_3$ (%)	Quartz (%)	Fit[2]?
III	261.7-271.3	858.6-890.1	First 28cm = calcareous chert, rest is carbonate claystone with nannofossils	L-E Pal	-0.043	N/A, 0-10	25-50, 100-90	75-50, 0-10	n m
III	271.3-272.3	890.1-893.4	Foraminifer claystone with nannofossils and carbonate grains	L-E Pal	-0.018	90-75	10-25	10-25	y
III	272.3-280.9	893.4-921.6	Claystone with nannofossils and carbonate grains	L-E Pal	-0.066	90-75	10-25	10-25	y
III	280.9-290.5	921.6-953.1	Nannofossil claystone that grades into nannofossil claystone with foraminifers	L-E Pal	-0.057	90-75	10-25	10-25	y
III	290.5-296.0	953.1-971.1	Carbonate chalk with clay and foraminifers alternating with chalk with zeolite and foraminifers	L-E Pal	-0.053	0-10	100-90	0-10	n
III	296.0-298.0	971.1-977.7	Clayey foraminifer chalk with quartz silt, numerous glauconitic pellets	L-E Pal	-0.064	25-50	75-50	25-50	m
III	298.0-300.1	977.7-984.6	Clayey foraminifer chalk	L-E Pal	-0.057	25-50	75-50	N/A	n
IV	301.6-477.4	984.6-1566.3	Clayey nannofossil chalk, nannofossil chalk with clay and nannofossil chalk.	L Maast	0.018	N/A	N/A	N/A	y
IV	300.1-319.3	984.6-1047.6	Nannofossil chalk with foraminifers and calicispheres, nannofossil chalk with clay	L Maast	0.001	0-10, 10-25	100-90, 90-75	N/A	y
IV	319.3-386.7	1047.6-1268.5	Nannofossil claystone	L Maast	0.019	90-75	10-25	N/A	y m
IV	386.7-396.3	1268.5-1300.2	Carbonate claystone with foraminifers, claystone with foraminifers and carbonate grains, and foraminifer carbonate chalk with nannofossils	L Maast	0.009	90-75, 0-10	10-25, 100-90	N/A	y m
IV	396.3-405.9	1300.2-1331.7	Clayey nannofossil chalk and clayey nannofossil chalk with carbonate grains	L Maast	0.015	25-50	75-50	N/A	y
IV	405. 9-444.3	1331.7-1457.7	Nannofossil claystone, claystone with calcareous microfossils	L Maast	0.022	100-90	0-10	N/A	y m
IV	444.3-453.9	1457.8-1489.2	Carbonate claystone and foraminifer claystone with nannofossils	L Maast	0.022	100-90	0-10	N/A	y
IV	453.9-473.2	1489.2-1552.5	Nannofossil claystone with carbonate grains, nannofossil claystone	L Maast	0.023	100-90	0-10	N/A	y
VA	477.4-511.8	1566.3-1679.1	Dark olive silty claystone, calcareous claystone	Cen-L Alb	0.010	N/A	N/A	N/A	y

Lith. unit	Lith. unit depth (mbsf)	Lith unit depth (fbsf)	Description	Age[1]	Mean density dev. (g/cm^3)	Clay (%)	$CaCO_3$ (%)	Quartz (%)	Fit[2]?
VA	473.2-482.8	1552.5-1584.0	Nannofossil limestone with foraminifers and clay, micritic limestone with foraminifers and calcispheres, and clayey foraminiferal limestone	Cen-L Alb	0.006	0-10, 25-50	100-90, 75-50	N/A	y
VA	482. 8-492.4	1584.0-1615.5	Clayey nannofossil chalk and nannofossil chalk with clay	Cen-L Alb	0.023	25-50, 0-10	75-50, 100-90	N/A	y
VA	492.8-502.0	1615.5-1647.0	Nannofossil limestone with clay and Micritic limestone with clay and calcispheres	Cen-L Alb	0.019	10-25	90-75	N/A	y
VA	502.0-510.6	1647.0-1675.2	Nannofossil limestone with clay, silty limestone and claystone with nannofossils and foraminifers	Cen-L Alb	-0.010	10-25, 25-50, 100-90	90-75, 75-50, 0-10	N/A	y m
VB	511.3-633.5	1677.5-2078.4	Dark claystone, black shale, calcareous claystone, silty claystone, clayey limestone with foraminifers and quartz and clayey siltstone. These alternate beginning and ending with black "shale." R rich in pyrite, contain clay with varying amounts of calcareous nannofossils, fine silt sized quartz, fish remains, and organic debris. This one has terrigenous material. There is a lot of calcium material judging from the core descriptions.	L Alb	-0.004	N/A	N/A	N/A	y
VB	510.6-520.3	1675.2-1707.0	The upper most portion contains nannofossil claystone with zeolite and claystone with organic remains. The rest is black shale alternating with coarse grained foram rich claystone	L Alb	0.012	90-75, 100-90	10-25, 0-10	N/A	n m
VB	520.3-523.0	1707.0-1715.9	Nannofossil claystone with pyrite and carbonate claystone with nannofossils and limestone	L Alb	0.010	90-75	10-25	N/A	y
VB	523.0-529.9	1715.9-1738.5	Carbonate claystone with nannofossils grading into massive limestone-bottom portion contains pyritized laminae	L Alb	-0.038	90-75, 0-10	10-25, 100-90	N/A	n m

Lith. unit	Lith. unit depth (mbsf)	Lith unit depth (fbsf)	Description	Age[1]	Mean density dev. (g/cm^3)	Clay (%)	$CaCO_3$ (%)	Quartz (%)	Fit[2]?
VB	529.9-539.5	1738.5-1770.0	Claystone with quartz silt and carbonate grains and claystone with quartz and feldspar silt and calcareous microfossils-at roughly 531m there is a clayey limestone interval	L Alb	-0.016	90-75	10-25	10-25	y
VB	539.5-548.1	1770.0-1798.2	Claystone with nannofossils	L Alb	-0.014	90-75	10-25	N/A	n
VB	548.1-558.7	1798.2-1833.0	Carbonate claystone	L Alb	-0.008	75-50	25-50	N/A	n
VB	558.7-568.3	1833.0-1864.5	Clayey limestone with foraminifers to carbonate claystone with quartz	L Alb	-0.028	25-50, 75-50	75-50, 25-50	25-50	m
VB	568.3-606.9	1864.5-1991.1	Claystone with carbonate grains	L Alb	0.005	90-75	10-25	N/A	y

[1]Age abbreviations:Olig=Oligocene; Eoc=Eocene; Pal=Paleocene; Maast=Maastrichtian; Sant=Santonian; Con=Coniacian; Tur=Turonian; Cen=Cenomanian; Alb=Albian; L=Late; M=Middle; E=Early

[2]Fit refers to whether the mean density deviation fits the overall lithology pattern: y=yes, n=no; m=mixed lithology

Table B-4. Hole 198-1207B (Shatsky Rise North; water depth 3103.0 m; total depth 622.8 mbsf; interval logged 125.5-622.0 mbsf).

Lith. unit	Lith. unit depth (mbsf)	Lith unit depth (fbsf)	Description	Age[1]	Mean density dev. (g/cm^3)	Clay (%)	$CaCO_3$ (%)	Quartz (%)	Fit[2]?
Ia & b?	157-166.5	515.1-546.3	Nannofossil ooze. Peak in gr at base = Campanian-Miocene unconformity and manganese nodule layer.	Hol-M Mio	0.021	0-10	100-90	0-10	y
II	166.5-335.3	546.3-1100.1	Nannofossil ooze with chert.	L Camp-E Tur	-0.001	N/A	90-75	25-Oct	y m
II	166.6-195.5	546.6-641.4	Nannofossil ooze with inorganic calcite	L Camp-E Tur	0.027	N/A	100-90	N/A	y
II	195.5-214.7	641.4-704.4	Nannofossil ooze with foraminifers	L Camp-E Tur	0.003	N/A	100-90	N/A	y
II	220.1-229.8	704.4-753.9	Chert	L Camp-E Tur	0.022	N/A	N/A	100-90	n
II	229.8-239.4	753.9-785.4	Nannofossil ooze, minor chert	L Camp-E Tur	-0.022	N/A	100-90, 0-10	0-10, 100-90	m
II	239.4-316.0	785.4-1036.8	Chert, minor porcellanite as inclusions or coating the chert	L Camp-E Tur	0.000	N/A	0-10, 100-90	100-90, 0-10	m
II	316.0-325.6	1036.8-1067.3	Chert, minor limestone	L Camp-E Tur	-0.038	N/A	0-10	100-90	m

Lith. unit	Lith. unit depth (mbsf)	Lith unit depth (fbsf)	Description	Age[1]	Mean density dev. (g/cm^3)	Clay (%)	$CaCO_3$ (%)	Quartz (%)	Fit[2]?
II	325.6-335.3	1067.3-1100.1	Chert, minor porcellanite as inclusions or coating the chert	L Camp-E Tur	-0.070	N/A	0-10, 100-90	100-90, 0-10	y m
III	335.3-603.5	1100.1-1980.0	Limestone and chert-VERY poor recovery throughout	E Tur-L Barr	0.003	N/A	0-10, 100-90	100-90, 0-10	y m
III	335.3-354.5	1980.0-1162.7	Chert with some porcellanite	E Tur-E Apt	-0.031	N/A	0-10, 100-90	100-90, 0-10	y m
III	354.5-364.1	1162.7-1194.6	Nannofossil chalk	E Tur-E Apt	-0.032	0-10	100-90	0-10	n
III	364.1-412.1	1194.6-1352.0	Chert with some porcellanite	E Tur-E Apt	-0.024	N/A	0-10, 100-90	100-90, 0-10	y m
III	412.1-421.7	1352.0-1383.5	Nannofossil ooze with clay	E Tur-E Apt	0.006	25-Oct	90-75	25-Oct	y
III	421.7-526.5	1383.5-1727.4	Chert with some porcellanite or chalk	E Tur-E Apt	0.018	N/A	0-10, 100-90	100-90, 0-10	n m
III	526.5-536.2	1727.4-1759.2	Nannofossil limestone with foraminifers	E Tur-E Apt	0.024	N/A	100-90	N/A	y
III	536.2-565.0	1759.2-1853.7	Chert and nannofossil limestone with clay	E Tur-E Apt	0.034	0-10, 10-0	0-10, 100-90	100-90, 0-10	n m
III	565.0-574.0	1853.7-1883.2	45cm thick corg rich dark yellowish brownmudstone. Core (198-1207B-44R-1, 60-105cm) OAE 1a	E Apt	-0.032	100-90	N/A	N/A	y
III	574.0-593.8	1883.2-1948.2	Chert, limestone and cherty limestone	E Apt-L Barr	0.003	0-10, 0-10, N/A	0-10, 100-90, 75-50	100-90, 0-10, 25-50	y m
III	593.8-622.8	1948.2-2043.3	Clayey limestone and clayey limestone with nannofossils	E Apt-L Barr	N/A	N/A	N/A	N/A	

[1]Age abbreviations:Hol=Holocene; Mio=Miocene; Camp=Campanian; Tur=Turonian; Cen=Cenomanian; Alb=Albian; Apt=Aptian; Barr=Barremian; L=Late; M=Middle; E=Early
[2]Fit refers to whether the mean density deviation fits the overall lithology pattern: y=yes, n=no; m=mixed lithology

Table B-5. Hole 198-1213B (Shatsky Rise North; water depth 3883.0 m; total depth 494.7 mbsf; interval logged 188.0-431.0 mbsf).

Lith. unit	Lith. unit depth (mbsf)	Lith unit depth (fbsf)	Description	Age[1]	Mean density dev. (g/cm^3)	Clay (%)	$CaCO_3$ (%)	Quartz (%)	Fit[2]?
IIIA	85.4-179.6	280.2-589.2	Dark Gray chert interbedded with light gray-various colored porcellanite and limestone.	E Cen-L Alb	N/A	N/A	N/A	N/A	
IIIB	179.6-256.8	589.2-839.9	Brown, red, yellow, gray porcellanite.	L Alb-E Apt	N/A	N/A	N/A	N/A	
IIIB	189.7-218.6	622.4-717.2	Chert with minor porcellanite	L Alb-E Apt	N/A	N/A	N/A	N/A	
IIIB	218.6-256.8	717.2-842.5	Chert with radiolarite or radiolarian porcellanite	L Alb-E Apt	0.012	N/A	N/A	N/A	m
IIIC	256.8-266.4	839.9-874.0	Pelegic environment. Interbedded clayey porcellanite, Corg rich, and radiolarian porcellanite, minor altered tuff. Partial core OAE1a = 198-1213B-8R.	E Apt	-0.016	25-50, N/A, N/A	75-50, 90-75, N/A	N/A, 10-25, N/A	y m
IIID	266.4-410.3	874 .0-1346.1	Chert, porcellanite, nannofossil chalk to clayey nannofossil chalk.	Haut-Berr	-0.001	N/A	N/A	N/A	y m
IIIE	410.3-447.8	1346.1-1469.2	Chert, porcellanite, claystone with nannofossils.	Berr	N/A	N/A	N/A	N/A	
IV	447.8-494.7	1469.2-1623.0	Igneous rock: dolerite and basalt.	Unkn	N/A	N/A	N/A	N/A	

[1]Age abbreviations:Cen=Cenomanian; Alb=Albian; Apt=Aptian; Haut=Hauterivian; Berr=Berriasian; L=Late; M=Middle; E=Early; Unkn=unknown

[2]Fit refers to whether the mean density deviation fits the overall lithology pattern: y=yes, n=no; m=mixed lithology

Table B-6. Hole 207-1258C (Demerara Rise; water depth 3192.2 m; total depth 485.0 mbsf; interval logged 86.0-488.0 mbsf).

Lith. unit	Lith. unit depth (mbsf)	Lith unit depth (fbsf)	Description	Age[1]	Mean density dev. (g/cm^3)	Clay (%)	$CaCO_3$ (%)	Quartz (%)	Fit[2]?
I	0.0-56.4	0-185.0	Nannofossil ooze with foraminifers * not cored in Hole C.	Camp	N/A	N/A	N/A	N/A	N/A
II	120.0-264.9	393.7-869.1	Nannofossil chalk with forams, calcareous chalk with forams.	M Eoc-Maast	-0.001	N/A	N/A	N/A	n

Lith. unit	Lith. unit depth (mbsf)	Lith unit depth (fbsf)	Description	Age[1]	Mean density dev. (g/cm^3)	Clay (%)	$CaCO_3$ (%)	Quartz (%)	Fit[2]?
II	120.0-129.4	393.7-424.5	Foraminifer nannofossil chalk with clay and nannofossil chalk with foraminifers	M Eoc-Maast	-0.018	0-10	90-10	0-10	n
II	129.4-139.0	424.5-456.0	Nannofossil chalk with clay, foraminifer and nannofossil chalk with radiolarians. Minor lithologies inlude nannofossil claystone with calcispheres and lepispheres	M Eoc-Maast	-0.006	25-10	75-90	25-10	n m
II	139.0-177.5	456.0-582.3	Radiolarian and nannofossil chalk with foraminifers	M Eoc-Maast	0.022	25-10	75-90	25-10	y m
II	177.5-264.6	582.3-869.1	Clayey nannofossil chalk with calcite and foraminifers, nannofossil chalk, and claystone.	M Eoc-Maast	-0.008	50-25, 10-0, 90-100	50-75, 90-100, 10-0	50-0, 10-0, 90-100	n
III	384.8-393.7	1262.5-1291.7	Clayey nannofossil chalk. Abundant barite & pyrite crystals	Camp	0.072	50-25	50-75	N/A	y
IV	389.8-394.4	1262.5-1292.7	Nannofossil chalk with clay or foraminifers	Camp	0.072	25-10	75-90	N/A	y
IV	393.7-449.6	1291.7-1294.0	Laminated black shale / chalk / limestone / clayey nannofossil chalk / limestone with organic matter.	Tur-M-L Alb	-0.016	N/A	N/A	N/A	m
IV	394.4-423.3	1292.7-1388.8	Nannofossil clay, limestone with foraminifers and organic matter, clayey nannofossil chalk with organic matter, clay with foraminifers and organic matter	Tur-M-L Alb	-0.039	75-90, 0-10, 90-100	25-10, 90-100, 10-0	N/A	y m
IV	423.3-428.3	1388.8-1405.2	Foraminifer nannofossil chalk with clay and calcareous sand with foraminifers	Tur-M-L Alb	-0.123	0-10, 50-75	100-90, 50-25	0-10, 50-75	m
IV	428.3-432.9	1405.2-1420.3	Black clayey nannofossil chalk	Tur-M-L Alb	-0.025	50-25	50-75	N/A	y m
IV	432.9-437.9	1420.3-1436.7	Nannofossil clay alternating with limestone with foraminifers and organic matter	Tur-M-L Alb	0.058	75-90, 10-0	25-10, 90-100	N/A	y m
IV	437.9-449. 6	1436.7-1473.1	Black clay with organic matter and nannofossils, and limestone with foraminifers and organic matter	Tur-M-L Alb	0.053	90-100, 10-0	10-0, 90-100	N/A	n m
V	449.6-484.9	1473.1-1590.9	Phosphatic calcareous claystone with organic matter.	E Alb	0.004	N/A	N/A	N/A	n m

Lith. unit	Lith. unit depth (mbsf)	Lith unit depth (fbsf)	Description	Age[1]	Mean density dev. (g/cm^3)	Clay (%)	$CaCO_3$ (%)	Quartz (%)	Fit[2]?
V	449.6-476.0	1509.9-1561.7	Black clay with nannofossils and organic matter, and limestone with foraminifers and organic matter, limestone nodules and phosphatic nodules through out	E Alb	N/A	N/A	N/A	N/A	
V	476.0-480.7	1561.7-1577.1	Nannofossil clay with foraminifers, calcite and opaques	E Alb	N/A	N/A	N/A	N/A	
V	480.7-485.0	1577.1-1591.2	Clay with carbonate and organic matter	E Alb	N/A	N/A	N/A	N/A	

[1]Age abbreviations:Eoc=Eocene; Maast=Maastrichtian; Camp=Campanian; Tur=Turonian; Cen=Cenomanian; Alb=Albian; L=Late; M=Middle; E=Early

[2]Fit refers to whether the mean density deviation fits the overall lithology pattern: y=yes, n=no; m=mixed lithology

Table B-7. Hole 207-1261B (Demerara Rise; water depth 1899.0 m; total depth 665.9 mbsf; interval logged 110.0-665.0 mbsf).

Lith. unit	Lith. unit depth (mbsf)	Lith unit depth (fbsf)	Description	Age[1]	Mean density dev. (g/cm^3)	Clay (%)	$CaCO_3$ (%)	Quartz (%)	Fit[2] ?
I	0.0-369.3	0.0-1211.6	Nannofossil ooze, nannofossil clay, clayey nannofossil ooze.	Pleist-L Mio	N/A	50-75	50-25	N/A	
II	369.3-491.7	1211.6-1613.2	Calcareous chalk, nannofossil chalk & limestone.	M Eoc-E Eoc	-0.008	50-25, 0-10	50-75, 100-90	50-25, 0-10	n
III	< 530.0-563.0	< 1738.8-1847.1	Clayey chalk with zeolites to calcareous claystone	L Pal-Camp	0.043	50-25	50-75	N/A	y
IV	563.0-650.21	1847.1-2133.2	Calcareous claystone (black laminated) with organic matter, clayey chalk with nannofossils and organic matter, glauconitic limestone with phosphatic nodules, and clayey limestone. The organic claystone is interbedded with limestone.	Sant-L Cen	N/A	50-75, 0-10	50-25, 100-90	N/A	

Lith. unit	Lith. unit depth (mbsf)	Lith unit depth (fbsf)	Description	Age[1]	Mean density dev. (g/cm^3)	Clay (%)	$CaCO_3$ (%)	Quartz (%)	Fit[2] ?
IV	563.0-568.4	1847.1-1864.8	Claystone, nannofossil, foraminifer and clay chalk with calcite and organic matter	Sant-L Cen	0.094	100-90, 25-10	0-10, 75-90	N/A	y
IV	568.4-578.0	1864.8-1896.3	Black clayey chalk with organic matter and chalk with clay	Sant-L Cen	0.044	50-25, 25-10	50-75, 75-90	N/A	y
IV	578.0-597.2	1896.3-1959.3	Calcareous claystone and clayey chalk	Sant-L Cen	0.023	50-75, 50-25	50-25, 50-75	N/A	y
IV	597.2-606.8	1959.3-1990.8	Claystone with foraminifers and micrite, limestone, and glauconitic limestone with phosphatic nodules	Sant-L Cen	-0.054	75-90, 0-10	25-10, 10-100	N/A	y m
IV	606.8-626.0	1990.8-2053.8	Calcareous claystone with foraminifiers and clayey chalk	Sant-L Cen	-0.045	50-75, 50-25	50-25, 50-75	50-25	y m
IV	626.0-635.6	2053.8-2085.3	Limestone, calcareous chalk with foraminifers	Sant-L Cen	-0.038	0-10	100-90	0-10	n
IV	635.6-650.2	2085.3-2133.2	Calcareous clay with nannofossils, and calcareous claystone. Minor lithology = limestone.	Sant-L Cen	N/A	N/A	N/A		
V	650.2-665.9	2133.2-2184.9	Quartz sandstone.	Alb?	N/A	N/A	N/A	90-100	

[1]Age abbreviations:Pleist=Pleistocene; Mio=Miocene; Eoc=Eocene; Pal=Paleocene; Camp=Campanian; Sant=Santonian; Cen=Cenomanian; Alb=Albian; L=Late; M=Middle; E=Early

[2]Fit refers to whether the mean density deviation fits the overall lithology pattern: y=yes, n=no; m=mixed lithology

APPENDIX C - BOREHOLE LOGS AND ORGANIC CARBON DATA THROUGH OAE INTERVALS IN ODP HOLES

Figure C-1. Hole 103-641C; log response and organic carbon percent through total logged interval of hole. The red line across logs indicates the upper boundary of Albian-age rocks, which continue below total depth of hole.

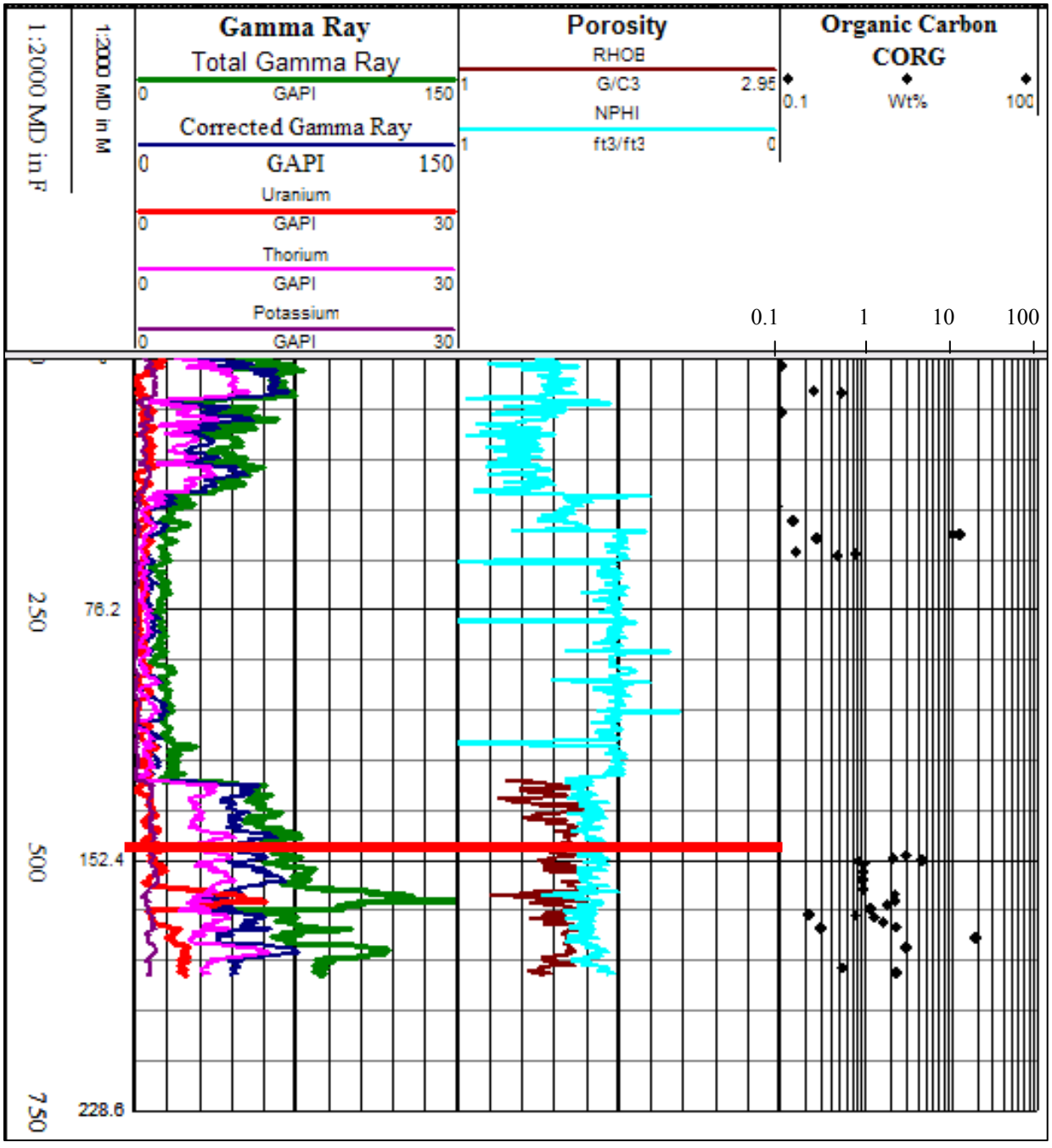

Figure C-2. Hole 103-641C; log response and organic carbon percent through Albian-age organic-rich, black claystone. The red line across logs indicates the upper boundary of Albian-age rocks, which continue past total depth of hole.

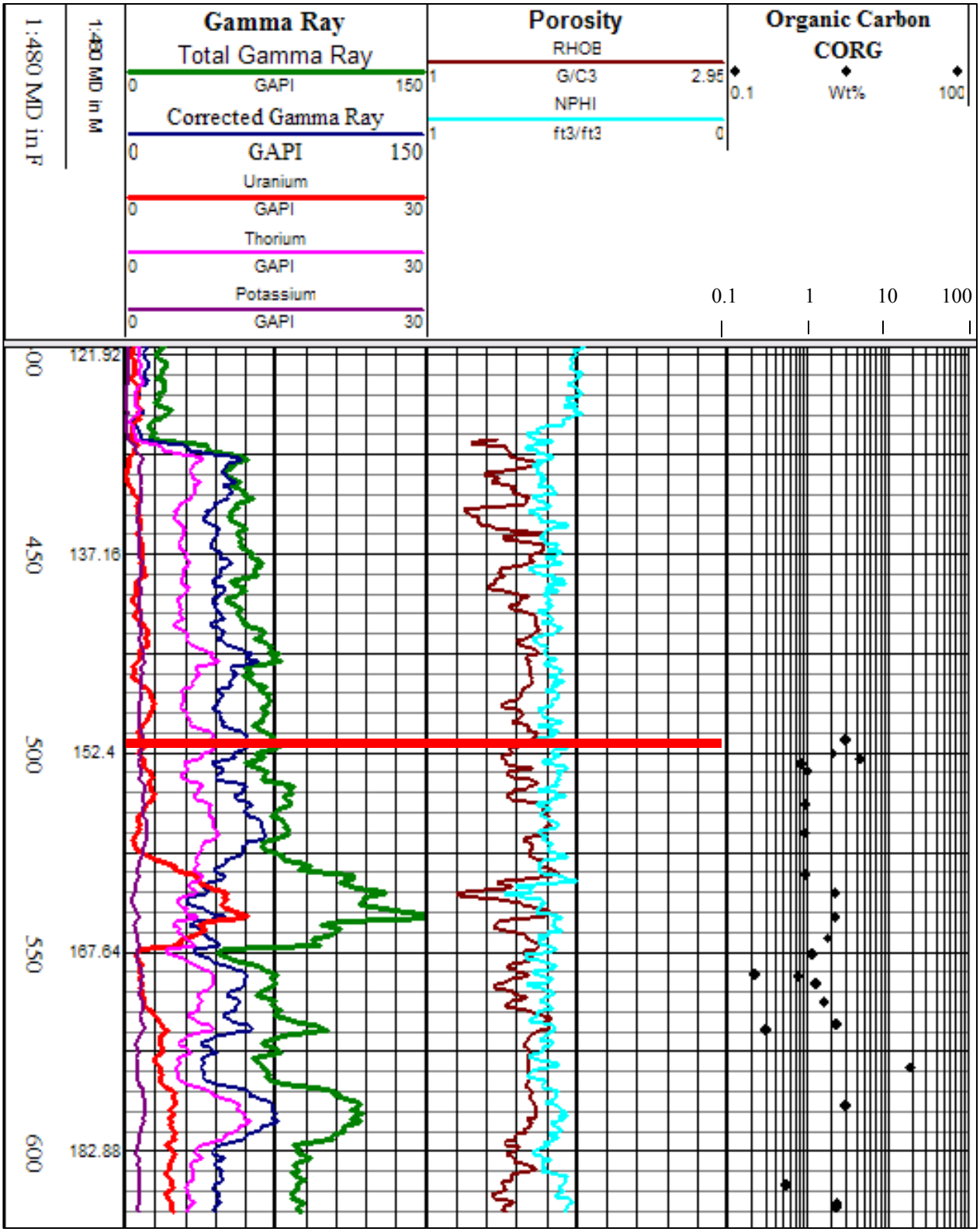

Figure C-3. Hole 159-959D; log response and organic carbon percent through total logged interval. The red lines across the logs indicate the upper boundary of lithologies associated with OAE 3 and a light green line indicates the lower boundary.

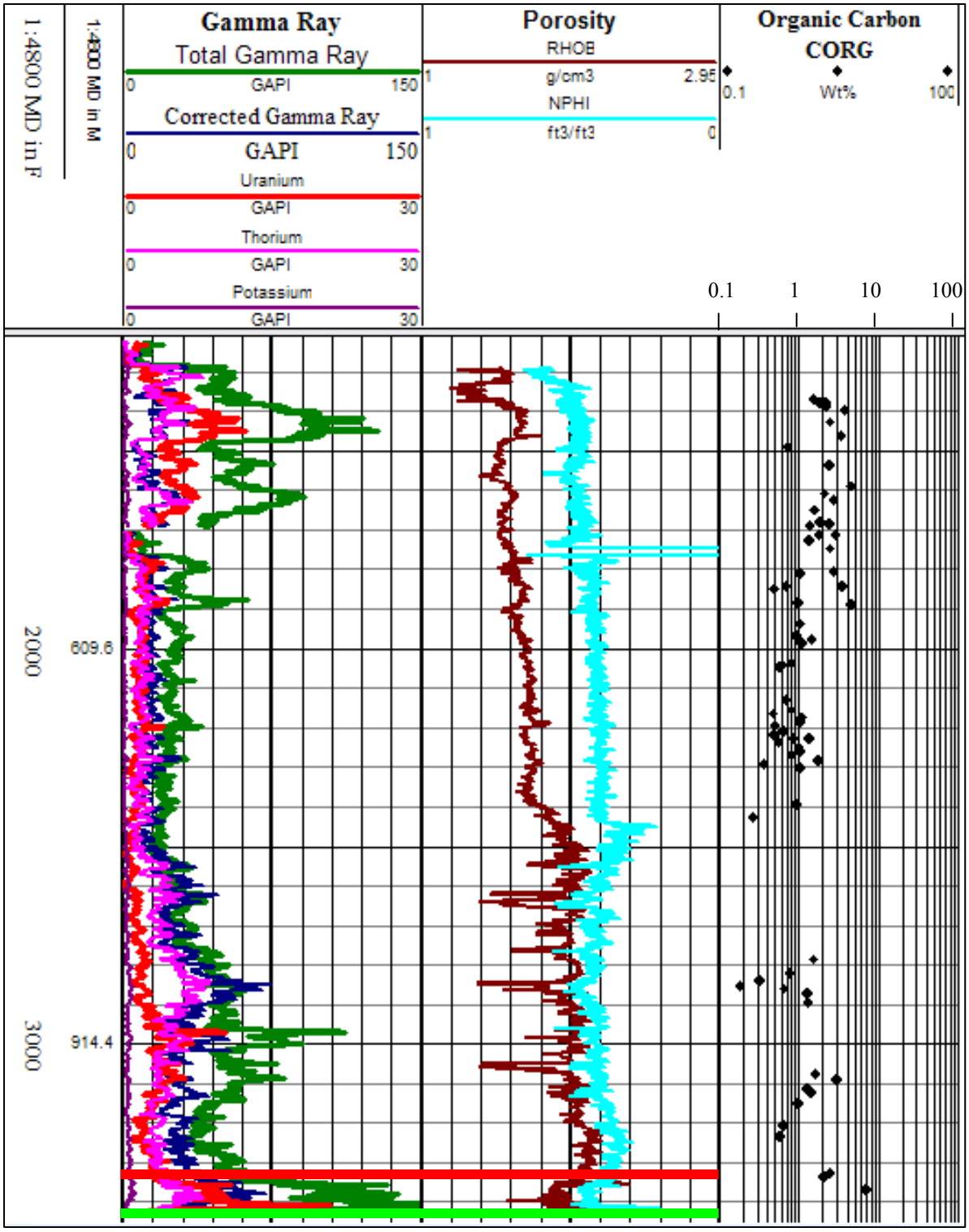

Figure C-4. Hole 159-959D; log response and organic carbon percent through OAE 3. The red lines across the logs indicate the upper boundary of lithologies associated with OAE 3 and a light green line indicates the lower boundary.

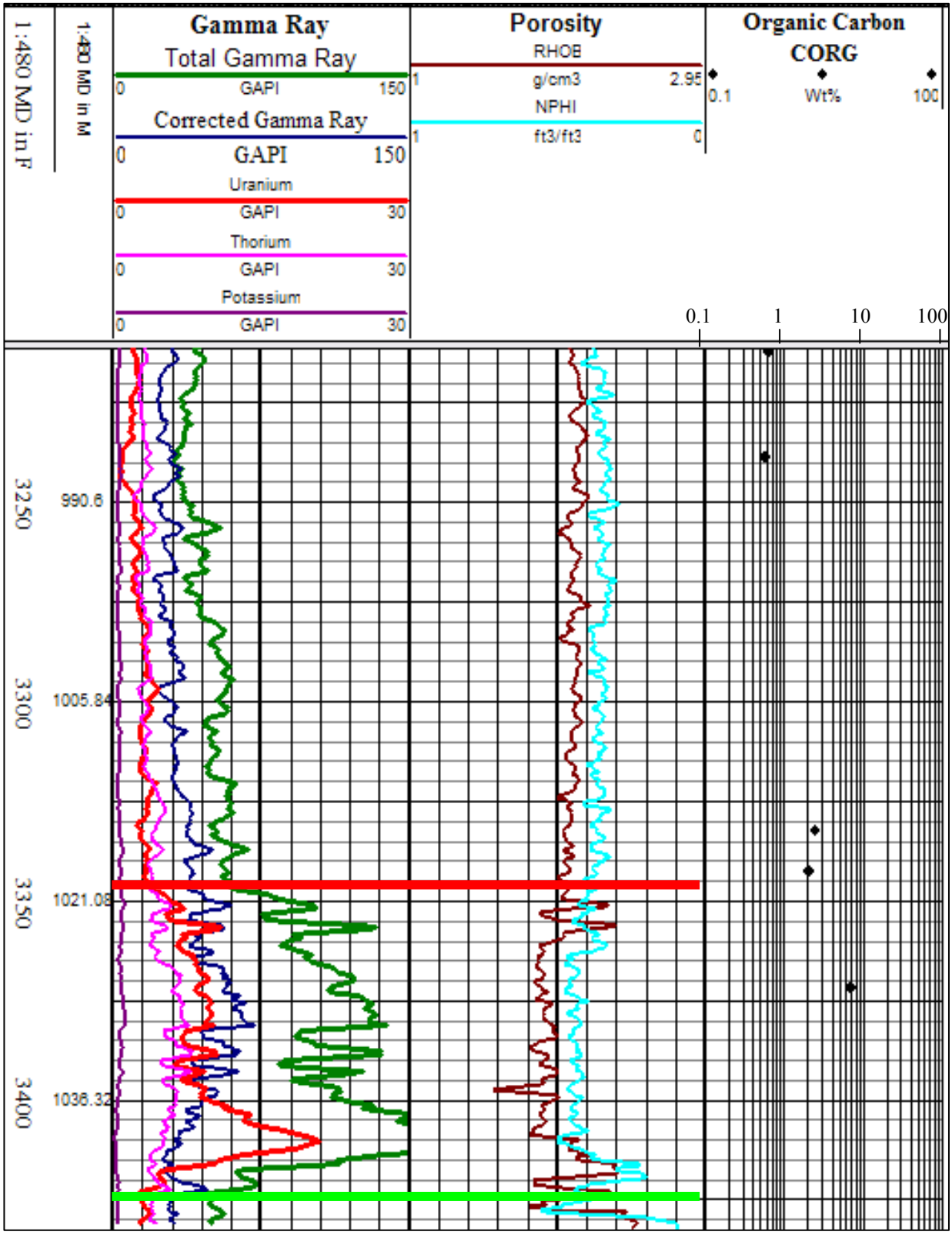

Figure C-5. Hole 171B-1052E; well log response and organic carbon percent through total logged interval. The red line across logs indicates the upper boundaries of OAE 1d and a light green line indicates the lower boundary.

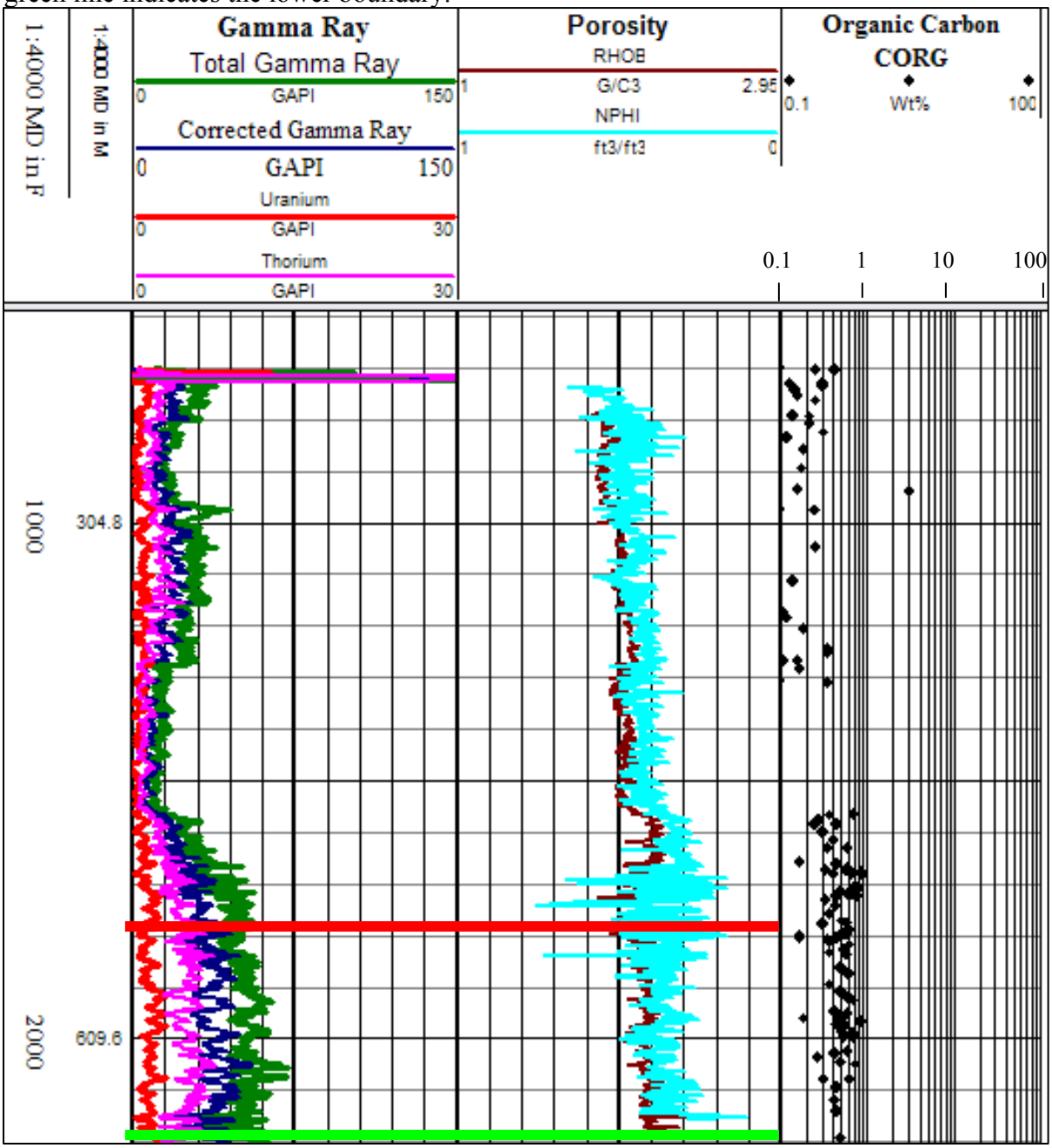

Figure C-6. Hole 171B-1052E; log response and organic carbon percent through black claystone associated with deposition during OAE 1d. The red line across logs indicates the upper boundaries of Late Albian-age organic-rich claystone and a light green line indicates the lower boundary.

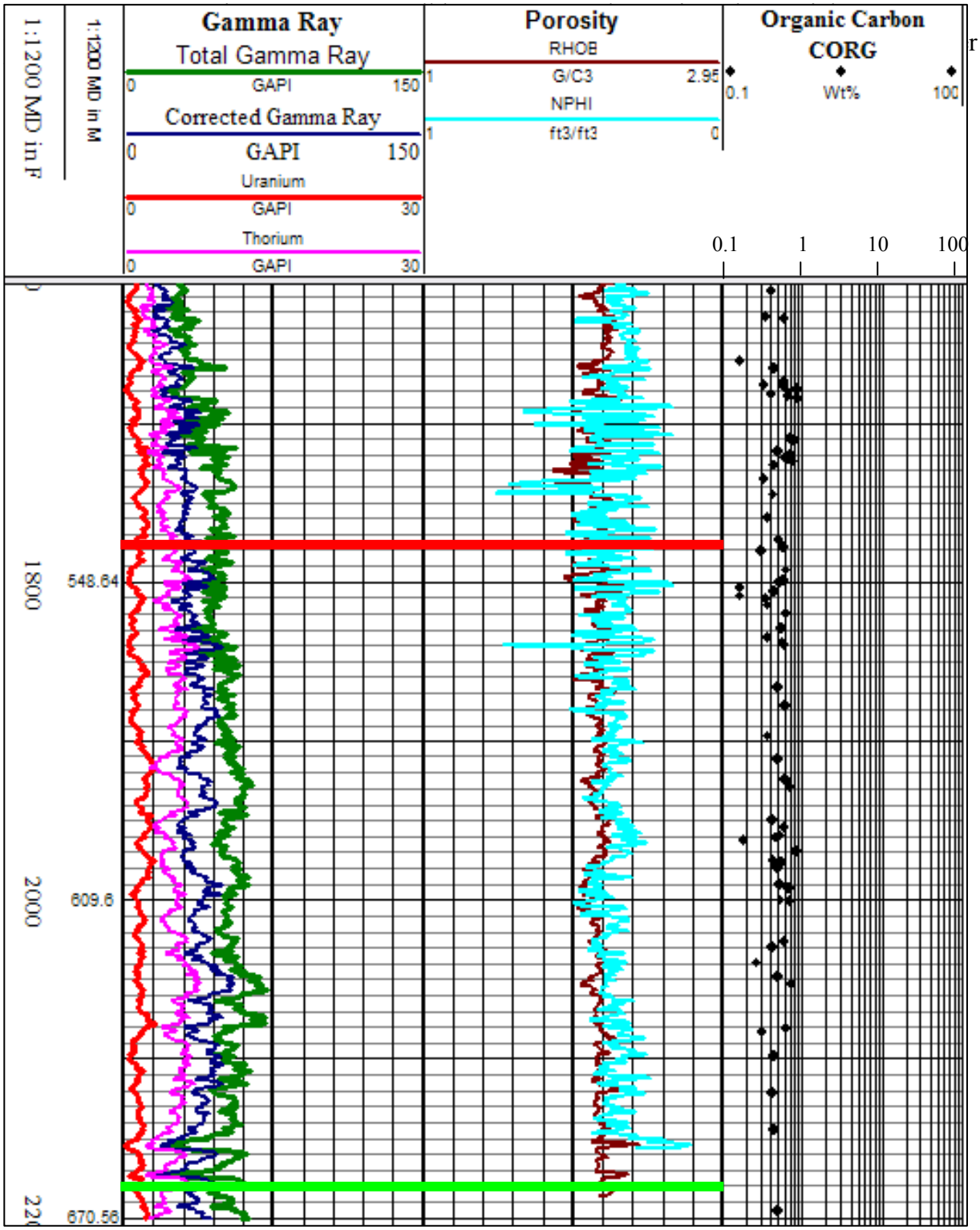

Figure C-7. Hole 198-1207B; log response and organic carbon weight percent through total logged interval. Orange arrow shows approximate depth at which lithologies associated with OAE 1a occur.

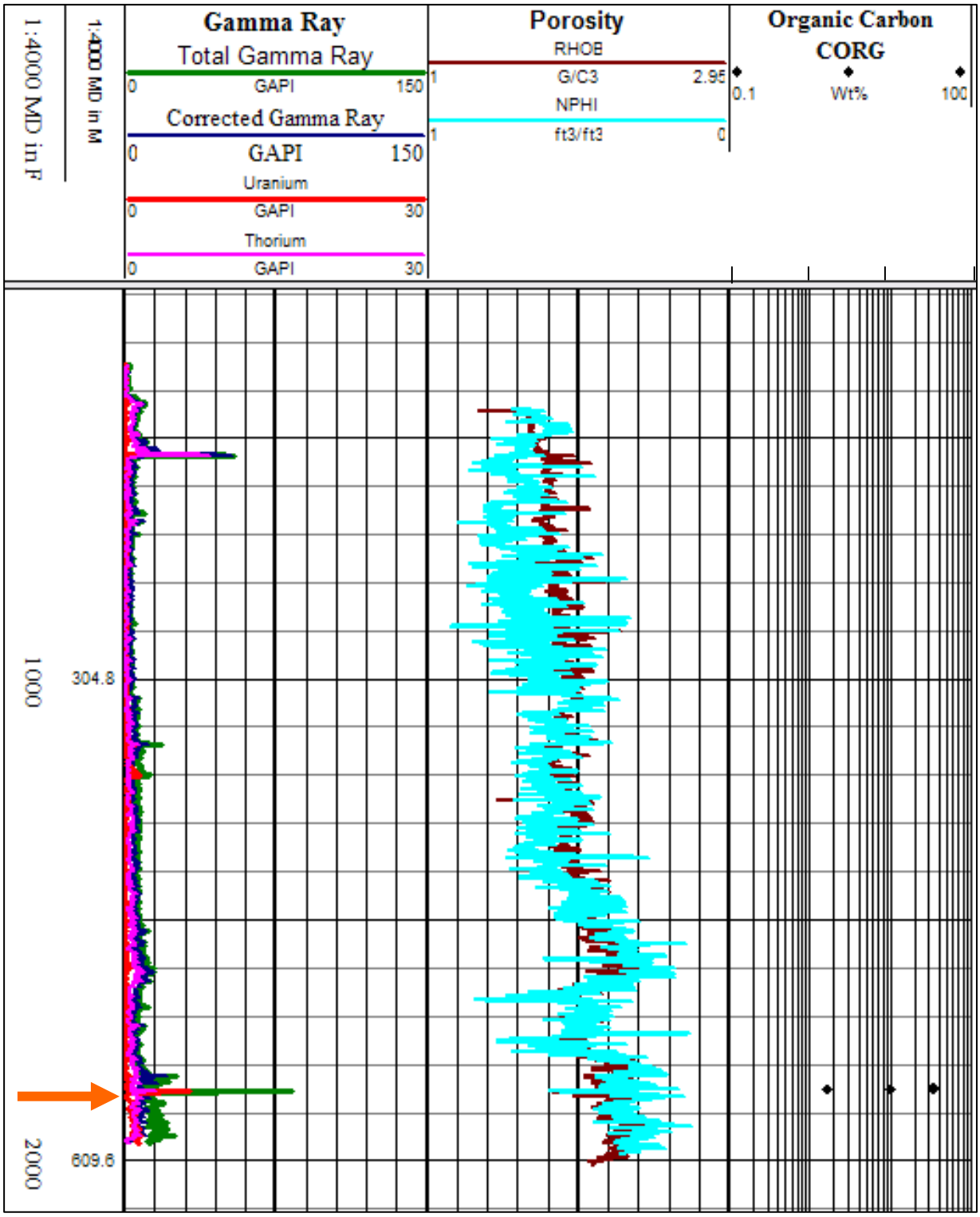

Figure C-8. Hole 198-1207B; log response and organic carbon percent through OAE 1a. The red line across logs indicates the upper boundaries of OAE 1a and a light green line indicates the lower boundary.

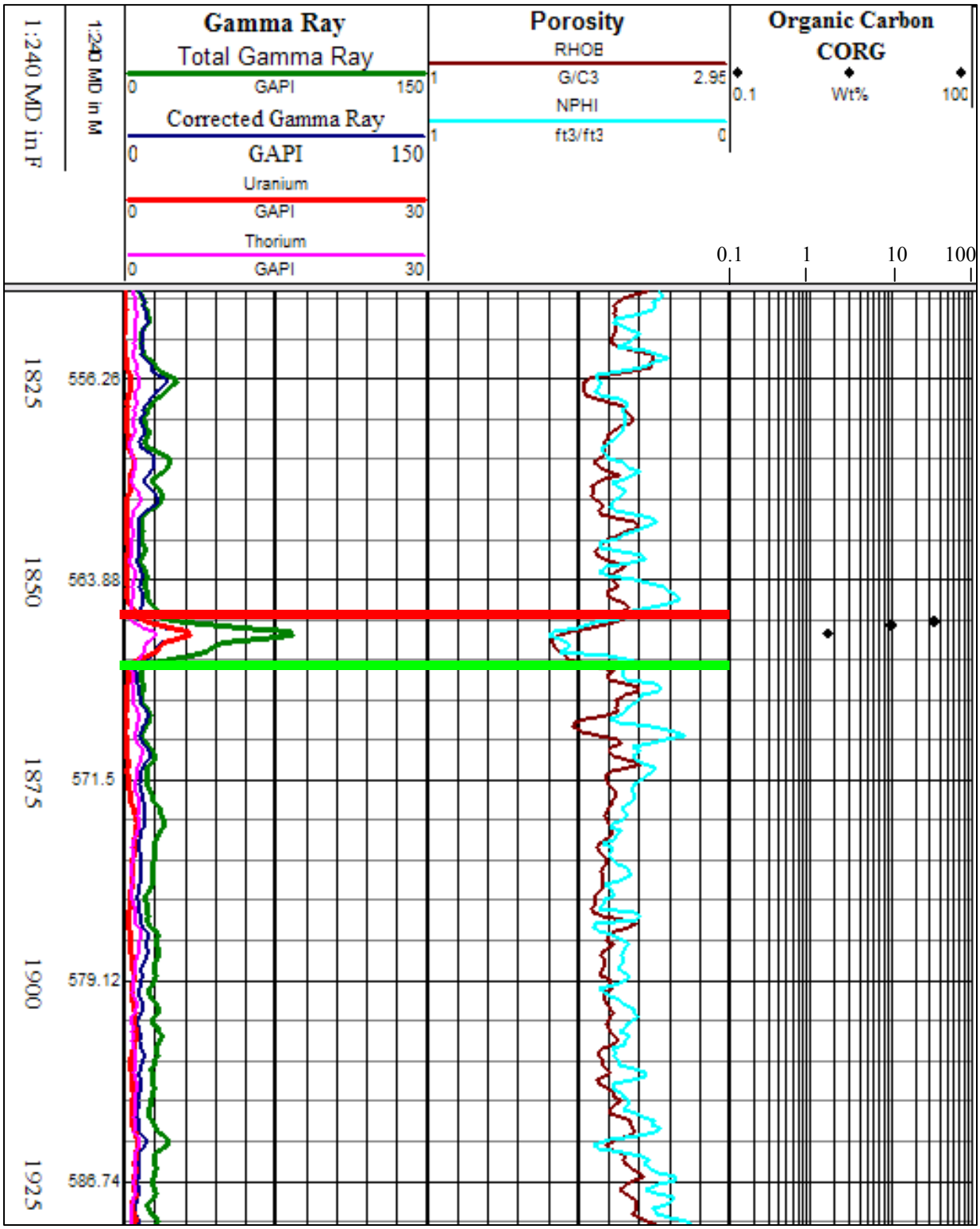

Figure C-9. Hole 198-1213B; log response and organic carbon percent through total logged interval. The red line across logs indicates the upper boundaries of OAE 1a and a light green line indicates the lower boundary.

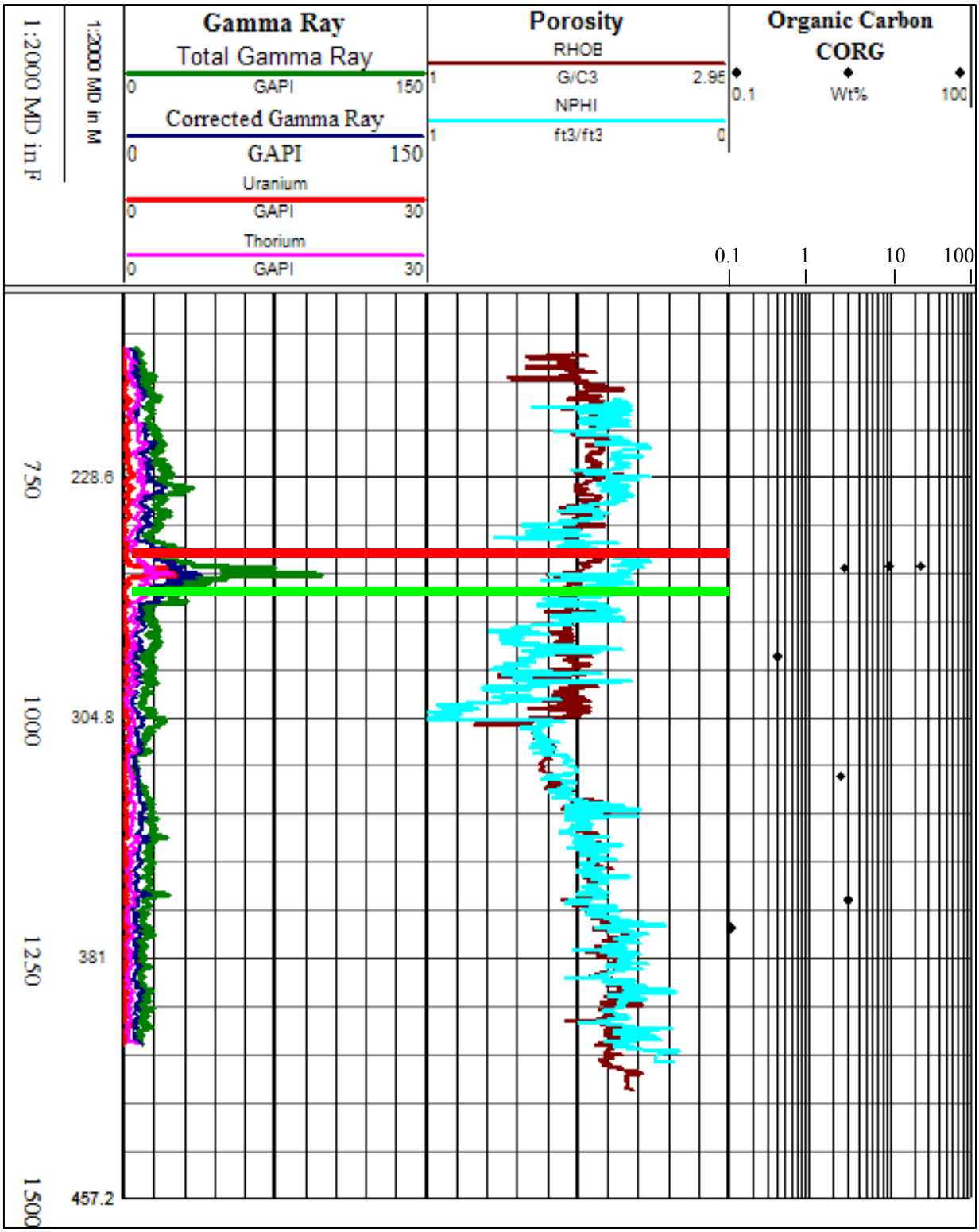

Figure C-10. Hole 198-1213B; log response and organic carbon percent through OAE 1a. The red line across logs indicates the upper boundaries of OAE 1a and a light green line indicates the lower boundary.

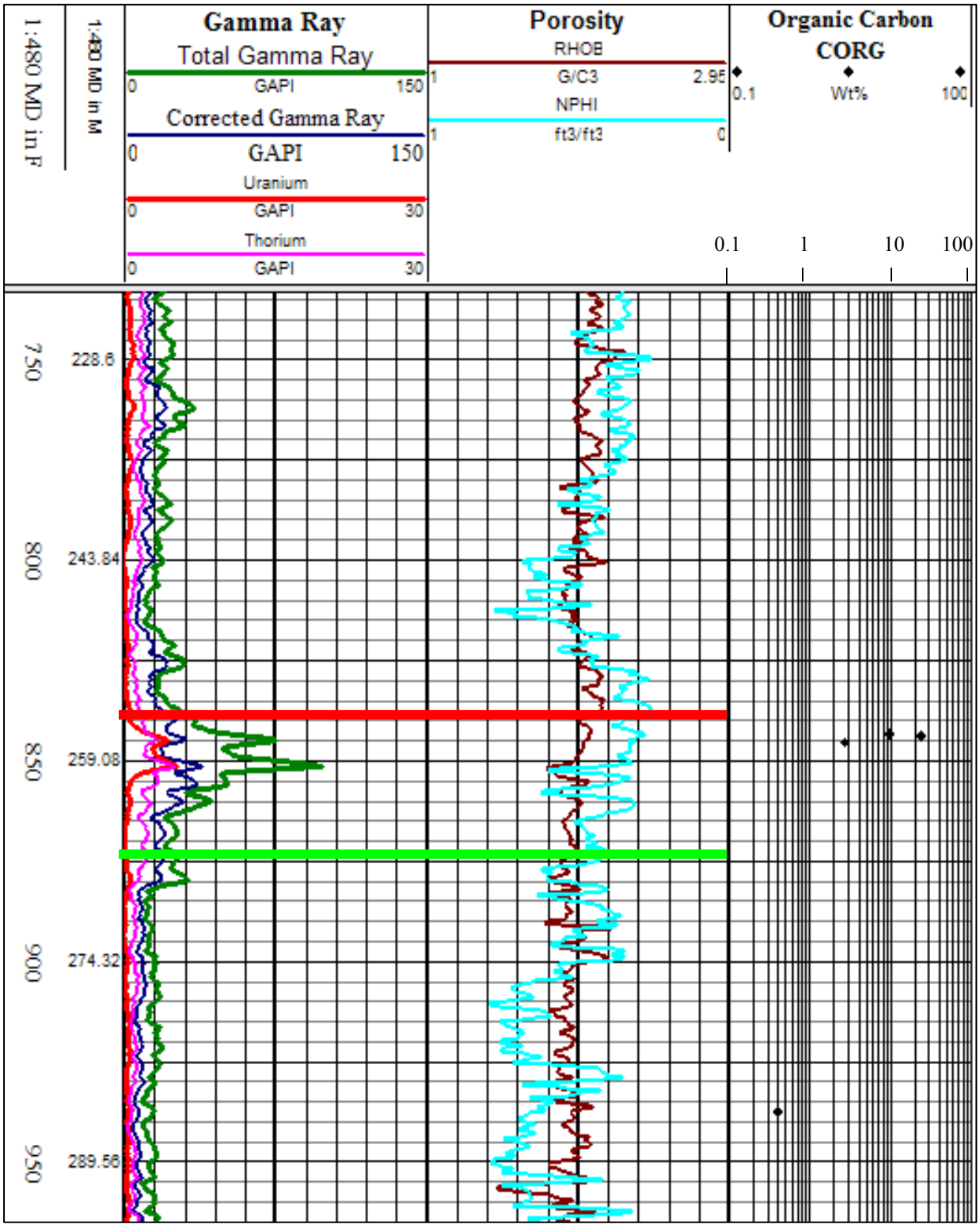

Figure C-11. Hole 207-1258C; log response and organic carbon percent through the total logged interval. Thick dark orange lines across logs indicate the upper and lower boundaries of lithologies associated with OAE 2 and the upper boundary of possible OAE 1d, which continues below the logged interval.

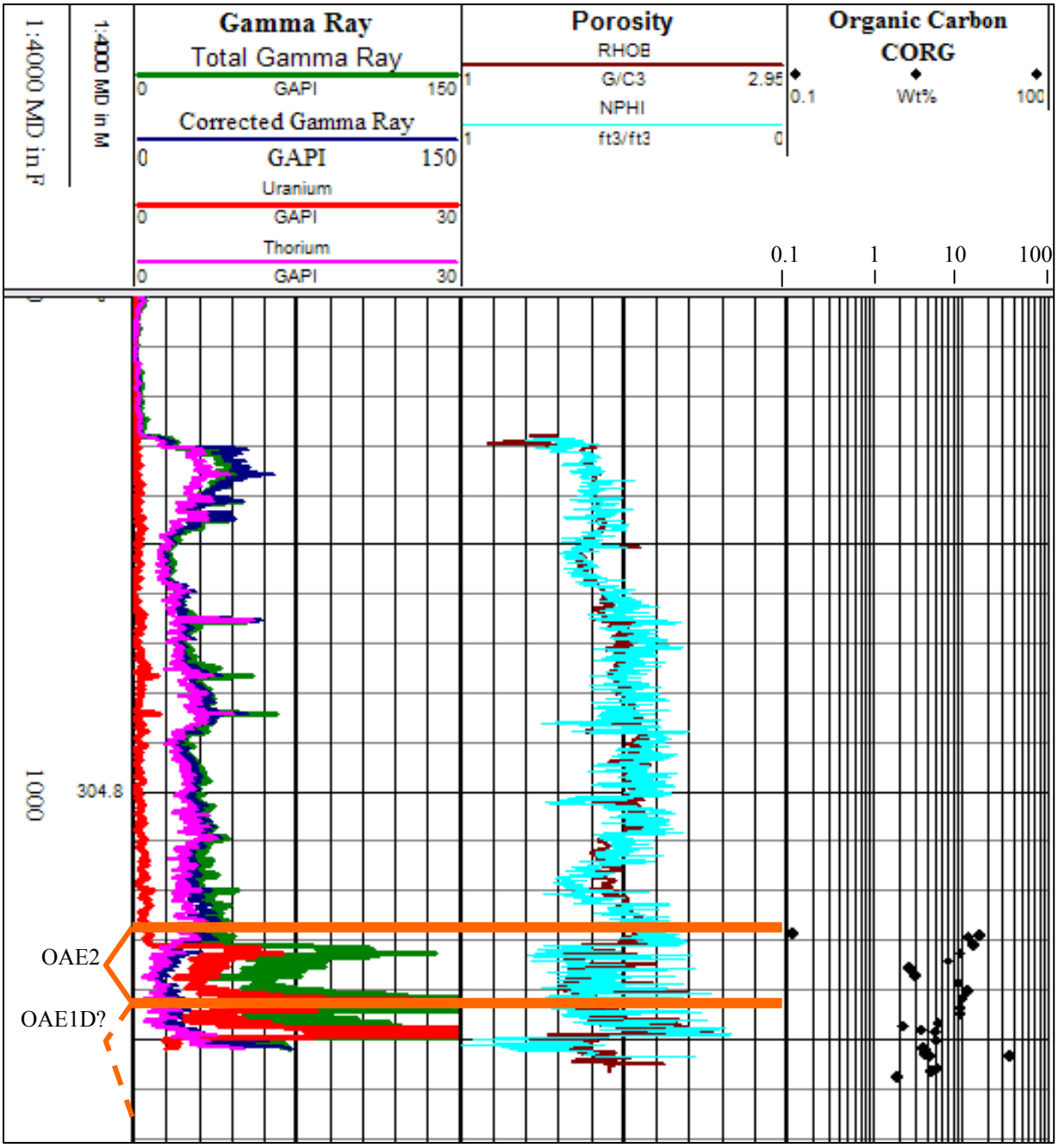

Figure C-12. Hole 207-1258C; log response and organic carbon percent through OAE 2 and a partial segment of what is likely OAE 1d. Thick dark orange lines across logs indicate the upper and lower boundaries of lithologies associated with OAE 2 and the upper boundary of possible OAE 1d, which continues below the logged interval.

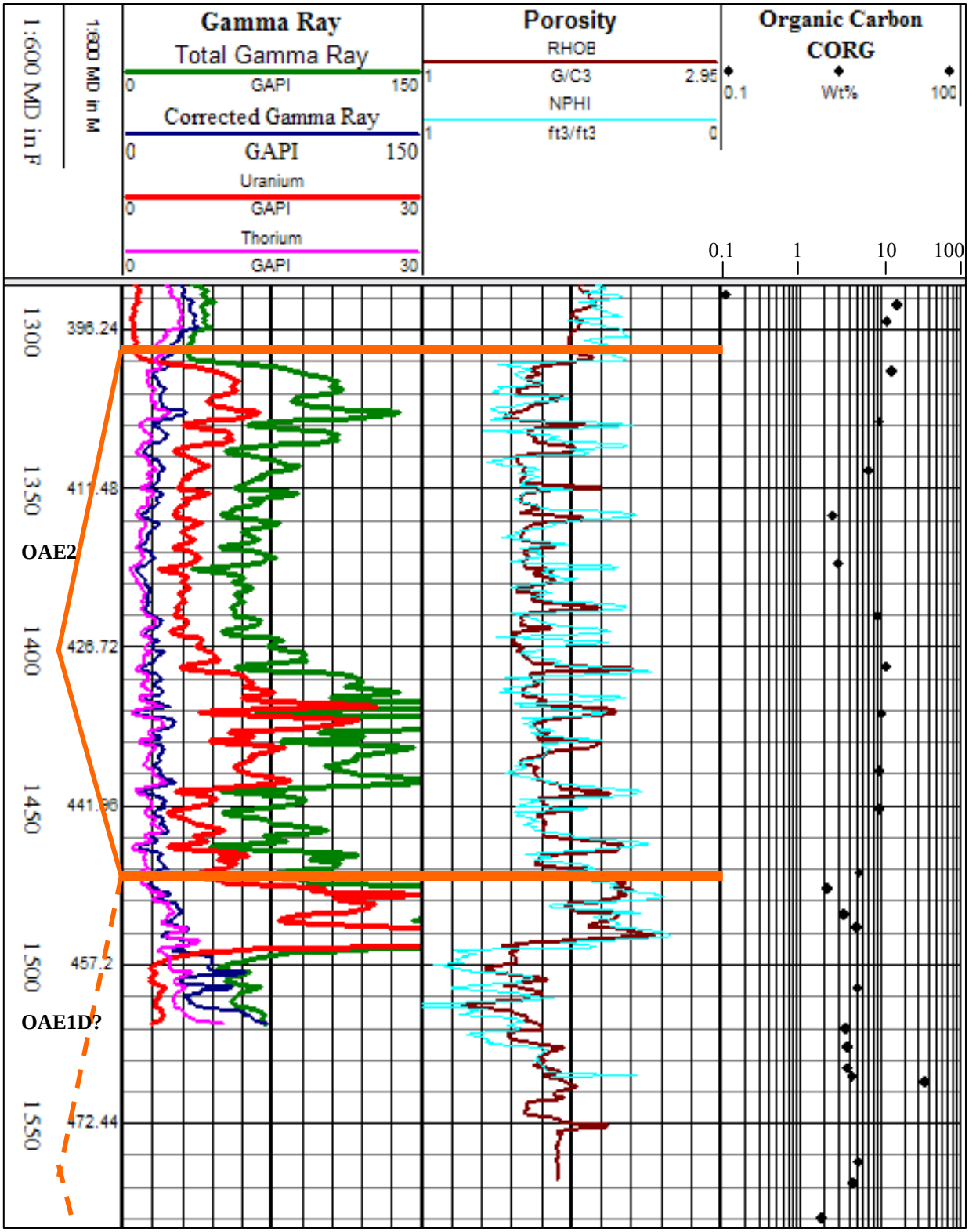

Figure C-13. Hole 207-1261B; log response and organic carbon percent through logged interval. The red line indicates the upper boundary of lithologies associated with OAE 2, which continues below the logged interval.

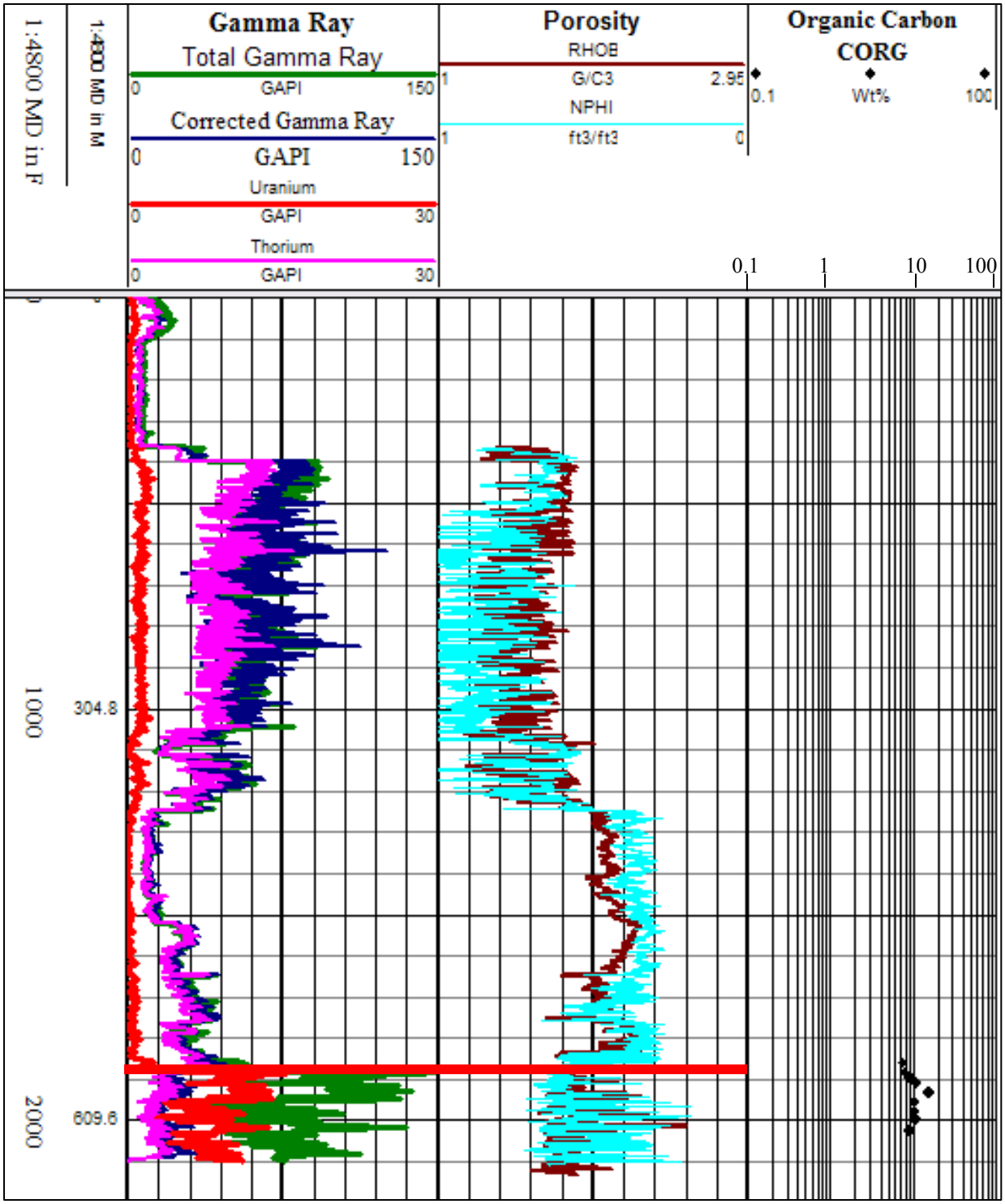

Figure C-14. Hole 207-1261B; log response and organic carbon percent through OAE 2. The red line indicates the upper boundary of lithologies associated with OAE 2, which continues below the logged interval.

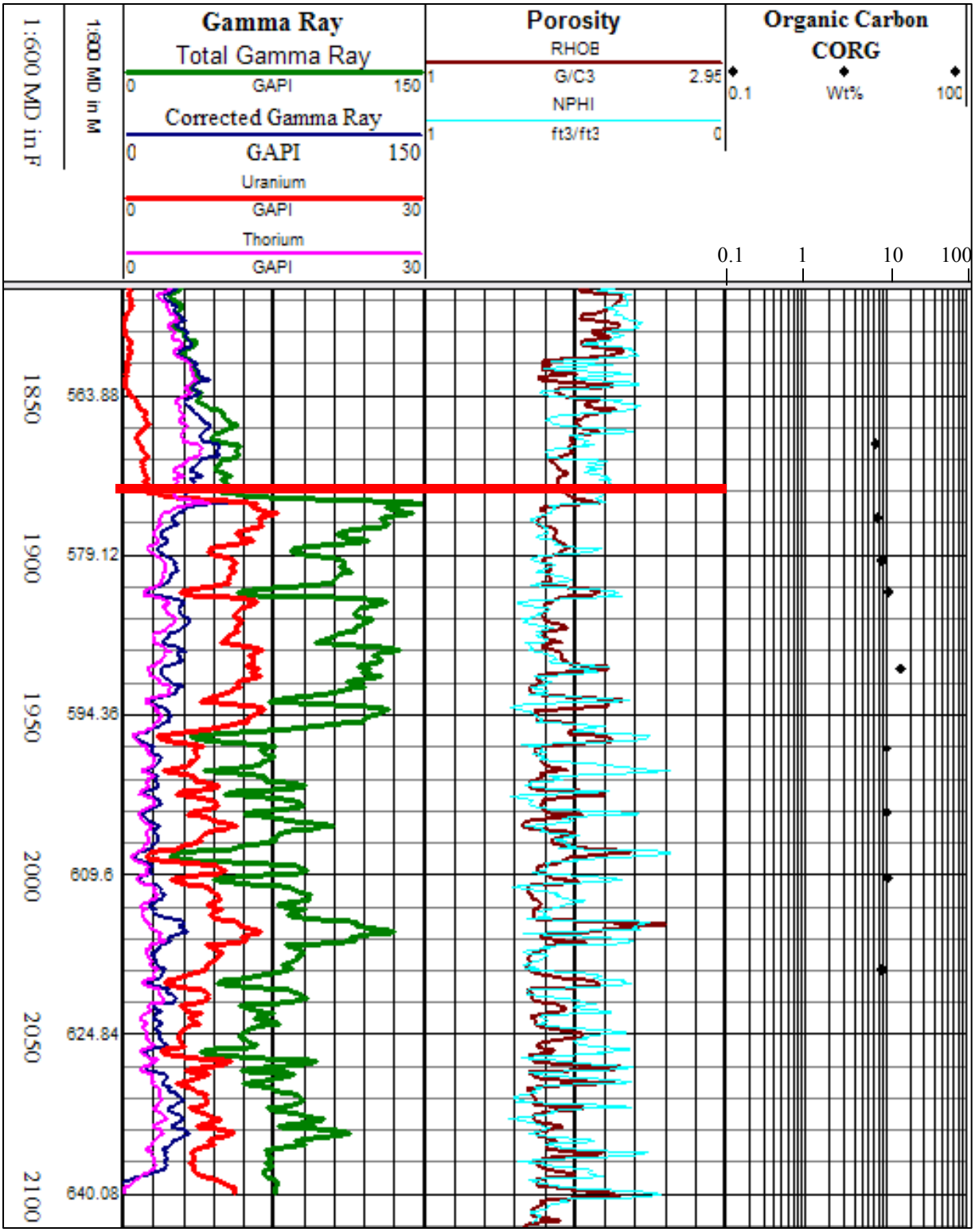

APPENDIX D - DEVIATION OF PSEUDO DENSITY CURVES FROM BULK DENSITY CURVES VERSUS DEPTH IN ODP HOLES

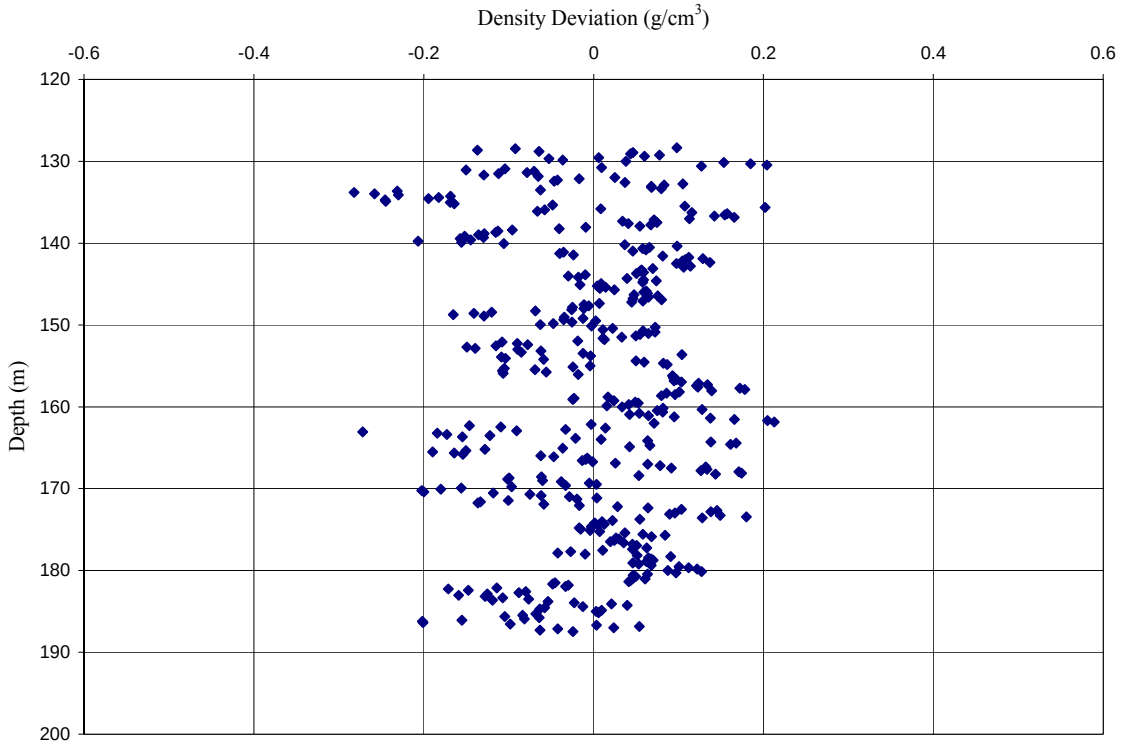

Figure D-1. Hole 103-641C deviation of pseudo density from bulk density.

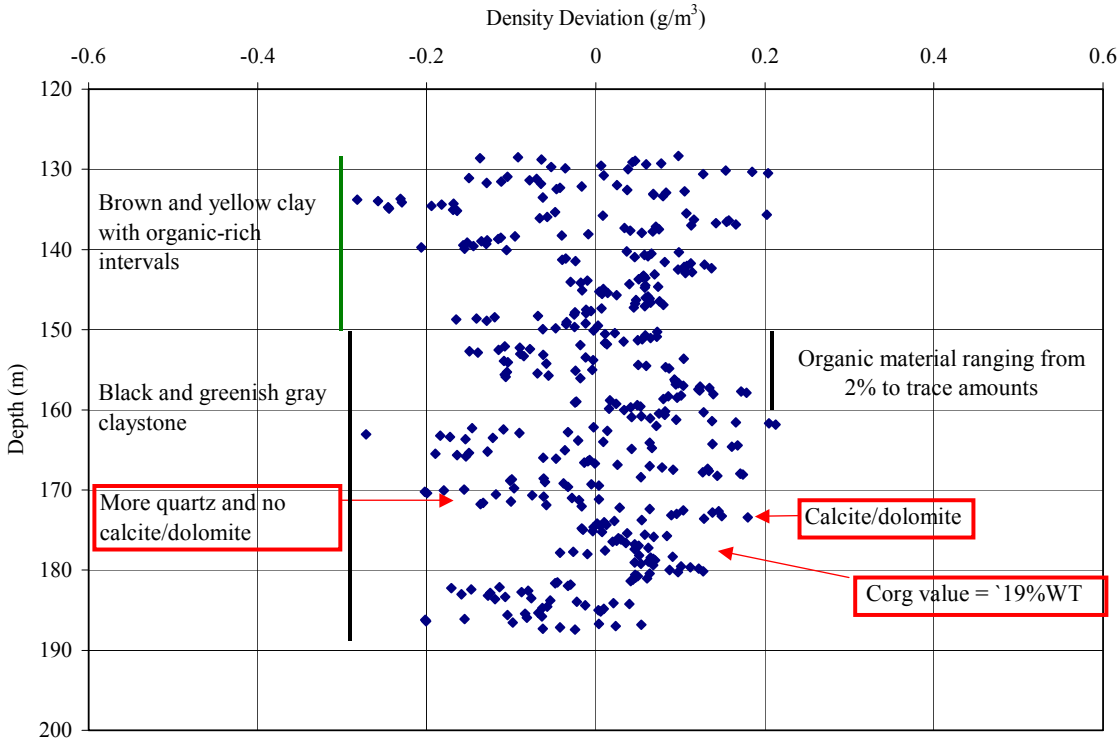

Figure D-2. Hole 103-641C deviation of pseudo density from bulk density with lithology descriptions.

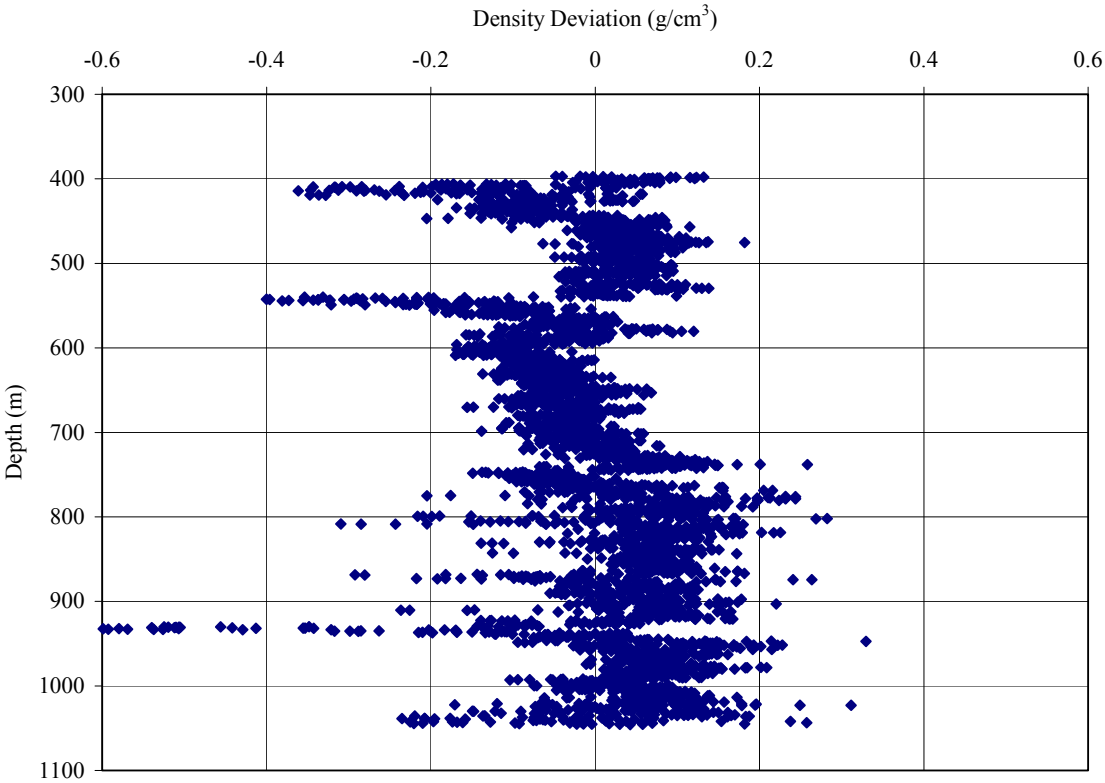

Figure D-3. Hole 159-959D deviation of pseudo density from bulk density.

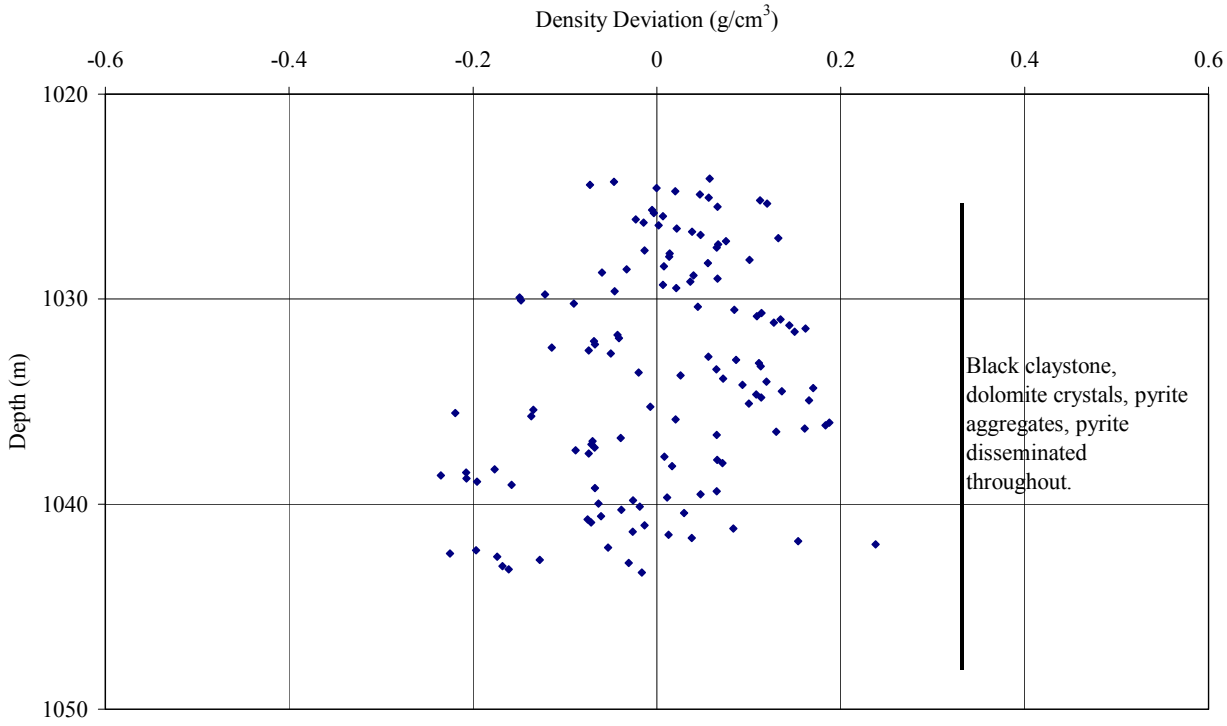

Figure D-4. Hole 159-959D deviation of pseudo density from bulk density and lithology descriptions through upper and lower boundary of lithologies associated with OAE 3.

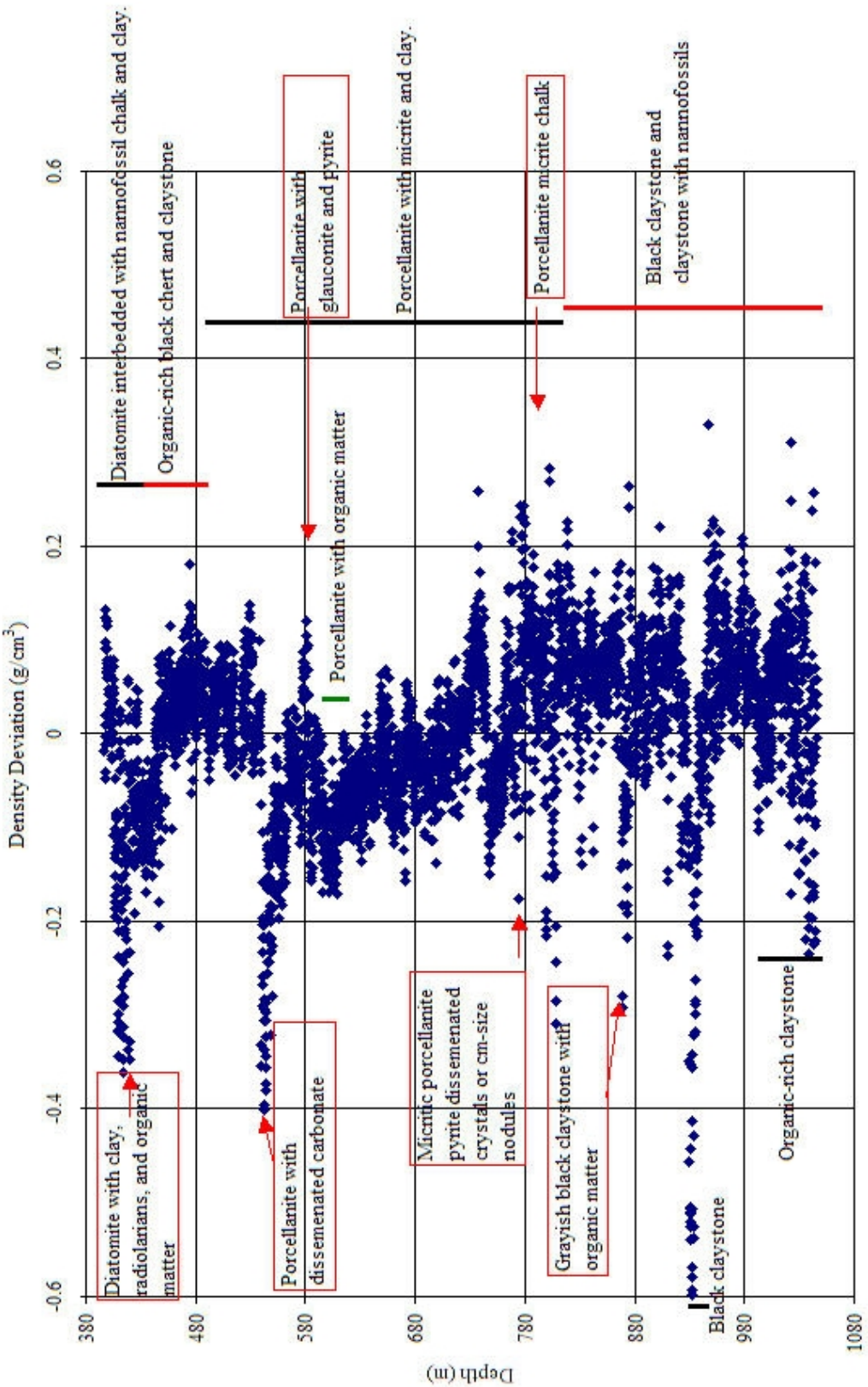

Figure D-5. Hole 159-959D deviation of pseudo density from bulk density and lithology descriptions.

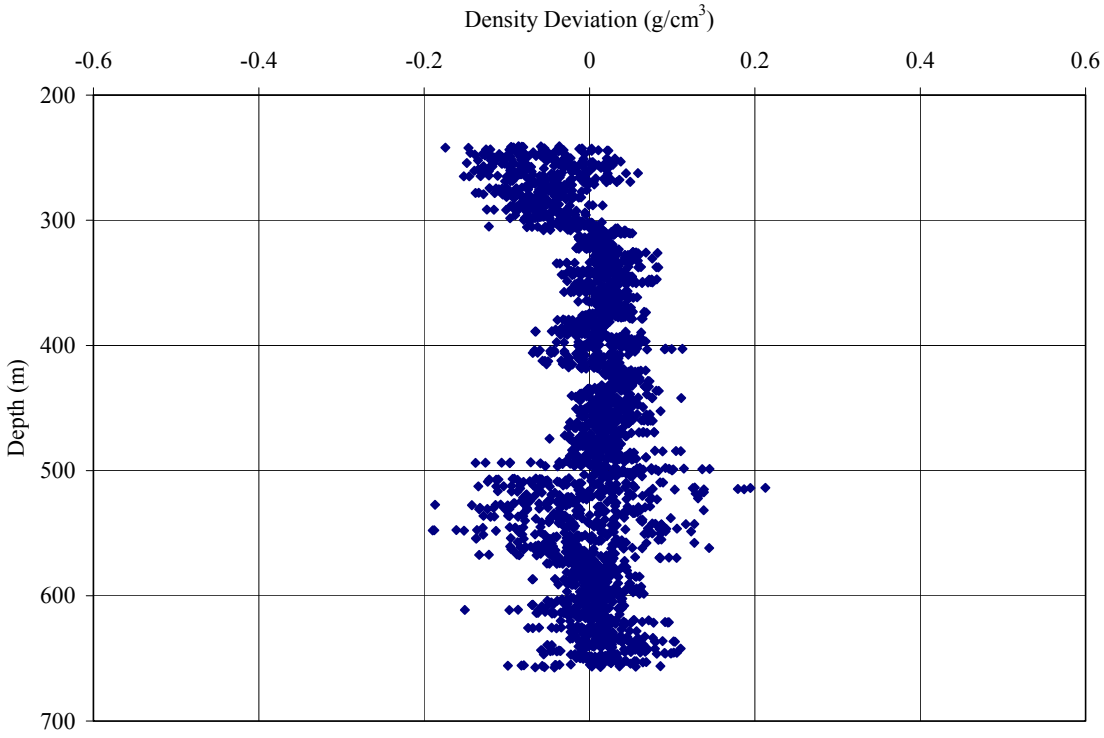

Figure D-6. Hole 171B-1052E deviation of pseudo density from bulk density.

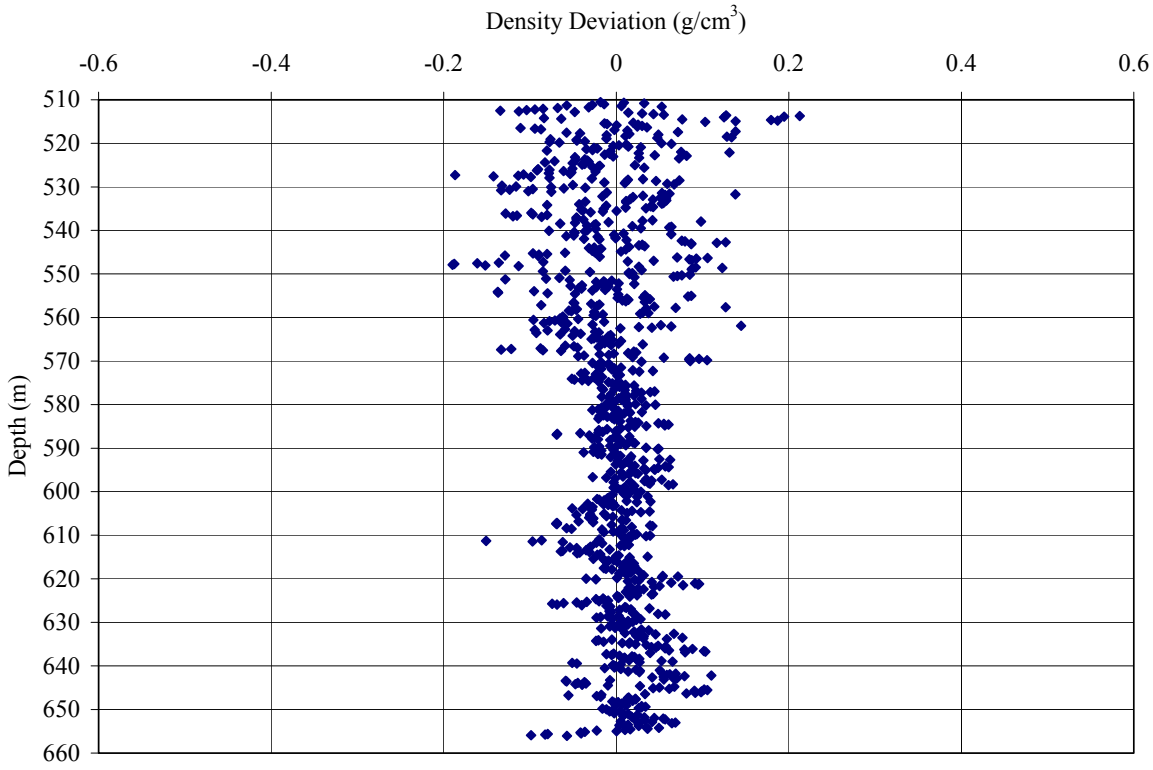

Figure D-7. Hole 171B-1052E deviation of pseudo density from bulk density through Late Albian lithologies associated with OAE deposition.

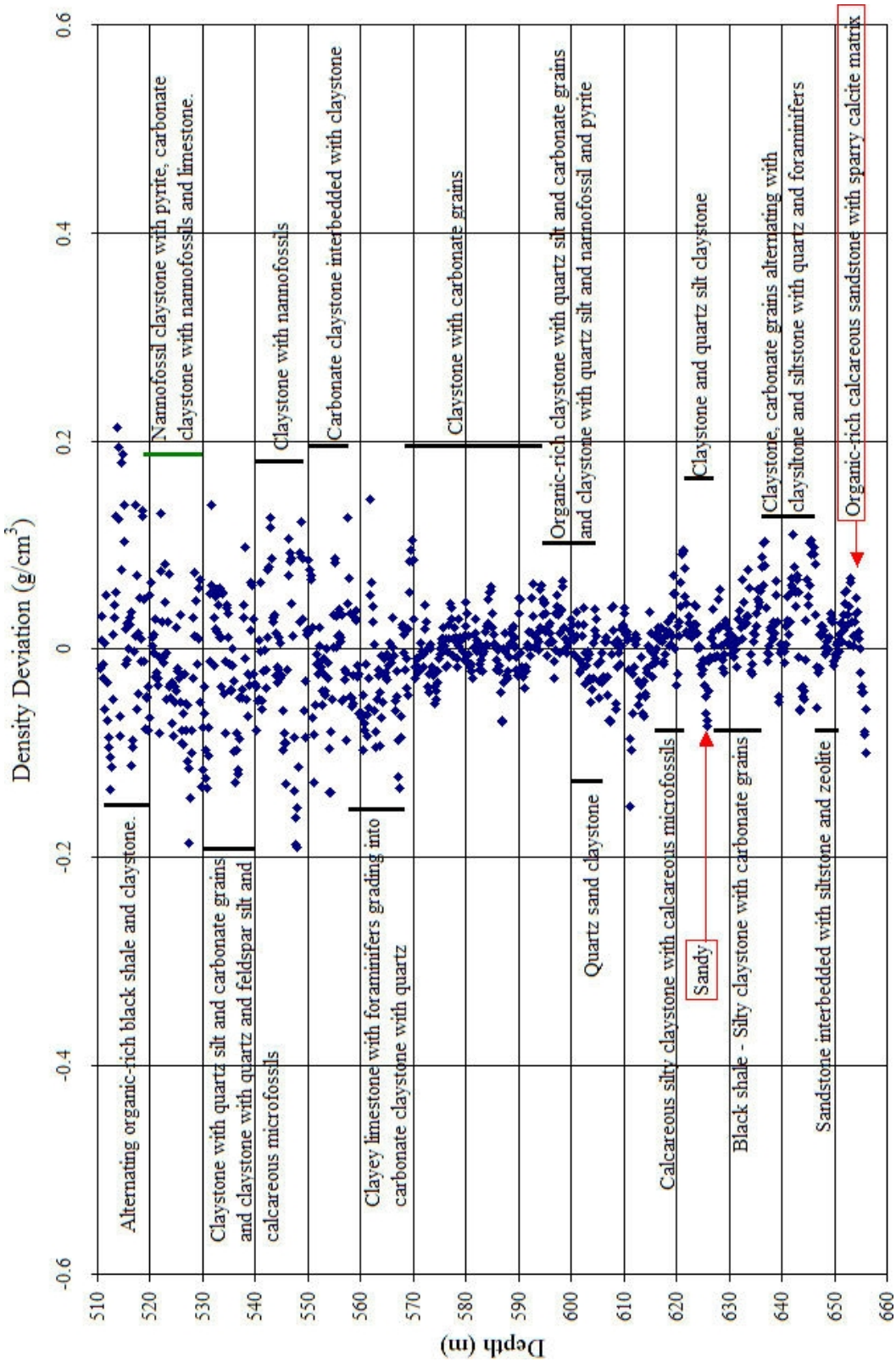

Figure D-8. Hole 171B-1052E deviation of pseudo density from bulk density through Late Albian lithologies associated with OAE deposition, with lithology information.

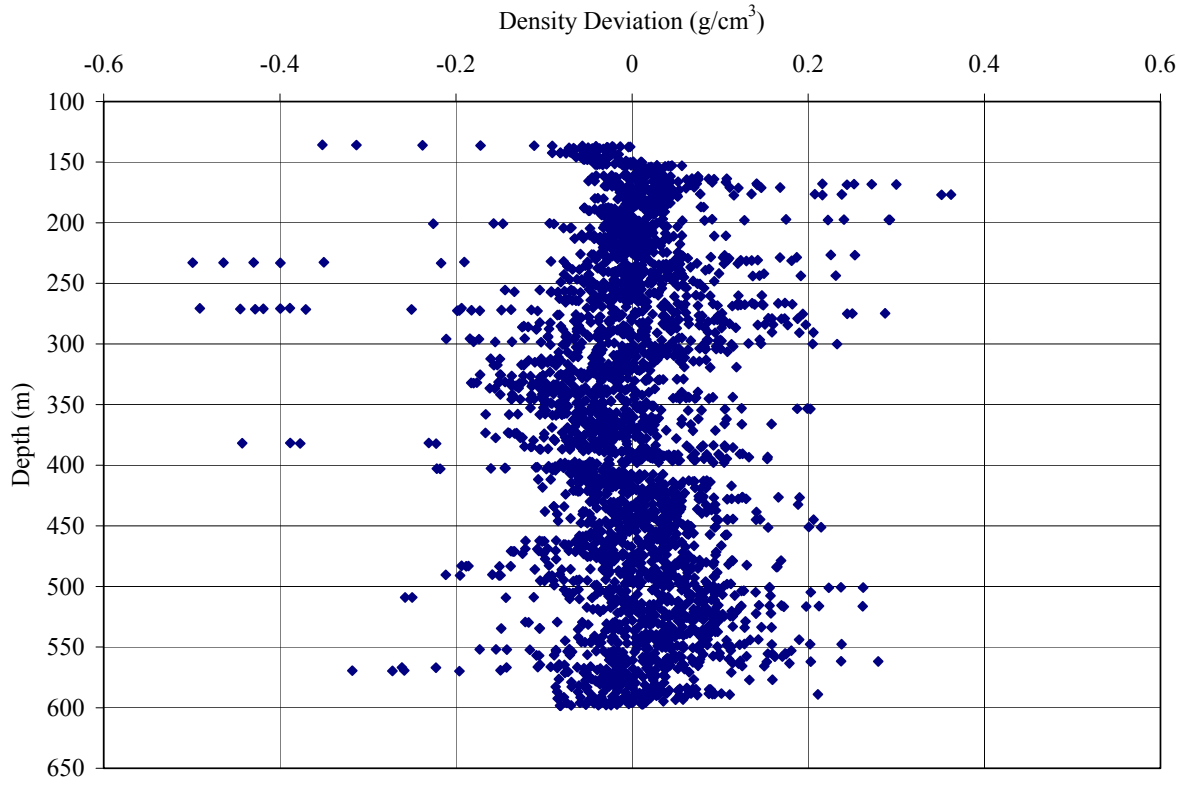

Figure D-9. Hole 198-1207C deviation of pseudo density from bulk density.

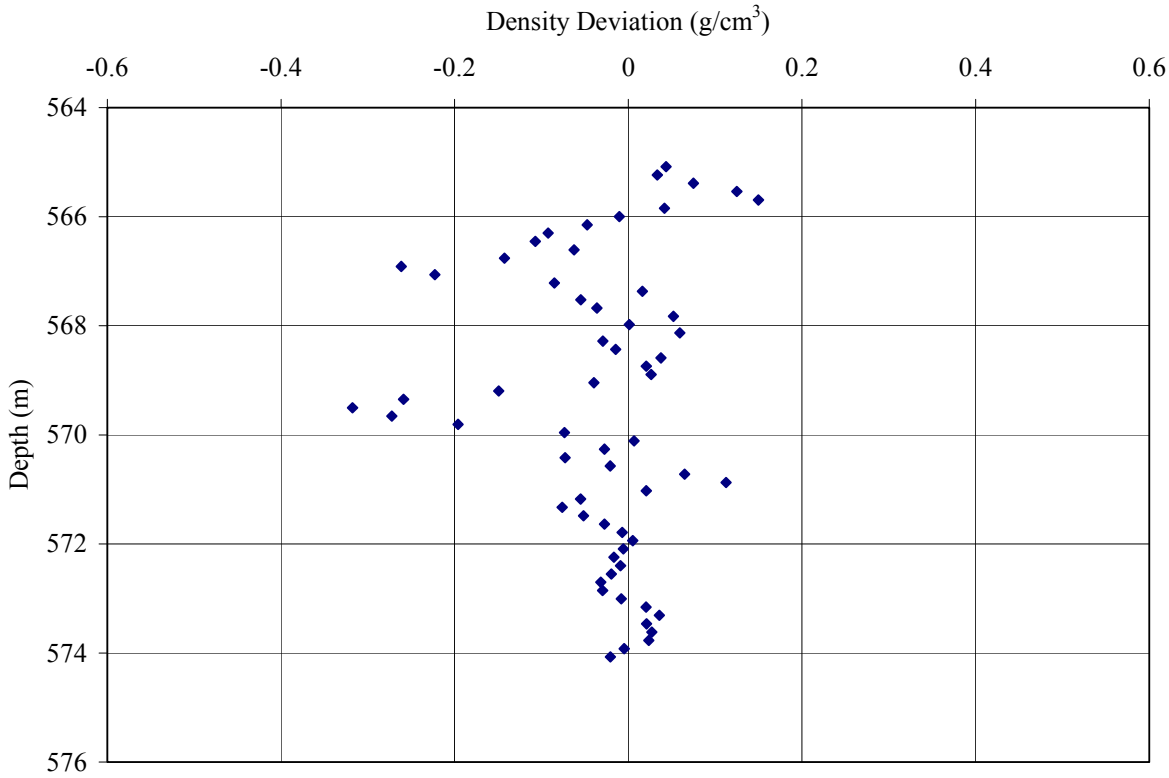

Figure D-10. Hole 198-1207C deviation of pseudo density from bulk density through lithologies associated with OAE 1a.

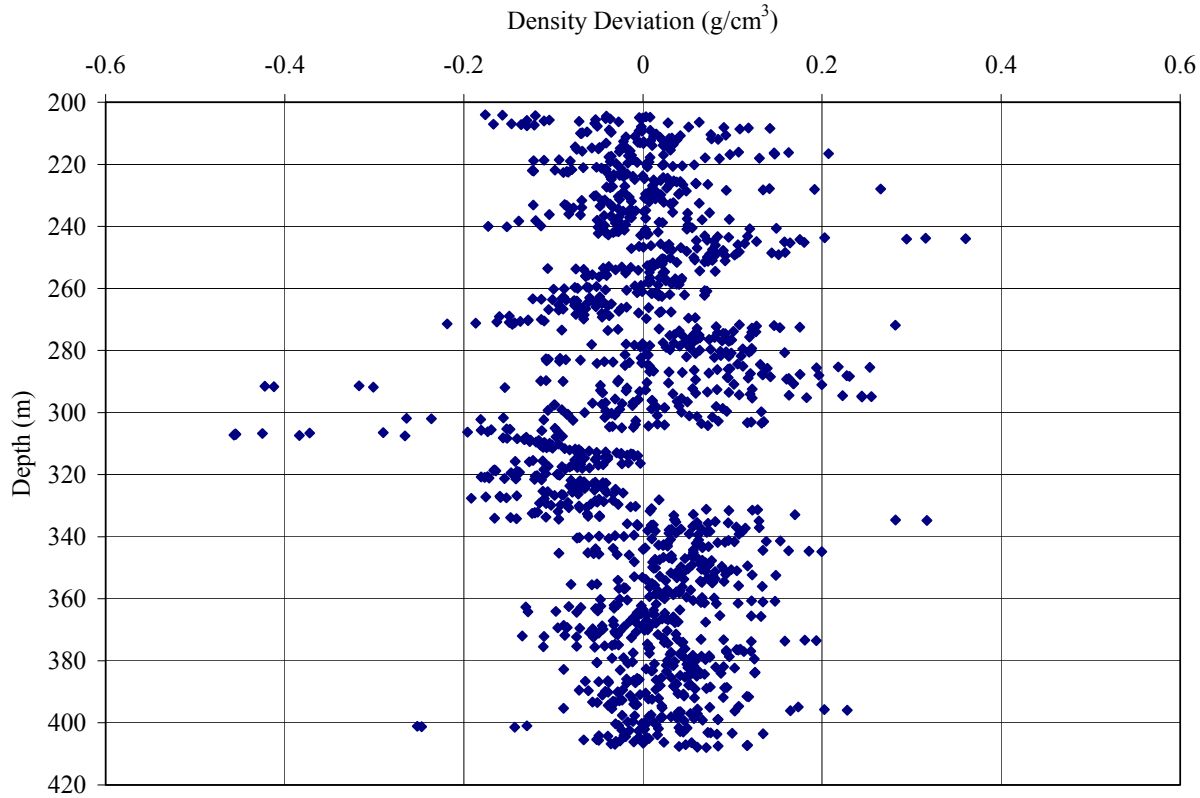

Figure D-11. Hole 198-1213B deviation of pseudo density from bulk density.

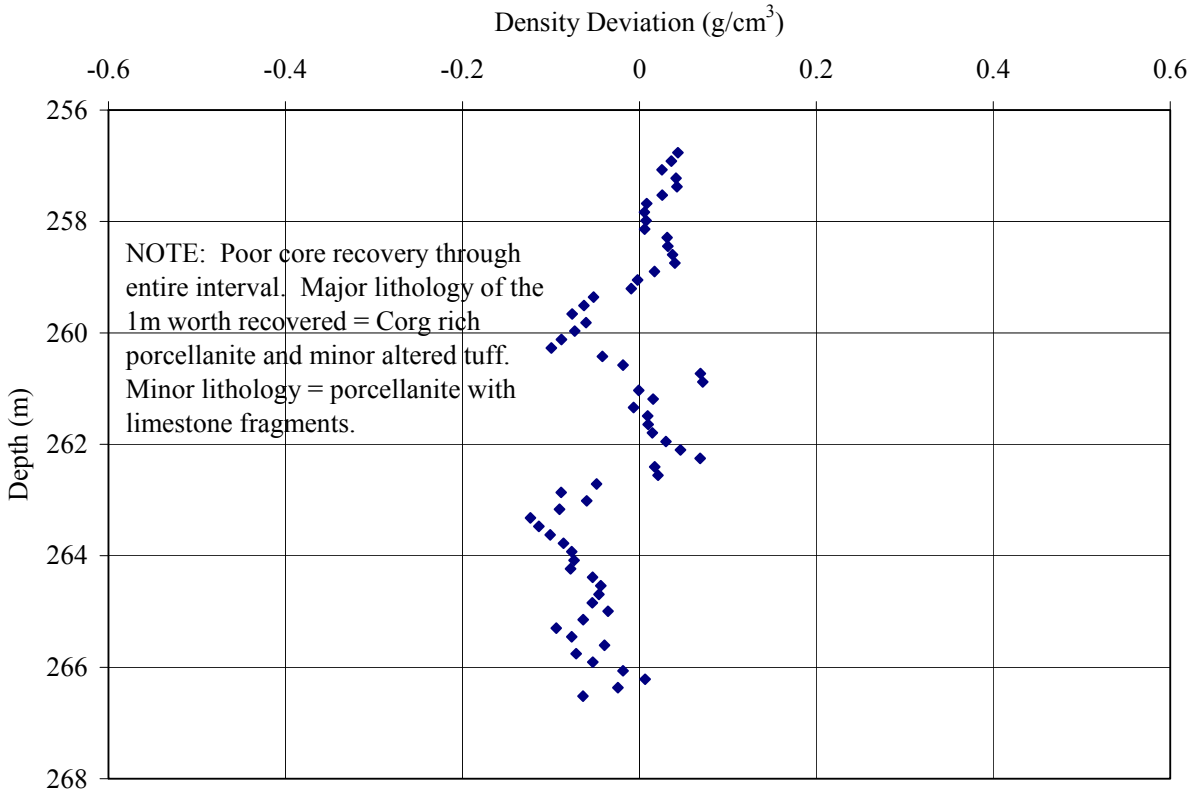

Figure D-12. Hole 198-1213B deviation of pseudo density from bulk density through OAE 1a.

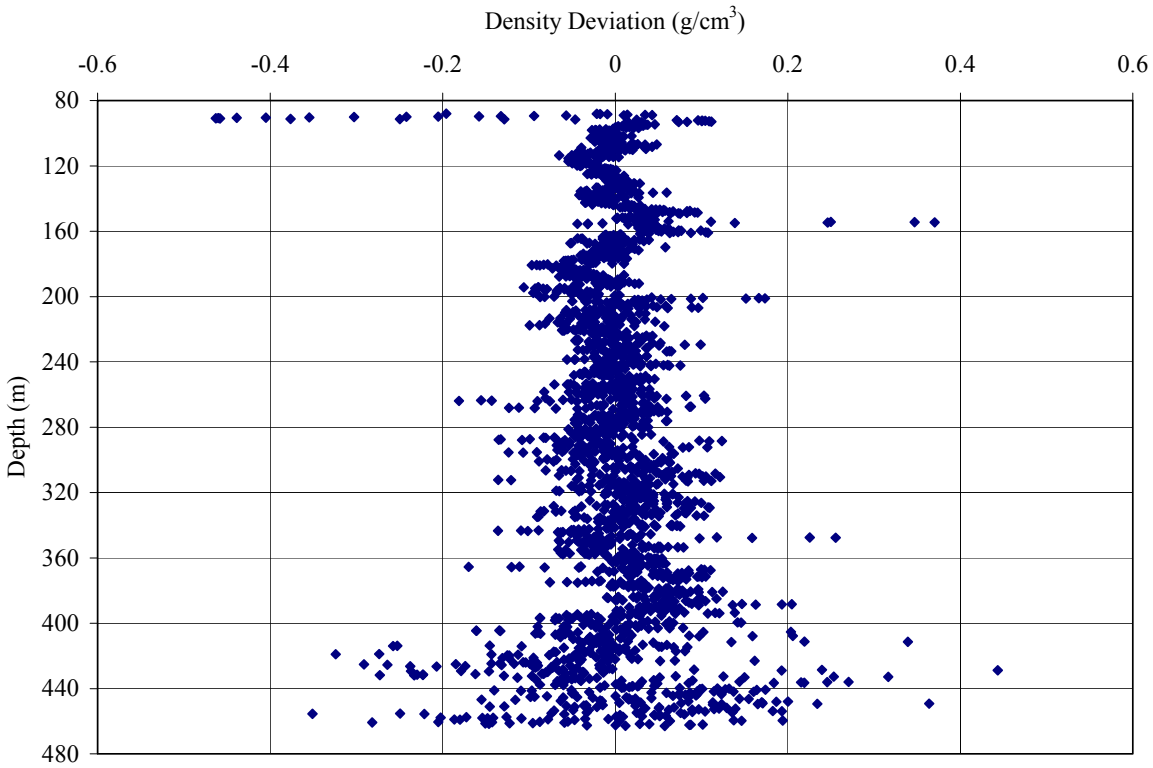

Figure D-13. Hole 207-1258C deviation of pseudo density from bulk density.

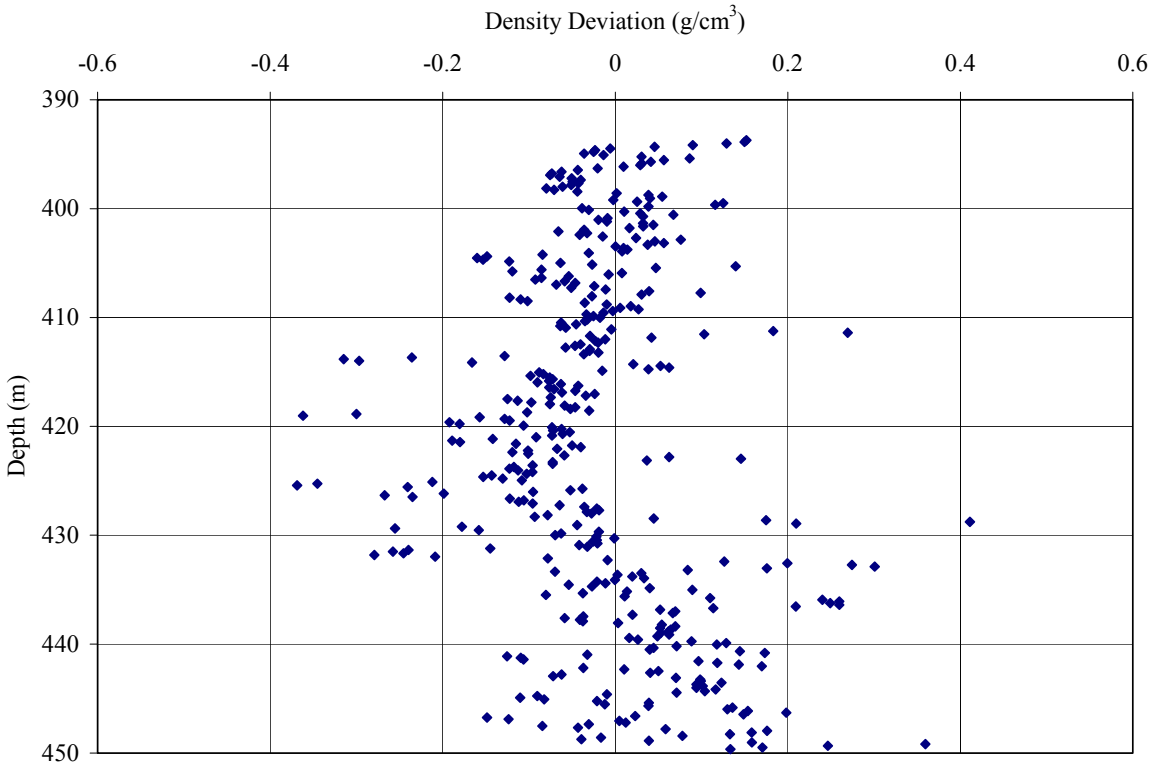

Figure D-14. Hole 207-1258C deviation of pseudo density from bulk density through lithologies associated with OAE 2.

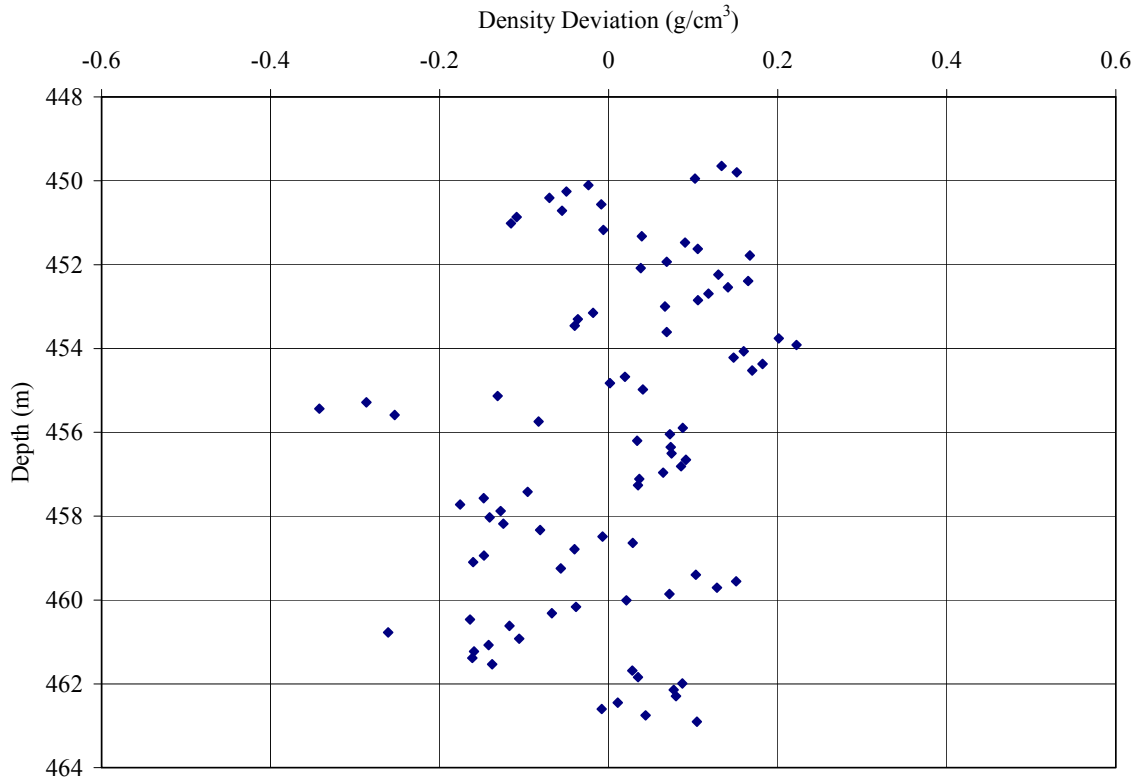

Figure D-15. Hole 207-1258C deviation of pseudo density from bulk density through lithologies associated with OAE 1d.

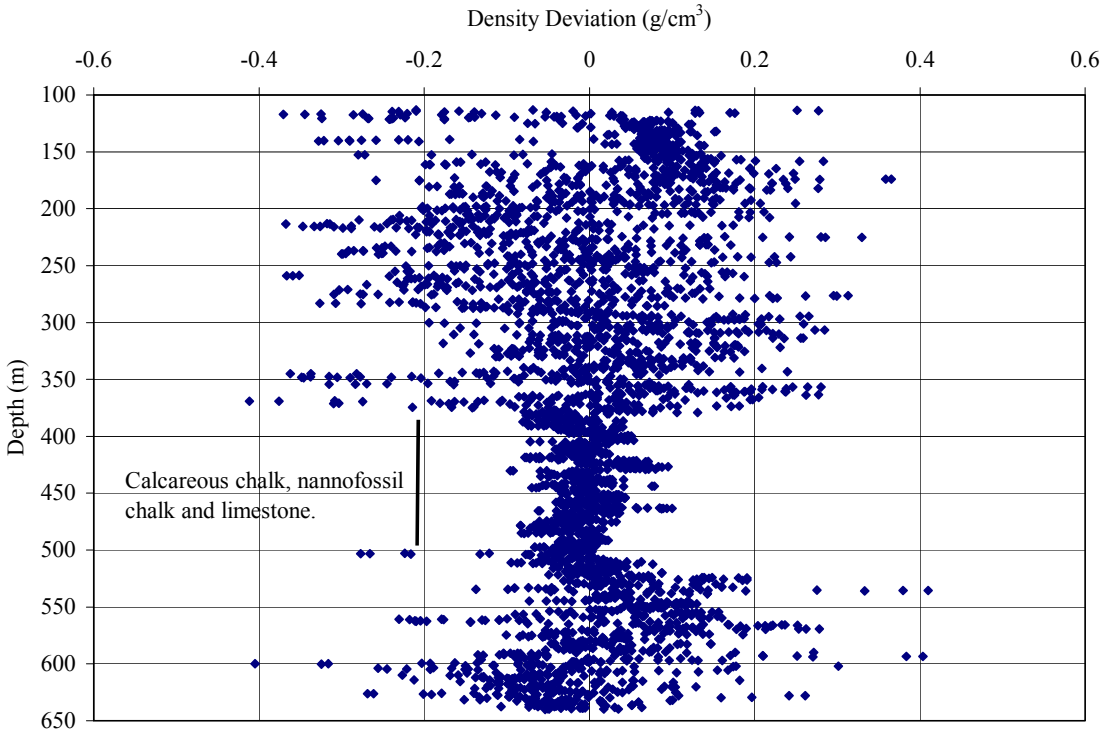

Figure D-16. Hole 207-1261B deviation of pseudo density from bulk density.

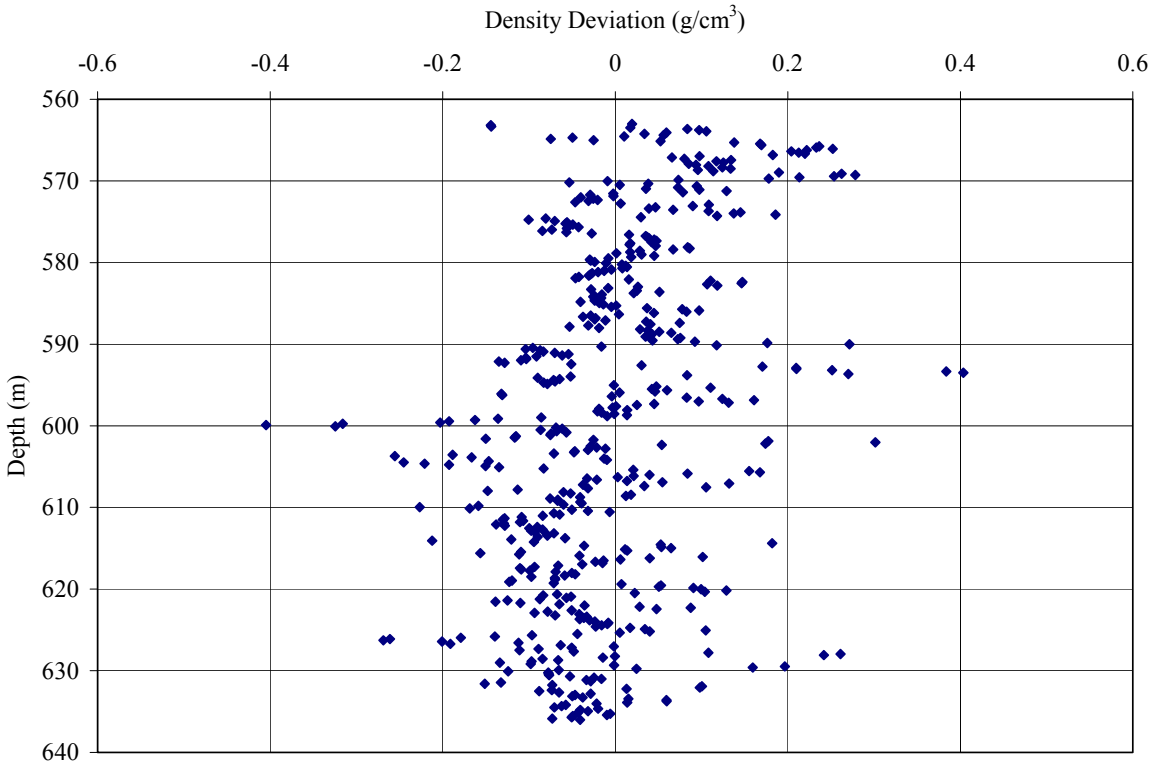

Figure D-17. Hole 207-1261B deviation of pseudo density from bulk density through OAE 2.

APPENDIX E - INDIVIDUAL SUMMARIES FOR THE GULF OF MEXICO WELLS

Table E-1. Well 177244005200 (Main Pass block number 264).

API	Well name	Side Track	By Pass	Area Code	Block	TD date	Water depth (m)	Logged interval (mbsf)
177244005200	002	00	00	MP	264	24-Aug-72	68.0	274.3-4480.6
Paleontology report version used:								
Paleo. notes								
Depth MD (ft)/(m)	Depth TVD	Age	Description					
Depth/Time of preceding non-interested interval:								
14250/4343.4		Maastrictian						
Depth/Time of 1st interested interval:								
14730/4489.7		Albian						
Depth/Time of last interested interval:								
Depth/Time of next non-interested interval:								
Notes from paleo. on impt. intervals:								
14450/4404.4		Cenomanian	Black shale					
Lithology notes								
Depth MD (ft)/(m)	Depth TVD	Age	Lithology description					
14360/4376.9		Santonian	Clay?/black splintery					
14400/4389.1		Cenomanian	Few pieces of black sandy shale					
14420/4395.2		Cenomanian	Light brown & black carbonated sand & shale					
14600/4450.1		Between Cenomanian & Albian	Dolomite & anhydrite					
14450/4404.4		Cenomanian	Shale, light brown and black with a dull gold and blue white flow and slow streaming cut are coming from the shale					
LESA Notes								
Depth MD (ft)/(m)	Depth TVD	Age	Description					
14450/4404.4		Cenomanian	Definite spike in the Gr, especially for that area, but not higher than other typical shales in the well, and a corresponding dip in the density.					
14360/4376.9		Santonian	The area is certainly less clean than immediately surrounding areas, but doesn't look particularly shalely compared to the rest of the well.					
14400/4389.1		Cenomanian	The area is certainly less clean than immediately surrounding areas, but doesn't look particularly shalely compared to the rest of the well.					
14420/4395.2		Cenomanian	The area is certainly less clean than immediately surrounding areas, but doesn't look particularly shalely compared to the rest of the well. BUT this is nearing the good spike in Gr found at 14450 (4404.4m) in this well.					

Table E-2. Well 177244005400 (Main Pass block number 253).

API	Well name	Side track	By pass	Area code	Block	TD date	Water depth (m)	Logged interval (mbsf)
177244005400	006	00	00	MP	253	04-Aug-72	82.3	670.6-5181.6
Paleontology report version used:								
Paleontology Notes								
Depth MD (ft)/(m)	Depth TVD	Age	Description					
Depth/Time of preceding non-interested interval:								
8700/2651.8		Maastrichtian						
Depth/Time of 1st interested interval:								
9960/3035.8		Cenomanian						
Depth/Time of last interested interval:								
16320/4974.3		Aptian						
Depth/Time of next non-interested interval:								
Notes from paleo. on impt. intervals:								
Lithology notes								
Depth MD (ft)/(m)	Depth TVD	Age	Lithology description					
14650/4465.3		Albian-Aptian	Limestone dark gray & black, dense, micritic, trace crystalline calcite					
14750/4495.8		Albian-Aptian	Limestone dark gray & black, dense, micritic, trace crystalline calcite					
LESA Notes								
Depth MD (ft)/(m)	Depth TVD	Age	Description					
14650/4465.3		Albian-Aptian	Between these two depths there are several spikes in the Gr with corresponding BIG dips in the density.					
14750/4495.8		Albian-Aptian						

Table E-3. Well 177244006300 (Main Pass block number 222; water depth 69.2 m; logged interval 304.8-3627.1 mbsf).

API	Well name	Side track	By pass	Area code	Block	TD Date	Water depth (m)	Logged interval (mbsf)
177244006300	001	00	00	MP	222	16-Jul-73	69.2	304.8-3627.1
Paleontology report version used:								
Paleontology notes								
Depth MD (ft)/(m)	Depth TVD	Age	Description					
Depth/Time of preceding non-interested interval:								
9241/2816.7		Campanian						
Depth/Time of 1st interested interval:								
9290/2831.6		Turonian-Cenomanian						

Depth/Time of last interested interval:		
11866/3616.8		Albian
Depth/Time of next non-interested interval:		
Notes from paleo. on impt. intervals:		

Lithology notes			
Depth MD (ft)/(m)	Depth TVD	Age	Lithology description
9410/2868.2		Cenomanian	Shale medium dark gray-black with pyrite
10850/3307.1		Albian	Shale dark gray-black fissile, silty, calcareous
9745-9785/ 2970.3-2982.5			Shale, medium gray, firm, calcareous
LESA Notes			
Depth MD (ft)/(m)	Depth TVD	Age	Description
N/A	N/A	N/A	In making the pseudo density curves SFL was not used because it did not cover the needed depths.
			The two depths mentioned in the mud logs as having "black" sediments did not show any promising peaks in the well logs.
9410/2868.2		Cenomanian	This area looks like it might have some very thin shalely bits, but nothing exciting.
9745-9785/ 2970.3-2982.5		Turonian-Cenomanian (Likely Cenomanian)	This area shows a sustained spike in Gr and corresponding dip in density.
10850/3307.1		Albian	At 10850 it looks shalely, BUT at 10875-10895 (3314.7-3320.8m) there is a definite spike in the GR and dip in density.

Table E-4. Well 608164003700 (Vioska Knoll block number 30).

API	Well name	Side track	By pass	Area code	Block	TD Date	Water depth (m)	Logged interval (mbsf)
608164003700	001	00	00	VK	30	26-Sep-77	32.6	365.8-3352.8
Paleontology report version used:		Conflicting dates in separate paleo. reports; using the newer 1993 report done by the operator.						

Paleo. notes			
Depth MD (ft)/(m)	Depth TVD	Age	Description
Depth/Time of preceding non-interested interval:			
7640/2328.7		Campanian	
Depth/Time of 1st interested interval:			
7820/2383.5		Santonian	
Depth/Time of last interested interval:			
10960/3340.6		Albian	

Depth/Time of next non-interested interval:		
Notes from paleo. on impt. intervals:		

Lithology notes			
Depth MD (ft)/(m)	Depth TVD	Age	Lithology description
7870/2398.8		Campanian	Gray/black, calcareous, micaceous silty soft trace limestone & pyrite
7940/2420.1		Campanian	Gray/black calcareous, black shale calcareous to calcareous micaceous silty & soft
8060-70/ 2457-2460		Santonian	Shale gray/black calcareous to very calcareous silty, micaceous soft
8090/2465.8			Limestone
8270/2520.7		Santonian	Black shale not calcareous
9200/2804.2		Turonian - Cenomanian	Shale gray/black, limestone trace sandstone fine
9600/2926.1		Cenomanian - Albian	Limestone black shaly grades into very calcareous shale
9870/3008.4		Albian	Shale red-calcareous black non-calcareous, limestone black - white, foram, shaley
N/A	N/A	N/A	Pyrite at many intervals throughout some glauconite
LESA Notes			
Depth MD (ft)/(m)	Depth TVD	Age	Description
7870/2398.8		Campanian	Not seeing anything promising on the GR.
7940/2420.1		Campanian	Not seeing anything promising on the GR.
8060-70/ 2457-2460		Santonian	Not seeing anything promising on the GR.
Depth MD (ft)/(m)	Depth TVD	Age	Description
8270/2520.7		Santonian	Looks shaley compared to immediately surrounding GR but not really compared to the rest of the well
9200/2804.2		Turonian - Cenomanian	Looks shaley, but shallower in the well the GR does spike higher
9600/2926.1		Cenomanian - Albian	Shale signal in the Gr likely dampened by calcareous material
9870/3008.4		Albian	This area is fluctuating through shaley bits BUT their signal is likely dampened by calcareous material

Table E-5. Well 608224000600 (Destin Dome block number 166).

API	Well name	Side track	By pass	Area code	Block	TD Date	Water depth (m)	Logged interval (mbsf)
608224000600	001	00	00	DD	166	26-Feb-75	44.2	335.3-5334.0
Paleo. version used:								
Paleo. notes								
Depth MD (ft)/(m)	Depth TVD	Age	Description					
Depth/Time of preceding non-interested interval:								
4310/1313.7		Campanian						
Depth/Time of 1st interested interval:								
4490/1368.6		Santonian						
Depth/Time of last interested interval:								
10130/3087.6		Aptian						
Depth/Time of next non-interested interval:								
Notes from paleo. on impt. intervals:								
4491/1368.8		Santonian	"Upper" Eutaw Formation					
4900/1493.5			Tuscaloosa Formation					
5030/1533.1			Tuscaloosa Formation					
5150/1569.7			Tuscaloosa Formation					
5211/1588.3			Tuscaloosa Formation					
Lithology notes								
Depth MD (ft)/(m)	Depth TVD	Age	Lithology description					
4491/1368.8		Santonian	Shale, gray, firm, calcareous					
4900/1493.5		Turonian-Cenomanian	Shale, light-dark gray-brown, soft, limey, sandy, splity					
Depth MD (ft)/(m)	Depth TVD	Age	Lithology description					
5030/1533.1		Turonian-Cenomanian	Shale, light-dark gray-brown, soft, limey, sandy, splity					
5150/1569.7		Turonian-Cenomanian	Shale, brown to dark gray, laminated, very sandy					
5211/1588.3		Cenomanian	Sand, white-light gray, very firm, graded (?)					
5280/1609.3		Cenomanian-Albian	Shale, dark gray to black, firm, silty, flaky, SL (?), calcareous					
9800/2987		Albian-Aptian	Limestone, gray-black-white, dense, brittle, mottled, microcrystalline					
10430/3179.1		Jurassic	Coal, black, glossy, hard					
10600/3230.9		Jurassic?	LIG (?), black, firm-hard, shale, soft, sli (?), calcareous					

Depth MD (ft)/(m)	Depth TVD	Age	Lithology description
17000/5181.6		Jurassic?	Limestone, black, very firm, micaceous, no porosity
LESA notes			
Depth MD (ft)/(m)	Depth TVD	Age	Description
4491/1368.8		Santonian	Doesn't show up as a shale on the log-possibly very thin
4900/1493.5		Turonian-Cenomanian	Definitely a shale, but no big spike in GR and no real dip in density
5030/1533.1		Turonian-Cenomanian	Definitely a shale, but no big spike in GR and no real dip in density
5150/1569.7		Turonian-Cenomanian	Start of a non-shalely bit
5211/1588.3		Cenomanian	At 5215' it starts looking shalely again but still no dip in density
5280/1609.3		Cenomanian-Albian	Shaley area, small extra spike here, low density comparatively
9800/2987		Albian-Aptian	Tiny spike in a less shaley area, big dip in density
10430/3179.1		Jurassic	Shaley but nothing special
10600/3230.9		Jurassic?	Nothing promising
17000/5181.6		Jurassic?	Nothing promising

Table E-6. Well 608224001400 (Destin Dome block number 162).

API	Well name	Side track	By pass	Area code	Block	TD Date	Water depth (m)	Logged interval (mbsf)
608224001400	003	00	00	DD	162	29-May-75	78.6	1005.8-5364.5
Paleo version used:								
Paleo. notes								
Depth MD (ft)/(m)	Depth TVD	Age				Description		
Depth/Time of preceding non-interested interval:								
3100/944.9		Campanian						
Depth/Time of 1st interested interval:								
3219/981.3	3219	Santonian						
Depth/Time of last interested interval:								
9430/2874.3	9429	Aptian						
Depth/Time of next non-interested interval:								
9490/2892.6	9489	Berriasian						
Notes from paleo. on impt. intervals:								

Lithology notes			
Depth MD (ft)/(m)	Depth TVD	Age	Lithology description
3730/1136.9		Turonian-Cenomanian	Shale black limestone brown, tan, black
4545/1385.3		Albian	Shale with traces of limestone
6355-6360/ 1937-1938.5		Aptian	Shale with traces of sand and limestone
6505/1982.7		Aptian	Shale with sand, trace of LIG (?)
6785/2068.1		Aptian	Shale with traces of sand and limestone
9227/2812.4		Aptian	Sand, clear to tan, shale black and bladed
9400/2865.1		Aptian	Shale black?, limestone tan / dense
9510/2898.6		Berriasian	Shale black / red siliceous calcareous; sandstone clear-tan
LESA notes			
Depth MD (ft)/(m)	Depth TVD	Age	Description
3730/1136.9		Turonian-Cenomanian	Definitely a shale, but not nearly as big a spike in GR as in others and no dip in density
4545/1385.3		Albian	Big spike in GR big dip in density
6355-6360/ 1937-1938.5		Aptian	Big spike in GR big dip in density
6505/1982.7		Aptian	Big spike in GR but no big dip in density
6785/2068.1		Aptian	Big spike in GR but no big dip in density
9227/2812.4		Aptian	Big dip in GR, moderate dip in density
Depth MD (ft)/(m)	Depth TVD	Age	Description
9400/2865.1		Aptian	Above or below this spot looks shalely with low density- but @ 9400 directly there is a GR low & peak in density, possibly it is a limestone
9500/2895.6		Berriasian	Dip in density & more shalely GR but 9510 is the opposite

Table E-7. Well 608224001700 (Destin Dome block number 529).

API	Well name	Side track	By pass	Area code	Block	TD Date	Water depth (m)	Logged interval (mbsf)
608224001700	001	00	00	DD	529	14-Jun-80	69.2	914.4-6157.0
Paleo. version used:		Using paleo. report 2 because it is newer, more detailed and has slight conflicts with paleo. report 1.						
Paleo. notes								
Depth MD (ft)/(m)	Depth TVD	Age		Description				
Depth/Time of preceding non-interested interval:								
8680/2645.7	8680	Maastrichtian						

Depth/Time of 1st interested interval:		
8860/2700.5	8860	Turonian
Depth/Time of last interested interval:		
18900/5760.1	18898	Aptian
Depth/Time of next non-interested interval:		
20250/6172.2	20247	Tithonian (Jurassic)
Notes from paleo. on impt. intervals:		

Lithology notes			
Depth MD (ft)/(m)	Depth TVD	Age	Lithology description
11300ish/ 3444.2ish		Albian	Shale gray to black
11600/3535.7		Albian	Shale gray to black-pyrite interbedded with gray-white limestone
12050/3672.8		Albian	Shale gray to black-pyrite, calcite
17230/5251.7		Albian-Aptian	Limestone, brown to gray, with pyrite, integrated with gray to black siltstone to shale (this is less than 10% of total sample)
17600-17625/ 5364.5-5372.1		Albian-Aptian	Limestone, white-buff-tan, intermixed with crystalline sparite, with pyrite, traces of siltstone-shale with oolites
18525/5646.4		Aptian	Limestone, micrite intermixed with sparite
18600/5669.3		Aptian	Limestone, micrite intermixed with sparite
18650-18675/ 5684.5-5692.1		Aptian	Siltstone, dark to light gray, moderately hard, blocky and friable
18800/5730.2		Aptian	Limestone, micrite, oolite and pelite inclusions, sparite crystals, traces of pyrite
18950/5776		Aptian-older	Siltstone, medium to light gray, moderately hard to very soft and friable, traces of pyrite occasionally as veins,
18980/5785.1		Aptian-older	Siltstone, medium to light gray, moderately hard to very soft and friable, traces of pyrite occasionally as veins

LESA notes			
Depth MD (ft)/(m)	Depth TVD	Age	Description
11300/3444.2		Albian	Nothing promising in the logs
11600/3535.7		Albian	Nothing promising in the logs
12050/3672.8		Albian	Small spike in the GR and dip in the density-but nothing dramatic
17230/5251.7		Albian-Aptian	Big spike in Gr and big dip in density
17600-17625/ 5364.5-5372.1		Albian-Aptian	Big spike in Gr and big dip in density
18525/5646.4		Aptian	Big spike in Gr and big dip in density
18600/5669.3		Aptian	Big spike in Gr and big dip in density

Depth MD (ft)/(m)	Depth TVD	Age	Description
18631-18675/ 5678.7-5692.1		Aptian	Several Big spikes in Gr and big dips in density
18800/5730.2		Aptian	Big spike in Gr and big dip in density
18950/5776		Aptian-older	Big spike in Gr and big dip in density
18980/5785.1		Aptian-older	Big spike in Gr and big dip in density

Table E-8. Well 608224002200 (Destin Dome block number 284).

API	Well name	Side track	By pass	Area code	Block	TD Date	Water depth (m)	Logged interval (mbsf)
608224002200	001	00	00	DD	284	06-Nov-85	185.0	487.6-5334.0
Paleo. version used:								
Paleo. notes								
Depth MD (ft)/(m)	Depth TVD	Age						Description
Depth/Time of preceding non-interested interval:								
5090/1551.4		Campanian						
Depth/Time of 1st interested interval:								
5990/1825.8		Santonian						
Depth/Time of last interested interval:								
10460/3188.2		Aptian						
Depth/Time of next non-interested interval:								
10820/3297.9		Barremian						
Notes from paleo. on impt. intervals:								
6290/191.7								Tuscaloosa Formation

Lithology notes			
Depth MD (ft)/(m)	Depth TVD	Age	Lithology description
6180/1883.7		Santonian-Coniancian	Shale black, calcareous, trs. sand, fossils, platey
6290/191.7		Santonian-Coniancian	Shale black, calcareous, trs. sand, fossils, platey, traces of chalk
6400/1950.7		Coniancian-Turonian	Shale medium gray-black slity
6500ish/1981.2ish		Turonian	Shale black, abundant fossils, traces of chalk
LESA notes			
Depth MD (ft)/(m)	Depth TVD	Age	Description
6185/1885.2		Santonian-Coniancian	Compared to the immediately surrounding rocks there's a spike in GR here, but no corresponding decrease in density
6290/191.7		Santonian-Coniancian	Gr looks like its moving into shaley-er material, but nothing very promising
6400/1950.7		Coniancian-Turonian	Nothing promising in the logs
6500/1981.2		Turonian	Nothing promising in the logs

APPENDIX F - LITHOLOGY AND AGE SUMMARIES FOR THE GULF OF MEXICO WELLS

Table F-1. Gulf of Mexico well 177244005200 lithology and age summary.

Depth (m)	Depth (ft)	Lithology	Age
731.5-2042.2	2400.0-6700.0	Interbedded unconsolidated sands and shales	Pliocene-Late Miocene
2042.2-2987.0	6700.0-9800.0	Interbedded consolidated sands and shales	Late Miocene
2987.0-3139.4	9800.0-10300.0	Interbedded sands and shales with traces of limestone and pyrite	Late Miocene
3139.4-3767.3	10300.0-12360.0	Interbedded sands with traces of calcareous sediments and shales with traces of limestone and pyrite	Late Miocene
3767.3-3822.2	12360.0-12540.0	Chalk	Late Miocene
3822.2-3913.6	12540.0-12840.0	Interbedded shales and sandstone with calcareous sediment and pyrite	Late Miocene
3913.6-3922.8	12840.0-12870.0	Marl	Late Miocene
3922.8-3931.9	12870.0-12900.0	Shale-black, waxy, brittle	Late Miocene
3931.9-3992.9	12900.0-13100.0	Marl	Late Miocene
3992.9-4114.8	13100.0-13500.0	Chalk-with some interbedded pyrite	Middle Miocene
4114.8-4322.1	13500.0-14180.0	Limestone	Middle Eocene-Maastrichtian
4322.1-4376.9	14180.0-14360.0	Chalk with traces of pyrite and limestone	Maastrichtian
4376.9-4395.2	14360.0-14420.0	Shale-black, limey, and chalky with traces of pyrite	Santonian
4395.2-4431.8	14420.0-14540.0	Shale-brown to black, carbonated	Santonian-Cenomanian
4431.8-4456.2	14540.0-14620.0	Limestone	Cenomanian
4456.2-TD	14620.0-TD	Dolomite and Anhydrate	Cenomanian-Albian

Table F-2. Gulf of Mexico well 177244005400 lithology and age summary.

Depth (m)	Depth (ft)	Lithology	Age
2407.9-2438.4	7900.0-8000.0	Chalk with limestone	Late Paleocene-Early Eocene
2438.4-2468.9	8000.0-8100.0	Limestone	Late Paleocene-Early Eocene
2468.9-2505.5	8100.0-8220.0	Chalk with pyrite	Early Eocene
2505.5-2743.2	8220.0-9000.0	Interbedded shale and limestone	Early Eocene-Maastrichtian
2743.2-2798.1	9000.0-9180.0	Limestone	Maastrictian-Cenomanian
2798.1-2834.6	9180.0-9300.0	Interbedded limestone, sandstone and shale	Maastrictian-Cenomanian
2834.6-2971.8	9300.0-9750.0	Interbedded limestone and sandstone	Maastrictian-Cenomanian
2971.8-2993.1	9750.0-9820.0	Shale	Maastrictian-Cenomanian
2993.1-3200.4	9820.0-10500.0	Limestone with traces of pyrite	Maastrictian-Albian
3200.4-3459.5	10500.0-11350.0	Limestone	Albian
3459.5-3505.2	11350.0-11500.0	Interbedded limestone and dolomite	Albian
3505.2-4450.1	11500.0-14600.0	Limestone	Albian-Aptian

Depth (m)	Depth (ft)	Lithology	Age
4450.1-4541.5	14600.0-14900.0	Limestone-dark gray to black	Aptian
4541.5-4602.5	14900.0-15100.0	Limestone	Aptian
4602.5-4648.2	15100.0-15250.0	Limestone-dark gray to black	Aptian
4648.2-TD	15250.0-TD	Limestone	Aptian

Table F-3. Gulf of Mexico well 177244006300 lithology and age summary.

Depth (m)	Depth (ft)	Lithology	Age
883.9-1950.7	2900.0-6400.0	Interbedded shales and sandstones	Early Pliocene-Late Miocene
1950.7-2036.1	6400.0-6680.0	Interbedded shales, limestone and sandstone	Late Miocene
2036.1-2255.5	6680.0-7400.0	Interbedded shales and sandstones	Late-Early Miocene
2255.5-2468.9	7400.0-8100.0	Interbedded shales, limestone and sandstone	Early Miocene-Middle Eocene
2468.9-2529.8	8100.0-8300.0	Limestone	Middle-Early Eocene
2529.8-2712.7	8300.0-8900.0	Interbedded shale and limestone with traces of pyrite and glauconite	Early Miocene-Maastrichtian
2712.7-2731.0	8900.0-8960.0	Interbedded black shale and limestone with glauconite	Maastrichtian
2731.0-2880.4	8960.0-9450.0	Interbedded shale and limestone	Maastrichtian-Cenomanian
2880.4-2956.6	9450.0-9700.0	Limestone	Maastrichtian-Cenomanian
2956.6-2999.2	9700.0-9840.0	Interbedded shale and limestone	Maastrichtian-Cenomanian
2999.2-3011.4	9840.0-9880.0	Interbedded shale, limestone and sandstone	Maastrichtian-Cenomanian
3011.4-3307.1	9880.0-10850.0	Limestone	Cenomanian-Albian
3307.1-3383.3	10850.0-11100.0	Interbedded shale-black to dark gray and limestone-traces of pyrite and glauconite	Albian
3383.3-TD	11100.0-TD	Interbedded shale and limestone	Albian

Table F-4. Gulf of Mexico well 608164003700 lithology and age summary.

Depth (m)	Depth (ft)	Lithology	Age
1280.2-1463.0	4200.0-4800.0	Interbedded limestone and shale	Unknown
1463.0-1585.0	4800.0-5200.0	Limestone	Unknown-Late Oligocene
1585.0-1667.3	5200.0-5470.0	Interbedded sandstone and shale	Late Oligocene
1667.3-1780.5	5470.0-5840.0	Limestone	Late-Early Oligocene
1780.5-1807.5	5840.0-5930.0	Shale	Early Oligocene-Late Eocene
1807.5-1853.2	5930.0-6080.0	Interbedded limestone and shale with traces of pyrite and glauconite	Late-Middle Eocene
1853.2-1950.7	6080.0-6400.0	Shale	Early Eocene

Depth (m)	Depth (ft)	Lithology	Age
1950.7-2042.2	6400.0-6700.0	Interbedded limestone and shale	Early Eocene-Late Paleocene
2042.2-2148.8	6700.0-7050.0	Shale	Late Paleocene
2148.8-2179.3	7050.0-7150.0	Limestone	Late Paleocene-Maastrichtian
2179.3-2209.8	7150.0-7250.0	Shale-black with some limestone	Maastrichtian-Campanian
2209.8-2279.9	7250.0-7480.0	Limestone	Campanian
2279.9-2310.4	7480.0-7580.0	Shale	Campanian
2310.4-2331.7	7580.0-7650.0	Shale-black and calcareous	Campanian
2331.7-2398.8	7650.0-7870.0	Interbedded limestone and shale	Campanian
2398.8-2423.2	7870.0-7950.0	Shale-black, calcareous, traces of pyrite	Campanian
2423.2-2456.7	7950.0-8060.0	Limestone	Campanian
2456.7-2520.7	8060.0-8270.0	Shale-black and calcareous	Campanian
2520.7-2615.2	8270.0-8580.0	Shale-black, non-calcareous	Campanian-Santonian
2615.2-2770.6	8580.0-9090.0	Shale-weakly calcareous	Santonian-Turonian
2770.6-2804.2	9090.0-9200.0	Limestone	Turonian-Cenomanian
2804.2-2880.4	9200.0-9450.0	Interbedded shale-black and limestone	Cenomanian
2880.4-2886.5	9450.0-9470.0	Limestone	Cenomanian
2886.5-2926.1	9470.0-9600.0	Shale-calcareous	Cenomanian
2926.1-2944.4	9600.0-9660.0	Limestone	Cenomanian
2944.4-2968.8	9660.0-9740.0	Limestone with traces of sandstone	Cenomanian-Albian
2968.8-3109.0	9740.0-10200.0	Shale	Albian
3109.0-TD	10200.0-TD	Limestone	Albian

Table F-5. Gulf of Mexico well 608224000600 lithology and age summary.

Depth (m)	Depth (ft)	Lithology	Age
396.2-426.7	1300.0-1400.0	Sandstone	Unknown
426.7-1005.8	1400.0-3300.0	Limestone	Unknown
1005.8-1036.3	3300.0-3400.0	Shale-calcareous	Unknown
1036.3-1127.8	3400.0-3700.0	Limestone	Unknown
1127.8-1140.0	3700.0-3740.0	Shale-calcareous	Unknown
1140.0-1249.7	3740.0-4100.0	Interbedded limestone and shale	Unknown
1249.7-1261.9	4100.0-4140.0	Sandstone	Maastrichtian
1261.9-1322.8	4140.0-4340.0	Limestone	Maastrichtian-Campanian
1322.8-1368.6	4340.0-4490.0	Shale-calcareous	Campanian-Santonian
1368.6-1399.0	4490.0-4590.0	Limestone	Santonian
1399.0-1569.7	4590.0-5150.0	Shale-limey	Santonian-Turonian
1569.7-1585.0	5150.0-5200.0	Interbedded shale-dark gray to black and sandy limestone	Turonian-Cenomanian
1585.0-1615.4	5200.0-5300.0	Interbedded shale and sandstone	Cenomanian-Albian
1615.4-1947.7	5300.0-6390.0	Interbedded shale, sandstone and limestone	Cenomanian-Albian
1947.7-1996.4	6390.0-6550.0	Interbedded shale and sandstone	Cenomanian-Albian
1996.4-2011.7	6550.0-6600.0	Chalk	Cenomanian-Albian

Depth (m)	Depth (ft)	Lithology	Age
2011.7-2560.3	6600.0-8400.0	Interbedded shale and sandstone with traces of anhydrate throughout	Cenomanian-Albian
2560.3-2651.8	8400.0-8700.0	Interbedded shale, sandstone and limestone	Albian
2651.8-2728.0	8700.0-8950.0	Interbedded limestone, shale and anhydrate	Albian
2728.0-2743.2	8950.0-9000.0	Interbedded shale and limestone	Albian
2743.2-2773.7	9000.0-9100.0	Sandstone	Albian
2773.7-2788.9	9100.0-9150.0	Limestone	Albian
2788.9-2834.6	9150.0-9300.0	Interbedded limestone, dolostone and anhydrate	Albian
2843.6-2895.6	9300.0-9500.0	Interbedded sand and shale with some anhydrate throughout	Albian
2895.6-3048.0	9500.0-10000.0	Interbedded shale, sandstone and limestone	Albian
3048.0-3169.9	10000.0-10400.0	Interbedded sand and shale	Albian-Late Jurassic
3169.9-3185.2	10400.0-10450.0	Coal	Late Jurassic
3185.2-3307.1	10450.0-10850.0	Interbedded sand and shale	Late Jurassic
3307.1-3444.2	10850.0-11300.0	Interbedded shale, sandstone and limestone	Late Jurassic
3444.2-3992.9	11300.0-13100.0	Interbedded limey sand and shale	Late Jurassic
3992.9-4267.2	13100.0-14000.0	Interbedded sand and shale with traces of anhydrate throughout	Late Jurassic
4267.2-5090.2	14000.0-16700.0	Interbedded sand and shale	Late Jurassic
5090.2-5181.6	16700.0-17000.0	Interbedded dolostone and limestone	Late Jurassic
5181.6-5196.8	17000.0-17050.0	Limestone-black	Late Jurassic
5196.8-5242.6	17050.0-17200.0	Interbedded dolostone, shale and limestone	Late Jurassic
5242.6-5288.3	17200.0-17350.0	Interbedded shale, sandstone and limestone	Late Jurassic
5288.3-5318.8	17350.0-17450.0	Dolostone	Late Jurassic
5318.8-5346.2	17450.0-17540.0	Limestone	Late Jurassic
5346.2-TD	17540.0-TD	Salt	Late Jurassic

Table F-6. Gulf of Mexico well 608224001400 lithology and age summary.

Depth (m)	Depth (ft)	Lithology	Age
304.8-798.6	1000.0-2620.0	Limestone	Late Oligocene-Middle Eocene
798.6-838.2	2620.0-2750.0	Shale	Middle Eocene
838.2-887.0	2750.0-2910.0	Limestone	Middle-Early Eocene
887.0-960.1	2910.0-3150.0	Chalk	Early Eocene-Campanian
960.1-1140.0	3150.0-3740.0	Limestone	Campanian-Albian
1140.0-1274.1	3740.0-4180.0	Shale	Campanian-Albian
1274.1-1325.9	4180.0-4350.0	Limestone	Albian-Early Cretaceous
1325.9-1429.5	4350.0-4690.0	Shale	Albian-Early Cretaceous
1429.5-1432.6	4690.0-4700.0	Shale-calcareous	Albian-Early Cretaceous
1432.6-1606.3	4700.0-5270.0	Shale	Albian-Early Cretaceous
1606.3-1676.4	5270.0-5500.0	Limestone	Albian-Early Cretaceous
1676.4-2100.1	5500.0-6890.0	Shale	Albian-Early Cretaceous
2100.1-2164.1	6890.0-7100.0	Sandstone	Albian-Early Cretaceous
2164.1-2218.9	7100.0-7280.0	Shale	Albian-Early Cretaceous
2218.9-2340.9	7280.0-7680.0	Interbedded shale and sandstone	Albian-Early Cretaceous

Depth (m)	Depth (ft)	Lithology	Age
2340.9-2511.6	7680.0-8240.0	Interbedded shale and limestone	Albian-Early Cretaceous
2511.6-2542.0	8240.0-8340.0	Anhydrate	Albian-Early Cretaceous
2542.0-2590.8	8340.0-8500.0	Limestone and anhydrate	Albian-Early Cretaceous
2590.8-2804.2	8500.0-9200.0	Interbedded shale and limestone	Albian-Early Cretaceous
2804.2-2865.1	9200.0-9400.0	Sandstone	Early Cretaceous-Late Jurassic
2865.1-2880.4	9400.0-9450.0	Limestone	Late Jurassic
2880.4-2956.6	9450.0-9700.0	Shale-black	Late Jurassic
2956.6-3352.8	9700.0-11000.0	Shale	Late Jurassic
3352.8-5105.4	11000.0-16750.0	Interbedded sandstone and shale	Late Jurassic
5105.4-5120.6	16750.0-16800.0	Limestone	Late Jurassic
5120.6-TD	16800.0-TD	Interbedded shale and limestone	Late Jurassic

Table F-7. Gulf of Mexico well 608224001700 lithology and age summary.

Depth (m)	Depth (ft)	Lithology	Age
2255.5-2286.0	7400.0-7500.0	Siltstone	Middle Eocene
2286.0-2316.5	7500.0-7600.0	Siltstone-calcareous	Middle Eocene
2316.5-2621.3	7600.0-8600.0	Siltstone	Early Eocene-Maastrichtian
2621.3-2651.8	8600.0-8700.0	Limestone	Maastrichtian
2651.8-2682.2	8700.0-8800.0	Siltstone-calcareous	Maastrichtian-Turonian
2682.2-2712.7	8800.0-8900.0	Silty limestone	Turonian-Cenomanian
2712.7-2773.7	8900.0-9100.0	Limestone	Cenomanian-Albian
2773.7-2804.2	9100.0-9200.0	Silty limestone	Albian
2804.2-2865.1	9200.0-9400.0	Siltstone	Albian
2865.1-2895.6	9400.0-9500.0	Sandy limestone	Albian
2895.6-2987.0	9500.0-9800.0	Limestone	Albian
2987.0-3017.5	9800.0-9900.0	Shale	Albian
3017.5-3109.0	9900.0-10200.0	Siltstone	Albian
3109.0-3169.9	10200.0-10400.0	Limestone	Albian
3169.9-3200.4	10400.0-10500.0	Siltstone	Albian
3200.4-3261.4	10500.0-10700.0	Shale	Albian
3261.4-3322.3	10700.0-10900.0	Limestone	Albian
3322.3-3413.8	10900.0-11200.0	Siltstone	Albian
3413.8-3444.2	11200.0-11300.0	Shale	Albian
3444.2-3505.2	11300.0-11500.0	Limestone	Albian
3505.2-3535.7	11500.0-11600.0	Shale-gray to black	Albian
3535.7-3596.6	11700.0-11800.0	Siltstone-gray to black	Albian
3596.6-3627.1	11800.0-11900.0	Limestone	Albian
3627.1-3657.6	11900.0-12000.0	Siltstone	Albian
3657.6-3749.0	12000.0-12300.0	Shale-gray to black	Albian
3749.0-3810.0	12300.0-12500.0	Limestone	Albian
3810.0-3840.5	12500.0-12600.0	Siltstone	Albian
3840.5-3931.9	12600.0-12900.0	Limestone	Albian
3931.9-3962.4	12900.0-13000.0	Shale	Albian

Depth (m)	Depth (ft)	Lithology	Age
3962.4-3992.9	13000.0-13100.0	Siltstone	Albian
3992.9-4236.7	13100.0-13900.0	Interbedded limestone and siltstone	Albian-Aptian
4236.7-4267.2	13900.0-14000.0	Shale	Albian-Aptian
4267.2-4419.6	14000.0-14500.0	Limestone	Albian-Aptian
4419.6-4450.1	14500.0-14600.0	Sandstone and siltstone	Albian-Aptian
4450.1-4480.6	14600.0-14700.0	Siltstone	Albian-Aptian
4480.6-5699.8	14700.0-18700.0	Limestone	Albian-Aptian
5699.8-5730.2	18700.0-18800.0	Siltstone	Aptian
5730.2-5852.2	18800.0-19200.0	Interbedded limestone and siltstone	Aptian
5852.2-5974.1	19200.0-19600.0	Limestone	Aptian
5974.1-6035.0	19600.0-19800.0	Dolomite	Aptian
6035.0-6065.5	19800.0-19900.0	Siltstone	Aptian
6065.5-6187.4	19900.0-20300.0	Limestone	Aptian-Late Jurassic
6187.4-TD	20300.0-TD	Interbedded limestone and siltstone	Late Jurassic

Table F-8. Gulf of Mexico well 608224002200 lithology and age summary.

Depth (m)	Depth (ft)	Lithology	Age
1036.3-1280.2	3400.0-4200.0	Chalk	Early Oligocene-Middle Eocene
1280.2-1402.1	4200.0-4600.0	Siltstone	Middle-Early Eocene
1402.1-1524.0	4600.0-5000.0	Shale	Middle-Early Eocene
1524.0-1585.0	5000.0-5200.0	Chalk	Early Eocene-Santonian
1585.0-1706.9	5200.0-5600.0	Interbedded clay, shale and chalk	Campanian-Santonian
1706.9-1828.8	5600.0-6000.0	Chalk	Santonian
1828.8-2103.1	6000.0-6900.0	Shale-black	Santonian-Cenomanian
2103.1-2133.6	6900.0-7000.0	Shale	Cenomanian-Albian
2133.6-2164.1	7000.0-7100.0	Sandstone	Cenomanian-Albian
2164.1-2468.9	7100.0-8100.0	Interbedded shale, limestone and siltstone	Cenomanian-Albian
2468.9-2621.3	8100.0-8600.0	Anhydrate	Albian
2621.3-2804.2	8600.0-9200.0	Interbedded shale and limestone	Albian-Aptian
2804.2-2865.1	9200.0-9400.0	Sandstone	Aptian
2865.1-2926.1	9400.0-9600.0	Shale	Aptian
2926.1-3078.5	9600.0-10100.0	Interbedded limestone and siltstone	Aptian
3078.5-3261.4	10100.0-10700.0	Sandstone	Aptian-Barremian
3261.4-3352.8	10700.0-11000.0	Interbedded sandstone and limestone	Aptian-Barremian
3352.8-3657.6	11000.0-12000.0	Interbedded sandstone, limestone, siltstone, and dolomite	Barremian
3657.6-4084.3	12000.0-13400.0	Limestone with occassional anhydrate	Barremian-Hauterivian
4084.3-4236.7	13400.0-13900.0	Interbedded sandstone, limestone, siltstone, and shale	Hauterivian
4236.7-4267.2	13900.0-14000.0	Anhydrate	Hauterivian-Berriasian
4267.2-4633.0	14000.0-15200.0	Limestone	Hauterivian-Berriasian
4633.0-4724.4	15200.0-15500.0	Interbedded shale and sandstone	Berriasian
4724.4-4785.4	15500.0-15700.0	Limestone	Berriasian-Valanginian
4785.4-4815.8	15700.0-15800.0	Siltstone	Unknown
4815.8-4563.4	15800.0-16100.0	Sandstone	Unknown
4563.4-4998.7	16100.0-16400.0	Interbedded shale-black and sandstone	Unknown

Depth (m)	Depth (ft)	Lithology	Age
4998.7-5212.1	16400.0-17100.0	Interbedded limestone and sandstone	Unknown
5212.1-5334.0	17100.0-17500.0	Siltstone	Unknown
5334.0-TD	17500.0-TD	Sandstone	Unknown

APPENDIX G - BOREHOLE LOGS THROUGH POTENTIAL OAE INTERVALS IN THE GULF OF MEXICO WELLS

Figure G-1. Well 177244005200; gamma ray log, density and neutron porosity response from 1524.0 mbsf to 4572.0 mbsf. The red arrow indicates depth of Cenomanian-age shale potenitally associated with deposition during an OAE.

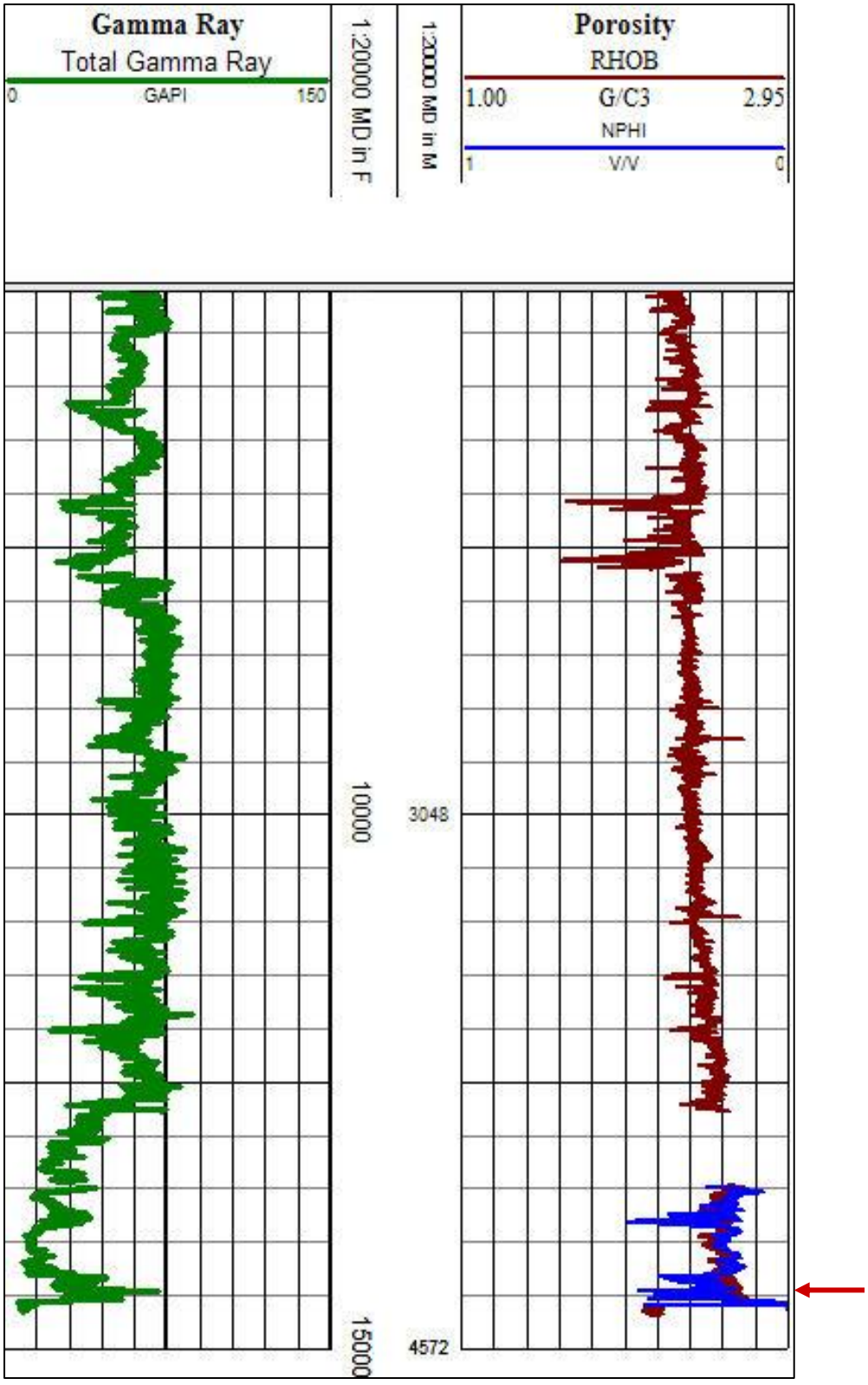

Figure G-2. Well 177244005200; gamma ray log, density and neutron porosity response detail through Cenomanian-age brown to black shale potentially associated with OAE deposition. The upper boundary of the section of interest is indicated with a red line and the lower boundary is indicated with a light green line.

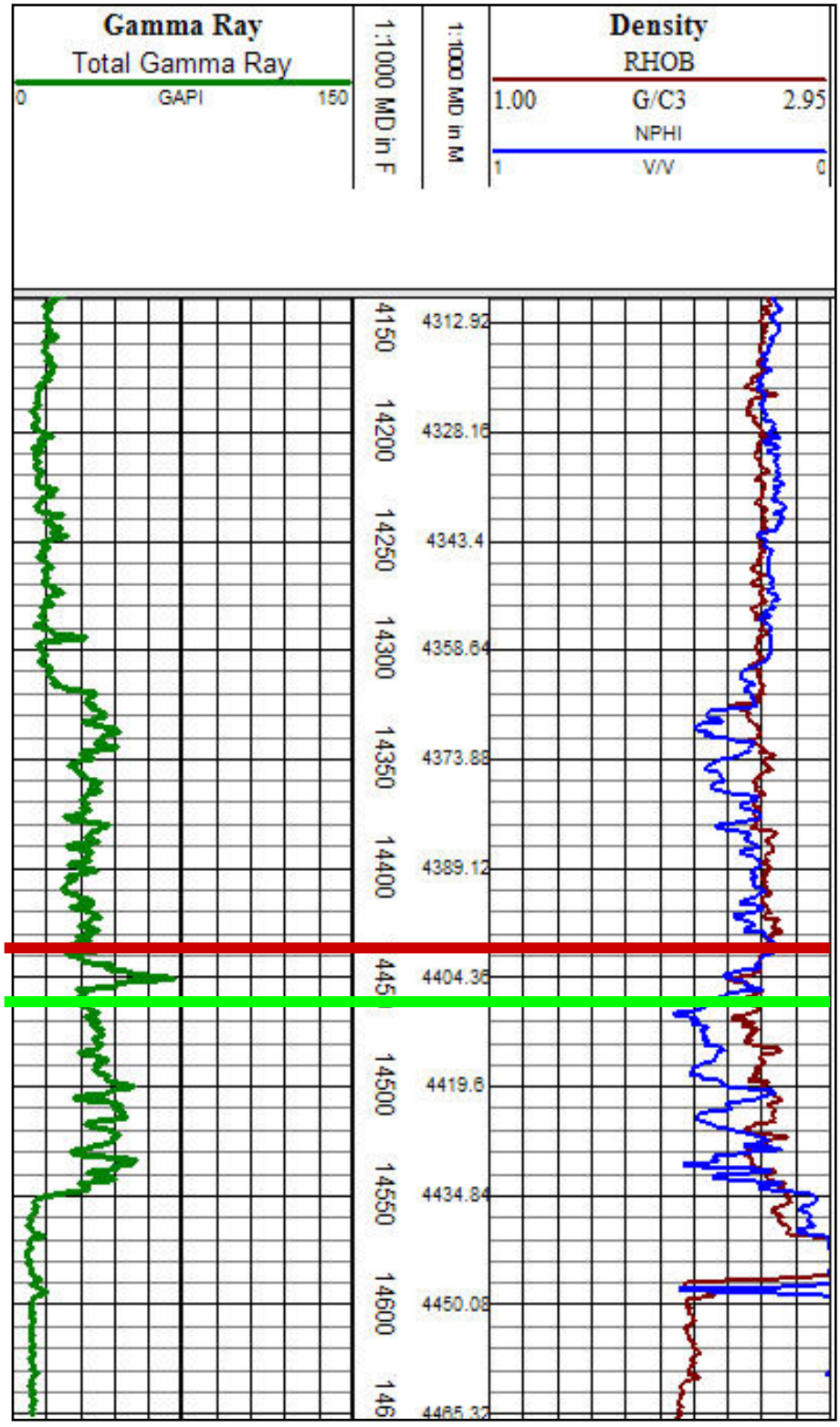

Figure G-3. Well 177244005400; gamma ray log, density and neutron porosity response over total logged interval. Red lines indicate depth of Albian-Aptian-age black to dark gray limestone potenitally associated with deposition during an OAE.

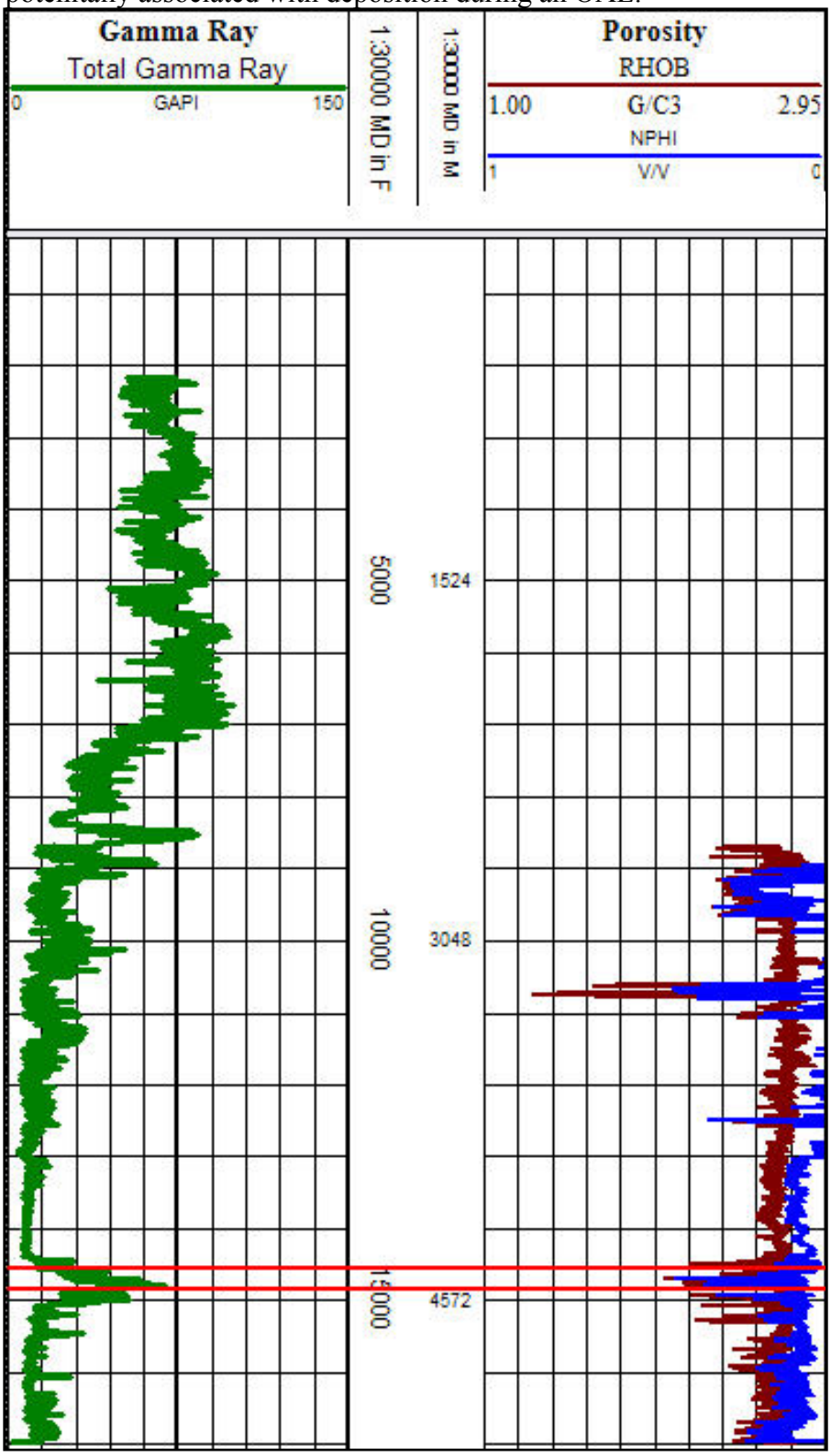

Figure G-4. Well 177244005400; gamma ray log, density and neutron porosity response detail through Albian-Aptian-age black to dark gray limestone potentially associated with OAE deposition. The upper boundary of the section of interest is indicated with a red line and the lower boundary is indicated with a light green line.

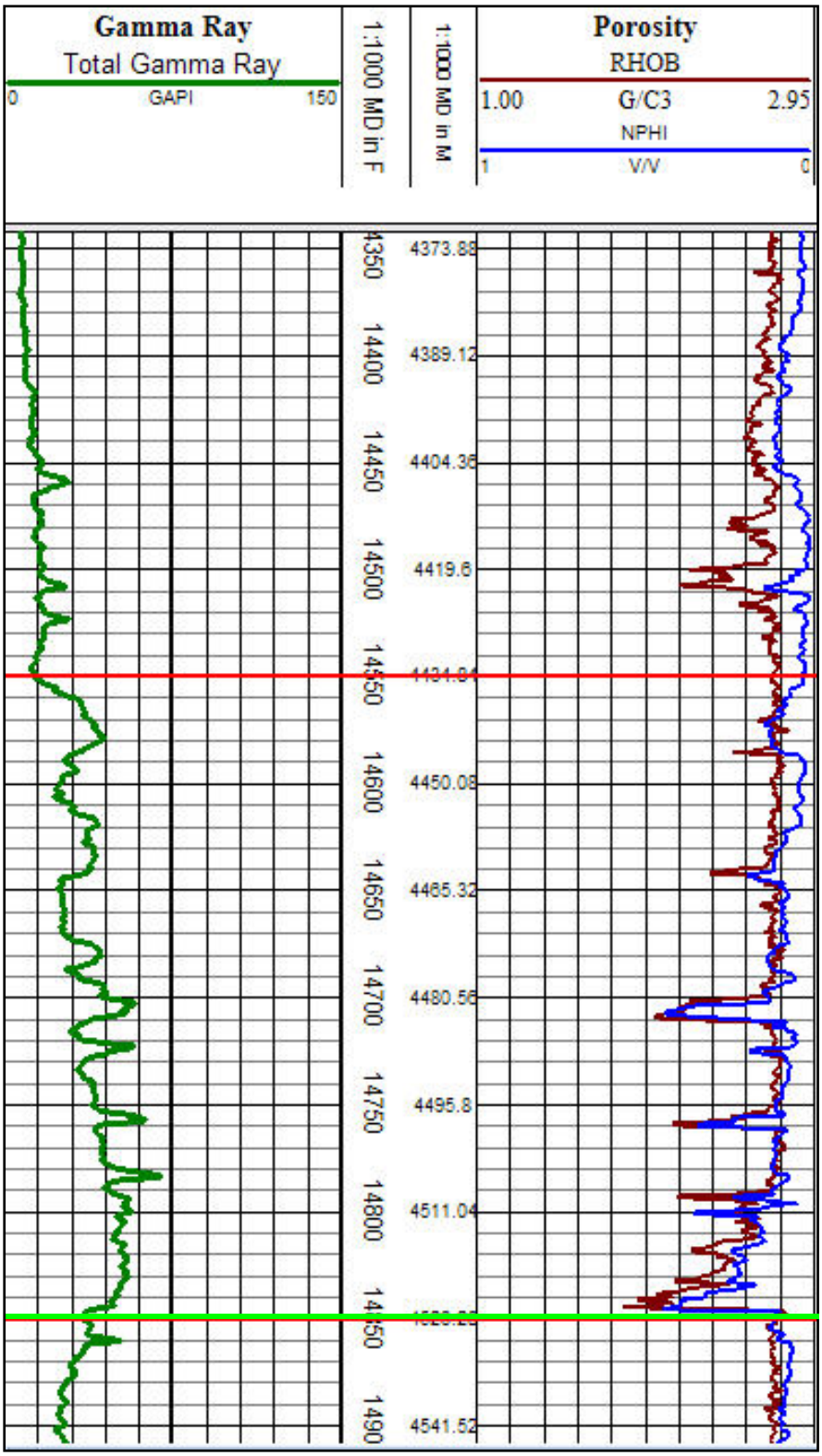

Figure G-5. Well 177244006300; gamma ray log, density and neutron porosity response over total logged interval. A red line indicates the upper boundary of a Turonian-Cenomanian-age calcareous shale potentially deposited during an OAE, the lower boundary is marked with a light green line. The depth of an Albian-age black calcareous shale potenitally associated with deposition during an OAE is marked with a dark orange line.

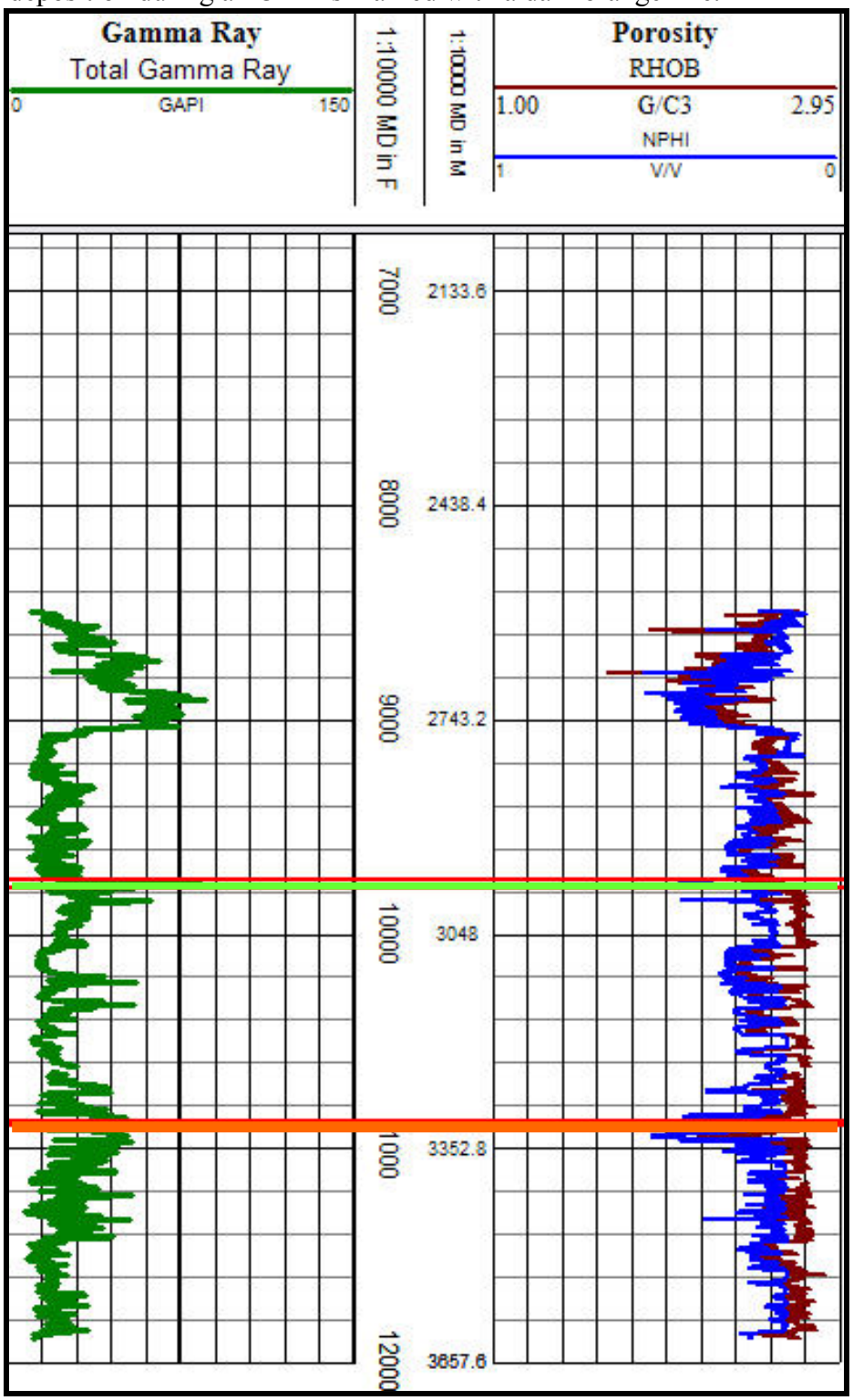

Figure G-6. Well 177244006300; gamma ray log, density and neutron porosity response detail through Turonian-Cenomanian-age calcareous shale potentially associated with OAE deposition. The upper boundary of the section of interest is indicated with a red line and the lower boundary is indicated with a light green line.

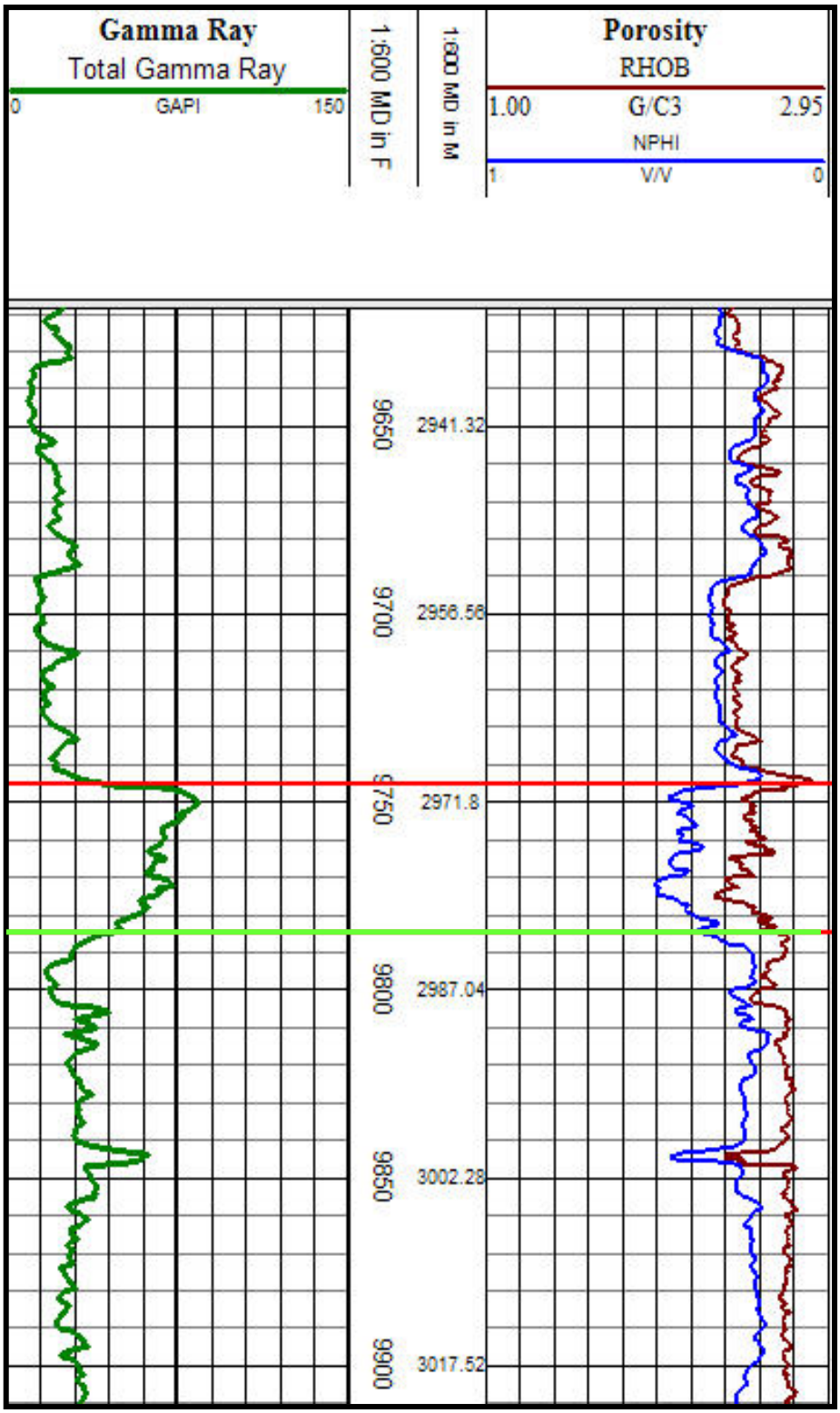

Figure G-7. Well 177244006300; gamma ray log, density and neutron porosity response detail through Albian-age dark gray-black shale potentially associated with OAE deposition. The upper boundary of the section of interest is indicated with a red line and the lower boundary is indicated with a light green line.

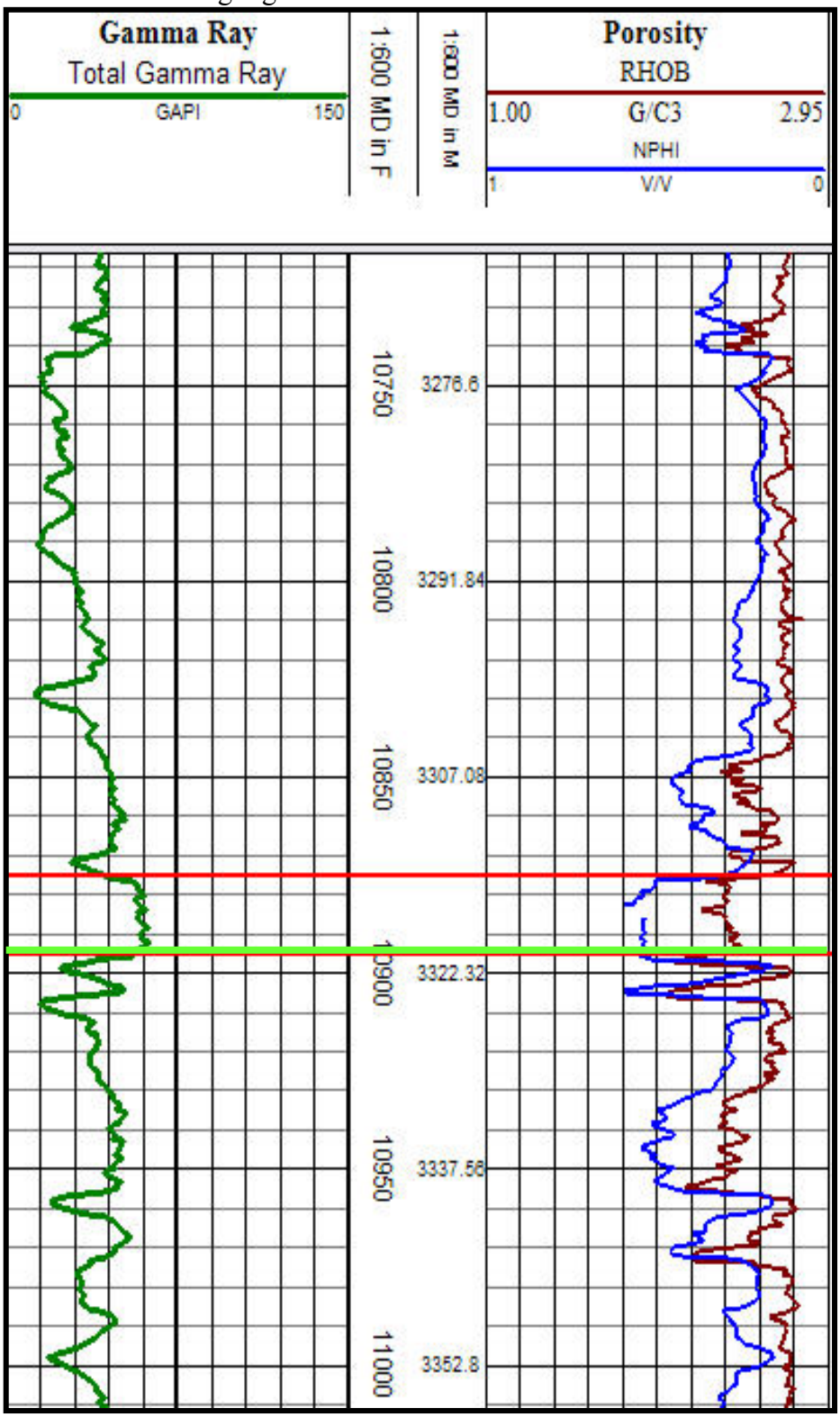

Figure G-8. Well 608164003700; gamma ray log, density and neutron porosity response over total logged interval. Red line indicates aproxiamte depth of Turonian-Cenomanian-age black/gray shale potenitally associated with deposition during an OAE.

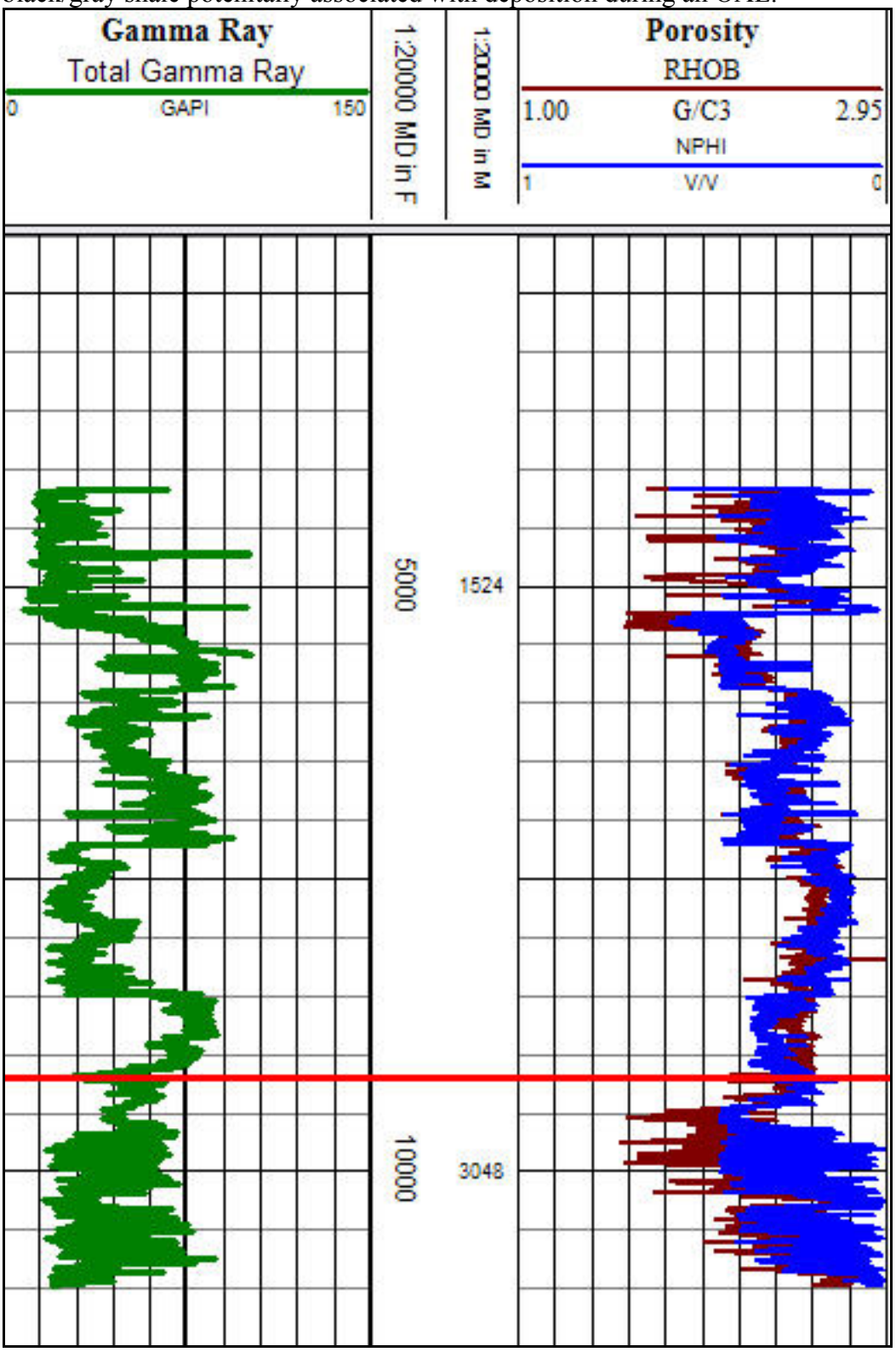

Figure G-9. Well 608164003700; gamma ray log, density and neutron porosity response detail through Turonian-Cenomanian-age black/gray shale potentially associated with OAE deposition. The upper boundary of the section of interest is indicated with a red line and the lower boundary is indicated with a light green line.

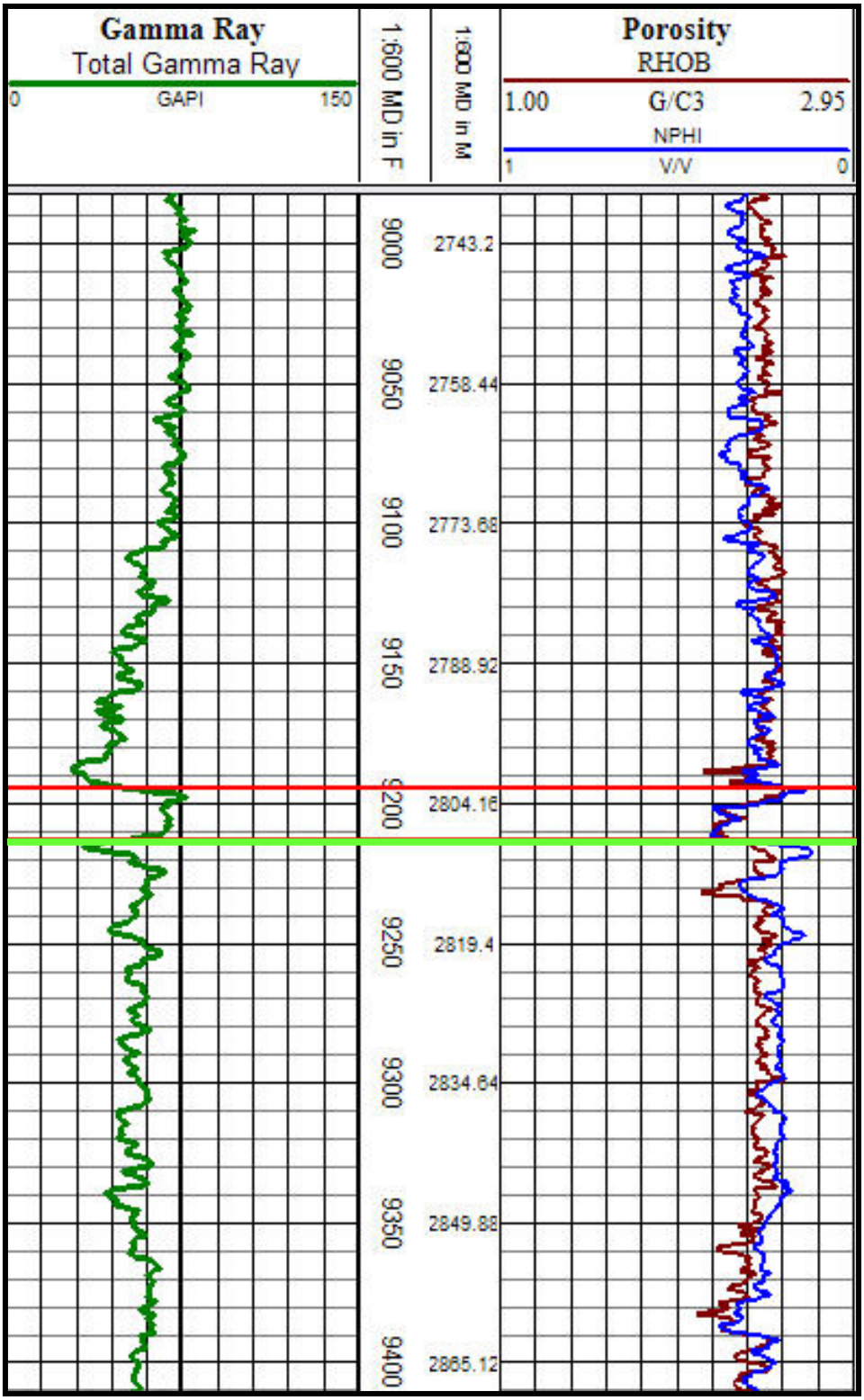

Figure G-10. Well 608224000600; gamma ray log, density and neutron porosity response over total logged interval. Red line indicates approximate depth of Turonian-Cenomanian-age Tuscaloosa Formation shale potenitally associated with deposition during an OAE.

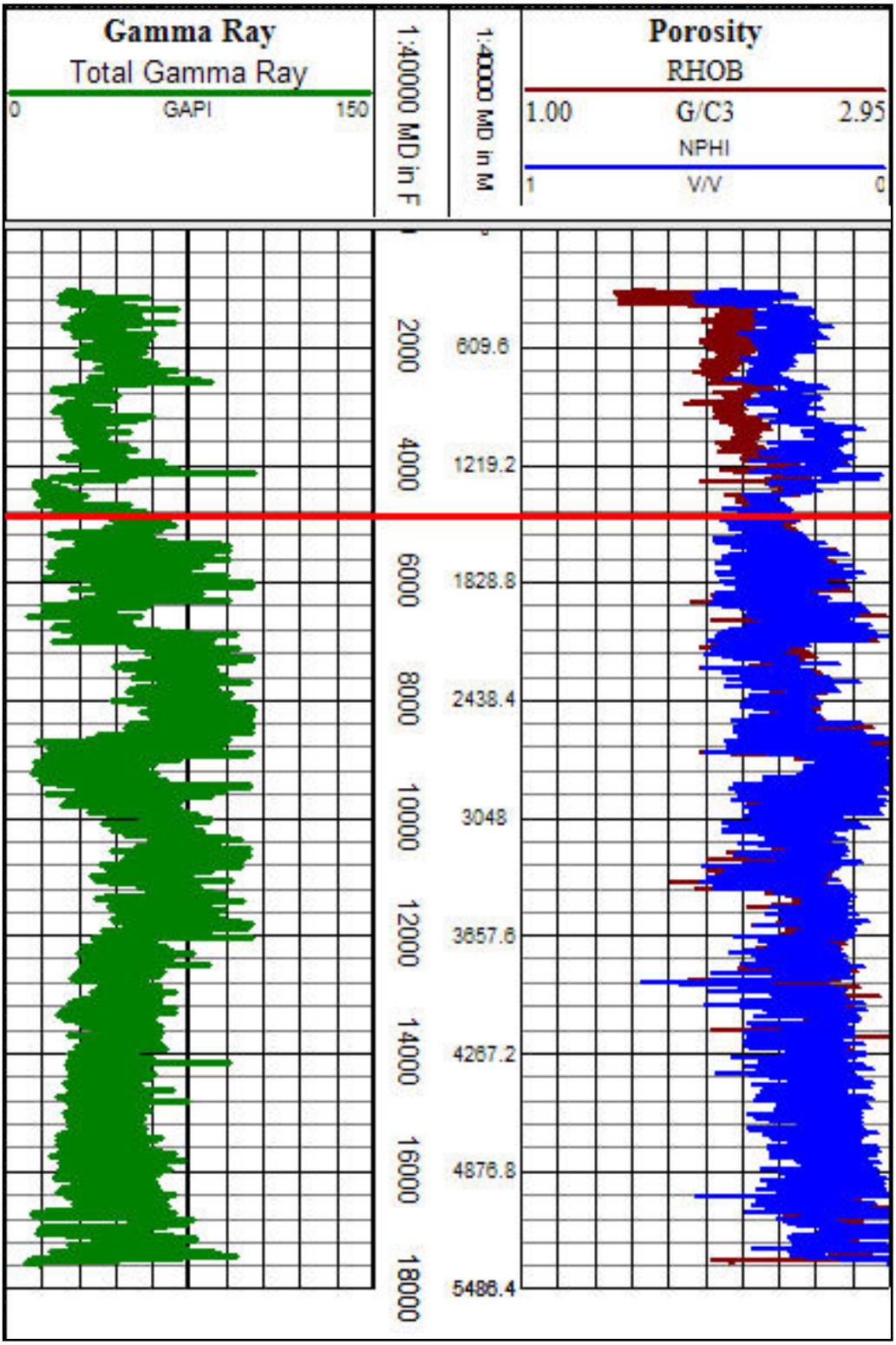

Figure G-11. Well 608224000600; gamma ray log, density and neutron porosity response detail through Turonian-Cenomanian-age Tuscaloosa Formation shale potentially associated with OAE deposition. The upper boundary of the section of interest is indicated with a red line and the lower boundary is indicated with a light green line.

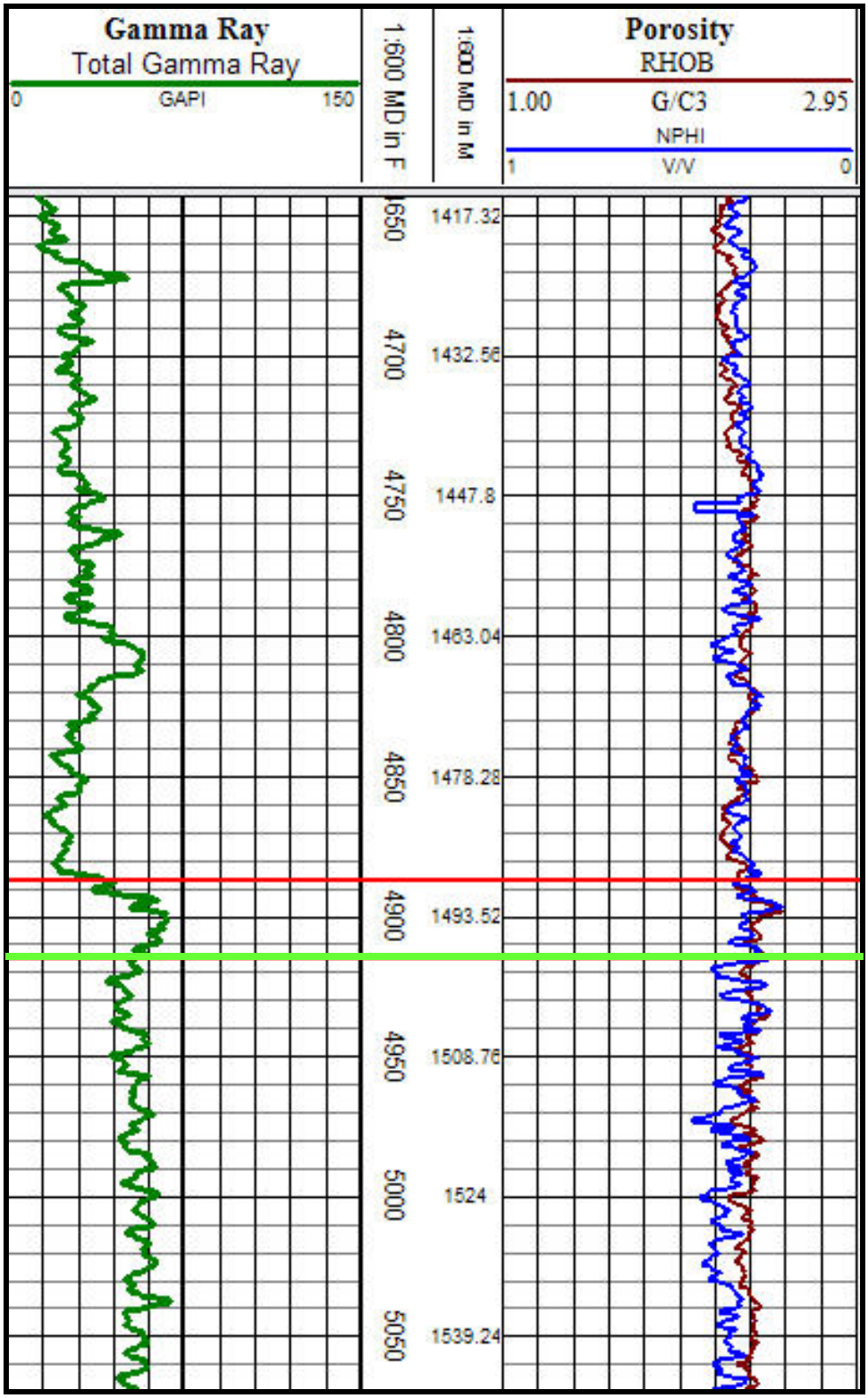

Figure G-12. Well 608224001400; gamma ray log, density and neutron porosity response over total logged interval. Red lines indicate approximate depths of multiple Albian and Aptian-age shales potenitally associated with deposition during an OAE.

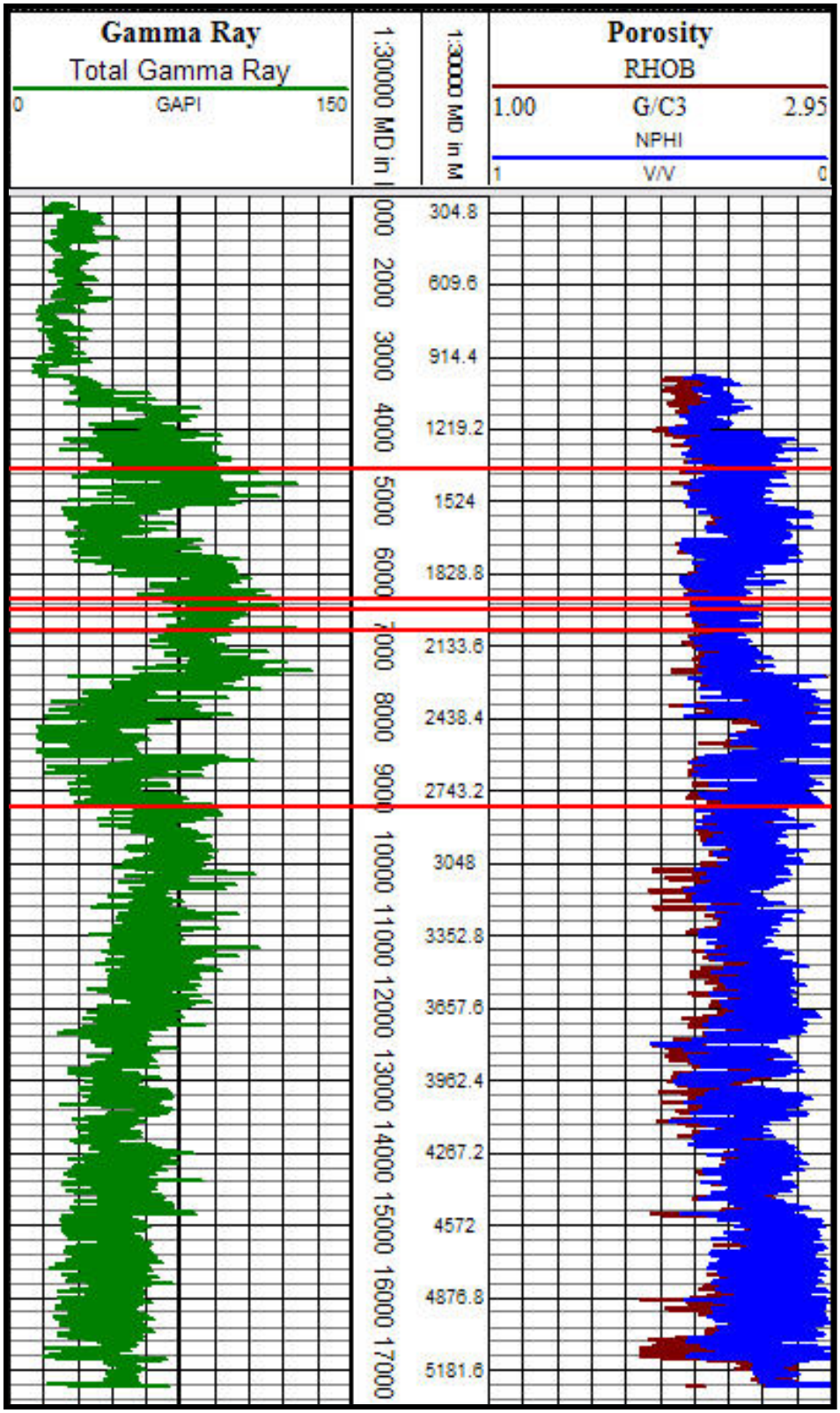

Figure G-13. Well 608224001400; gamma ray log, density and neutron porosity response detail through Albian-age shale potentially associated with OAE deposition. The upper boundary of the section of interest is indicated with a red line and the lower boundary is indicated with a light green line.

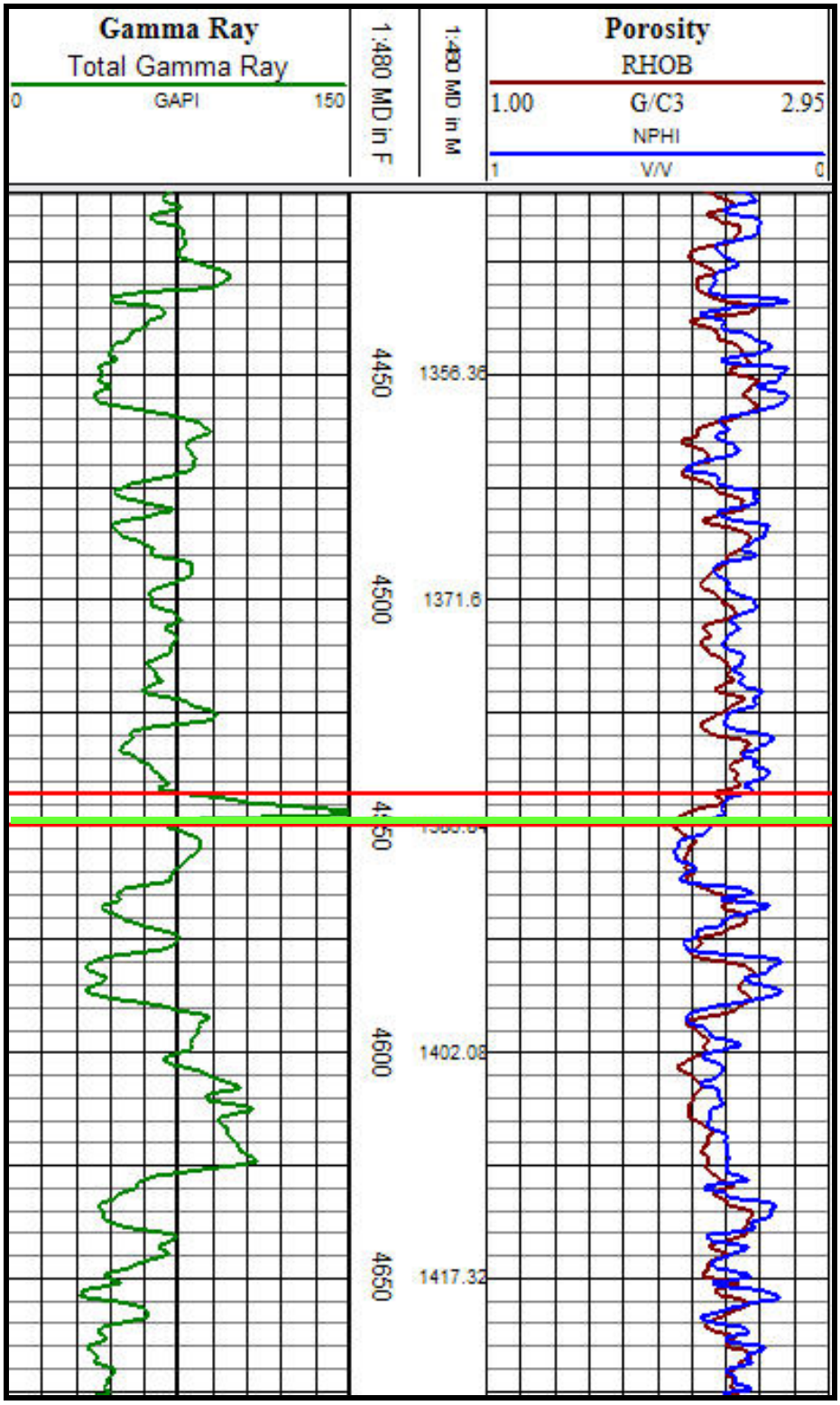

Figure G-14. Well 608224001400; gamma ray log, density and neutron porosity response detail through two Aptian-age shales potentially associated with OAE deposition. The upper boundaries of the sections of interest are indicated with red lines and the lower boundaries are indicated with light green lines.

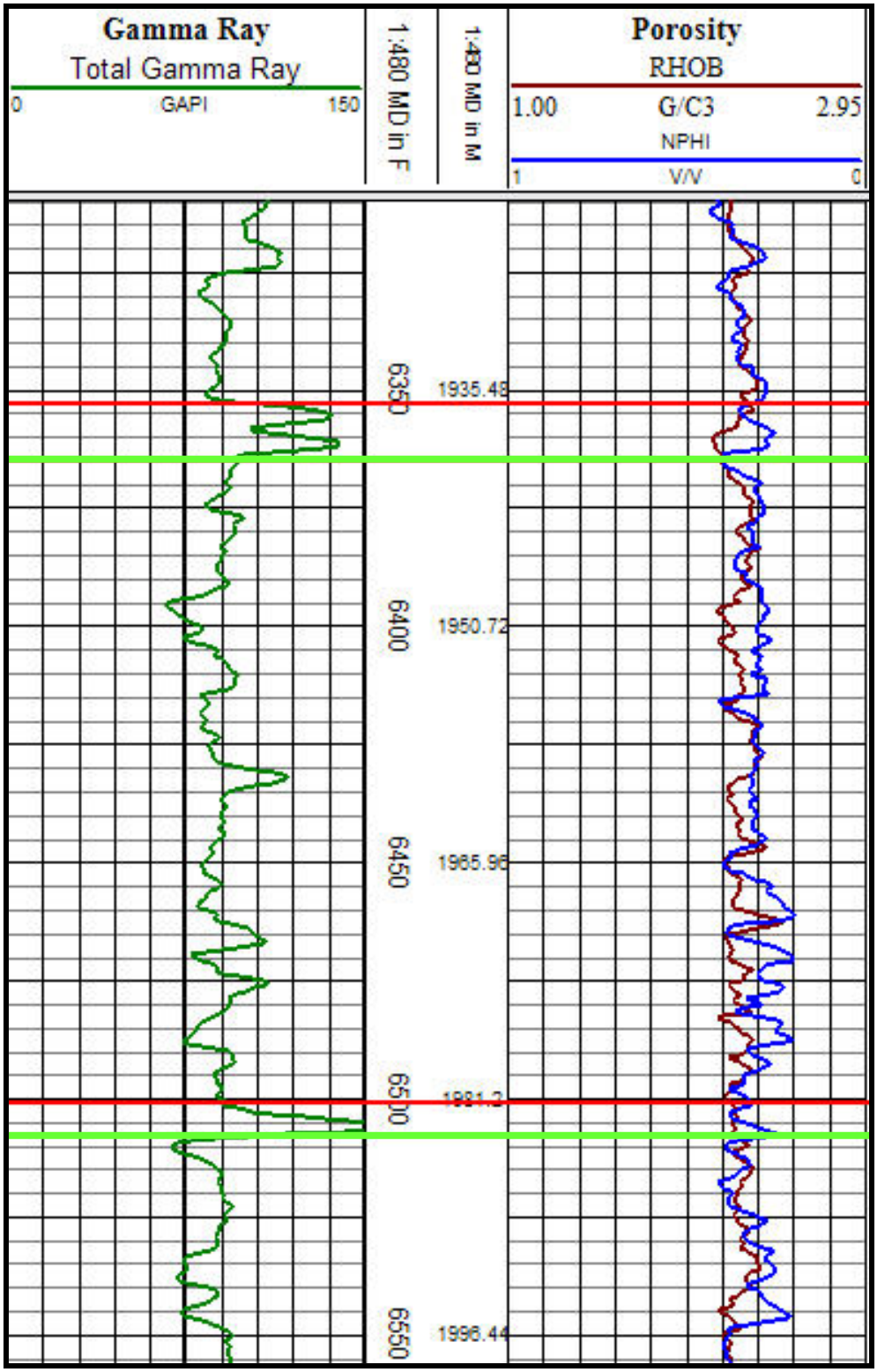

Figure G-15. Well 608224001400; gamma ray log, density and neutron porosity response detail through Aptian-age shale potentially associated with OAE deposition. The upper boundary of the section of interest is indicated with a red line and the lower boundary is indicated with a light green line.

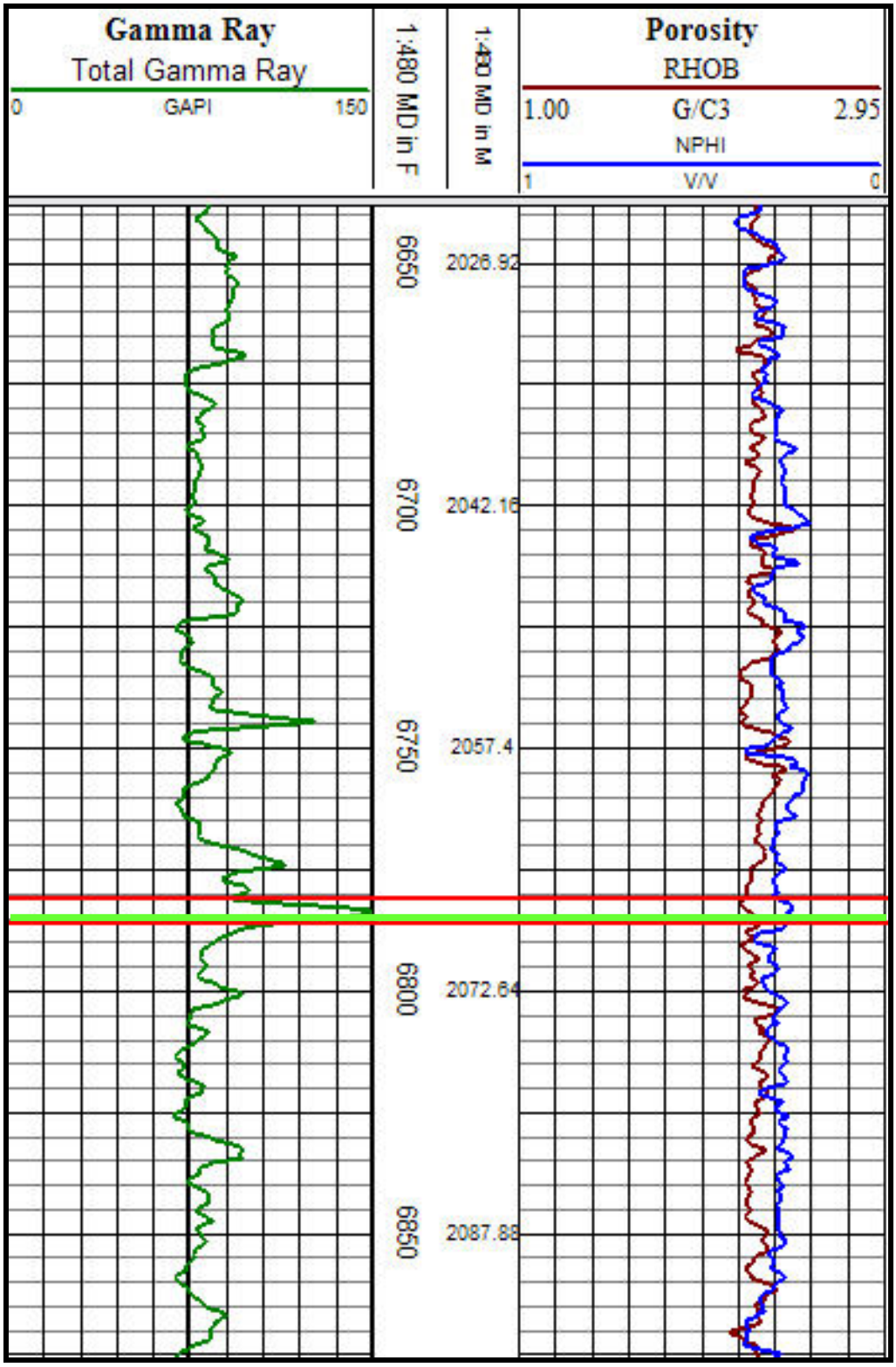

Figure G-16. Well 608224001400; gamma ray log, density and neutron porosity response detail through Aptian-age shale potentially associated with OAE deposition. The upper boundary of the section of interest is indicated with a red line and the lower boundary is indicated with a light green line.

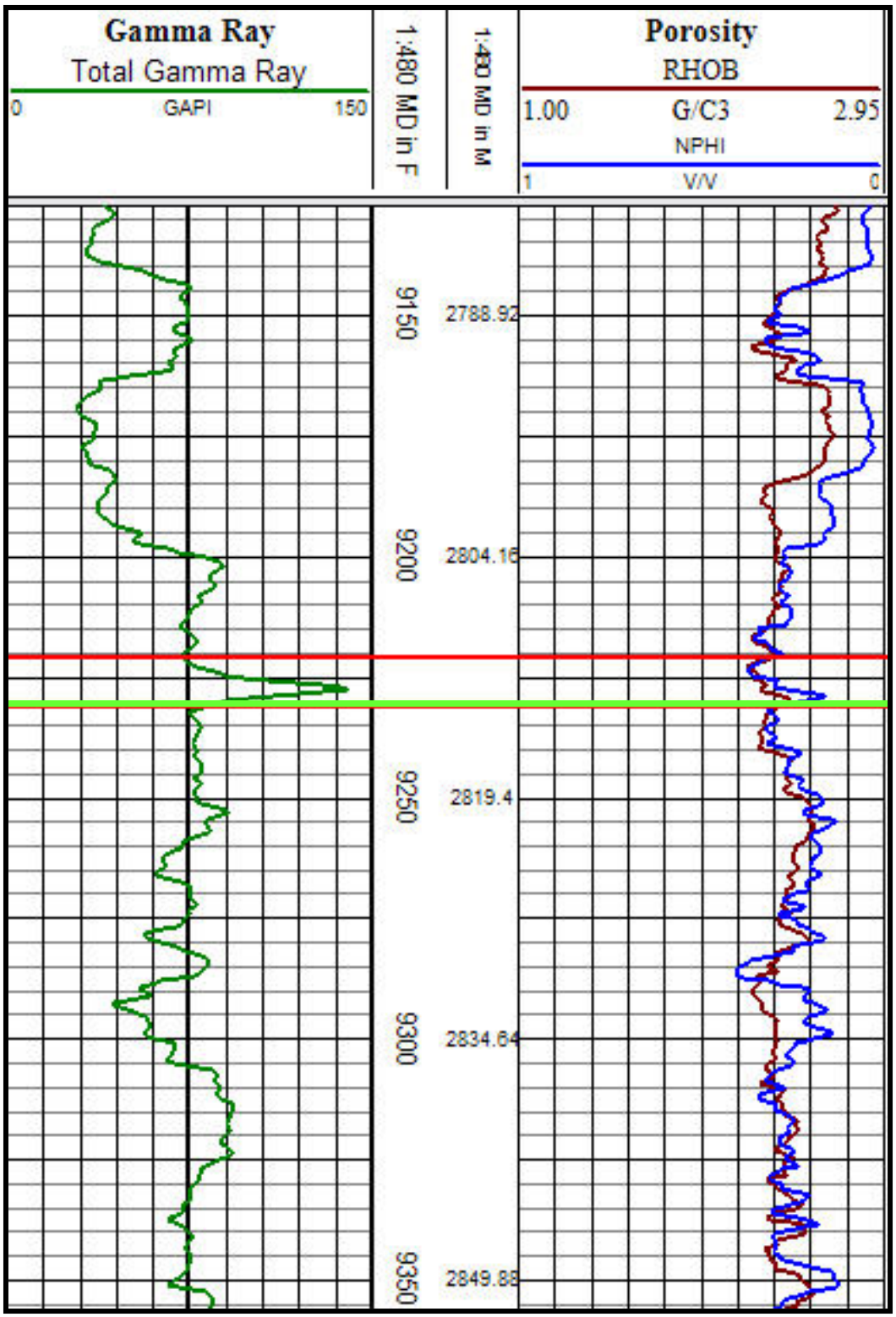

Figure G-17. Well 608224001700; gamma ray log, density and neutron porosity response over total logged interval. Red lines indicate approximate depths of multiple Albian and Aptian-age limestones and siltstones potentially associated with deposition during an OAE.

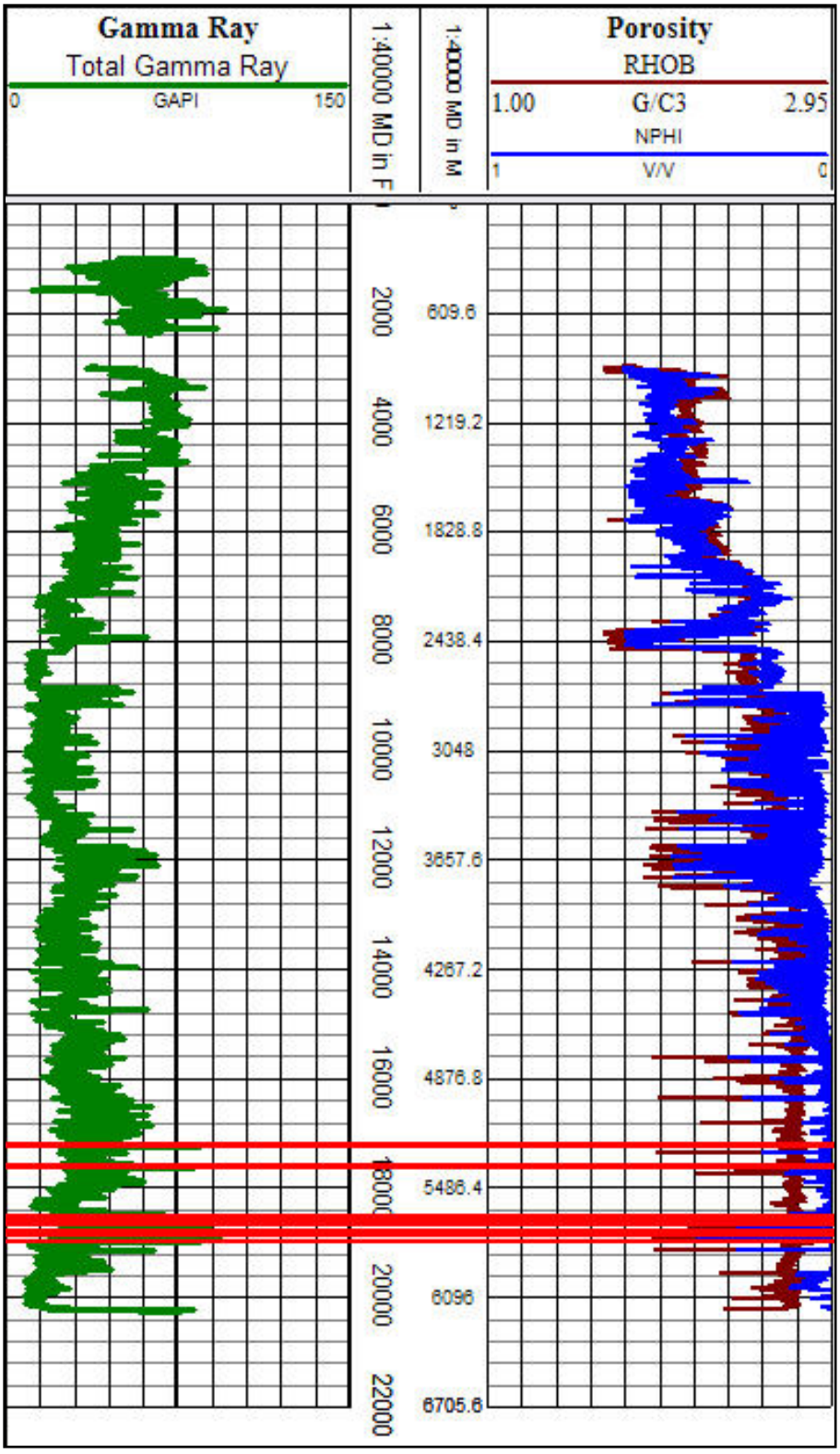

Figure G-18. Well 608224001700; gamma ray log, density and neutron porosity response detail through Albian-Aptian-age limestone potentially associated with OAE deposition. The upper boundary of the section of interest is indicated with a red line and the lower boundary is indicated with a light green line.

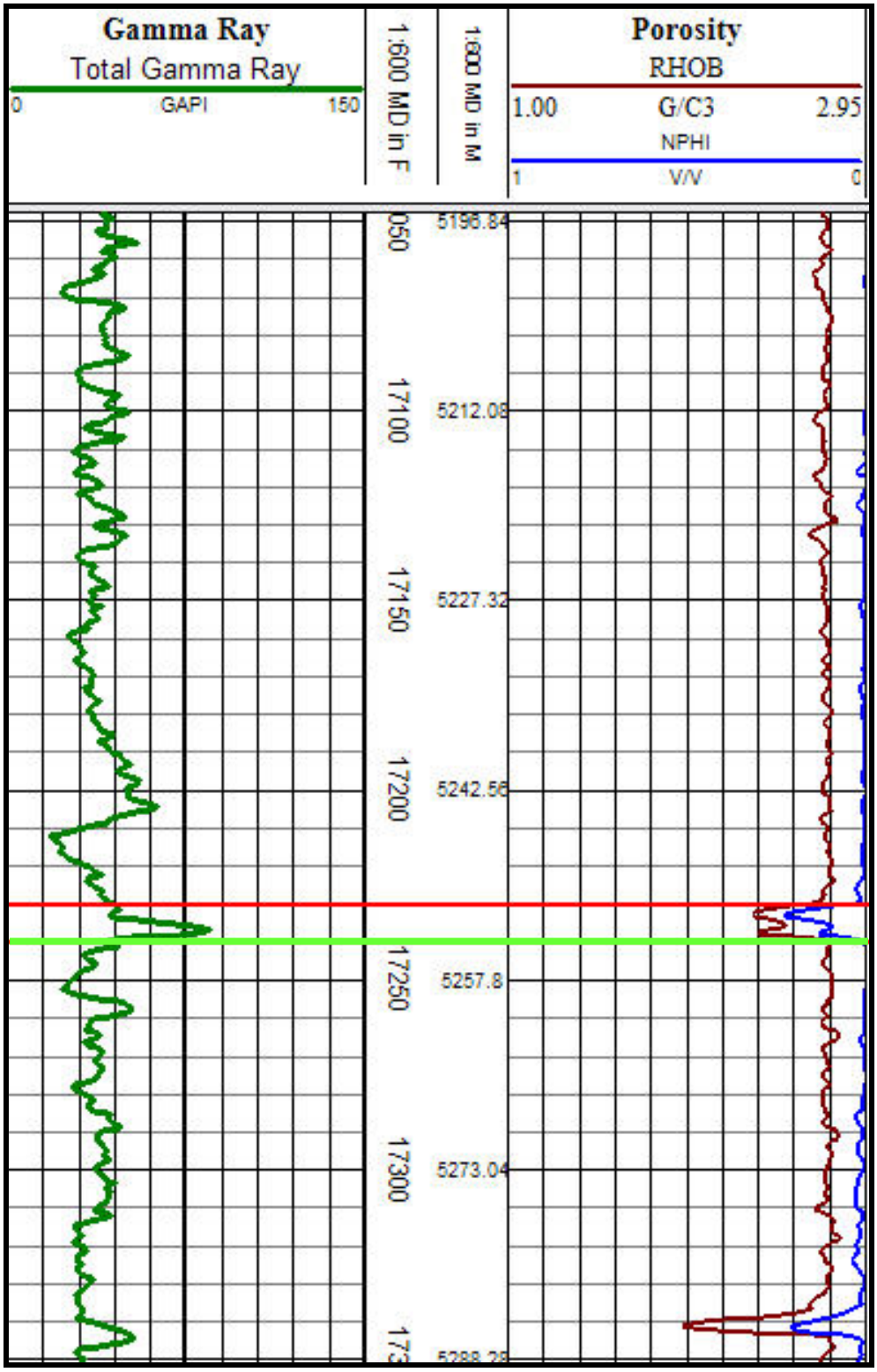

Figure G-19. Well 608224001700; gamma ray log, density and neutron porosity response detail through Albian-Aptian-age limestone potentially associated with OAE deposition. The upper boundary of the section of interest is indicated with a red line and the lower boundary is indicated with a light green line.

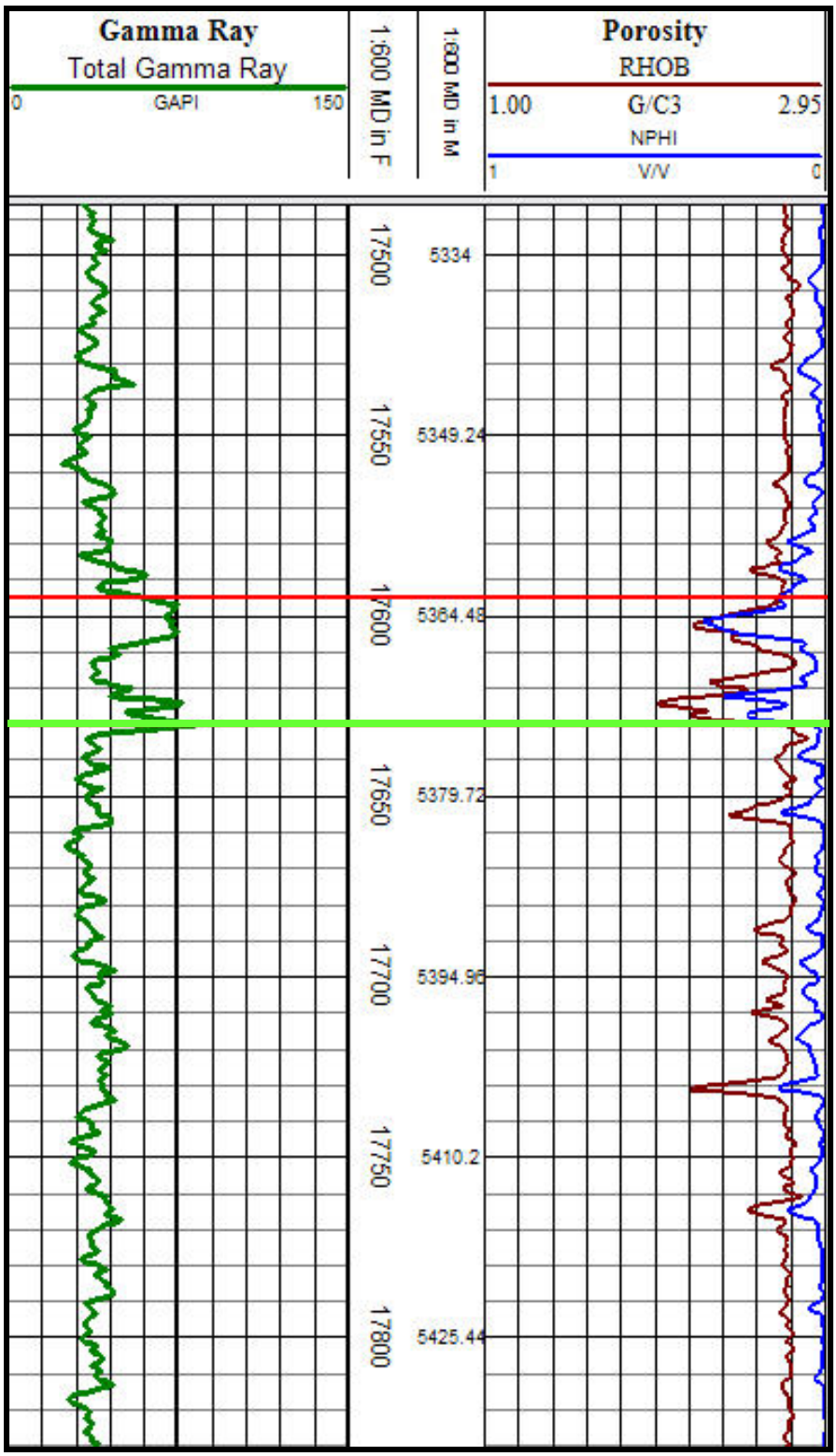

Figure G-20. Well 608224001700; gamma ray log, density and neutron porosity response detail through multiple Aptian-age limestones and siltstone potentially associated with OAE deposition. The upper boundaries of the sections of interest are indicated with red lines and the lower boundaries are indicated with light green lines.

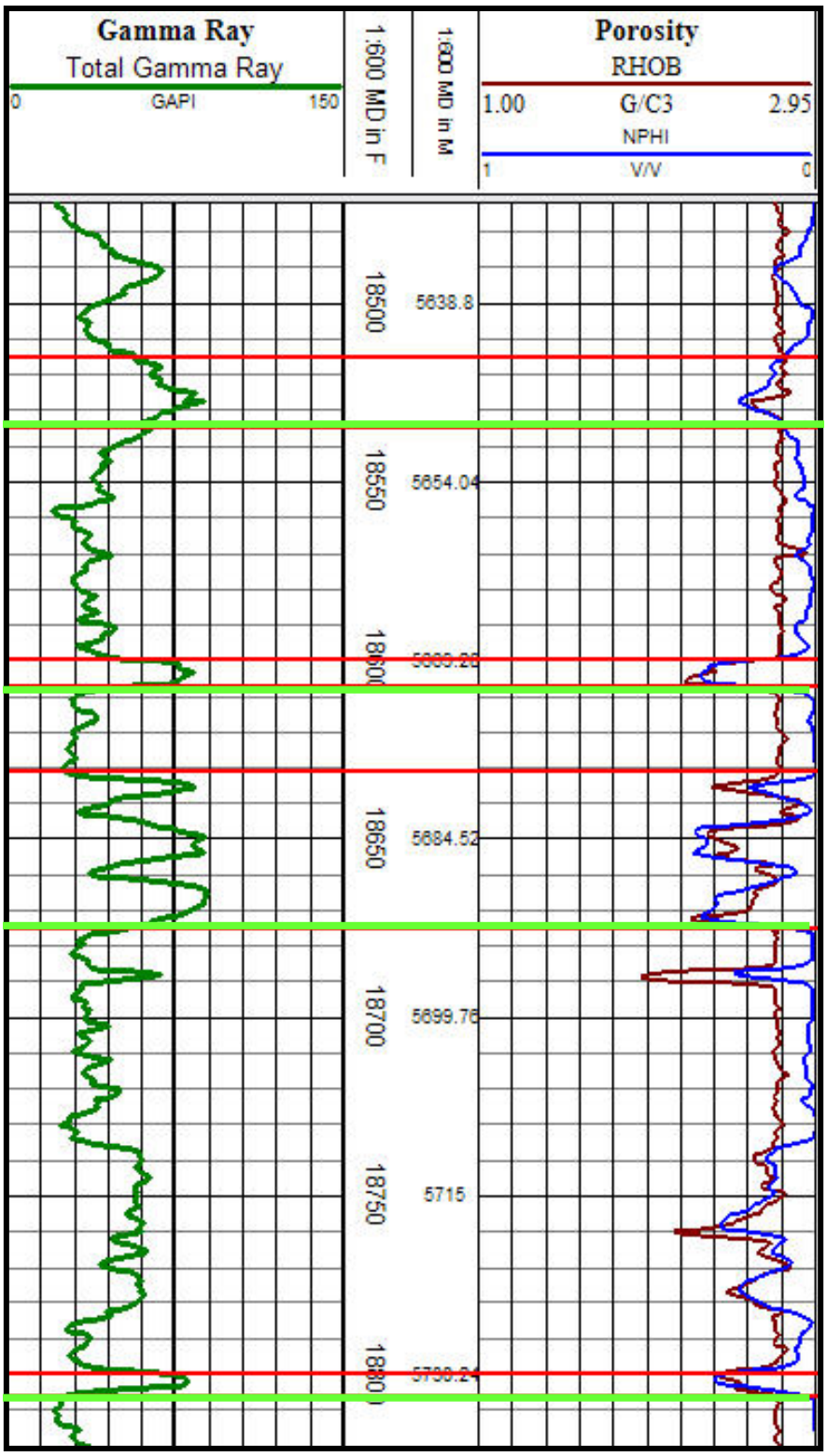

Figure G-21. Well 608224001700; gamma ray log, density and neutron porosity response detail through Aptian-age siltstone potentially associated with OAE deposition. The upper boundary of the section of interest is indicated with a red line and the lower boundary is indicated with a light green line.

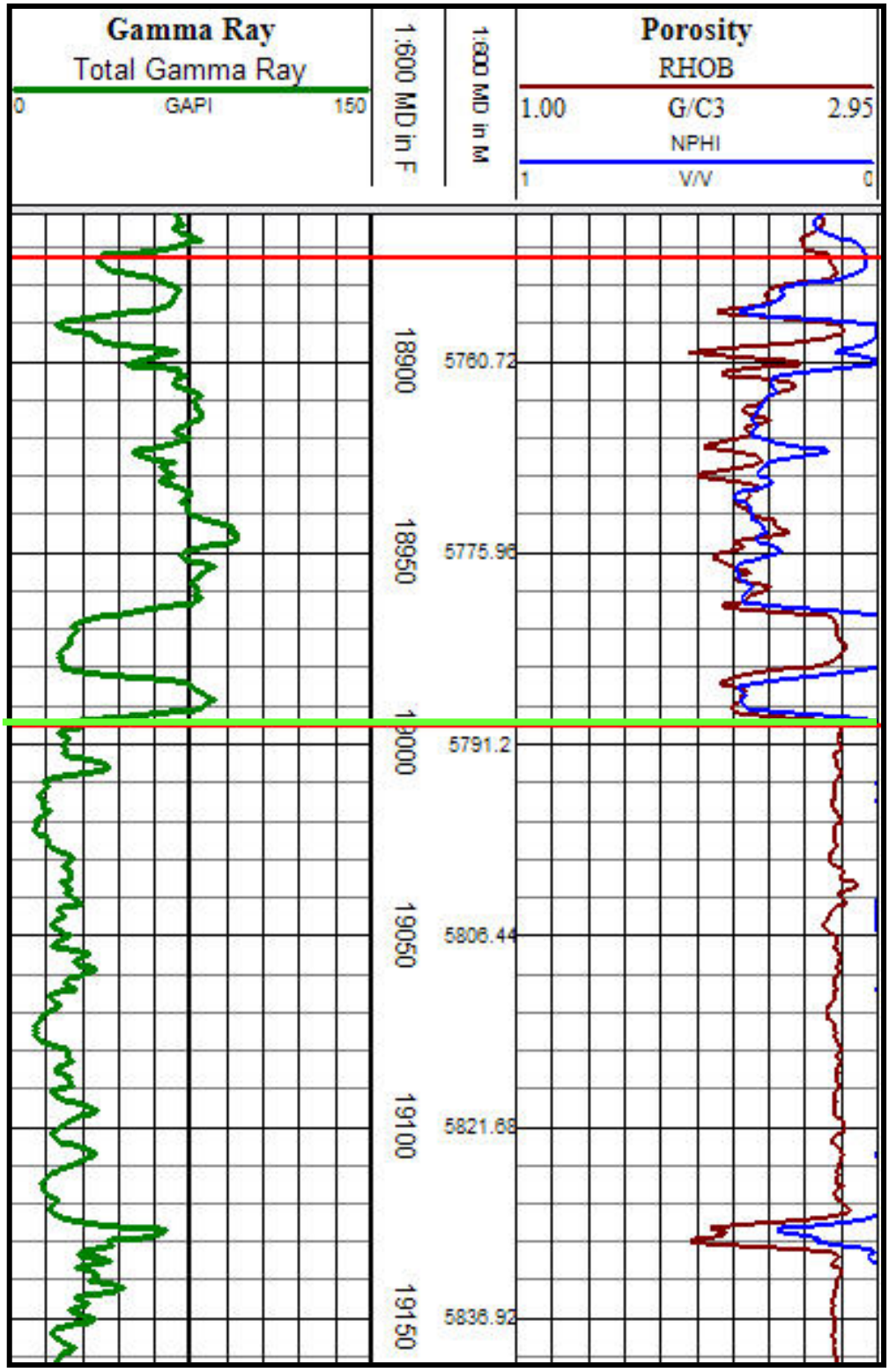

Figure G-22. Well 608224002200; gamma ray log, density and neutron porosity response over total logged interval. Red lines indicate approximate depths of multiple Santonian-Coniancian-age black shales potentially associated with deposition during an OAE.

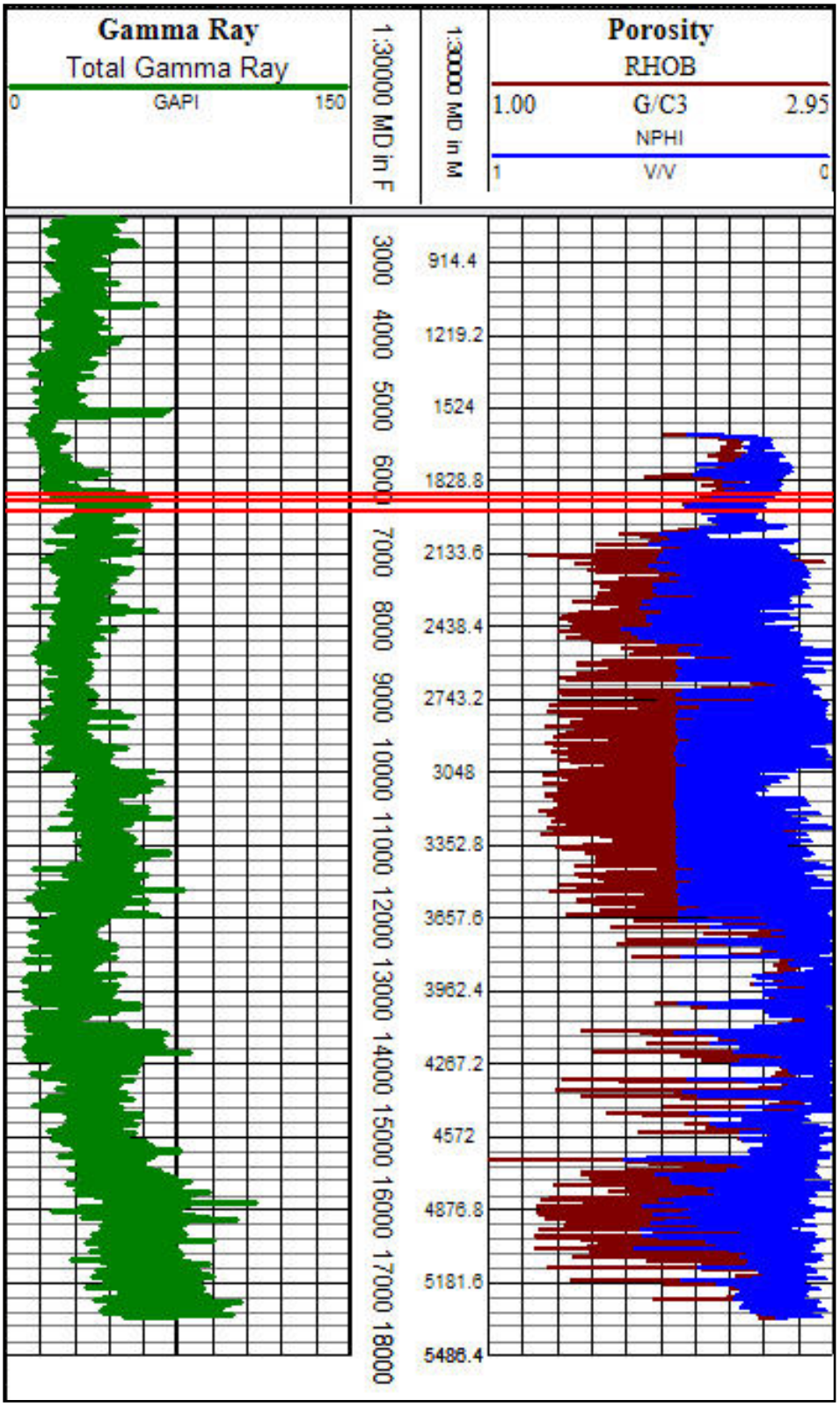

Figure G-23. Well 608224002200; gamma ray log, density and neutron porosity response detail through Santonian-Coniancian-age calcareous black shale and Tuscaloosa Formation black shale potentially associated with OAE deposition. The upper boundary of the section of interest is indicated with a red line and the lower boundary is indicated with a light green line.

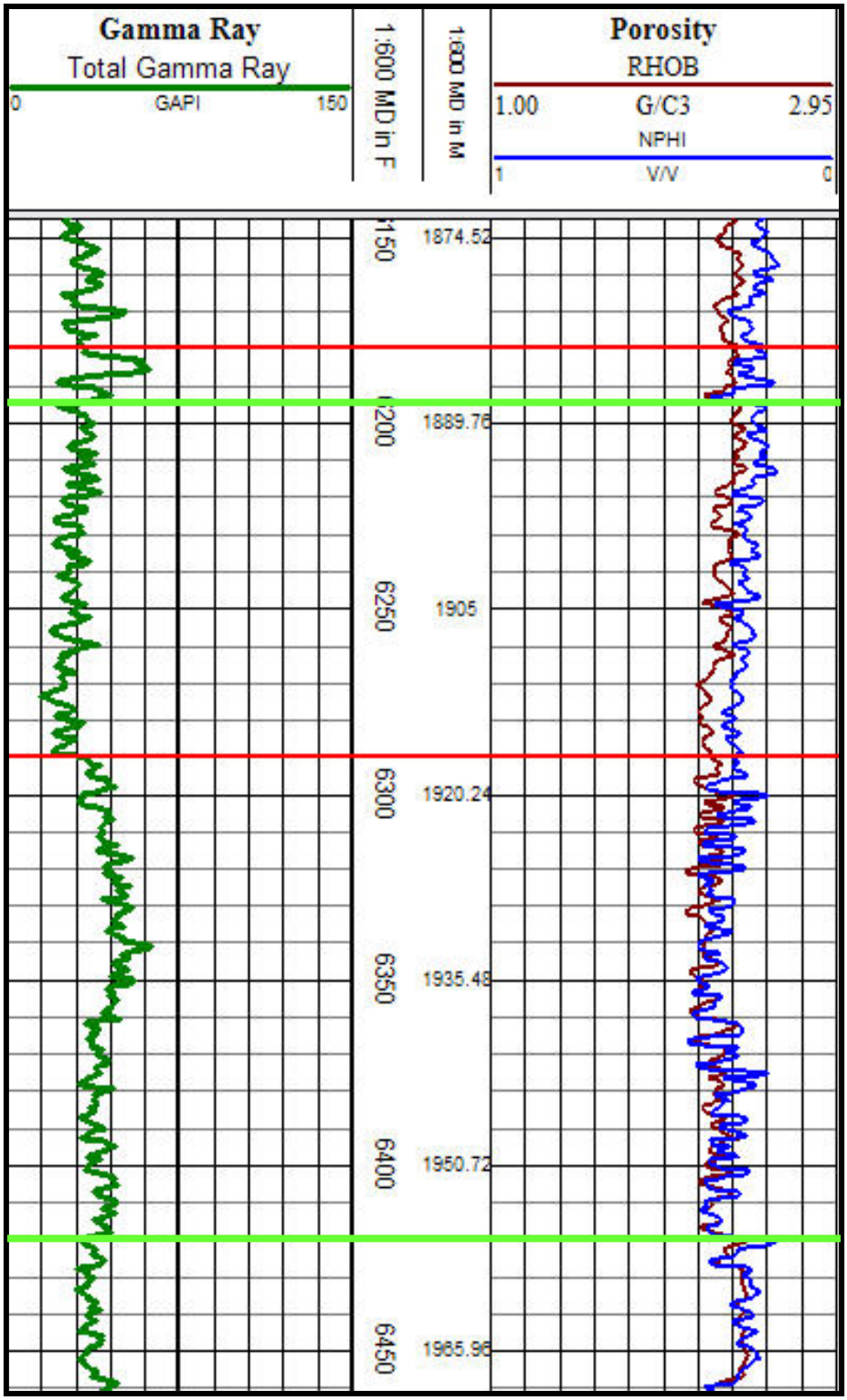

APPENDIX H - DEVIATION OF PSEUDO DENSITY CURVES FROM BULK DENSITY CURVES VERSUS DEPTH IN GULF OF MEXICO WELLS

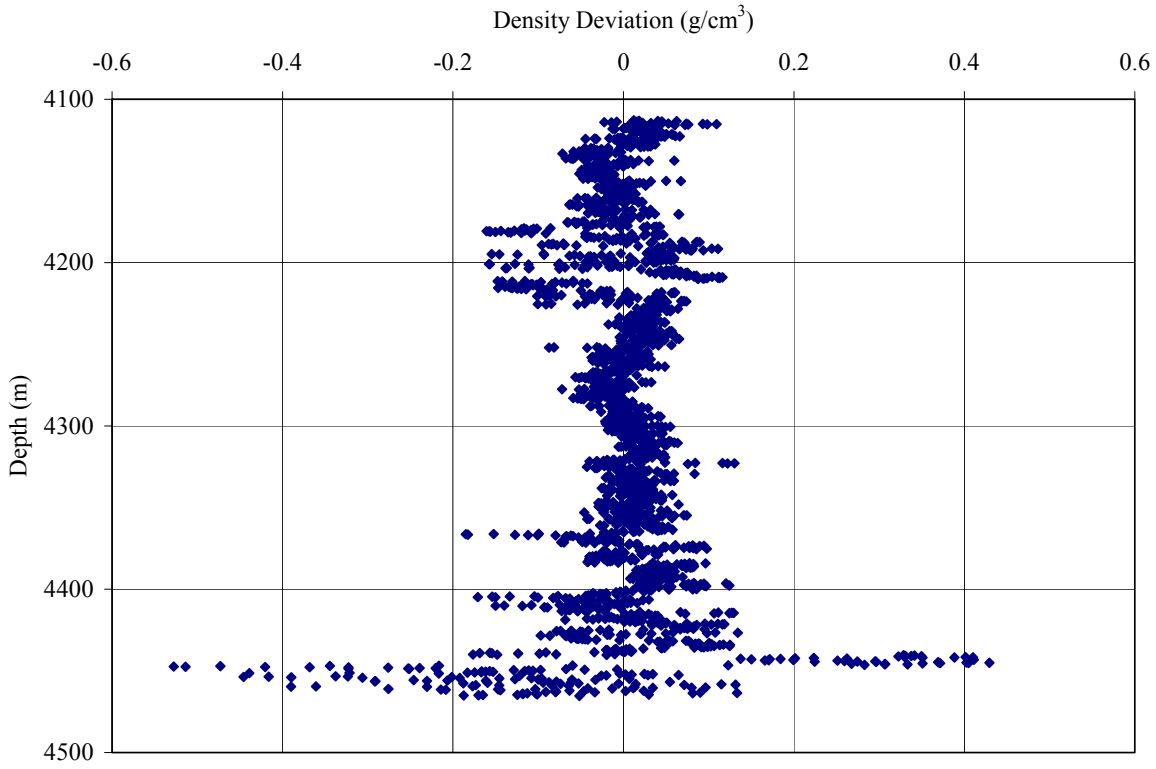

Figure H-1. Well 177244005200 pseudo density deviation from bulk density.

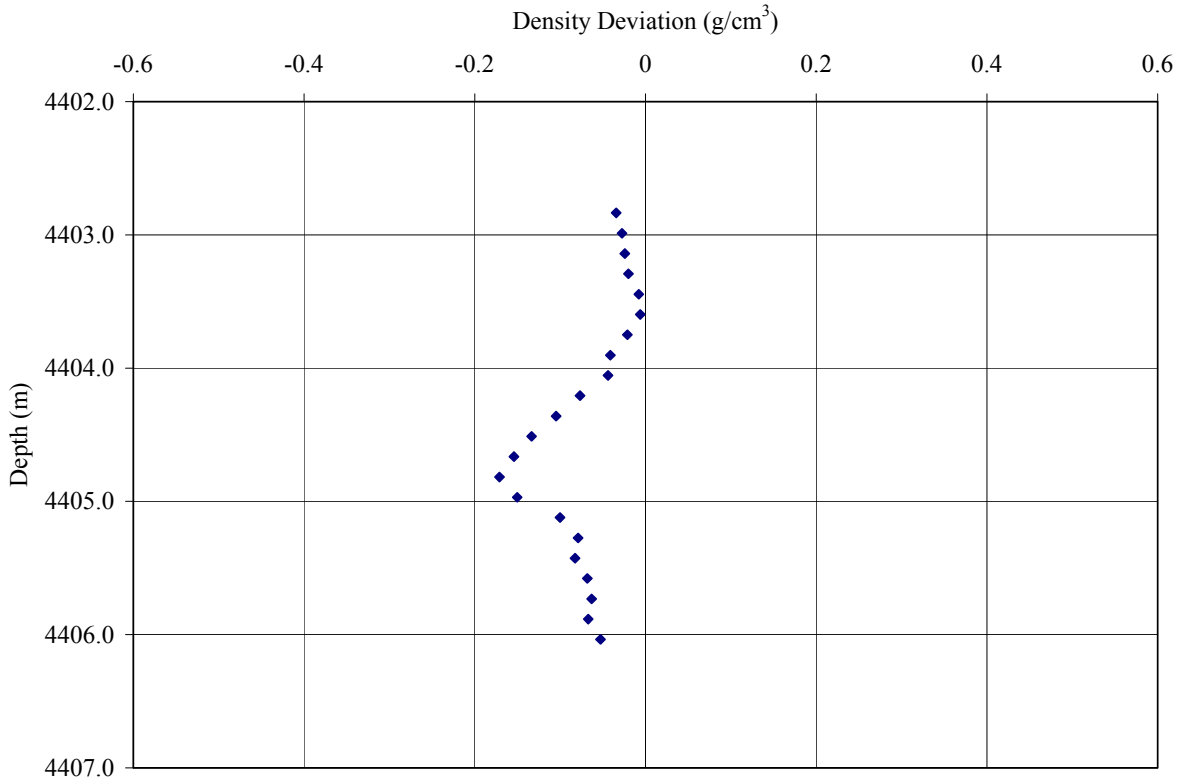

Figure H-2. Well 177244005200 pseudo density deviation from bulk density through Cenomanian-age shale potentially associated with deposition during an OAE.

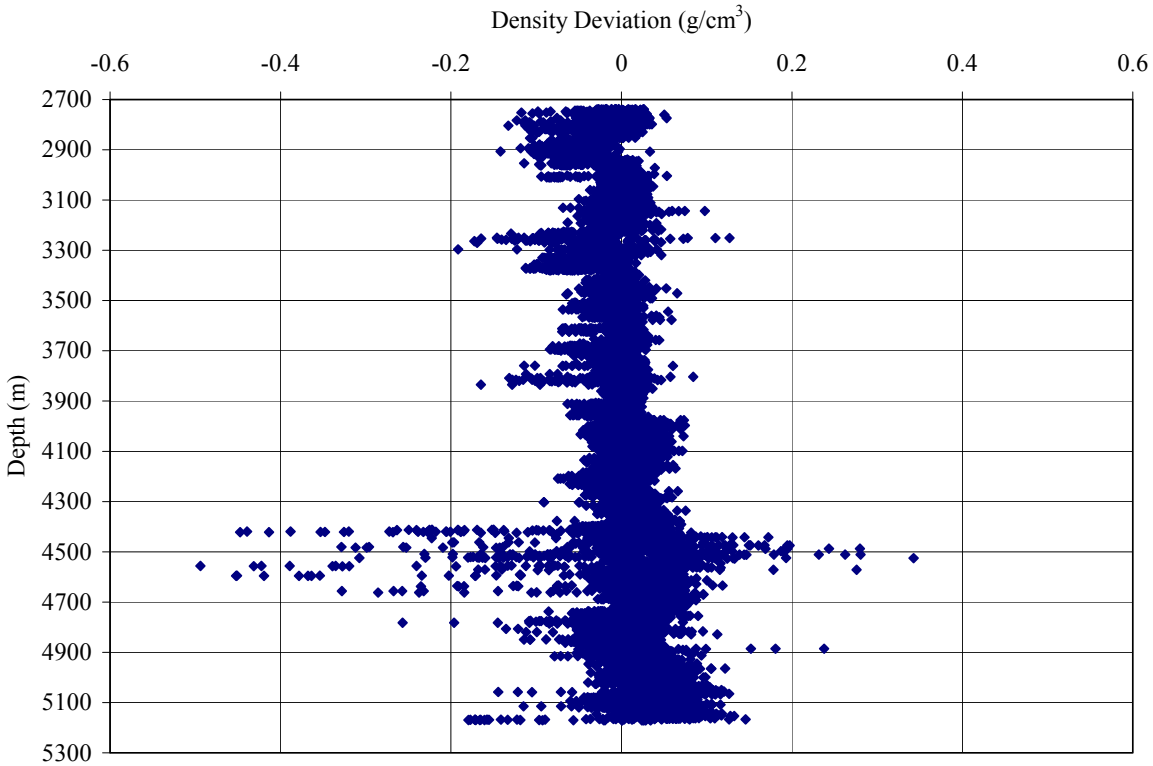

Figure H-3. Well 177244005400; pseudo density deviation from bulk density.

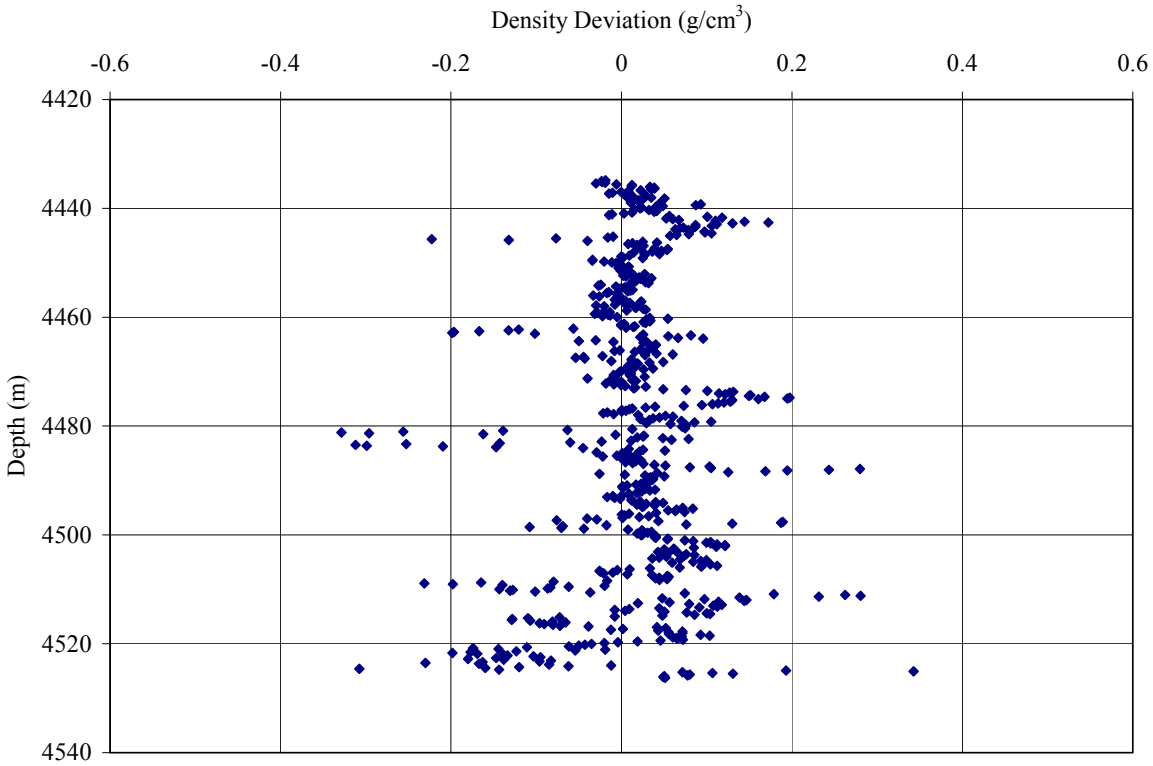

Figure H-4. Well 177244005400; pseudo density deviation from bulk density through Albian-Aptian-age limestone potentially associated with deposition during an OAE.

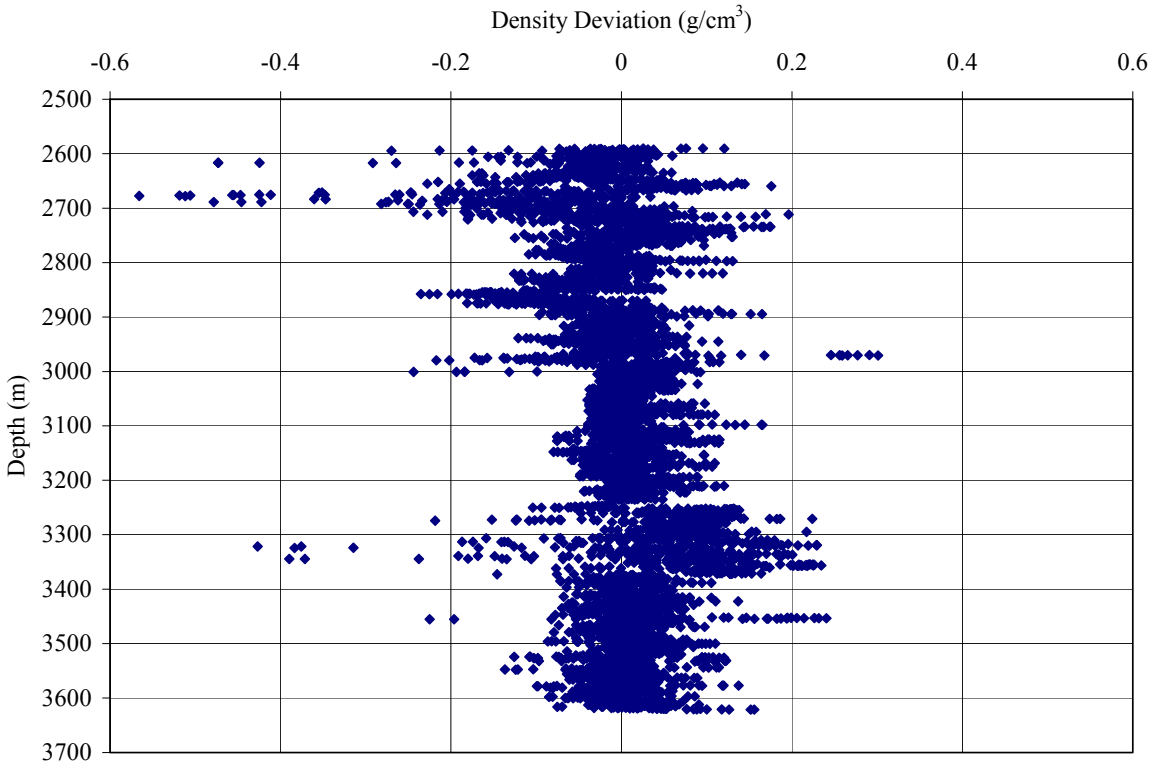

Figure H-5. Well 177244006300; pseudo density deviation from bulk density.

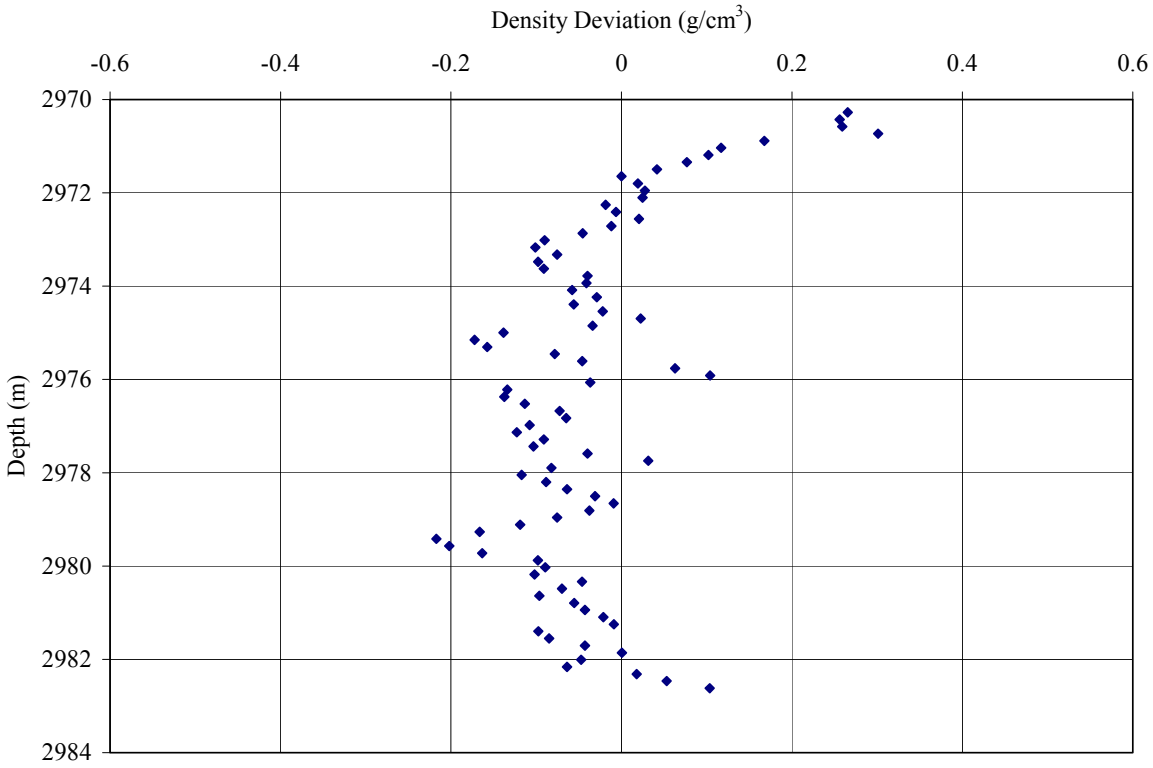

Figure H-6. Well 177244006300; pseudo density deviation from bulk density through Turonian-Cenomanian-age shale potentially associated with deposition during an OAE.

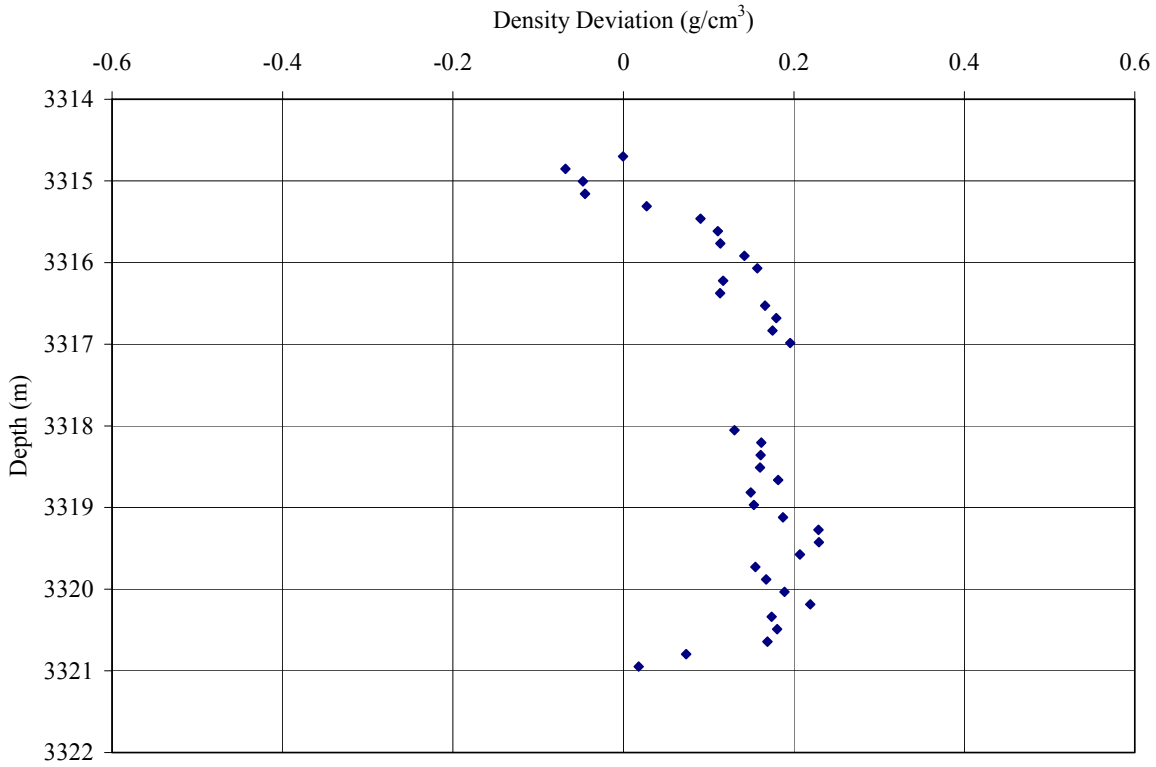

Figure H-7. Well 177244006300; pseudo density deviation from bulk density through Albian-age black shale potentially associated with deposition during an OAE.

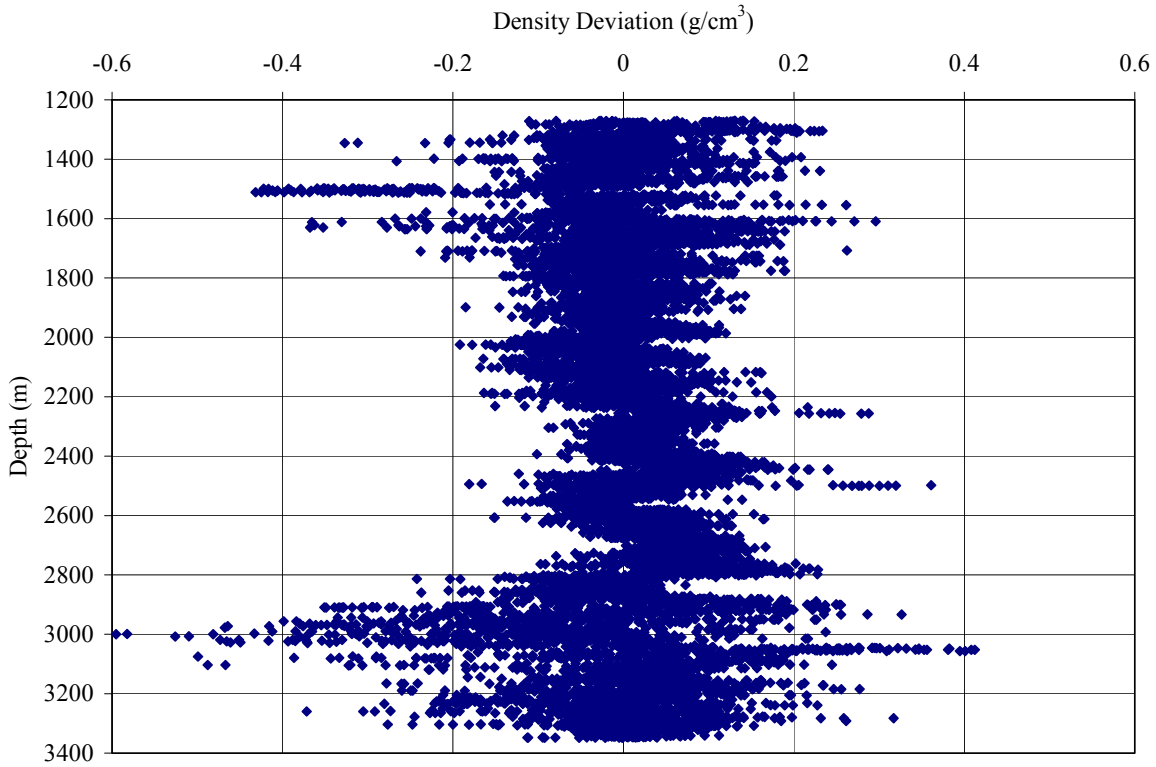

Figure H-8. Well 608164003700; pseudo density deviation from bulk density.

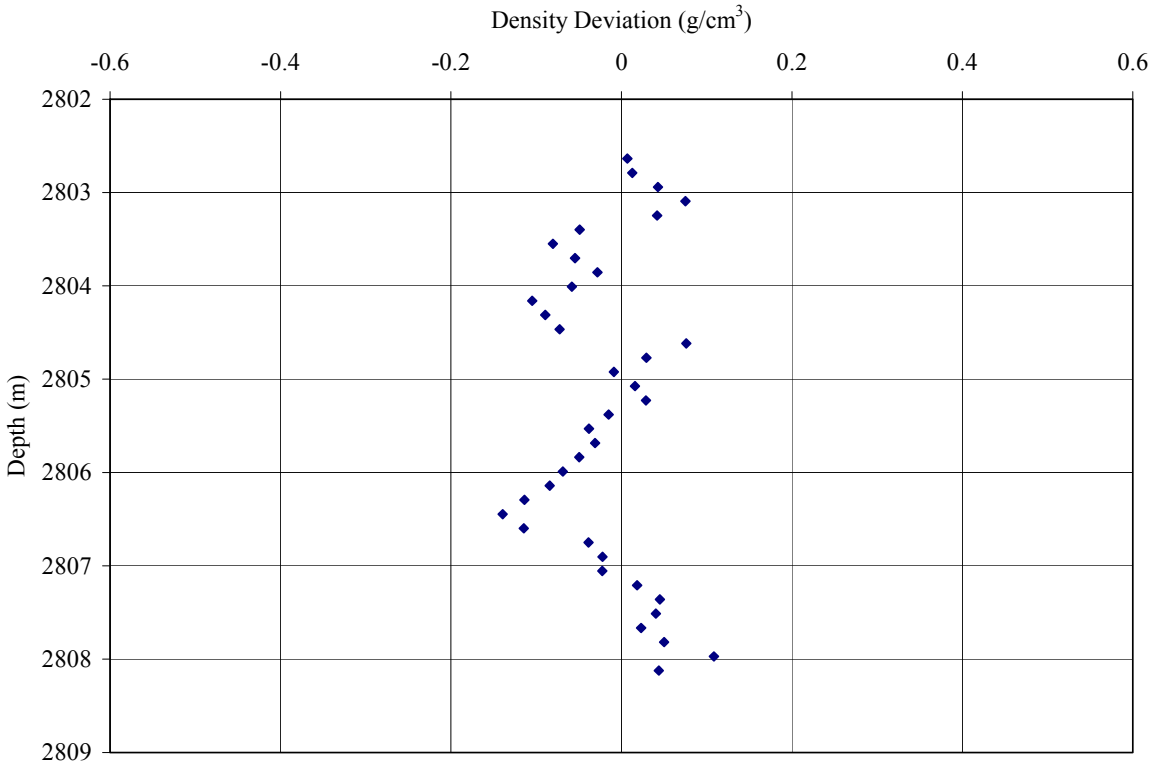

Figure H-9. Well 608164003700; pseudo density deviation from bulk density through Turonian-Cenomanian-age black shale potentially associated with deposition during an OAE.

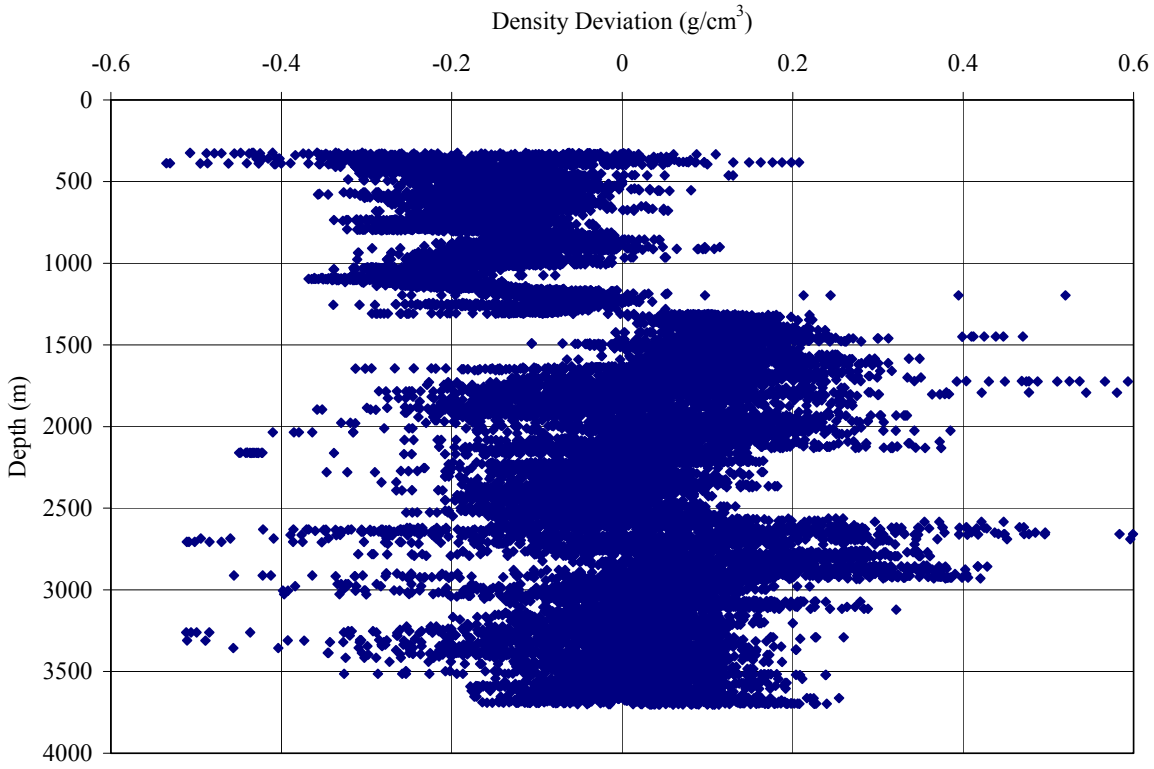

Figure H-10. Well 608224000600; pseudo density deviation from bulk density.

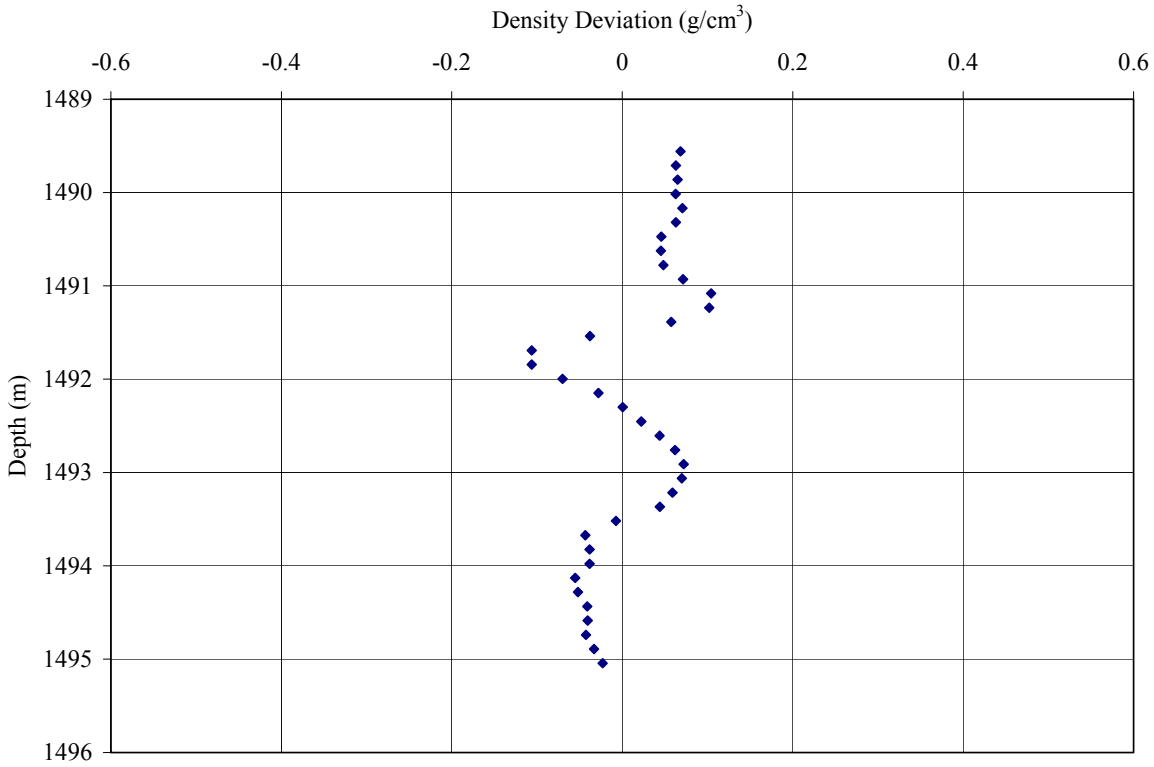

Figure H-11. Well 608224000600; pseudo density deviation from bulk density through Turonian-Cenomanian-age Tuscaloosa Formation shale potentially associated with deposition during an OAE.

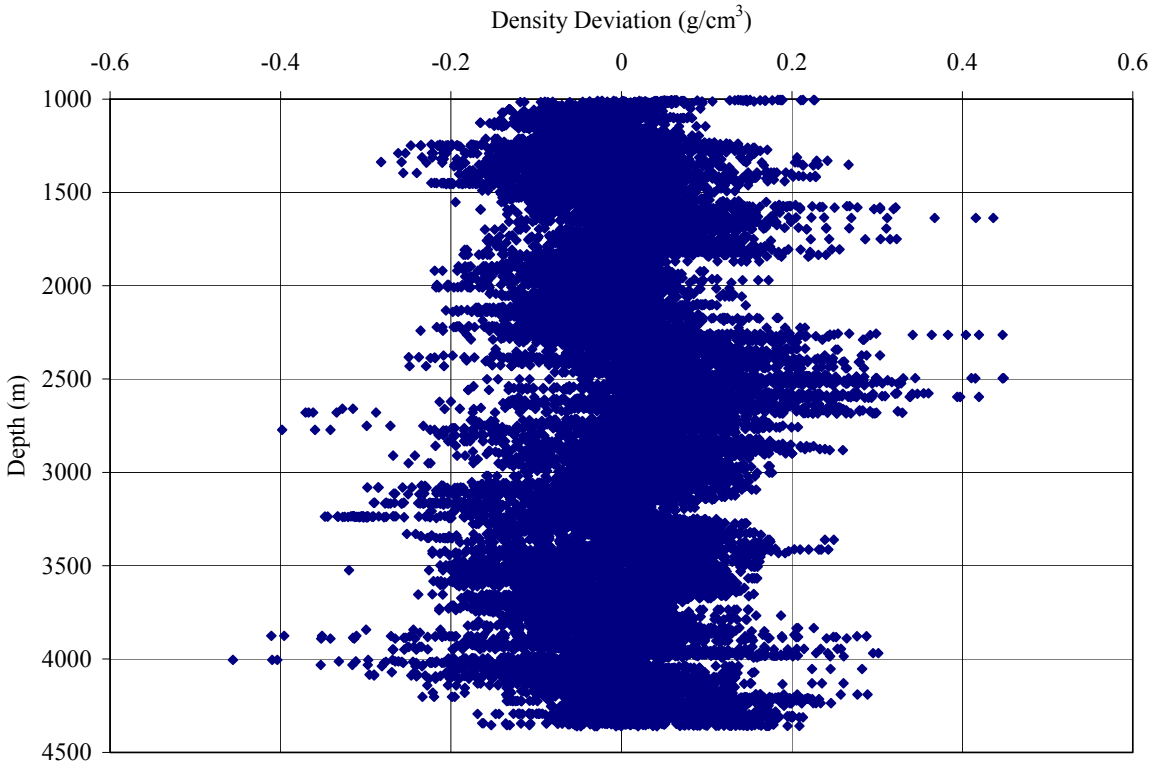

Figure H-12. Well 608224001400; pseudo density deviation from bulk density.

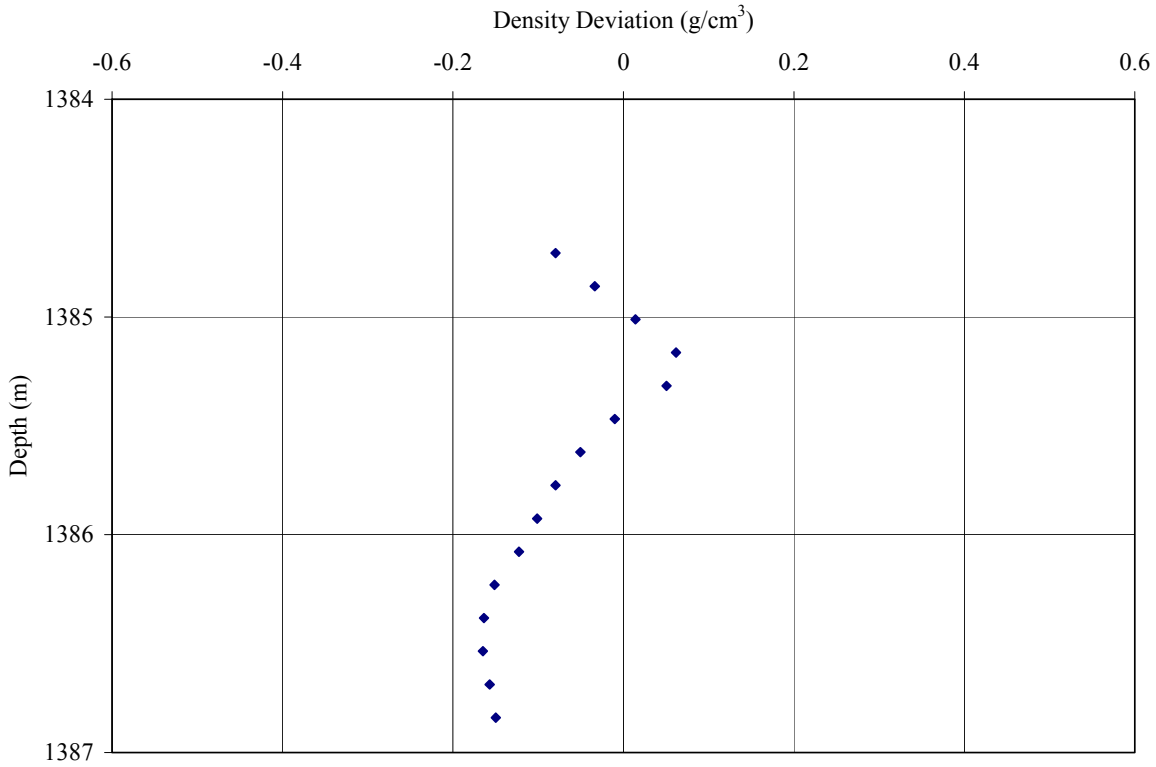

Figure H-13. Well 608224001400; pseudo density deviation from bulk density through Albian-age shale potentially associated with deposition during an OAE.

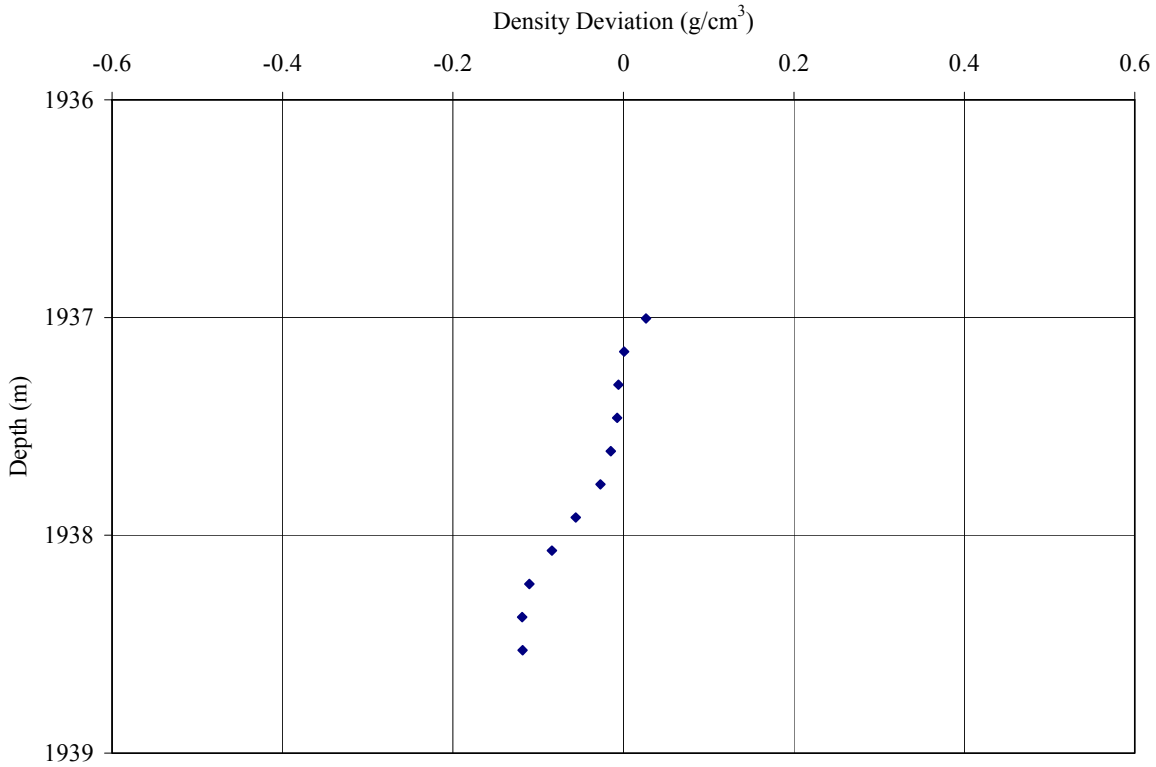

Figure H-14. Well 608224001400; pseudo density deviation from bulk density through Aptian-age shale potentially associated with deposition during an OAE.

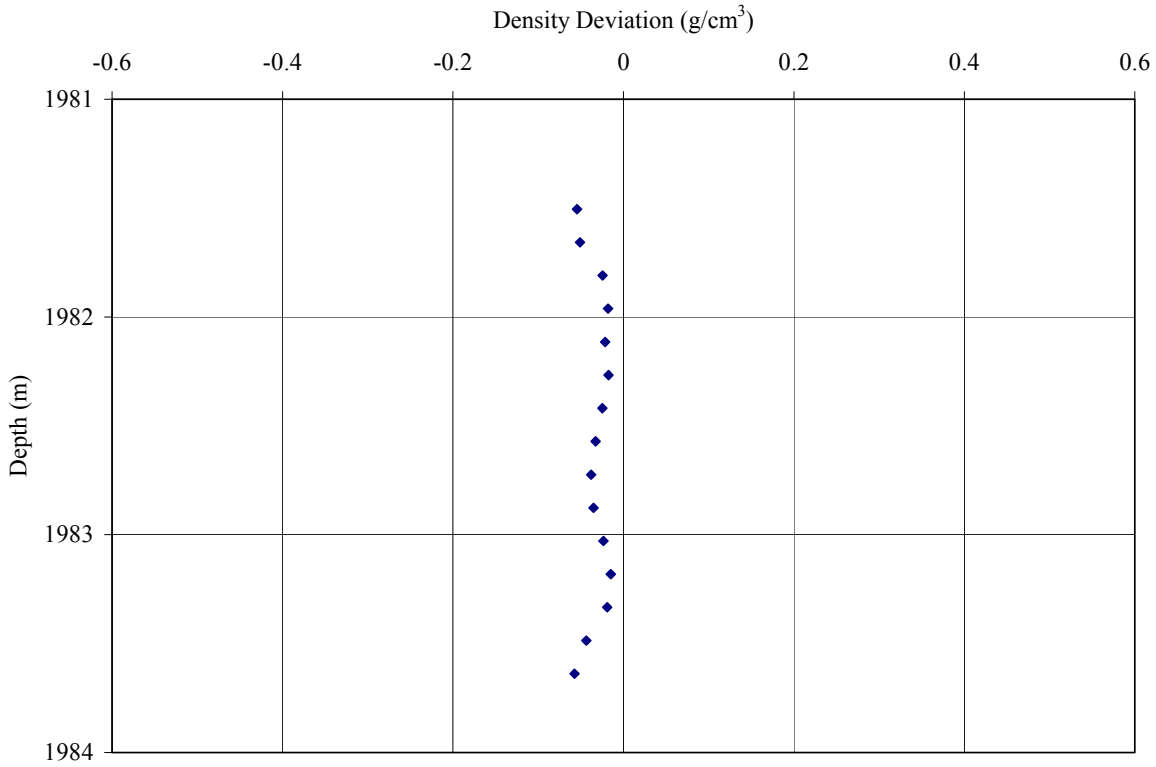

Figure H-15. Well 608224001400; pseudo density deviation from bulk density through Aptian-age shale potentially associated with deposition during an OAE.

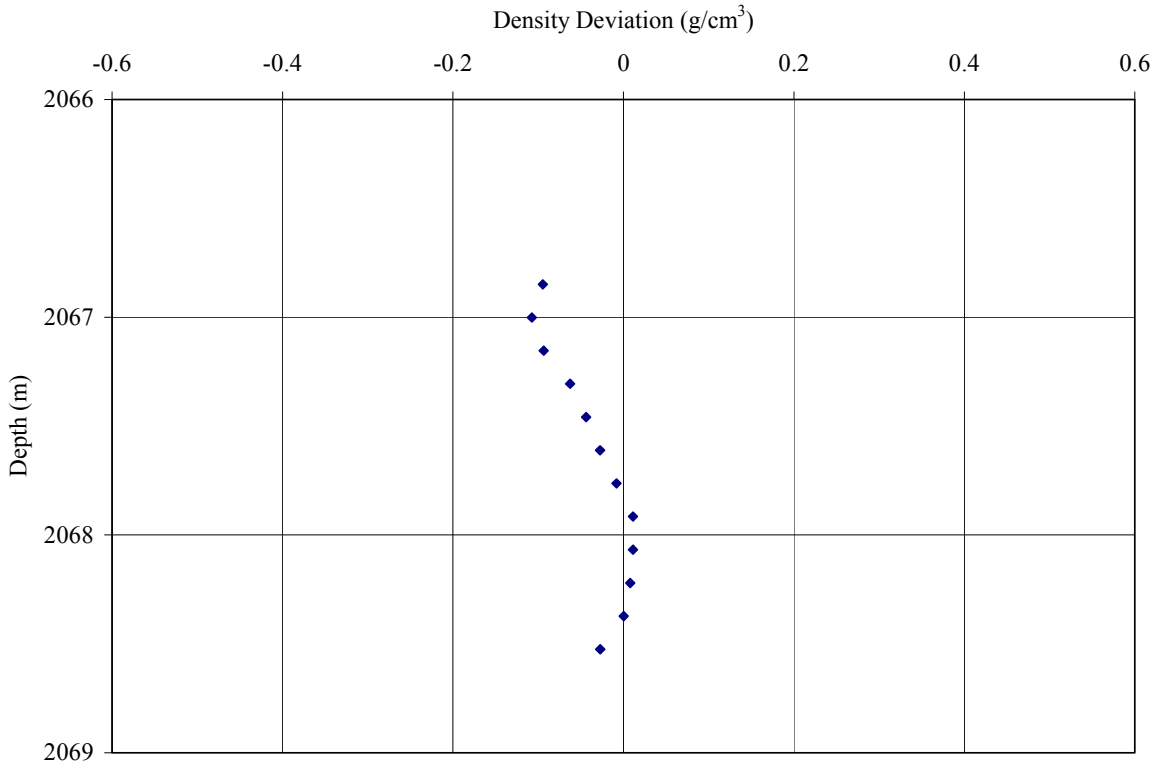

Figure H-16. Well 608224001400; pseudo density deviation from bulk density through Aptian-age shale potentially associated with deposition during an OAE.

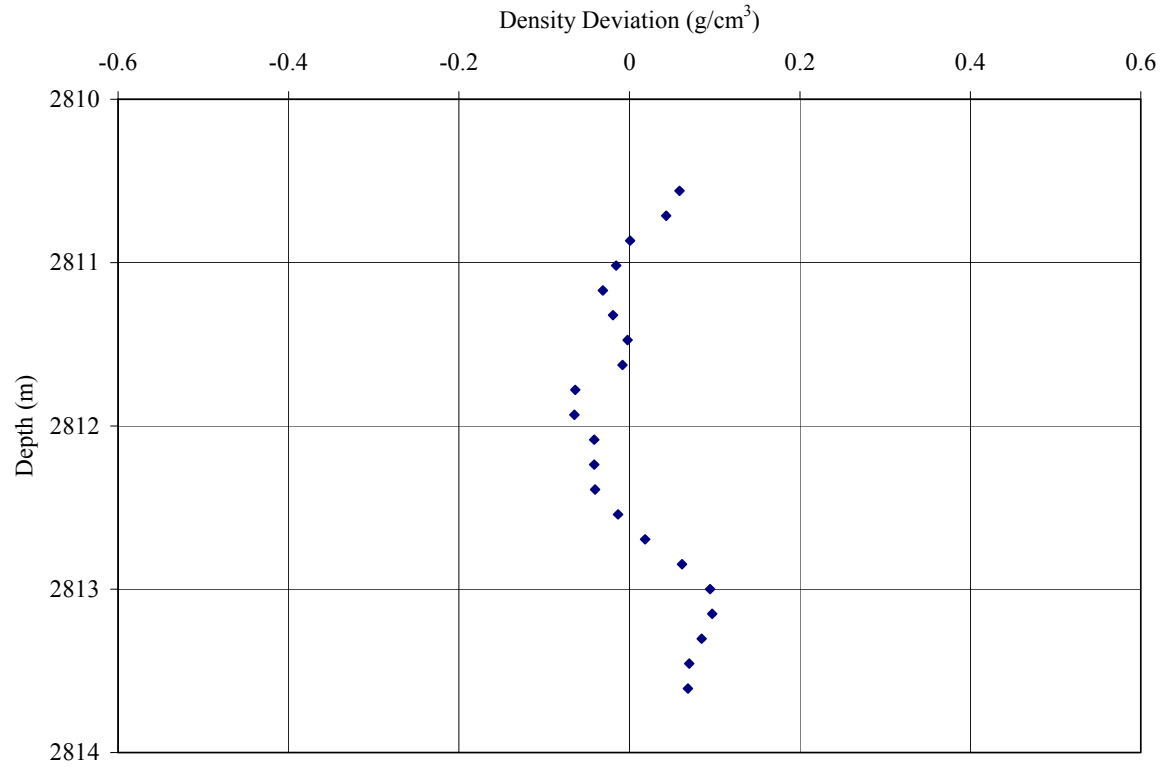

Figure H-17. Well 608224001400; pseudo density deviation from bulk density through Aptian-age sand and black shale potentially associated with deposition during an OAE.

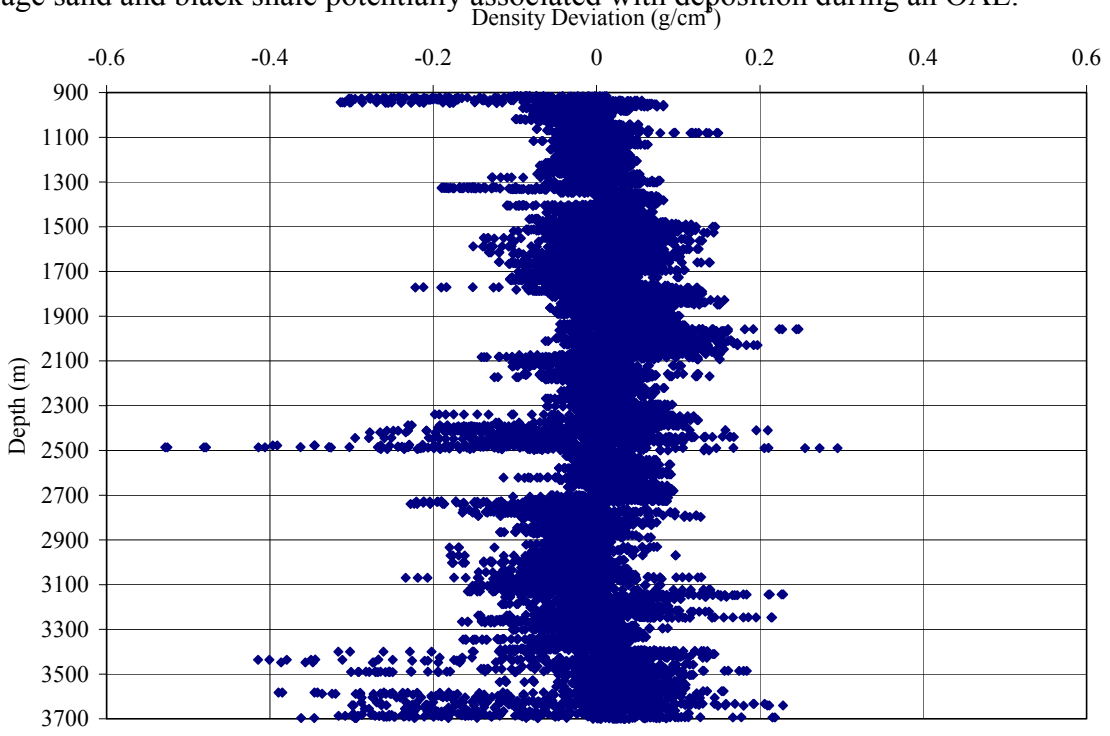

Figure H-18. Well 608224001700; part A; pseudo density deviation from bulk density. The pseudo density chart for this well is split into a part A and part B due to the number of data points within the well exceeding the total number of points Excel charts are able to hold.

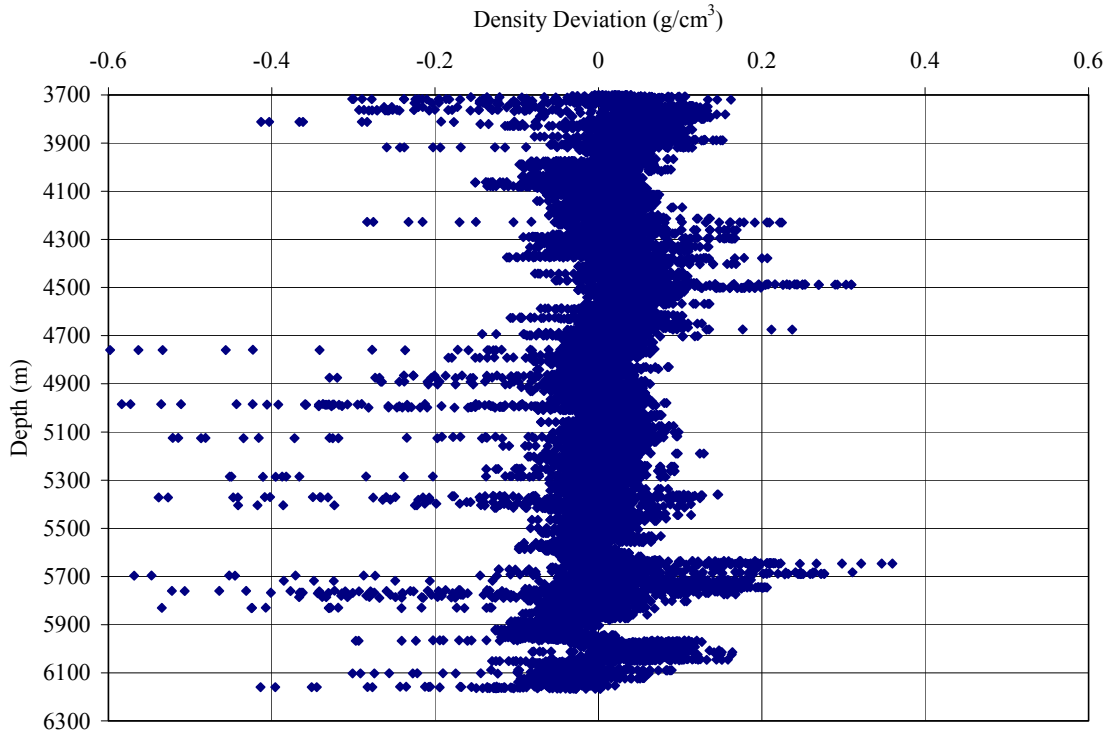

Figure H-19. Well 608224001700; part B; pseudo density deviation from bulk density. The pseudo density chart for this well is split into a part A and part B due to the number of data points within the well exceeding the total number of points Excel charts are able to hold.

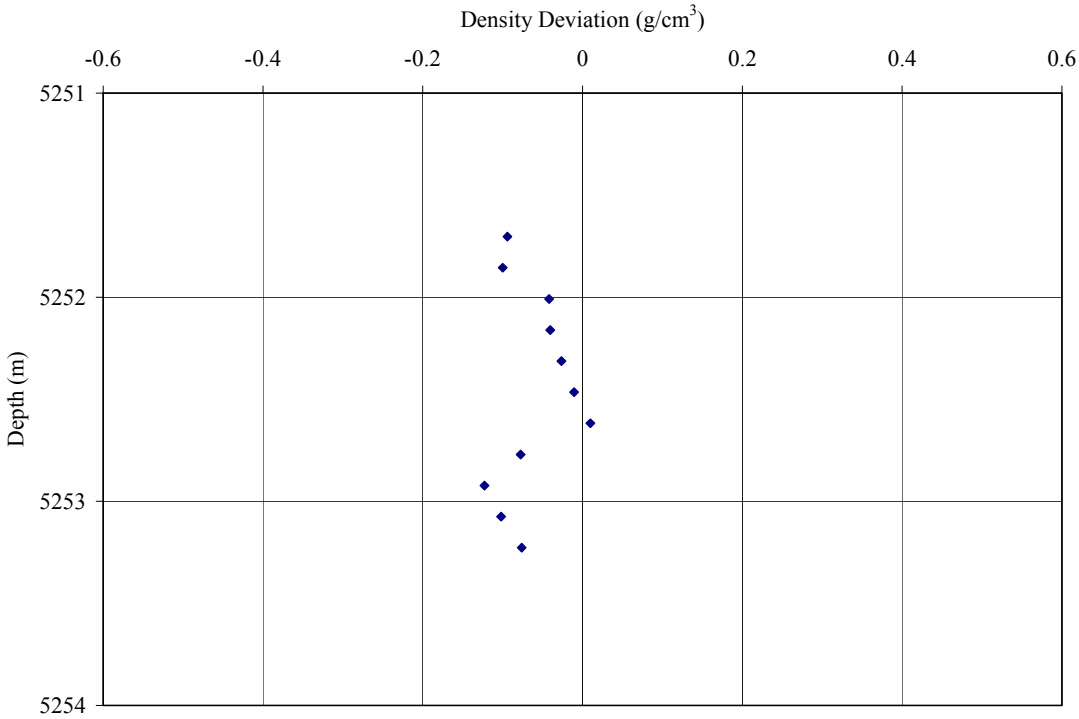

Figure H-20. Well 608224001700; pseudo density deviation from bulk density through Albian-Aptian-age limestone and black shale potentially associated with deposition during an OAE.

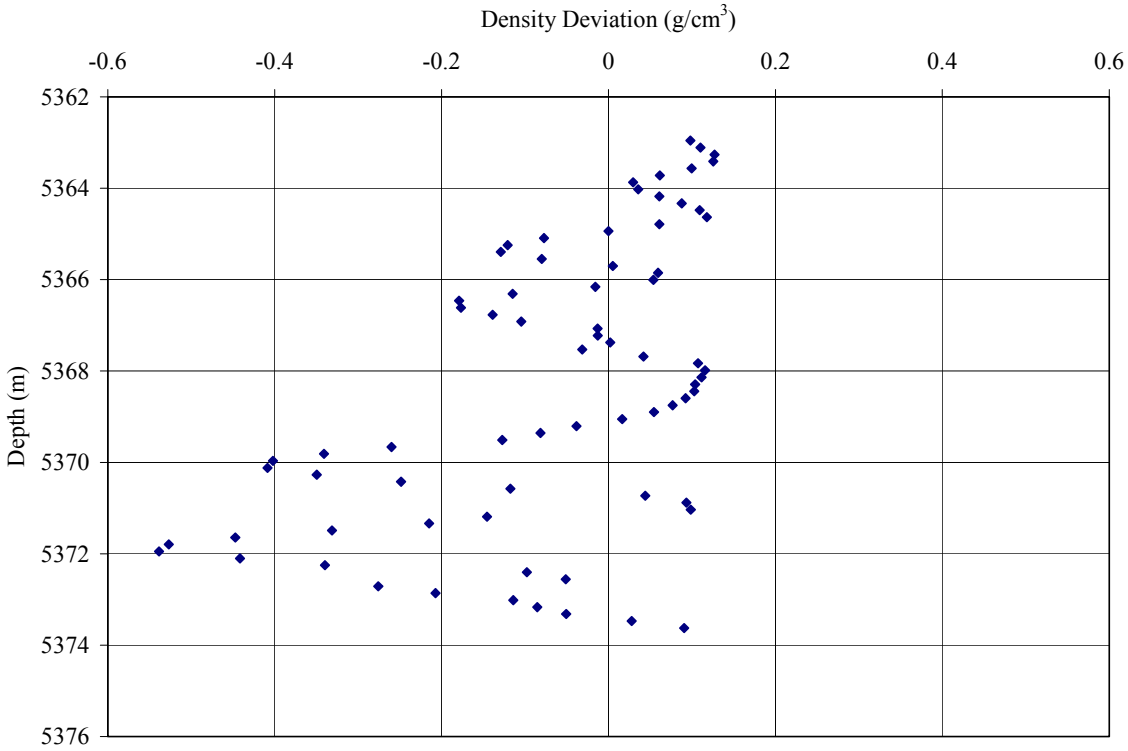

Figure H-21. Well 608224001700; pseudo density deviation from bulk density through Albian-Aptian-age limestone potentially associated with deposition during an OAE.

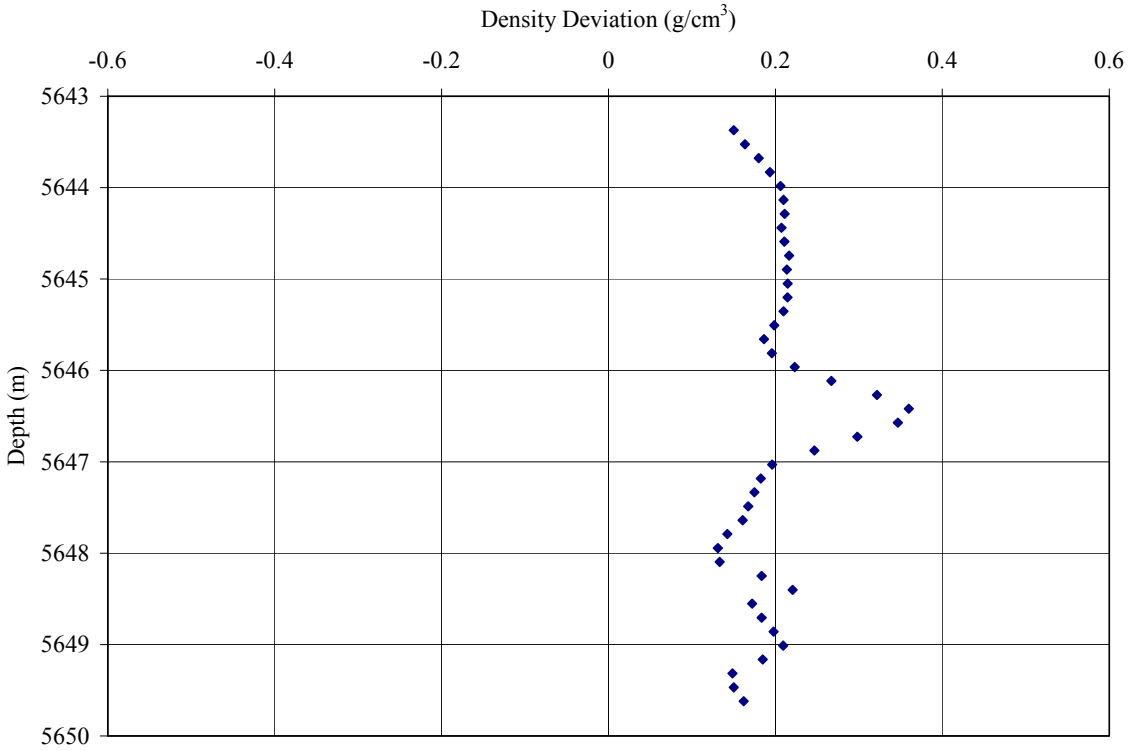

Figure H-22. Well 608224001700; pseudo density deviation from bulk density through Aptian-age limestone potentially associated with deposition during an OAE.

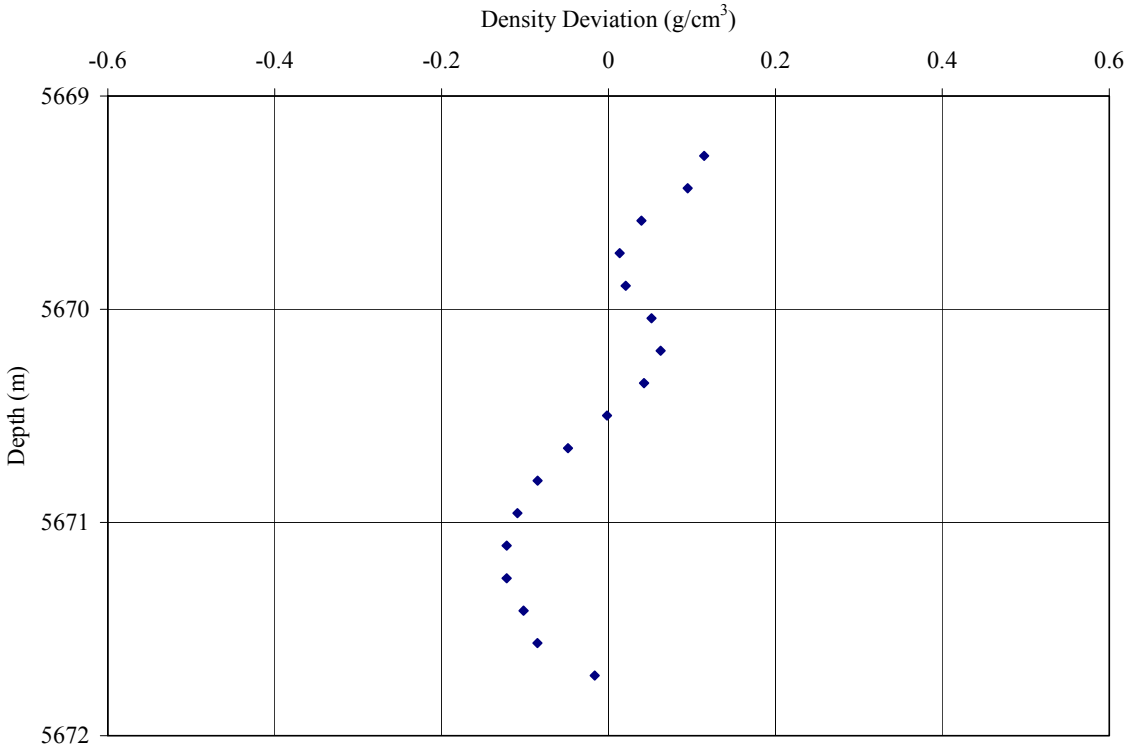

Figure H-23. Well 608224001700; pseudo density deviation from bulk density through Aptian-age limestone potentially associated with deposition during an OAE.

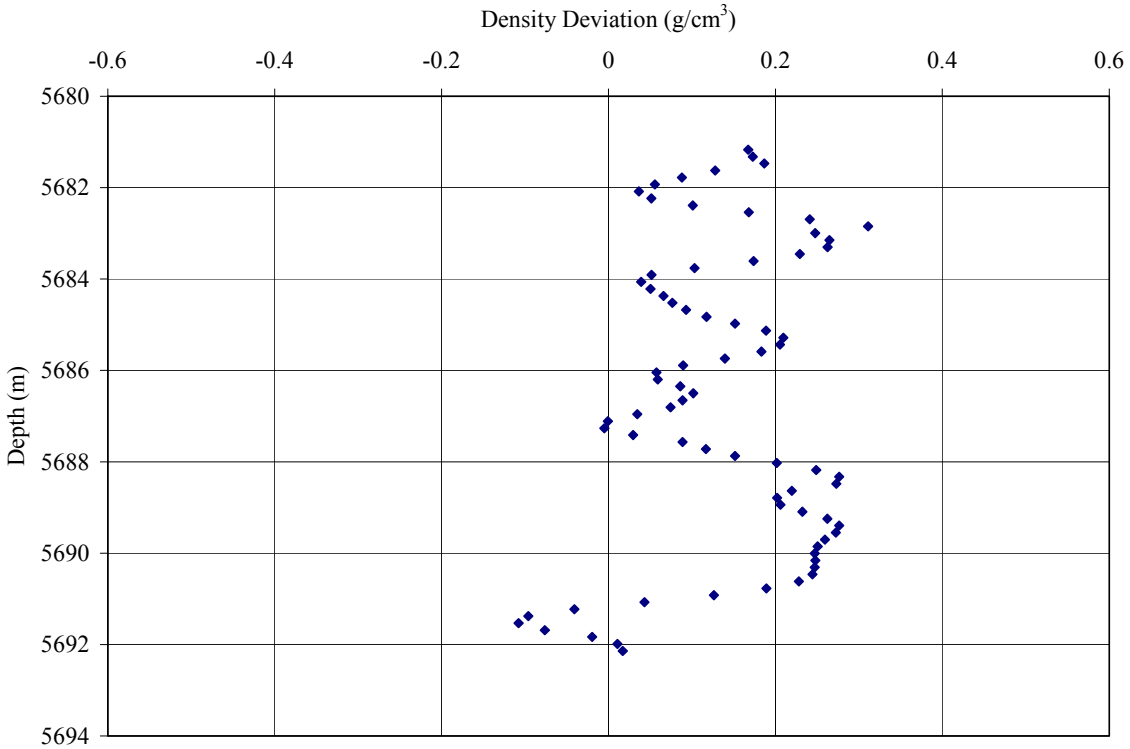

Figure H-24. Well 608224001700; pseudo density deviation from bulk density through Aptian-age siltstone potentially associated with deposition during an OAE.

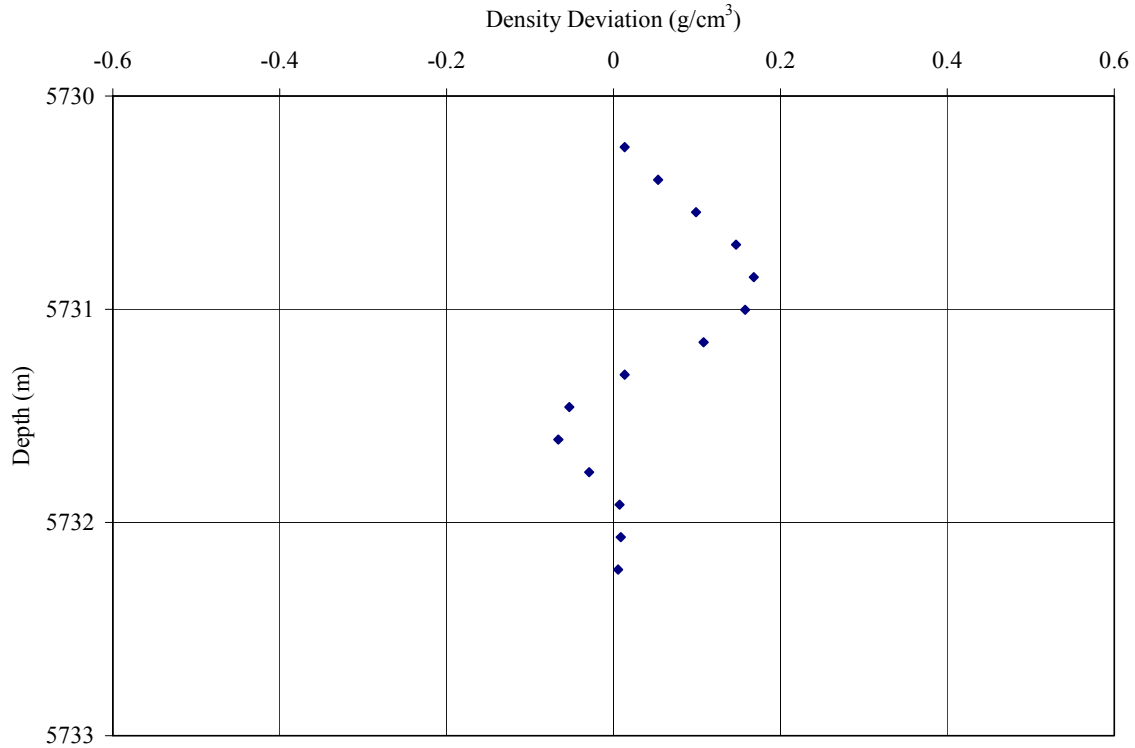

Figure H-25. Well 608224001700; pseudo density deviation from bulk density through Aptian-age limestone potentially associated with deposition during an OAE.

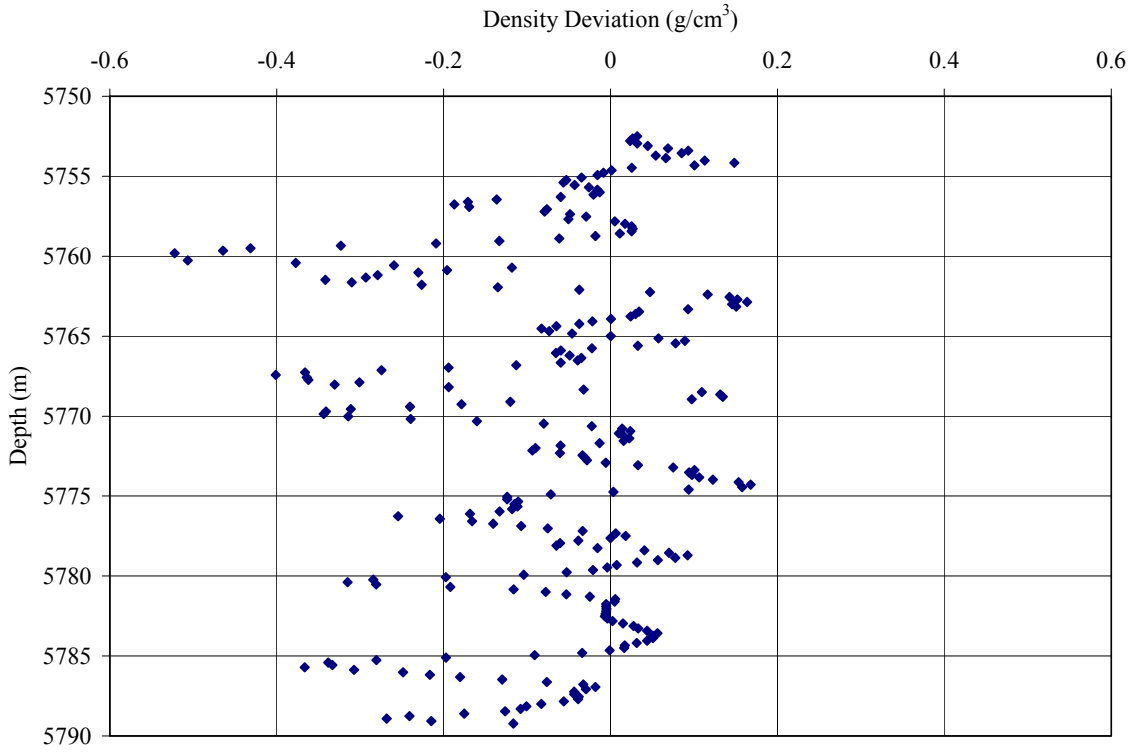

Figure H-26. Well 608224001700; pseudo density deviation from bulk density through Aptian or older aged siltstone potentially associated with deposition during an OAE.

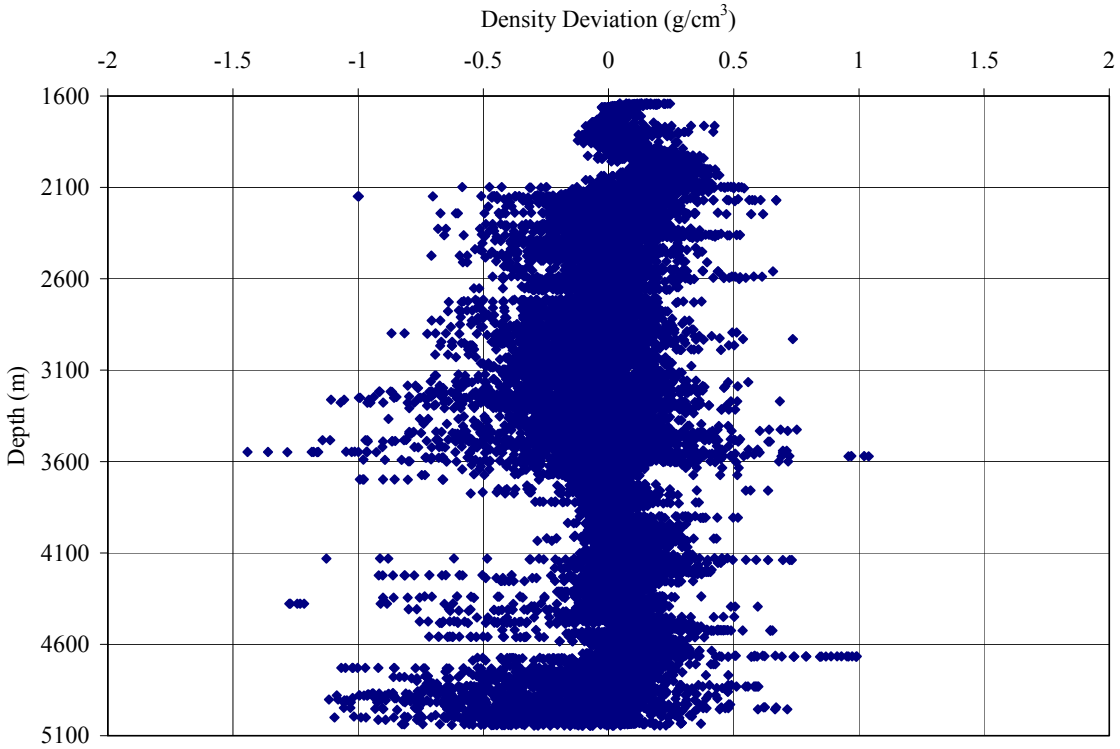

Figure H-27. Well 608224002200; pseudo density deviation from bulk density.

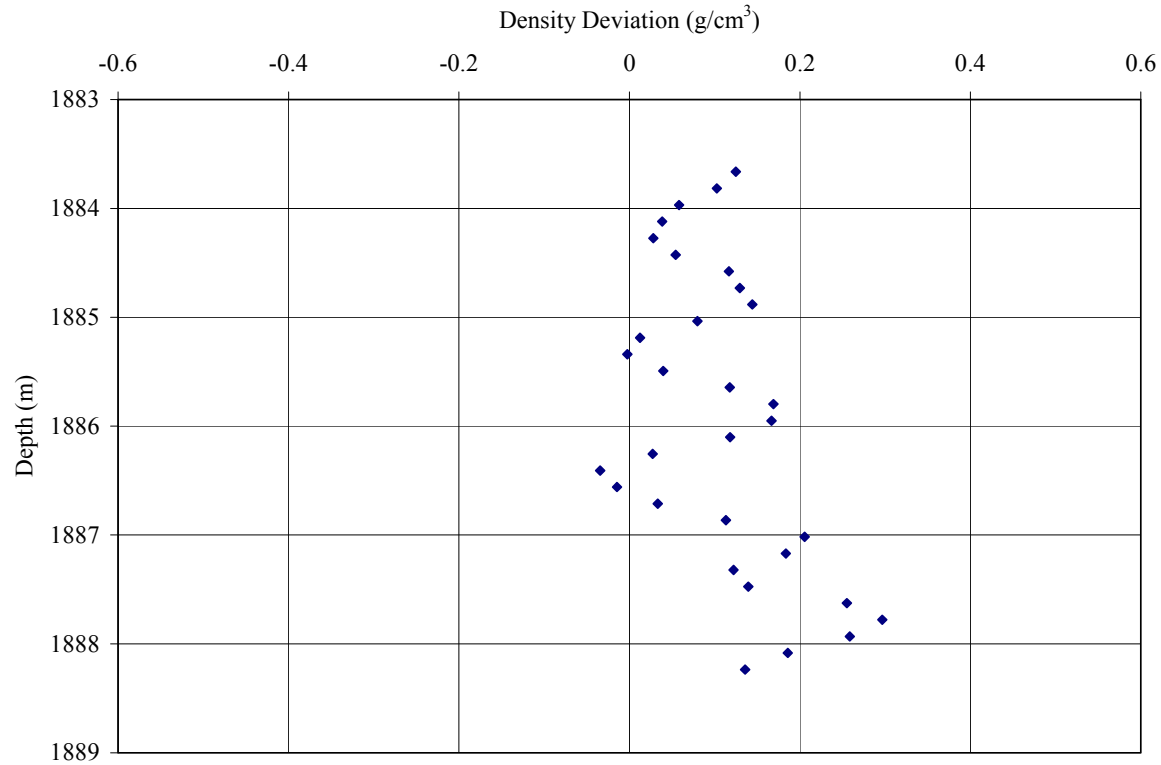

Figure H-28. Well 608224001700; pseudo density deviation from bulk density through Santonian-Coniancian-age black shale potentially associated with deposition during an OAE.

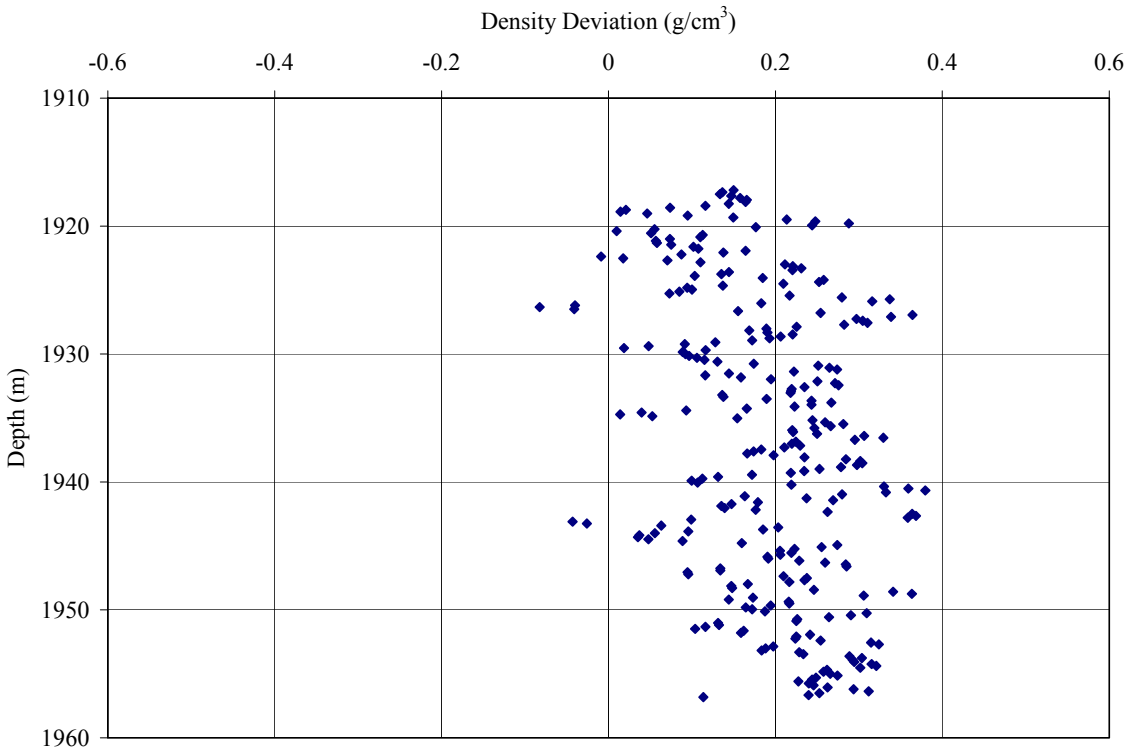

Figure H-29. Well 608224001700; pseudo density deviation from bulk density through Santonian-Coniancian-age Tuscaloosa Formation black shale potentially associated with deposition during an OAE.

VITA

Asani Brewton was born in Pensacola, Florida in 1983. In 2005 she obtained her bachelor's degree in Geology from Elizabeth City State University in Elizabeth City, North Carolina. She is currently pursuing a master's degree in Geology at the University of New Orleans, in New Orleans, Louisiana. Asani was a co-author for a geologic field guide for the American Association of Petroleum Geologists for their 2005 eastern section meeting. In the summer of 2003, she was employed as an intern by the United States Forest Service in Wise, Virginia. She is currently employed with the Department of the Interior, Minerals Management Service in New Orleans, Louisiana. She is currently a part of the Production and Development Unit, working on Conservation Information Documents in the deepwater Gulf of Mexico.